Hydrogen-bonding Receptors for Anion Recovery in a Capacitive Deionisation System.

Calum S. Hope

Submitted in fulfilment of the requirements for the

Degree of Doctor of Philosophy

School of Chemistry

College of Science and Engineering

University of Glasgow

September 2022

COVID-19 Statement

The work undertaken in the following body of work was greatly affected by the global pandemic. At the start of 2020 the direction of my research project changed, from a metal-coordination based project to one that more directly resembles the presented thesis. In early January/February 2020, I had just started the initial synthetic reactions that are presented in this thesis, specifically chapter 3. Based on this, the scope of the project was extended to include a second receptor for a different anion- chapter 4. By March 2020 and the start of the pandemic, I had successfully synthesised the first molecule in one of the suggested routes and was trying to purify the other.

During the pandemic, when it was possible to go into the lab, the available lab-time was severely impacted by the implementation of a rota system; either half-days or one- or two-days week. As a primarily synthetic research project, this had a drastic impact upon the output of the work that I was able to complete, consequently, a shift second alternative research project was proposed that would be better suited to the limited practical lab-time that was authorised. The results of this project are not detailed in this thesis.

Upon the easing of lab restrictions, it was possible to return once again to working on the synthetic projects presented in this thesis. Due to the length of time away from the project it was prudent to start the projects again from the beginning. This was to ensure that any of the previously synthesised material had not degraded and also to 'start fresh' after having not worked on the project for such a long period of time. The length of time whereby the laboratory/building was under some form of restrictions exceeded 15 months. Consequently, problems with the synthetic route were encountered at a much later stage, such as issues with removing protecting groups and the subsequent resign of the synthetic procedure. This led to a third receptor being proposed that had a much less intensive synthetic route. This third receptor that required only three synthetic steps, with minimal workup.

The final receptor complexes, all three, were finally synthesised by early February 2022. As such, work was begun on the implementation of the receptors within the proposed capacitive deionisation system. This included work on the binding of the receptors to the electrode surface, as well as trying to attain an idea of the binding of the anions to the receptor. In order to obtain this data, further receptor needed to be synthesised, purified, and characterised to ensure that there was enough material to test using NMR spectroscopy

and Ultraviolet-visible spectroscopy. By May/June 2022, enough receptor had been synthesised for preliminary testing. Concurrent experiments to graft the alkyne groups directly to the surface were being conducted but would require more time.

Despite being given a five-month extension, this did not negate fully the time away from experimental work. Given more time, repeat experiments on the binding of the receptors to other anions to investigate promiscuity would need to be done, this would further confirm the receptors suitability in a selective capacitive deionisation system. As detailed in this body of work, there are a number of ways that the receptors can be grafted to an electrode surface. Initial tests through the direct oxidation of the alkyne proved to be unsuccessful and would require more work. Alternative methods, i.e., Click reaction, have been proposed should this route not work; however, no work has been undertaken on this method. Once the receptors have been grafted to an electrode surface, work on the design and optimisation of a capacitive deionisation system could begin.

Abstract

Receptors are ubiquitous throughout nature and are found heavily within biological systems. This has led to synthetic supramolecular chemists to modify or develop analogous mimics of these receptors with high affinity and specificity for a range of target compounds, for potential commercial use. One group of particular interest are receptors that function through the formation of hydrogen bonds to the guest species. This class of receptor has been shown to have a range of different structural geometries and binding motifs, that allow for the sequestration of a number of different species. In the context of this work, anionic hydrogen-bonding receptors, specifically for 'phosphate'- in most cases dihydrogenphosphate- and bicarbonate are of interest. Phosphate is an integral part of the DNA backbone, however a organophosphorus containing compounds also comprise a large group of chemical weapons which can have a devasting impact on the bodies ability to function. Chemical weapon compounds, such as sarin and Novichok, are based on the functionalisation of a central phosphate core which can be biotransformed into a highly potent active species within the body. Phosphate is also an essential component of plant fertilizers and is used on a huge scale in order to maintain global food security. However, phosphate loss as a consequence of agricultural run-off leads to reduced availability of essential minerals as well as large scale eutrophication. One such method that could be utilised for the recovery of phosphate is electrochemical capacitive deionisation. The principle and idea of capacitive deionisation has been around since the late 1960's to early 1970's and has been shown to be a suitable method for the desalination of low-to-medium salinity input streams. The purpose of the work within this thesis was to modify and synthesise receptors that could be covalently attached to porous carbon electrodes and impart selectivity to a capacitive deionisation system.

In Chapter 1, the importance of 'phosphate', biologically and commercially is addressed before an in depth look at some of the phosphate specific hydrogen bonding receptors that have been reported in the literature. The design of a successful hydrogen bonding receptor relies on the correct orientation of the binding motifs and the range of structural scaffolds have been shown to be useable. Following this, the electrochemical principles of capacitive deionisation and its suitability for the recovery of phosphate are detailed, including some examples of capacitive deionisation set-ups and the overall processes involved. Chapter 2 details the theory of the techniques used throughout this thesis, which include, but not limited to, ^{1}H and ^{13}C NMR for the structural elucidation of the

synthesised receptors and cyclic voltammetry which was used for the attachment of organic groups to an electrode. The historical and theoretical background established in Chapters 1 and 2 will lead into the work undertaken in Chapters 3-5.

Chapter 3 focusses on the first of three hydrogen bonding receptors synthesised. Building upon previous work within the field, two neutral indole-based receptors were modified to include two different potential attachment points for the electrode- a carboxylic acid and an alkyne. Following the successful synthesis of the alkyne-based receptor, ^{1}H NMR titrations were used to confirm the affinity of the new receptor for dihydrogenphosphate. Chapter 4 introduces the second anion of interest, bicarbonate. The underlying principles for hydrogen bonding are the same for bicarbonate, as in phosphate, however a different receptor was synthesised. The carbazole receptor synthesised contained free amine groups that were proposed to act as points of attachment to an already surface bound organic spacer group. ^{1}H NMR titrations are once again used to determine the affinity of the receptor for the bicarbonate anion. Finally, Chapter 5 introduces the second of the dihydrogenphosphate-specific receptors, this time based on the amino acid leucine. UV-Vis titrations with a number of different anions were used to determine the affinity of the receptor. Within this chapter, methods for the attachment of organic groups are detailed including the electroreduction of 4-nitrobenzene diazonium and the direct oxidation of the alkyne.

Table of Contents

COVID-19 Statement i

Abstract iii

Table of Contents v

List of Conferences and Courses x

Acknowledgements xi

Author's Declaration xiii

List of Abbreviations xiv

Anion Receptors and Capacitive Deionisation Systems 1

1.1 Phosphate 2

1.2 Hydrogen bonding: factors affecting association constants. 6

1.3 Calculating association constants: NMR vs. UV-Vis vs. Fluorescence Spectroscopy. 11

1.3.1NMR Spectroscopy 11

1.3.2 UV-Vis Spectroscopy 12

1.3.3 Fluorescence Spectroscopy 12

1.3.4 Isothermal Calorimetry 13

1.4 Stoichiometry: Job's plots and the alternatives 13

1.5 Developments in Anion Receptors for Phosphate species 17

1.6 Capacitive Deionisation Systems 41

1.6.1 Electric Double Layer 44

1.6.2 Developments in Capacitive Deionisation systems 49

1.7 Conclusions 53

1.8 References 55

Analytical and Electrochemical Techniques 59

Synopsis 59

2.1 NMR Spectroscopy 60

2.1.1 Fundamentals of NMR and Chemical Shift 60

2.1.2 Distortionless Enhancement by Polarization Transfer (DEPT) **64**
2.2 UV-Vis 64
2.3 Infrared Spectroscopy (IR) 65
2.4 Mass Spectrometry (MS) 67
2.4.1 Ion source- Electron Ionization **68**
2.4.2 Ion Source- Electrospray Ionization (ESI) **69**
2.4.3 Mass analyser **69**
2.4.4 Ion Detection **70**
2.4.5 Data Receiver **71**
2.5 Electrochemical Techniques 71
2.5.1 Cell Setup **71**
2.5.2 Cyclic Voltammetry (CV) **72**
2.5.3 Electrolysis **74**
2.6 References 75
Acknowledgments and Declaration 76
Synopsis 77
3.1 Introduction 78
3.2 Proposed reaction Scheme 79
3.2.1 GABA esterification **81**
3.2.2 CDIm amide coupling **83**
3.2.3 Reduction of nitro moiety using Pd/C **85**
3.2.4 Urea coupling- Triphosgene **87**
3.2.5 Methyl ester deprotection **89**
3.3 Revised Reaction Scheme 90
3.3.1 Reduction of the nitro moiety- Béchamp reduction **91**
3.4 ^{1}H NMR Titrations 93
3.5 Conclusions and Future Work 95
3.6 Experimental 102
3.6.1 Materials and reagents **102**
3.6.2 General synthetic methods **102**

3.6.3 ^{1}H NMR Titrations **108**

3.7 References 110

Bis-carbazolylurea Receptor for Anion Recovery **113**

Acknowledgements and Declaration 113

Synopsis 114

4.1 Introduction 115

4.2 Proposed Reaction Scheme 119

4.2.1 Synthesis of 1-nitrocarbazole (4.5) **120**

4.2.1.1 Nitration with HNO_3 120

4.2.1.2 Buchwald-Hartwig cross-coupling 121

4.3 Revised Reaction Scheme 126

4.3.1 Friedel-Crafts alkylation of carbazole (4.9) **128**

4.3.2 Bromination of 3,6-di-*tert*-butyl-*9H*-carbazole (4.11) **131**

4.3.3 Amination of 1,8-dibromo-3,6-di-*tert*-butyl-*9H*-carbazole (4.12) **132**

4.3.4 Mono-Boc protection of 3,6-di-*tert*-butyl-*9H*-carbazole-1,8-diamine (4.13) **134**

4.3.5 CDIm coupling; synthesis of 1,3-Bis(3,6-di-*tert*-butyl-8-(*tert*-butoxycarbonylamino)-*9H*-carbazol-1-yl)urea (4.14) **136**

4.3.6 Deprotection of 1,3-Bis(3,6-di-*tert*-butyl-8-(*tert*-butoxycarbonylamino)-*9H*-carbazol-1-yl)urea (4.15) **138**

4.4 ^{1}H NMR Titrations of TEA·HCO_3 139

4.5 Conclusions and Future Work 141

4.6 Experimental 143

4.6.1 Materials and Reagents **143**

4.6.2 General Synthetic methods **143**

4.6.2.1 NMR Analysis 143

4.7 References 151

1,3-dicarboxamide Receptor for Anion Recovery and Electrochemical methods for electrode attachment **153**

Acknowledgements and Declaration 153

Synopsis 154

5.1 Introduction 155

5.1.1 Capacitive Deionisation **157**

5.2 Proposed Reaction Scheme 158

5.2.1 *N*-boc-*L*-leucine and 2-aminoquinoline coupling using *N,N'*-dicyclohexylcarbodiimide (5.8) **162**

5.2.2 Deprotection of trimethyl-1,3,5-benzenetricarboxylate (5.11) **164**

5.2.3 Benzylation of dimethyl-1,3,5-benzenetricarboxylate (5.12) **165**

5.3 Revised Reaction Scheme 168

5.4 Binding Studies- UV-Vis titrations 169

5.5 Electrode Attachment 173

5.5.1 Electroreduction of 4-nitrobenzene diazonium salt **174**

5.6 Conclusions and Future Work 178

5.7 Experimental 180

5.7.1 Materials and Reagents **180**

5.7.2 General synthetic methods **180**

5.7.2.1 NMR Analysis 180

5.7.3 UV-Vis titrations **184**

5.7.4 Electrode attachment **184**

5.8 References 185

Final Conclusions and Future Work **188**

Final Conclusions and Future Work 189

References 193

Appendix **194**

NMR Spectra 195

Compounds- Chapter 3 ..... **195**

Compounds- Chapter 4 ..... **202**

Compounds- Chapter 5 ..... **210**

Association Constant Fitting (BindFit)[1,2] **214**

Chapter 3- Compound 3.12 214

Chapter 4- Compound 4.16 214

Chapter 5- Compound 5.16 214

References 215

List of Conferences and Courses

- Energy Storage and Conversion Section Colloquia, School of Chemistry, University of Glasgow, UK.
  Oral Presentation: "Capacitive Deionisation for Anion Recovery".

- Royal Society of Chemistry Electrochem, Glasgow, UK, 2019 [26/8-28/8/2019].
  Poster presentation: "Capacitive Deionisation for Anion Recovery".

- Universities of Scotland Inorganic Chemistry (USIC), Glasgow, UK, 2019 [29/8-30/8/2019].
  Poster presentation: "Capacitive Deionisation for Anion Recovery".

- Basics of Nuclear Magnetic Resonance, 5 weeks online course, University of Lille, France, 2021.

Acknowledgements

I would like to take this opportunity to thank Professor Mark Symes for the opportunity afforded to me four years ago. Thank you for all your help and support along the way. At times when things were perhaps not working as intended, or even at all, your advice and guidance were invaluable and have allowed me to reach a point, that two years ago, seemed so far away, so for that thank you again. I would also like to thank all of the Symes group, past and present, for all the help and chats that made the whole PhD process that little bit more bearable! A big thank you also to all the technical and support staff who helped to make everything so much easier.

Patrick McHugh and Thanasis, I don't think my experience would have been the same if it wasn't for the both of you. Four years ago, we were complete strangers and now, I can honestly say you are two of my best friends. Coming in everyday was that much easier knowing I had some friendly faces around for support. I have nothing but fond memories, both in and out of work, of the past four years, although I'm not too sure about Patrick….Hala Madrid!

Ali, a thank you isn't nearly enough. From living together in the dingy, dark and porous basement flat in the West End, to welcoming me into your much warmer, brighter and ,more importantly, waterproof flat in the Southside. Your friendship, help and support are things I truly cherish and, I look forward to many more inane conversations about nothing in the many years to come.

To the boys back home, thank you for all the support over the years, from coming all the way up to visit to a simple text just checking in, it means the world to me. The pandemic was hard for all and being so far away made it that bit more difficult, but the countless hours/days playing with all of you made that time so much easier, so thank you. Here's to many more years of unspecified kaos to come!

To Laura. When I started, we were just beginning to get to know each other, but since then, you have been with me every step of the way. Thank you for your kind, and sometimes unkind words when needed, that have gotten me through. I'm so glad that we met when we did as I cannot imagine making it through all of this without your love and support. I just want to say how proud I am of you and all you have achieved. Thank you for making me a better person. All my love.

Mum and Dad, you have always been my biggest believers, always pushing me to better myself and have no fear of failure, so thank you. Thank you for politely, telling me to pull my finger out at times, or offering a kind shoulder when I needed it. I have never not, not once, felt like I was ever alone. Thank you for always making me feel loved and welcome when I come back home. I could not ask for more loving or caring parents. Thank you for making me believe I could do anything. I love you both.

And Milo; Woof.

Author's Declaration

I declare that, expect where explicit reference is made to the contribution of others, this thesis is the result of my own work and has not been submitted for any other degree at the University of Glasgow or any other institution.

I declare that this thesis has been produced in accordance with the University of Glasgow's Code of Good Practice in Research.

I acknowledge that if any issues are raised regarding good research practice based on review of the thesis, the examination may be postponed pending the outcome of any investigation of the issues.

Printed name: **Calum S. Hope**

Signature:

List of Abbreviations

ΔE	Potential Difference
2A4NT	2-amino-4-nitrotoluene
4A2NT	4-amino-2-nitrotoluene
4HA2T	4-hydroxylamine-2-nitrotoluene
A	Area or Absorbance
AcO^-	Acetate
AcOOH	Acetic Acid
ACTD	Actinomycin D
Ar	Aromatic
B_0	Applied Magnetic Field
B_{eff}	Effective Magnetic Field
B_i	Induced Magnetic Field
BINAP	2,2′-Bis(diphenylphosphino)-1,1′-binaphthalene
Bn	Benzyl
Boc	*tert*-Butyloxycarbonyl
Boc_2O	Di-*tert*-butyl dicarbonate
BzO^-	Benzoate
C	Capacitance
c	Concentration
Cbz	Carbazole
CDI	Capacitive Deionisation
CDIm	1,1'-carbonyldiimidazole
CEM	Cation Exchange Membrane
CV	Cyclic Voltammetry

dba	Dibenzylideneacetone
DCC	*N*,*N'*-Dicyclohexylcarbodiimide
DCM	Dichloromethane
DCU	Dicyclohexylurea
DEPT	Distortionless Enhancement by Polarization Transfer
DMAP	Dimethylaminopyridine
DMEDA	1,2-dimethylethylenediamine
DMF	Dimethylformamide
DMSO	Dimethylsulfoxide
DNA	Deoxyribonucelic acid
DNAT	2,2’-dinitro-4,4’-azoxytoluene
DPB	4,4’-dipyrrolyl-2,2’-bipyridine
e	Electronic Charge
E	Potential
e^-	Electron
EDL	Electric Double Layer
E_{pzc}	Potential of Zero Charge
ESI	Electrospray Ionisation
Et_2O	Diethyl ether
EtOAc	Ethyl Acetate
F	Faraday's Constant
FCA	Friedel-Crafts Alkylation
GABA	Gamma/γ-aminobutyric acid
GC	Gas Chromatography
GCE	Glassy Carbon Electrode

Glu	Glutaraldehyde
h	Planck's Constant
H-bond/bonding	Hydrogen bonding
HCP	Hypercrosslinked Polymer
HDC	Huisgen 1,3-dipolar cycloaddition
HMBC	Heteronuclear Multiple Bond Correlation
HOBt	1-Hydroxybenzotriazole hydrate
HPLC	High Performance Liquid-Chromatography
HSQC	Heteronuclear Single Quantum Coherence
I	Spin Quantum Number
i	Current
Icbz	Indolo[3,2,1-jk]carbazole
ICDI	Inverted Capacitive Deionisation
Ind	Indole
IR	Infrared
J	Coupling Constant
k	Spring Constant
K_a	Association Constant
l	Pathlength
Ln	Ligand
m	Mass or Moles
m/z	Mass-to-charge
M_0	Bulk Magnetic Moment
MCDI	Membrane Capacitive Deionisation
Me	Methyl

MEA	Monoethanolamine
MeCN	Acetonitrile
MeOH	Methanol
MS	Mass Spectrometry
n	Number of electrons
n-Bu	*n*-Butyl
NMR	Nuclear Magnetic Resonance
NO_2Me	Nitromethane
Nu^-	Nucleophile
OLED	Organic Light Emitting Diode
PBP	Phosphate Binding Protein
Pet. Ether	Petroleum ether
PG	Protecting Group
Ph	Phenyl
POP	Porous Organic Polymers
Q	Charge
r	Radius
R	Resistance
RNA	Ribonucleic acid
Sat.	Saturated
t	Time
TBA	Tetrabutylammonium
t-Bu	*tert*-Butyl
TEA	Tetraethylammonium
TFA	Trifluoroacetic acid

TFB	Tetrafluoroborate
TfO^-	Triflate
THF	Tetrahydrofuran
TPB	1,3,5,-triphenylbenzene
TriEA	Triethanolamine
Triphos.	Triphosgene
UV-Vis	Ultraviolet-Visible
wt%	Percentage weight
δ	Chemical Shift
ε	Molar Extinction Coefficient
μ	Magnetic Moment or Reduced Mass
ν	Frequency
ρ	Resistivity
γ	Gyromagnetic Ratio

Note: Conventional abbreviations for units and physical quantities are not included.

Chapter 1

Anion Receptors and Capacitive Deionisation Systems

1.1 Phosphate

Anion recognition has, and continues to be, of great interest to supramolecular and synthetic chemists worldwide. Anions have been shown to be of great commercial value in catalysis[1] and are often targets for molecular sensors.[2,3] From a biological standpoint, anion transporters are often targets of chemotherapeutics.[4,5]

The design of receptors for the complexation of anions in water is not an easy feat, as anions in water are hydrated and any such complexation with a receptor must first exceed the large energy gap for dehydration. This, coupled with receptor-solvent and solvent-solvent interactions, makes anion recognition highly challenging.[4] Dihydrogenphosphate is one such anion that has huge industrial, environmental, and biological impact. Phosphorus (as phosphate) is used heavily in fertilisers, and in conjunction with nitrogen and potassium, has greatly increased crop yields and food security globally. In 2016, the Food and Agriculture Organization of the United Nations estimated that the global demand for fertiliser would reach approximately 202 million tonnes annually, and that demand would continue to increase.[5] Typically, phosphorus is mined from phosphorite- a family of rocks that are phosphorus-rich- of which global supplies are estimated to be depleted in less than 200 years. It is therefore essential that phosphorus containing compounds can be efficiently recovered and recycled. Eutrophication- the excessive growth of plant life in an aquatic body of water due to agricultural run-off of essential nutrients- is the main environmental problem associated with fertiliser loss and leads to the decrease of crop yields and algal bloom. Consequently, phosphate (as dihydrogenphosphate, under aqueous conditions) can be recovered chemically, through precipitation, as the mineral struvite, or biologically using phosphorus accumulating organisms.

Organophosphorus compounds also comprise a large group of chemical warfare agents that include sarin, **1.1** and Novichok related compounds, **1.2** and **1.3**.

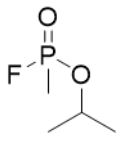

1.1

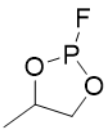

1.2

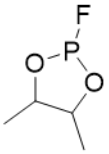

1.3

Many of these agents are biotransformed into their active species, through oxidation or cleavage of a functional group, leading to their extremely toxic effect. These compounds often work by binding to the enzyme acetylcholinesterase, which acts to inhibit the recovery of acetylcholine, which plays a vital role in the muscle contraction and heart rate regulation. During the biotransformation process, functional groups may be removed which increase the strength of the bond between the warfare agent and the enzyme leading to an irreversible bond and rapid death soon follows. Current methods for the neutralization of organophosphorus agents include the use of scavenger enzymes that bind and inactivate the organophosphorus compounds, hydrolysis of the compounds to nontoxic products and a combinatorial therapy of both the aforementioned methods.[6]

Biologically, phosphate is the backbone of DNA and RNA (Figure. 1.1) and is therefore an integral part in many genetic processes including transcription, translation, and molecular signalling.[7,8]

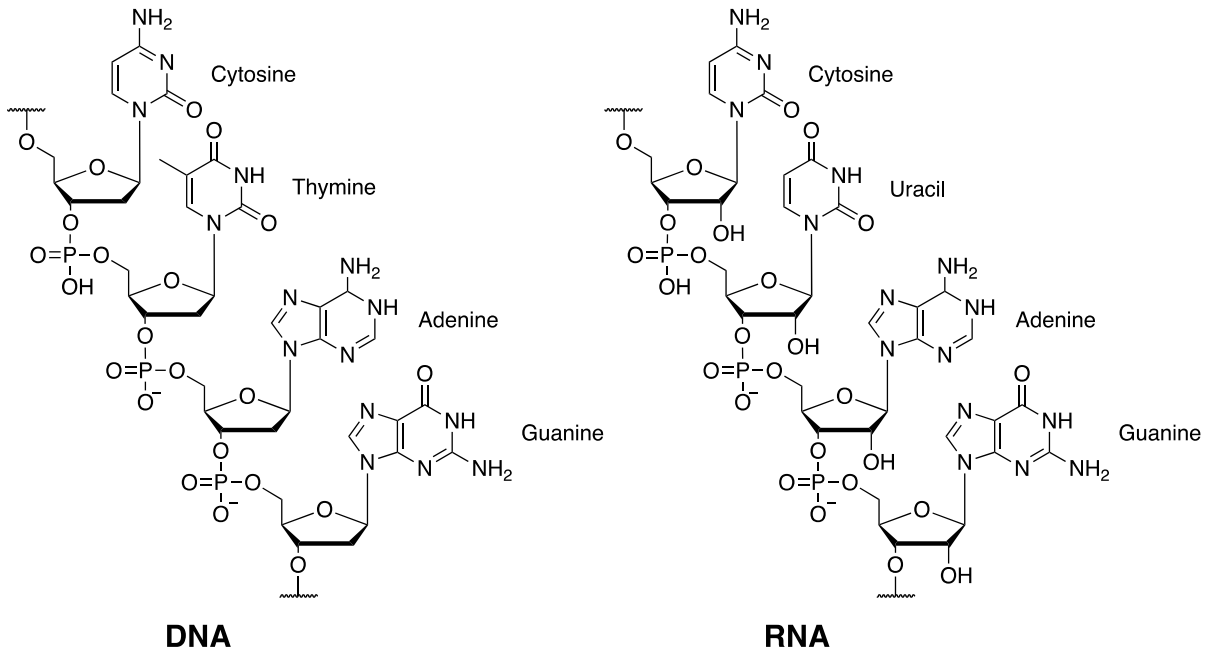

Figure 1:1: Chemical structures of DNA and RNA, showing nucleobases and phosphodiester linkages.

In the 1860's, Boettcher first described the synthesis of a crystalline solid obtained from human semen, which in 1878 was subsequently demonstrated to be a compound made from an organic base and phosphoric acid, henceforth called spermine, **1.4**. The spermine base has been identified in a range of cell types- testis, ovary, pancreas, muscle, liver, brain, spleen, thymus, thyroid, and yeast- as well as in animals. In 1927, the true structure of the spermine bas was identified– $NH_2(CH_2)_3NH(CH_2)_4NH(CH_2)_3NH_2$ – and shown to contain the trimethylenediamine group.[9]

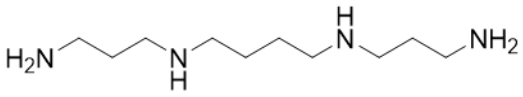

1.4

At physiological pH, polyamines carry multiple positive charges, that can interact with the nucleic acid backbone through both electrostatic and hydrogen-bond interactions. These interactions with DNA/RNA phosphate groups can promote conformational change, aid in condensation of the chain and also play a role in translation and transcription.[10] In addition to this, polyamines have been shown to protect DNA from denaturation and damage from a variety of sources, such as reactive oxygen species and mutagenic agents.[11,12] Polyamine metabolism, like spermine synthesis, has been shown to be deregulated in cancerous cells. As a result, concentrations of these polyamines have been detected in the millimolar range in cell nuclei, which could potentially be exploited. In 2012, Wang et al. demonstrated the effect that spermine had on a known DNA intercalating agent, Actinomycin D (ACTD), **1.5**. [8]In their study, they investigated how effectively ACTD could interact with DNA in the presence of spermine. They showed that not only did the binding of spermine directly block the intercalation of ACTD, through the formation of intrastrand bonds, but when present, especially at higher concentrations, spermine actively interfered with the affinity of ACTD for DNA.

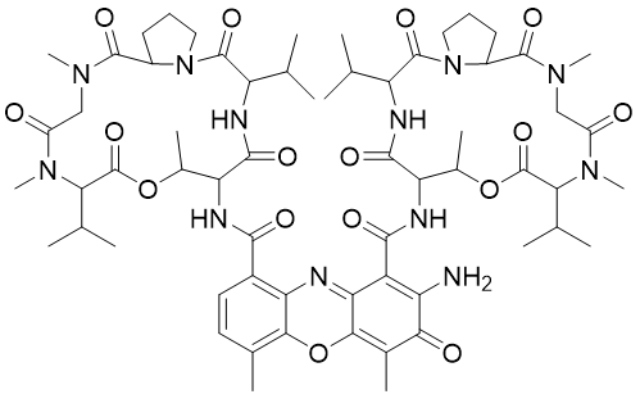

1.5

As a direct consequence of this, synthetic and supramolecular chemists across the globe have endeavoured to design synthetic receptors that have even greater affinity for phosphate containing species, that may have use in environmental remediation, sensors, or biological mimics.[13,14]

Receptor design has proven to be a challenging concept with several crucial factors needing to be addressed, firstly, the nature of the interaction between receptor and anion. Non-covalent interactions dominate in the complexation of ionic species, and the various types of interaction can be seen in Figure 1.2.

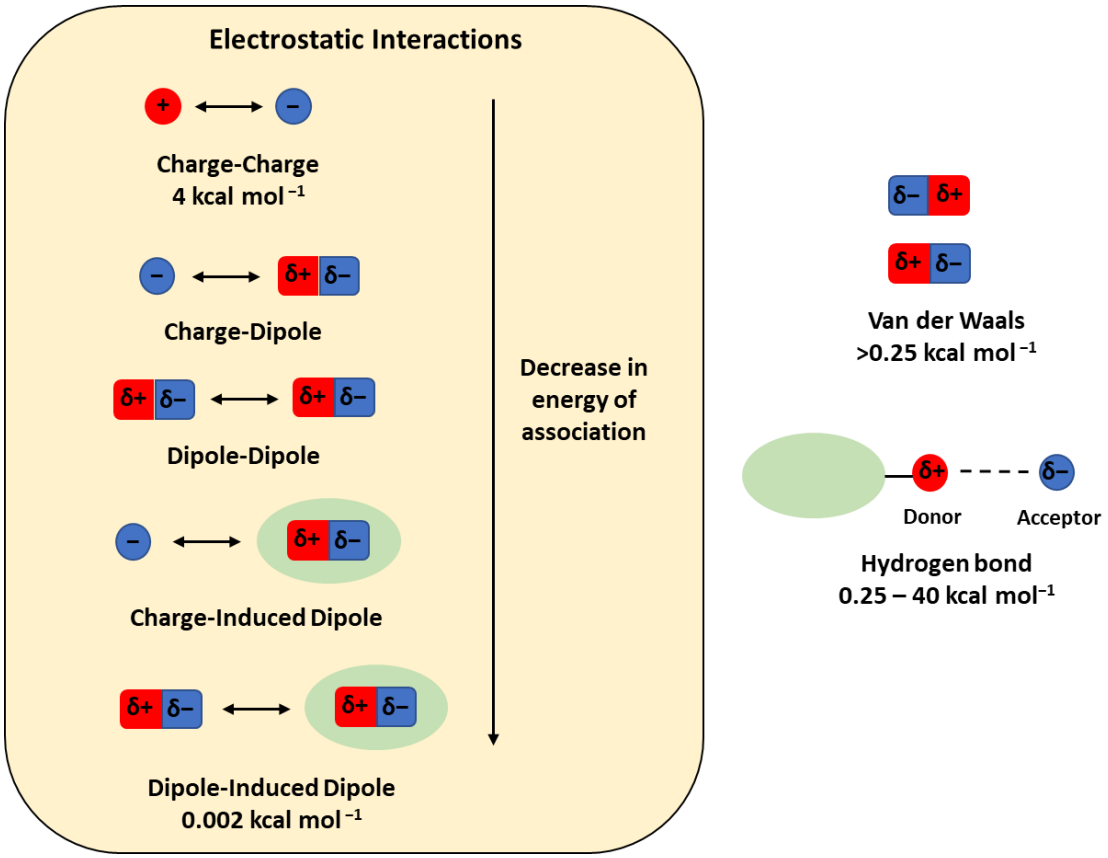

Figure 1.2: Types of non-covalent interactions.

Of particular importance is hydrogen bonding as it has been proven to be a highly effective, directional method for the complexation of anions, with a range of functional groups acting as H-bond donors or acceptors, or both in some cases. Hydrogen bonding has been shown to be highly directional with the strength of the interaction scaling with the difference in electronegativity between the donor and acceptor species- 0.25-40 kcal mol^{-1} -from an almost Van der Waals type interaction, which are weak in isolation but can have a large effect *en masse*, to a more covalent interaction between more polarised groups.[15] Typically, within receptor species, groups responsible for hydrogen bonding often contain oxygen or nitrogen atoms. Electrostatic interactions can enhance these H-bond interactions but have no directionality and can be broken down into different sub-types, depending on the type of species present. The strength of the interaction rapidly falls off with an increase in the ionic distance between the interacting species. Anion-π systems have been designed that incorporate electron withdrawing groups allowing for the interaction of the π-system with the anion.[16] Classic metal-coordination based receptors have also been shown to be effective in the complexation and sequestration of various anions.[17] Ion-pair systems, which are capable of binding both anions and cations simultaneously, have been developed

as they are a means to overcome the effects of anion-cation interactions that may perturb or interfere with the calculated binding constants.[18,19] Secondly, geometry, of both receptor and anion, must be considered. Anion geometry can vary dramatically from the simple spherical halides to tetrahedral dihydrogenphosphate to trigonal planar bicarbonate, consequently binding motifs associated with the receptor must be designed to maximise the efficacy of contacts between the two. It is important to consider both charge density and anion size when designing a suitable receptor, however, it has been demonstrated that the receptor binding cavity can show diverse capability to coordinate anions of various sizes and shape, at a cost to selectivity.[20,21]

1.2 Hydrogen bonding: factors affecting association constants.

As previously discussed, how efficiently and effectively a guest can bind and it what ratio, is perhaps the most important aspect of guest receptor complexes (both anionic and cationic). In the context of this body of work, hydrogen bonding is responsible for the association of the guest and receptor. Hydrogen, although the smallest atom, when polarised by an adjoining electronegative atom has a large charge density which can interact transiently with neighbouring electronegative atoms.[22] These intermolecular interactions, whereby no covalent bonds are formed, occur between a sufficiently electronegative atom, such as oxygen or nitrogen, and a hydrogen bonded to a second electronegative atom, -OH and -NH, for example, Figure 1.3a.[22–25] The strength of the bond formed is directly related to the electronegativity of the atoms involved, the distance between them and the geometry. The optimal geometry and bond distance is 180° and 2.7 – 3.3 Å, respectively.[26] Due to the increased electronegativity of oxygen versus nitrogen, the -OH bond is more polarised than the analogous -NH, and as such is a stronger H-bonding donor group. The relative strength of a hydrogen bond can vary dramatically from over 160 kJ mol^{-1} in some cases such as $[F\ldots H\ldots F]^-$ and P-OH…O=P, whereby the interaction is more covalent in nature, to less than 17 kJ mol^{-1} in cases involving C-H…O, with more transient, dipolar interaction characteristics.[22,25]

Hydrogen bonds have been demonstrated to be incredibly important in both nature and for industry. In industry, hydrogen bonding between the repeating amide units in nylon fibres, impart increased material strength, relative to other non-hydrogen bond containing materials, making them suitable for use as protective clothing, Figure 1.3b.

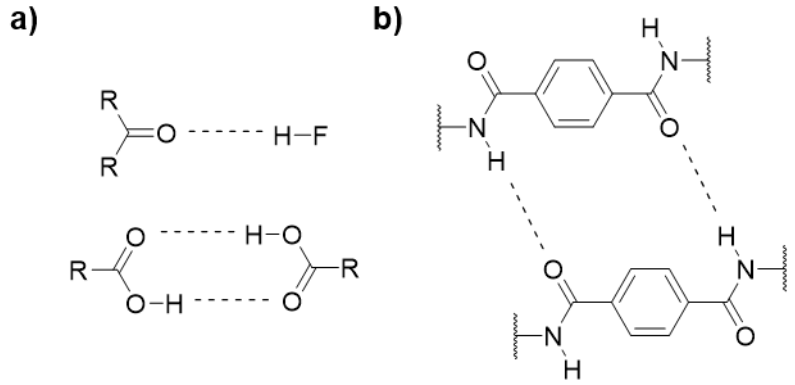

Figure 1.3: Hydrogen bonding examples involving a) different carbonyl and electronegative groups; b) polymeric Nylon strands. Both show the optimal bond angle of 180°.

As previously described, hydrogen bonds can form between -OH groups and as such, hydrogen bonding is present in water. The presence of H-bonds in water is what gives water some of its unusual properties, e.g., lower density as ice (compared to liquid), high surface tension and boiling point. In the field of receptor-guest chemistry, where a vast number of receptor-guest interaction is the result of receptor -NH donor groups, the tendency of water to form H-bonds is problematic as the increased polarization of the -OH means that investigating artificial receptor-guest complexes in aqueous media is generally not possible or requires more labour-intensive methods. Consequently, the solvent of choice for receptor-guest interactions are more often than not, investigated in a suitable aprotic solvent, such as $CHCl_3$ and DMSO, in order to increase the noncovalent interactions.[24] However, numerous examples can be seen in the literature that show water being spiked into receptor-guest mixes at increasing concentrations, and as such increase the competition between the receptor and its intended guest and solvent, in this case water. As a result of this, it is often seen that the calculated binding constants for a receptor in an aprotic/water mix are significantly lower to their solely aprotic counterparts. The role of the solvent in guest-receptor chemistry is therefore an incredibly important factor when considering calculations involving the determination of binding constants. The solvent utilised in guest-receptor experiments first and foremost, is dominated by the solubility of the receptor and guest-it would be impossible to determine the affinity of the receptor for a specific guest if aggregation was to occur. Secondly, considerations of the potential effects of the solvent-receptor interactions, which could complicate the calculation of the desired receptor-guest binding association, through the competing association reaction, should be a factor. During an association event, both the receptor and guest must be desolvated before association can occur. Entropically, it is favourable for the release of solvent molecules from the solvation shells of the receptor and guest, however, due to the nature of the H-

bond donor and acceptor groups of the receptor and guest, solvent molecules may interact more favourably and have an increased enthalpic cost of desolvation, this competing receptor-or guest-solvent interactions can decrease the stability of the desired complexes.[27] Therefore, in all cases, the accurate comparison of binding constants of different receptors can only be compared when the solvent media are the same.

A second important consideration when calculating and comparing binding constants, in this case anions, is the cationic counterion used. In the body of this work, the anions were added as their tetrabutylammonium. **1.6**, or tetraethylammonium salt, **1.7**.

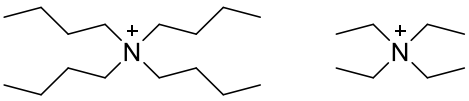

1.6 **1.7**

Typically, counterions are chosen to improve the solubility of a desired salt. This is perhaps most well evidenced in the pharmaceutical industry and the large library of safe counterions that can be accessed.[28] In the field of receptor-guest chemistry, the effects of the counterion not only affect the solubility but can also have an impact on the effectiveness of the desired binding event. It should first be noted that the counterion selected should possess only weakly coordinating ability, if any, to the receptor as to not interfere with the guest binding event. As previously described, typical guest-receptor are conducted in non-polar solvents which can dramatically increase the ion-pair strength (of the added salt), and consequently, the counterion can have an impact on the association of the receptor and guest through a number of different processes, such as sterics, electrostatics and charge density, stability of the separated ion and counterion pair and any interactions of the counterion with other ionic species in the reaction mixture.

In the solvent systems typically employed- non-polar, organic solvents- the ion-counterion pair can generally be thought of intimate ion-system (Type 3), whereby no solvent molecules separate the two ionic species, as opposed to a solvent separated (Type 1) or solvent shared system (Type 2), Figure1.4.

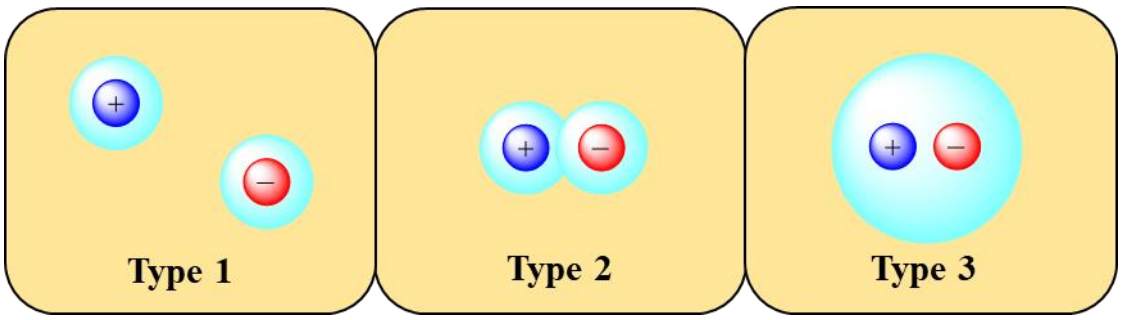

Figure 1.4: Typical ion-counterion pair interactions in organic solvents.

This tightly bound ion-pair can have significant implications during the receptor-guest complexation process, given the proximity of the counterion to the binding event. The steric effect would be greatest if the counterion remained tightly bound to the guest species and can drastically affect the complexation process if the binding cleft cannot adequately fit the ion pair.

The charge density of the counterion has been demonstrated to have a great impact on the ability of an ionic guest to bind to a neutral receptor complex. It follows that a large, sparsely charged counterion, will have a much more diminished polarising effect on the ionic guest, than a smaller, charge-rich counterion and as such, it is likely that an increase in the association between guest and receptor will be observed.[29] It therefore follows that small, charge-dense counterion species, will polarise the guest species more and subsequently reduce the strength of the binding event. One of the earliest experiments that investigated the effect of charge density of the counterion on the binding of an ionic guest was conducted by Bartoli and Roelens.[30] In their study they investigated the effect of varying the halide counterion- Cl^-, Br^- and I^- - on the binding of acetylcholine. The halide ions are spherical, monovalent ions that have an increasing ionic radius and as such made them prime candidates for investigations into the effect of charge density on the binding event. Using ^1H NMR in $CDCl_3$ at 296 K, they showed that the binding constant was shown to increase- 4 to 5 to 11 M^{-1}- as the ionic radius of the halide counterion increased.

The propensity for competition between the receptor host and counterion for binding sites on the ionic guest species has also been shown to affect the strength of the desired binding event. A weakly coordinating counterion species would likely have no discernible impact upon the binding of the guest to the receptor host, however this is very much dependent on the system that is in use and therefore should be reviewed on a case-by-case basis. A strongly binding ion-pair, such as the Type 3 described previously, would have a large impact on the binding of the guest to the receptor through both steric and charge polarisation of the guest.

In contrast, if the ion-pair is solvated, then there must be competition between both the receptor and the counterion, which would impact the efficacy of the guest binding to the receptor host.[29]

The stability of the separated ionic pair can have an influence on the stability of the formed receptor-guest complex. An increased distance between the cation and anion leads to an unfavourable thermodynamic contribution to the overall stability of the receptor-guest complex. This effect is further exacerbated if the counterion is only poorly stabilised by the solvent. In order to improve the stability of the guest-counterion pair, three properties of the ion pair can be modulated such as the polarity of the solvent, the distance between the ion-pair and the binding strength of the ion-pair. Investigative studies into the effects of these by Meijer et al. on the supramolecular assembly of guanosine monomers, **1.8**, into tetramers and the subsequent quadruplexes formed showed that the polarity of the solvent played a vital role in tuning the size of the complex formed.[31]

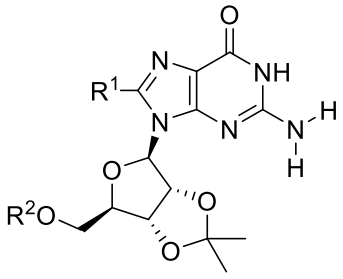

1.8

It was shown that in the relatively non-polar THF, the 8-mer was preferentially formed and in the highly polar acetonitrile medium, the 16-mer was formed. It was thought that the increased charge of the higher order complexes was stabilised better by a more polar solvent, such as acetone or acetonitrile. Further investigation on the same quadruplex substrates into the dependence of the anion-cation ion pair distance was demonstrated through the substitution of a bromine at the 8-position which forced the ribose units to adopt the all *syn*-conformation, as opposed to all the *anti*-conformation. This change in conformation caused an increase in the anion-cation distance and lead to a decrease in the quadruplexes stability.

1.3 Calculating association constants: NMR vs. UV-Vis vs. Fluorescence Spectroscopy.

In order to determine the strength of the interaction between the receptor and the anionic guest, titration experiments are typically the preferred experimental method. The titration of a known equivalence of anionic guest into a known concentration of receptor can be followed through a number of spectroscopic techniques such as NMR or Ultraviolet-Visible spectroscopy. In order to be studied by such techniques, it is integral that the binding of the guest causes a detectable change in the observed variable e.g., change in absorbance or change in chemical shift.

1.3.1NMR Spectroscopy

Proton NMR titration experiments often the yield the most information, however, other NMR forms such as ^{31}P and 1D-^{13}C can still give useful quantitative information. In addition, changes in the symmetry and chemical shifts can be used to probe the interaction between host and guest and even determine the binding association. During the NMR titration the change in the observed resonance is the average of both the free receptor and the bound receptor-guest species and can be described by Equation 1.1

$$\Delta\delta = \delta_{\Delta HG}\left(\frac{[HG]}{[H_0]}\right) \qquad Equation\ 1.1$$

With the advent of more powerful and sensitive NMR spectrometers, it is now possible to obtain NMR spectra for concentrations of receptor as low as 10^{-4} M^{-1}, which would allow for the K_a determination up to 10^6 M^{-1}. One consideration with NMR titration experiments is the relative exchange equilibrium between the association and dissociation of the guest and the receptor host and the timescale of the NMR experiment. This means that for a given titration experiment, the main limitation is whether the system being study exists in the slow- or fast-exchange range at the NMR timescale. The change in the observed chemical shift is related to the mole fraction of free receptor and the relative 'off' rate of the system. As mentioned previously, the timescale of the NMR experiment and whether or not the system is in fast or slow exchange are integral in dictating whether or not the observed changes can be related to the underlying equations- not spoke about in the body of this thesis. Simply, it has been shown that the assumptions and underpinning equations breakdown if the system

of interest is not in fast exchange. In analysing the obtained titration curves, practically it has been demonstrated that it is often best to focus attention on relatively small changes to the observed chemical shift as these are more likely to still be in the fast exchange region and as such be less prone to broadening effects.[32]

1.3.2 UV-Vis Spectroscopy

The second most utilised spectroscopic technique for investigating receptor-guest complexation is UV-Vis. A benefit of using UV-Vis over NMR is that with the correct chromophore group, binding constants, as high as 10^9 M^{-1}, in the sub-micromolar concentration range- 10^{-7} M^{-1} can be obtained. In order for UV-Vis to be applied, the chosen concentration must allow for both the absorption peaks of the receptor and the receptor-guest complex to fall with the limits of the Beer-Lambert law i.e. $A < 1$. Secondly, it is desirable, and aids in interpretation, for the added guest species to have no absorption within the region that is under investigation. Fortunately, for most simple ionic species employed within such binding studies, no absorption is observed. A final point of note, that although applicable to all the spectroscopic methods employed to determine binding constants, is particularly pertinent to UV-Vis, is the effect of temperature and diluting the receptor species, as well as the effect of impurities in either/both the receptor and guest species. It is therefore paramount, that if a particularly low concentration is required, then extra care should be taken during the weighing process as to accurately establish the concentration of the receptor.[32]

1.3.3 Fluorescence Spectroscopy

A third, highly popular technique- not used in the context of this thesis- is fluorescence spectroscopy. This technique is the most sensitive of the three described and measurements of nanomolar receptor concentrations are possible. As a result, fluorescence spectroscopy can be used for the determination of very large association constants. The low concentration is a necessity for the fluorescence titrations due to the linear dependence of the fluorescence response on the absorption of the incident light . At higher concentrations or when the excitation wavelength has absorption above 0.05, this linear dependence breaks down.

An additional benefit of fluorescence is the ability for the design or inclusion of a single fluorophore group, whether in the receptor host or the guest. Consequently, this means that

during a titration, the complexation of fluorescently active species can be either quenched or activated by the complexation of the other fluorescently 'silent' species. If quenching plays a role is observed, static and dynamic quenching must be differentiated, with only static quenching being of real importance during supramolecular complexation.

1.3.4 Isothermal Calorimetry

Calorimetry titration experiments measure the increase in enthalpy when the guest is added to a solution of the receptor guest. This is usually done through measuring the heat emitted or absorbed upon complexation. This heat measured can then be related to the molar enthalpy and the number of moles of the complex that can be formed. The power of calorimetric measurements is that not only is it possible to obtain values for the association constants, manipulation of equations for free energy, *G*, make it possible to obtain enthalpic and entropic values as well.[32]

1.4 Stoichiometry: Job's plots and the alternatives

For nearly 100 years, the primary method for determining complex stoichiometry has been the method of continuous variation, also known as Job's plot, after Paul Job who first described the method in 1928. In his seminal work, he monitored the change in the absorbance of $Tl(NO_3)/NH_3$ as the mole fraction of the thallium (III) nitrate was altered. Based on this, it is possible to plot the mole fraction versus the absorbance and obtain a graph that can be used to gauge the stoichiometry of the reaction.[33] In a Job's plot, a number of assumptions are made that oversimplify the reality of what is actually occurring. For example, an ideal Job's plot assumes that only the H_xG_y complex is formed and is the sole contributing factor to the change in the measured observable. For a Job's plot, the observed maxima is when $[H_0]:[G_0]=x:y$, however it is likely that the formation of the H_xG_y complex will be a competing complexation between all the other possible stoichiometries for the receptor host and guest species. Consequently, the maxima observed can be skewed and somewhere between the maxima of two stoichiometries.

Until recently Job's plots were considered the primary method for the determination of binding stoichiometry of receptors however, in 2016 Jurczak et al. demonstrated how the Job's plot method is perhaps too simplistic and required special care when interpreting any

obtained results.[34] In their studies they simulated Job's plots for theoretical 1:1 and 1:2 receptor-guest complexes, with typical association constants and concentration employed within supramolecular titration experiments. In their simulations, Figure 1.5 they showed that in only 4 of the 16 simulated cases, was the 'true' nature of a Job's plot of a HG_2 complex observed, and of these four, only one presented any real likeness to the actual value of $x = 0.33$.

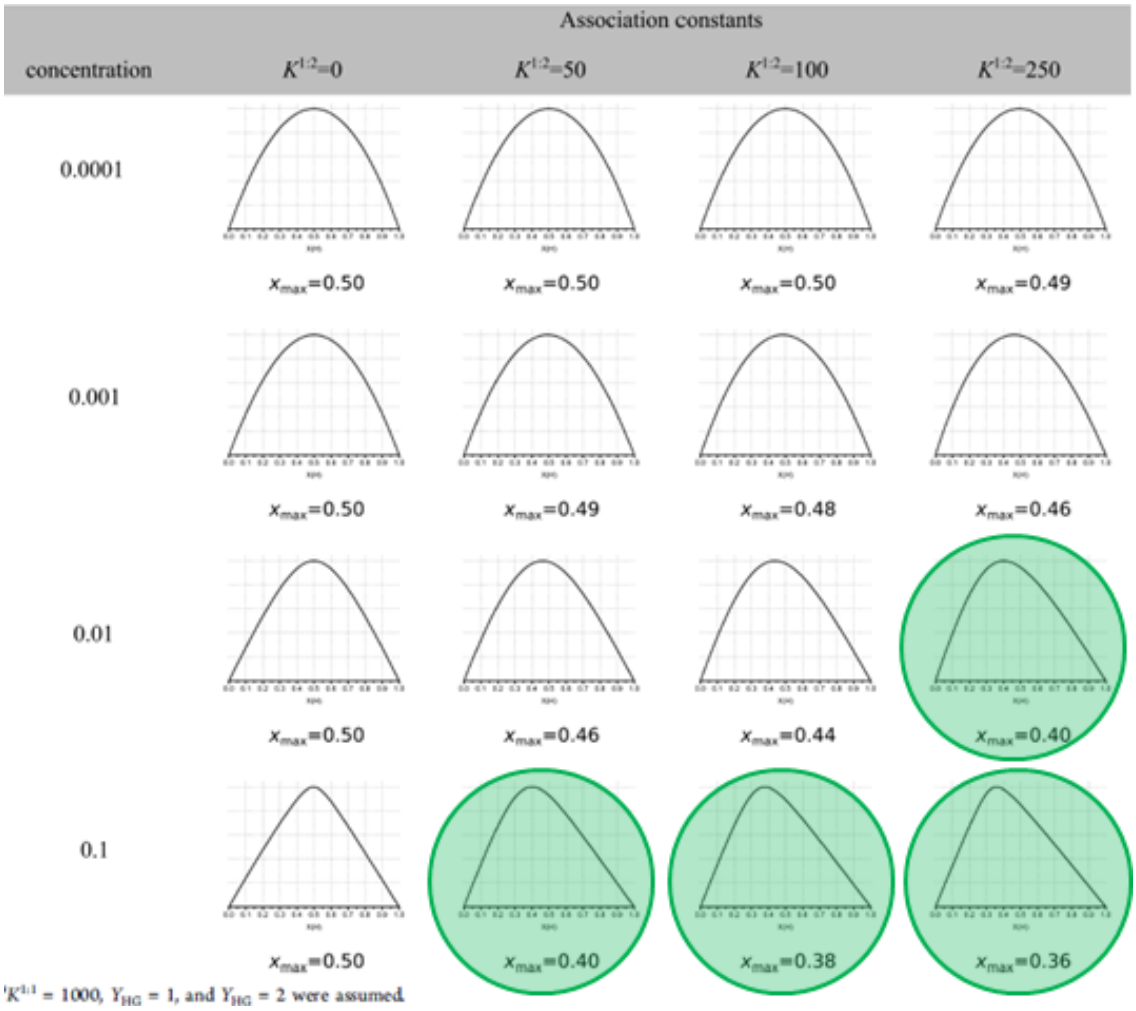

Figure 1.5: Job's plot simulations showing the effect of concentration and association constant on the shape of the Job's plot obtained.

At low concentrations, the maxima observed is at $x = 0.5$, regardless of the $K_{a\ 1:2}$ value. Increasing the concentration leads to the shifting of the observed maxima, but the effect of this can only be seen when the $K_{a\ 1:2} = K_{a\ 1:1}/20$. They further demonstrated that the observable monitored, Y, for the free host, HG and HG_2 complexes can have a drastic impact on the observed Job's plot. In four simulations (with $K^{1:1} = 1000$, $K^{1:2} = 250$ and $[H]_0 = 0.01$)- the observables were ($Y_{HG} = 1$; $Y_{HG2} = 1$), ($Y_{HG} = 1$; $Y_{HG2} = 0$), ($Y_{HG} = 0$; $Y_{HG2} = 1$) and

(Y_{HG} = 1; Y_{HG2} = −1)-.In the first of the simulations, the maxima occurred at x = 0.5, and not the 'true' 1:2 value of x = 0.33. the second simulation indicates that a H_2G complex is likely to be formed, without any being present in solution. The third has a maximum at x = 0.29, the midpoint between the expected value for a HG_2 and HG_3 complex. Finally, the opposite signs of the observable lead to a wave-like Job's plot containing both a minimum and maximum, neither of which indicated the correct stoichiometry of the HG_2 complex, Figure 1.6.

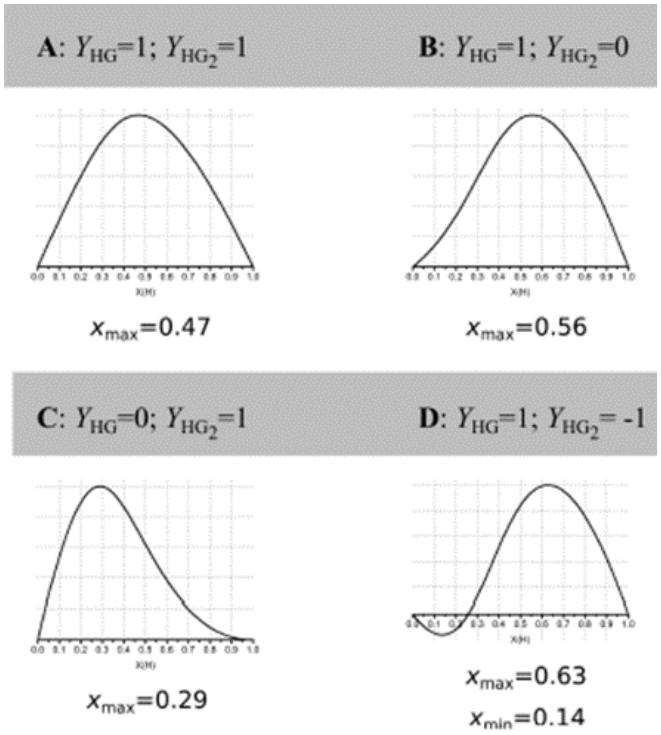

Figure 1.6: Effect of the sign of the observable being monitored, *Y*, on the shape of the Job's plot.

These results suggested that even if the formation of the 'desired' HG_2 complex is preferential and the concentration of both the reactants is high, then the observables, Y_{HG} and Y_{HG2}, can combine to give deceptive results and so consequently Job's plots, although not entirely without merit, require some care when interpreting the results.

Hibbert and Thordarson echoed this sentiment in their 2016 paper[35] and in turn aimed to shift the focus to more reliable methods that utilise non-linear regression methods, in order to best fit the data to a suitable binding model and obtain an association constant and stoichiometry of the complex. There are inherent problems associated with oversimplifying the equations that underpin the calculation of K_a and the effect this can have on accurately determining stoichiometry. Typical simplification plots employed include the Benesi-Hildebrand, the Scatchard and Hanse-Woolf. At one time, these linear transformations

would have been more powerful and useful, however, as computing power has increased, more complex mathematical models can be employed, and these simplified methods often do not give an accurate representation and the reliance on such models should be phased out. There are two main reasons why these linear methods are problematic, the first of which is that they misrepresent the experimental error and consequently infringe on the fundamental assumptions made during the linear regression and secondly, they often make broad assumptions, such as a large excess of guest or that the complex is fully formed at the end of the titration, which are often not the case and can break down, skewing the obtained results.[32] As a starting point is best to assume a simple 1:1 binding mode and gather evidence that either supports or contradicts this hypothesis. Aside from the Job's plot, there are a number of different methods that can be used to gain insight into the binding stoichiometry including:

1. *Comparing stability constants determined from a range of different methods.*
2. *Consistency between the host and the host-guest structure.*
3. *Experimental evidence, such as isosbestic points.*
4. *Increasing the concentration of the reactants leads to no change in the obtained stability constant.*

Of the aforementioned methods, 2) is the most simple and effective as it is now common practice to include crystallographic and 2D-NMR data when presenting supramolecular complexation. This coupled with the advent of molecular modelling allows for the visualisation of both the receptor host and the host-guest complex. Method 3) is perhaps the most utilised. The combination of altering the concentration and implementing a second alternative technique e.g., NMR followed by UV-Vis spectroscopy, and observing consistent results, is seen as good evidence for the correct model being employed.[32] An alternative to the Job's plot is the mole ratio method. This method is relatively simple to produce and is similar to the Job's plot, but instead of keeping the total molar concentration of both the host and guest constant (Job's plot), the molar concentration of one reactant- the host- is kept constant as the concentration of the guest is varied. Once plotted, a break point is then identified. It is at this point- the part of the graph with the most distinct change in gradient- that usually corresponds to the stoichiometry of the complex, Figure 1.7.

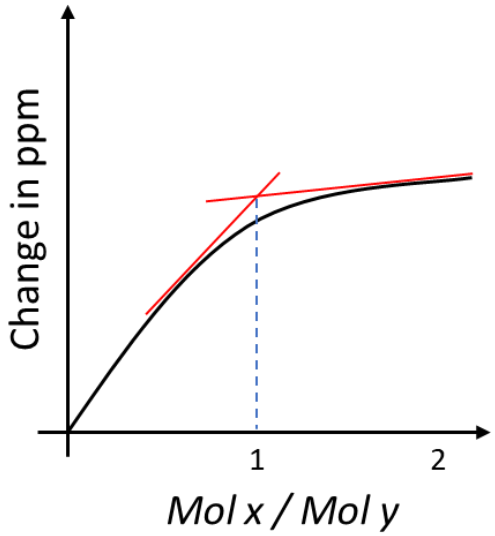

Figure 1.7: Simplified example of the mole ratio method for determination of complex stoichiometry. Break point shown demonstrates 1:1 complex formation.

1.5 Developments in Anion Receptors for Phosphate species

As previously stated, an important part of anion recognition has been the development of suitable biologically relevant mimics that can be used to better understand enzymatic binding pathways and lead to the design of better drugs; of particular interest in this context is phosphate binding protein (PBP). PBP is a member of a class of proteins that are produced by the cell in response to a lack of essential nutrients. This class contains such proteins with specificity for inorganic phosphate, amino acids and sulfate. PBP's role is to scavenge inorganic phosphate and deliver it to a membrane protein for transport into the cytoplasm.[36] In 2007, Katayev et al. synthesized a receptor, **1.9**, that functions as a PBP mimic. They showed that in the solid state, the receptor-anion complex— **1.9**$H_2^+ \cdot HPO_4^{2-}$ —bore structural similarities to the PBP binding site.[37] Receptor **1.9** was an expanded macrocycle based on previous work within the group- receptor **1.10**- that contains the same building blocks bonded through imine linkages. The use of imines adds extra H-bond donor sites which are also susceptible to protonation. At physiological pH, inorganic phosphate exists in a number of different protonated forms, and it was thought that by incorporating imines into the structure, these different protonated forms could be bound by the receptor. Their structural analysis into the binding mode of the **1.9**$H_2^+ \cdot HPO_4^{2-}$ complex and PBP showed that the average H-bond distance interactions were extremely similar in both the natural and synthetic models, with the bond angles being constrained in the synthetic model due to the rotational restriction of the macrocyclic structure. Unlike PBP, **1.9** showed some promiscuity

for the hydrogensulfate anion, HSO_4^-, because of the two positively charged residues which bind indiscriminately, these anions are confined within a H-bonding network that was shown to be similar. One more H-bond is formed between **1.9** and $H_2PO_4^-$ due to the orientation of the oxo-anion- however the binding affinities of the two anions were altered in acetonitrile solution, allowing for the discrimination of the two species.

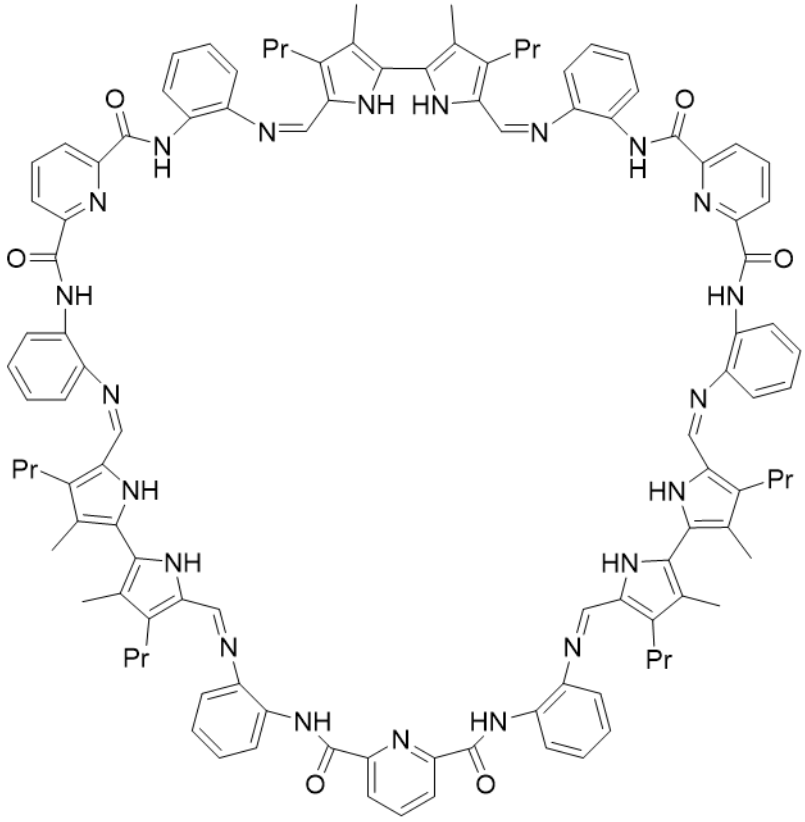

1.9

The binding affinity was determined in the solution state in acetonitrile through UV-Vis titrations of the tetrabutylammonium (TBA) salts of the anions at 296 K, with the neutral, free-base forms of the receptor. The neutral form of **1.9** was used to avoid issues that may arise from counterion effects and incomplete protonation. **1.9** was shown to have three absorption maxima that decreased in intensity with increasing wavelength. When 1 equiv. of $H_2PO_4^-$ was added, the solution turned from yellow to red, but upon subsequent addition of anion, the solution reverts to the original yellow colour. This change was determined to be the result of more than one stoichiometric equivalent of anion binding to the receptor. This was further confirmed through Job plot analysis, which showed receptor **1.9** bound dihydrogenphosphate with a 1:3 (receptor: anion) stoichiometry. The similarity in the UV-Vis spectra for **1.9** when binding both $H_2PO_4^-$ and HSO_4^- was ascribed to the change in receptor geometry when binding to the anion, creating a tight H-bonding network, as seen

in the solid state. The determined binding affinity for **1.9** and dihydrogenphosphate was determined to be log K_a = 6.74(6), 5.98(9) and 4.11(6) for the stepwise 1:1,
1:2 and 1:3 addition, respectively. The conformational change observed upon the addition of 1.0 equiv. of anion mirrors the change in conformation of PBP. This structural and functional similarity could be used to further understand anion recognition in natural systems.[38] Binding constants, in their various forms- K_a and logK_a – are the primary method for determining the effectiveness of which one species binds to another, in this case a receptor binding an anion target. The binding constant value is a measure of the equilibrium between the association and dissociation of the two species, with a large K_a /logK_a indicating a strong association between the receptor-anion and as such the equilibrium lies in the forward direction. Values for the association constant for receptors and anions can be calculated from a number of different techniques such as ^{1}H NMR, UV-Vis and fluorescence spectroscopic titrations and can be done by measuring the observed changes seen when the concentration of guest (anion) species is increased, and the receptor concentration remains the same. Fitting of these changes to a suitable binding model such as 1:1, 1:2 etc., gives a linear relationship, the gradient of which is the calculated association constant.

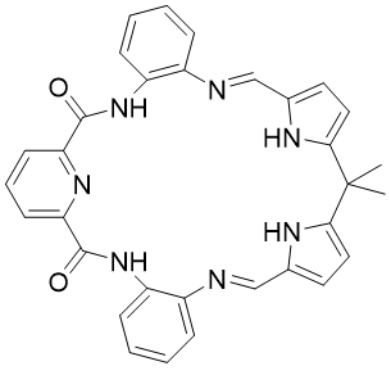

1.10

In 2017, Unguisin A, **1.11**, a cyclic heptapeptide from the marine fungus species *Emericella unguis*, was being investigated for potential antibacterial activity.[39] Being comprised primarily from D-amino acids with a γ-aminobutyric acid (GABA) residue, it was thought that this predetermined macrocyclic structure with multiple H-donor sites, along with the flexible GABA moiety, would function efficiently as an anion receptor. Selectivity of the receptor depends on the size of the binding cleft and the ability for it to sufficiently accommodate the anion- as previously stated, the GABA residue allows for flexibility and hence improved anion affinity.

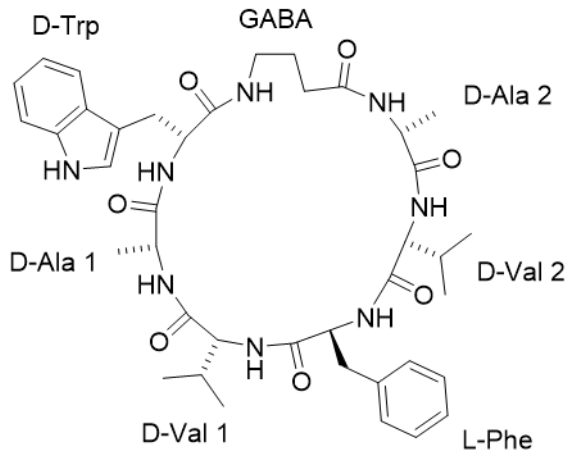

1.11

Proton NMR titration investigations, where up to 50 equivalents of a range of anions in a competitive d_6-acetone/d_6-DMSO (9:1) solvent system were added, showed the promiscuity of the binding cleft, but also the importance of the anion size. Smaller halides caused noticeable changes to the observed chemical shifts, but no such shifts were observed when large I^- was added, indicting the size limitation of **1.11**. Oxo-anions with a range of geometries, such as $H_2PO_4^-$, AcO^-, HCO_3^{2-} and $HP_2O_7^{3-}$, all showed some interaction with **1.11**, further emphasizing the conformational flexibility of **1.11**. Focussing on the phosphate anions, $H_2PO_4^-$ and $HP_2O_7^{3-}$, the binding stoichiometry, e.g., 1:1, 1:2 etc, of the **6**.anion complex could not be determined, however Ariawan et al. determined that due to the presence of a sigmoidal binding isotherm, a positive interaction was observed. The presence of such behaviour indicates a degree of positive cooperative binding whereby an allosteric effect is observed. The binding of the anion at one H-bonding site, leads to an increased binding affinity at a different site. This leads to a rapid increase in the formation of receptor-anion complex, with a very small change in the concentration of anion. Furthermore, ^{1}H-NMR analysis of the addition of anion showed a slow-exchange process occurring. The combination of both these results suggested that **1.11** and both phosphate species had a strong affinity. The NH signals of the receptor showed that when less than 0.1 eq. of anion was added significant broadening occurred. Addition of further anion- < 2.0 eq. caused the disappearance of the signal entirely. This observation can likely be explained by a proton transfer reaction occurring, between either the NH groups and the anion or bound and free anion. The occurrence of proton transfer is one possibility for shape of the sigmoidal isotherm as electrostatic interactions are also involved in the anion binding. Phosphorus NMR spectroscopy competition experiments, employed to determine which phosphate species has the higher affinity, showed that when **1.11** was added to a 1:1 mix of $H_2PO_4^{2-}$ and $HP_2O_7^{3-}$ in d_6-acetone/d_6-DMSO (9:1), below 0.5 eq, only the signals for $H_2PO_4^-$ were

shifted upfield, whilst at higher receptor equivalents (1.0-2.5 equiv.) only $HP_2O_7^{3-}$ signals were shifted and $H_2PO_4^-$ signals returned to normal. Therefore, at low receptor concentration a complex of **1.11**·H_2PO_4 is preferentially formed and $HP_2O_7^{3-}$ is bound as the receptor concentration increases. This may be the result of size versus. charge competition, where at lower concentrations the smaller dihydrogenphosphate anion is preferentially bound. As the concentration of pyrophosphate, with its tribasic charge, is increased, it outcompetes the monobasic, smaller phosphate species.

A broad range of heterocyclic scaffolds have been used as the core for a range of H-bonding anion receptors. Indoles are one such scaffold that finds itself within nature in a variety of proteins and enzymes. Gale et al. created a range of 2,7- amide or urea functionalised indoles, **1.12**-**1.14**, that showed binding activity with a range of anions.[40]The presence of both the amide and urea moieties allow for a large degree of rotation and consequently the receptors can adopt two planar conformations where either the NH groups angle into the cleft with carbonyl groups pointing out, or vice versa. In order to maximise binding, it is likely that during binding the NH-groups point inwards- repulsion between the NH-groups would likely ensure that this is geometry is not favoured for the free receptor. Binding constants were determined through ^{1}H-NMR spectroscopic titrations in a d_6-DMSO/0.5% H_2O mixture with the anions acetate, benzoate, dihydrogenphosphate and chloride.

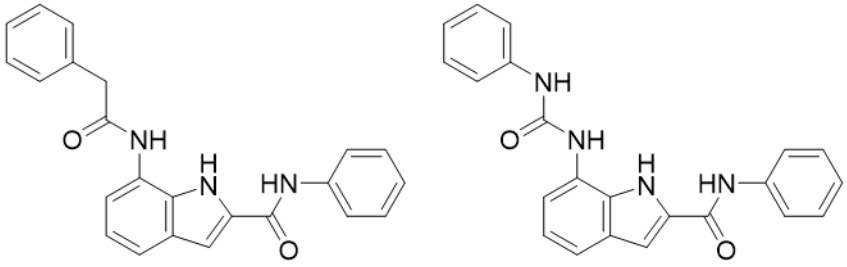

1.12

1.13

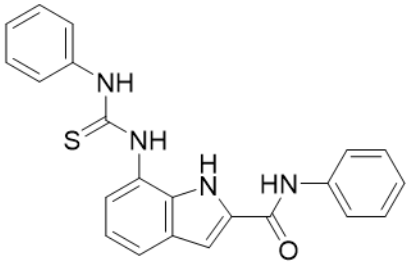

1.14

It was seen that each of the receptors, **1.12**-**1.14**, showed varying degrees of affinity for the anions tested, but all of them bound the anions in order of their basicity: $Cl^- < C_6H_5CO_2^- < H_2PO_4^- < CH_3CO_2^-$. The largest affinity, at 298 K, was observed for receptor **1.13**: 2-amide,

7-urea, followed by the thiourea, K_a = 4950 and 1600 M^{-1}, respectively. The bisamide showed relatively weak binding in comparison to the urea-based receptors with an association constant, K_a, of only 390 M^{-1}. Replacing the urea group with a more acidic thiourea, **1.14**, effectively reduced the calculated binding constant. This was ascribed to the '*syn-syn*' geometry adopted upon anion complexation, whereby steric interactions between the larger S-atom and CH-groups of the phenyl rings cause a destabilising effect. Subsequently, it was shown that all three receptors utilized all the NH-groups available suggesting that the receptor-anion complex formed through three H-bonds.

Building upon the work of the 2,7-disubstituted indoles, **1.12**-**1.14**, a series of substituted 1,3-diindolylureas, **1.15** and **1.16**, were designed.[41] The amide moiety was shown to only weakly bind to anions, whereas the indole and urea moieties were shown to have a strong affinity. On this basis, by removing a weakly binding amide group and replacing with a second indole, the affinities for anions could be improved.

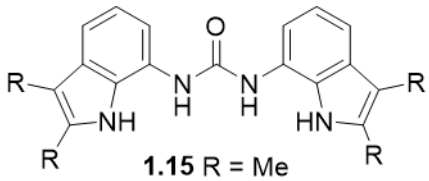

1.15 R = Me
1.16 R= H

Proton NMR titrations at 298 K in d_6-DMSO/H_2O mixtures were used to follow the shift in NH-resonances. K_a values calculated for **1.15** in a d_6-DMSO/0.5% H_2O mix showed a high affinity for the oxo-anions tested─ $C_6H_5CO_2^-$, $H_2PO_4^-$, $CH_3CO_2^-$ ─ with values >10^4 M^{-1}. Chloride was shown to only very weakly bind. The binding trend observed continued in a more polar solvent mixture containing 10% H_2O, where the greatest K_a, 4790 M^{-1}, was observed for $H_2PO_4^-$. Increasing the polarity further still, up to 25% H_2O/d_6-DMSO caused precipitation and no K_a was determined.

The same trend was observed with **1.16**- oxo-anions showed the largest affinity for the receptor, with $H_2PO_4^-$ once again showing the largest K_a, 5170 M^{-1}, in a 10% H_2O mixture. Complexes of **1.16**·$H_2PO_4^-$ were more soluble in a 25% H_2O mixture and allowed for a binding constant of 160 M^{-1} to be obtained.

In addition, both receptors were tested for their ability to bind bicarbonate, HCO_3^-, and showed comparable binding constants to that of the tested carboxylates, roughly 600 M^{-1}, however the use of a different counterion, tetraethylammonium vs. tetrabutylammonium, meant the results could not directly be compared. Solid state analysis of **1.15**, showed that a deprotonation event had occurred, and that the anion was bound as CO_3^{2-} to two receptor molecules (with tetraethylammonium counterions), through a network of eight H-bonds.

Figure 1.8. In similar fashion, crystallisation of **1.16** in d_6-DMSO/25% H_2O with excess $H_2PO_4^-$, yielded a fully deprotonated anion-receptor complex.

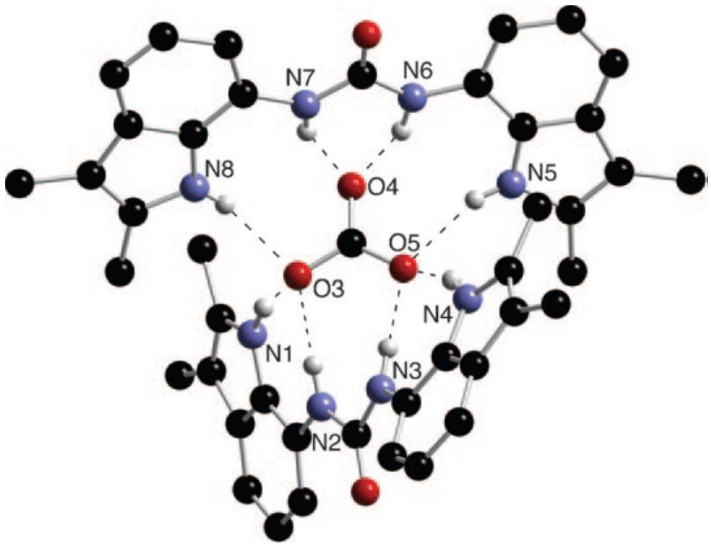

Figure 1.8: X-ray crystal structure of the complex of TEA·HCO_3 and **1.15**. [41]

Within the binding cleft, PO_4^{3-} was found to be complexed by three receptor molecules through twelve H-bonds, in which each receptor binds to three O-atoms. This was demonstrated to be the first example of a fully deprotonated urea-phosphate complex. The formation of twelve H-bonds is postulated to be the optimal coordination number for the binding of monoprotonated phosphate in biological systems as PBP itself forms twelve H-bonds- eleven H-bonds from the protein and the one H-bond from the anion. The diindolylurea based receptors were shown to have a high affinity for $H_2PO_4^-$ with the ability to form multiple H-bonds without filling the coordination sphere of the anion, allowing multiple receptors to coordinate simultaneously, which may account for the deprotonation observed in the solid state.

Deprotonation events, like those observed with **1.15** and **1.16**, have been shown to interfere with the complexation process. Basic anions, such as fluoride and dihydrogenphosphate, can abstract a proton from H-bond donor receptors. As seen with receptors **1.15** and **1.16**, HCO_3^{2-} and $H_2PO_4^-$ were deprotonated during the crystallisation process as a result of multiple receptors coordinating each anion, respectively, and causing sufficient lowering of the pK_a. In solution, it was demonstrated that a 1:1 binding stoichiometry was observed. Gale et al. further modified their diindolylurea receptors in order to maximise the number of H-bond donor sites, receptors **1.17** and **1.18**, with the aim of observing the deprotonation events in solution.[42]

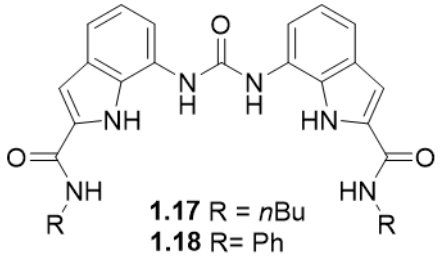

1.17 R = *n*Bu
1.18 R= Ph

Binding constants were determined through ^{1}H-NMR spectroscopy titrations at 298 K in d_6-DMSO with 0.5% or 10% water and by following shifts in NH-urea and indole-C**6**-H resonances. Receptors **1.17** and **1.18** were shown to bind strongly to oxo-anions, with calculated K_a values in excess of $>10^4$ M^{-1} for **1.17** for BzO^-, AcO^- and HCO_3^-. Binding models employed to fit the binding stoichiometry for **1.17** and $H_2PO_4^-$ were complex and showed characteristics of a deprotonation event. This was seen through both fast and slow exchange processes in the NMR. Slow NMR processes in 0.5% H_2O mixes exhibited shifts in the NH-amide resonance and above 1.0 eq. $H_2PO_4^-$ added, new downfield peaks emerged. It was postulated that at low concentrations of added anion, a 1:1 receptor-anion complex is rapidly formed and as the concentration of anion increases, a 2:1 anion-receptor complex is formed which is slow on the NMR timescale. However, the new peaks were shifted downfield by a considerable amount- 2 ppm in one instance – making it more likely that deprotonation had occurred. The presence of six H-bond donor sites in **1.17**, made it more likely that the pK_a of a bound $H_2PO_4^-$ species could be effectively lowered so that proton transfer could occur between the more basic free anion in solution. Consequently, the bound monohydrogen, double negative charged anion would interact stronger with the receptor. In order to confirm the formation of the monohydrogen HPO_4^{2-} complex, tetrabutylammonium hydroxide, up to 1.4 eq., was titrated into a solution of receptor and anion. It was seen that the new downfield shifts that had been previously observed increased in intensity, confirming that a deprotonated anion receptor complex had been formed. Control experiments in the absence of $H_2PO_4^-$, demonstrated that the new shifts observed were the result of the bound monohydrogen anion.

New peaks were not observed when $H_2PO_4^-$ was titrated into solutions of **1.18**, however this may be due to steric interactions that may destabilise the binding of the monohydrogen complex. Deprotonation may still have occurred as neither the NH-resonances' broadening, nor a binding isotherm could effectively be fitted, suggesting that the proton transfer equilibrium may have happened but is too fast on the NMR timescale.

The C_3 symmetric triptycene based receptor, **1.19**, designed by Granda et al. in 2015, aimed to improve upon the limitations of charged phosphate receptors with poor selectivity and neutral receptors that can only function in non-competitive media.[43] The functionalisation of a triptycene scaffold with pyrrole subunits was proposed to give structural rigidity while the addition of pyrrole adds NH H-bonding sites and the ability for further structural functionalisation.

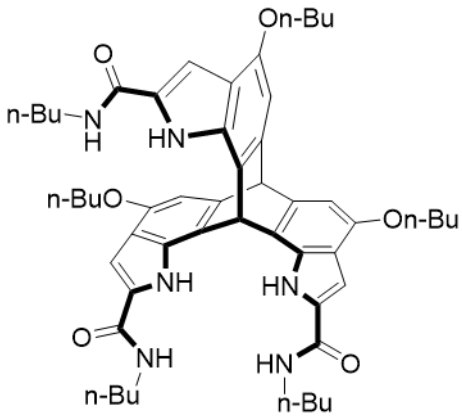

1.19

Binding studies of **1.19** were probed through ^{1}H-NMR titration experiments at 303 K in a competitive d_6-DMSO/0.5% H_2O mixture. On the NMR timescale, a slow exchange process was observed upon the addition of $H_2PO_4^-$, much like those observed with receptor **1.19**. Signals for the free receptor disappeared and new set of signals corresponding to a **1.19**·$H_2PO_4^-$ complex were seen. Continued addition of anion caused this 'new' set of signals to disappear and be replaced by more downfield signals ascribed to the deprotonation of the bound anion by more basic free anion in solution. Fluorescence quenching titrations were used to determine the binding affinity for **1.19** and $H_2PO_4^-$. At 430 nm- with excitation at 310 nm- the anion affinity, K_a, was shown to be 67608 M^{-1}, which showed that **1.19** had a very large affinity for dihydrogenphosphate.

The aforementioned receptors, **1.12**-**1.19**, all made use of the indole moiety as a binding motif and structural scaffold, however until 2006, little to no research into receptors that incorporated indoles had been conducted. One of the initial investigations into the suitability of the indole scaffold was done by Sessler et al. who synthesised the 2,3-diindol-3'-yl quinoxalines, **1.20** and **1.21**, which consisted of a quinoxaline core with β-connected indole moieties.[44] It was thought that the β-connections allow for a more flexible binding cavity and could accommodate larger anionic species.

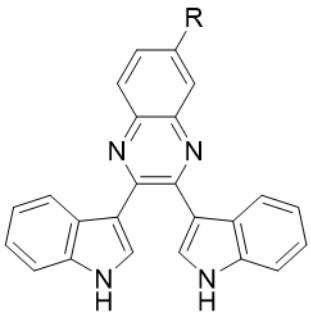

1.20 R= H
1.21 R= NO_2

Binding affinity was determined through UV-Vis titrations at 22°C in DCM and free **1.21** showed an absorption maximum at 434 nm, which showed a red-shift upon titration with $H_2PO_4^-$. Both receptors showed a highest affinity for dihydrogenphosphate, over the other anions tested - F^-, Cl^-, HSO_4^- and BzO^- - with K_a 6800 and 20000 M^{-1} for **1.20** and **1.21**, respectively. The large increase between these two values can be attributed to the presence of the electron-withdrawing nitro group, which subsequently increased the acidity of the binding cleft. Job's plots, in addition to solid state analysis, was used to determine a 1:1 binding stoichiometry. Interestingly, the addition of the $H_2PO_4^-$ caused a colour change from yellow to orange, meaning complexation could be followed by the naked eye.

Fluorescence detection is a simple and sensitive technique that has emerged as a method for following anion complexation. In 2005, Kondo et al., designed the tetraamide-based receptor, **1.22**, that had 2-pyridyl groups that acted as H-bond acceptors.[45] It was demonstrated that **1.22** showed selectivity for dihydrogenphosphate but contained no fluorophore group.

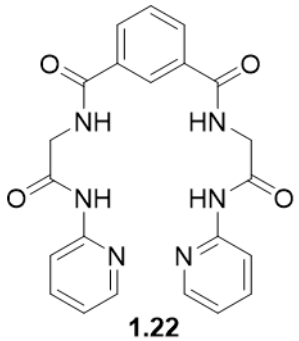

1.22

On this basis, receptors **1.23** and **1.24**, were designed that substituted the pyridyl units for the fluorophores 1-isoquinolyl and 2-quinolyl, respectively.[46]

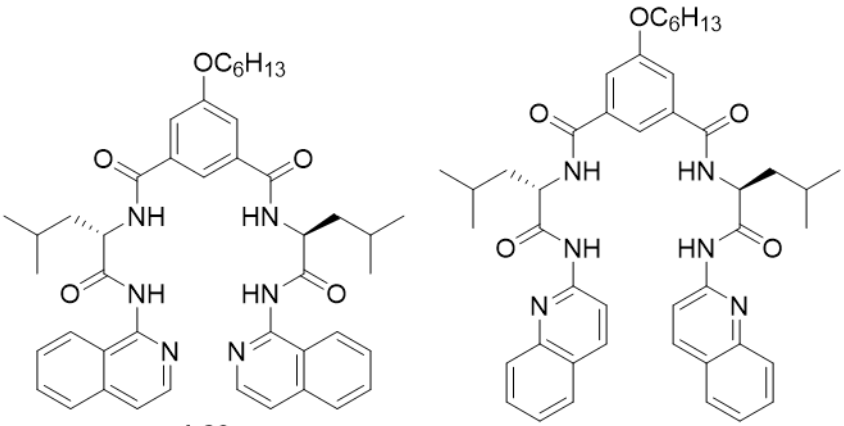

The pyridyl and related fluorophore capping groups provide additional H-bond acceptor sites to the hydroxyl group of the dihydrogenphosphate anion, and hence allow for improved discrimination against AcO^-. Anion binding constants for a range of anions- acetate, dihydrogenphosphate, sulfate, nitrate and halides – were determined through UV-Vis and fluorescence spectroscopy at 298 K. UV-Vis titrations of receptor **1.23** showed characteristic increases and decreases in the observed absorption through isobestic points. Receptor **1.24** showed similar behaviour but with much more pronounced changes in the observed peaks. Of the other anions tested, only AcO^- showed some affinity for **1.23**, whilst **1.24** showed affinity for $H_2PO_4^-$ almost exclusively. The presence of isobestic points in the UV-Vis spectrum suggested that a 1:1 receptor-anion complex was formed, which was further confirmed through Job's plot analysis. Binding constants, K_a, were determined from both UV-Vis and fluorescence measurements and showed high affinity for dihydrogenphosphate, with K_a, for **1.23,** $1.94 \pm 0.24 \times 10^6$ and $2.51 \pm 0.10 \times 10^6\ M^{-1}$, for UV-Vis and fluorescence, respectively, and $5.41 \pm 0.40 \times 10^6$ and $2.76 \pm 0.10 \times 10^6\ M^{-1}$ for **1.23**.

Both receptors showed strong fluorescence when excited at 332 nm and 318 nm for **1.23** and **1.24**, respectively. Gradual quenching was seen when both $H_2PO_4^-$ and AcO^- were titrated into **1.23**, however **1.24** showed almost complete quenching upon the addition of $H_2PO_4^-$ only, with little to no quenching recorded when titrated with other anions. The high selectivity of the receptors for dihydrogenphosphate over acetate, was thought to arise from the quinolyl and isoquinolyl motifs, which act as H-bond acceptors. Hydrogen bonds are formed between the hydroxyl groups of $H_2PO_4^-$ and the fluorophore moieties.

Electron-withdrawing groups, such as -NO_2, have been shown to increase the acidity of receptors and increase the affinity for negative anions. The addition of a positive charge, either through protonation or coordination of a transition metal has been shown to have the same effect. Plitt and co-workers built upon previous work for small fluoride anion recognition[47] by elongating the binding site to see if this caused a change in anion selectivity. 4,4'-dipyrrolyl-2,2'-bipyridine (DPB) based receptors, **1.25** and **1.26**, were synthesised.[48]

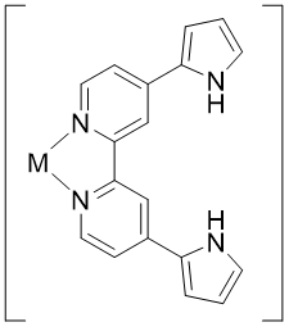

1.25 M= bpy_2Ru, *n*= 2
1.26 M= bpy_2Rh, *n*= 3

The larger bipyridine subunit that separated the pyrrole groups caused the selectivity of the receptors to change to that of the larger dihydrogenphosphate and benzoate. Much like other electron-withdrawing groups, the addition of the transition metal polarizes the binding site and improves the interaction with the negatively charged anions, whilst also acting as a conformational lock preventing rotation of the receptor. Proton NMR, UV-Vis and fluorescence spectroscopy at 22°C were used to probe the binding of various anions – F^-, Cl^-, Br^-, CN^- and $H_2PO_4^-$ - with Job's plots used to determine a 1:1 binding stoichiometry for **1.25**. Receptor **1.26** precipitated out of solution and as such stoichiometry could not be calculated. Elongation of the binding site was shown to dramatically improve the affinity of the receptor for oxo-anions. Proton NMR titrations of both **1.25** and **1.26** with millimolar amounts of $H_2PO_4^-$ caused precipitation. In order to calculate the binding affinity, K_a, fluorescence spectroscopy, with more dilute concentrations was performed. Receptor **1.25**, like other Ru^{2+} containing complexes, exhibited a red-orange emission, when excited at 464 nm, giving rise to an emission band of 630 nm. When titrated with $H_2PO_4^-$ this emission band was seen to decrease- an effect not seen when other anions were added. The observed results were ascribed to the formation of **1.25**·$H_2PO_4^-$ complex. A linear Beer-Lambert plot over the range tested further confirmed complexation and not aggregation caused the decrease in the emission band. Receptor **1.25** showed the highest affinity for $H_2PO_4^-$, with a K_a of 104,000 ± 18000 M^{-1}, which indicated a high degree of interaction between receptor and anion. In order to confirm the role of the pyrrole group in complexation, control experiments with a pyrrole free Ru^{2+} complex showed minimal spectral changes. This, in

addition to shifts in the observed ^{1}H-NMR NH-signals suggested that specific H-bond interactions were responsible for anion binding, rather than anion-cation interactions.

Proteins that bind phosphates often form ‘P-loops’; giant anion holes that are dominated by glycine, **1.27**, with other amino acids dispersed throughout.

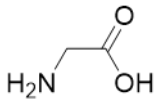

1.27

The glycine residues give structural flexibility and can lead to the formation of a cyclic binding pocket. Receptors **1.28** and **1.29**, both contain glycine residues and lead to either a tweezer-like or macrocyclic structure, respectively.[49]

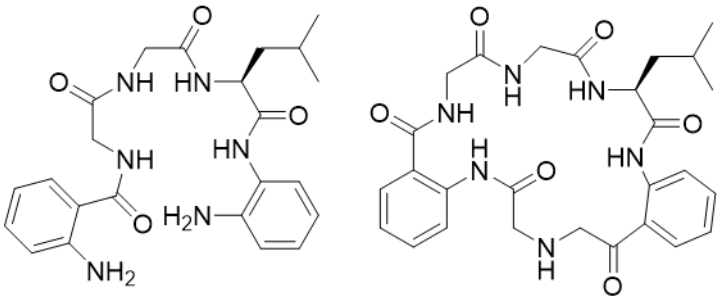

1.28 **1.29**

Receptor **1.28**, with two terminal amino groups, was expected to be able to bind all the tested tetrabutylammonium anion salts- Cl^{-}, CH_3COO^{-}, $H_2PO_4^{-}$ and HSO_4^{-}. It was shown that dihydrogenphosphate was bound in a 1:2 receptor-anion fashion. This was confirmed through Job’s plot analysis, whereby 1:1 curve fitting was too weak, and NMR spectroscopy. Binding affinity, *log* K_a for $H_2PO_4^{-}$ was determined to be 8.98 in d_3-acetonitrile by NMR at 25°C, which was in general agreement with those calculated by UV-Vis and fluorescence- *log* K_a 7.85 ± 0.01 and 7.95 ± 0.03, respectively. Fluorescence titrations with anions caused a hypsochromic shift in the observed emission band. This was thought to be the result of the formation of an H-bond between the anion and the anthranilic moiety of the receptor.

Like **1.28**, receptor **1.29** bound two dihydrogenphosphate anions in a stepwise manner, however the combined *log* K_a values, from the combined UV-Vis data at 25°C, was (10.51 ± 0.14) for dihydrogenphosphate were much larger than the other anions tested, implying selectivity as a result of the macrocyclic structure. Interestingly, both receptors **1.28** and **1.29** possess a cavity that is too small to accommodate the observed two anion binding. Three modes for this observation were postulated whereby firstly, $H_2PO_4^{-}$ dimerises in the

presence of receptor. Secondly, deprotonation of the protic anion and subsequent protonation of the amine group(s), leading to the binding of second anion through electrostatic interactions and finally, the two terminal amine groups, orientated in opposite direction, Figure 1.9, allowed for the coordination of the anion from either side.

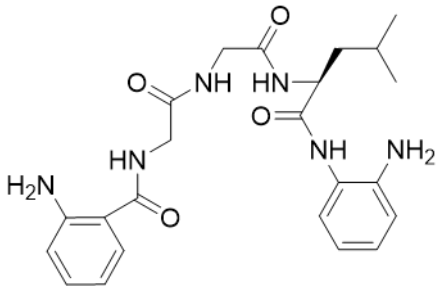

Figure 1.9: Orientation of **1.28** to allow binding of the anion from either side.

In order to determine the method of anion binding, UV-Vis spectra were compared to a solution of protonated receptor with a non-binding species, perchloric acid. The spectra indicated that the addition of dihydrogenphosphate did not cause protonation of the receptor, this was further confirmed through NMR analysis. Therefore, a hypothesis was proposed that that if only one anion was sequestered within the cavity, the total number bound would be two-one in the cavity and one electrostatically, and if the cavity could accommodate two species, then the total number bound would be three. By fitting of the UV-Vis data to appropriate models, it was determined that three $H_2PO_4^-$ were bound.

In addition to the quantitative determination of anion binding by spectroscopic techniques like UV-Vis and NMR, it has also been demonstrated that the binding of anions, such as $H_2PO_4^-$, can be assessed visually through the use of a colorimetric sensor. Pandian et al. developed a set of anthracene-based receptors, **1.30** and **1.31**, that contained acylhydrazone groups that showed affinity for the dihydrogenphosphate anion.[50]

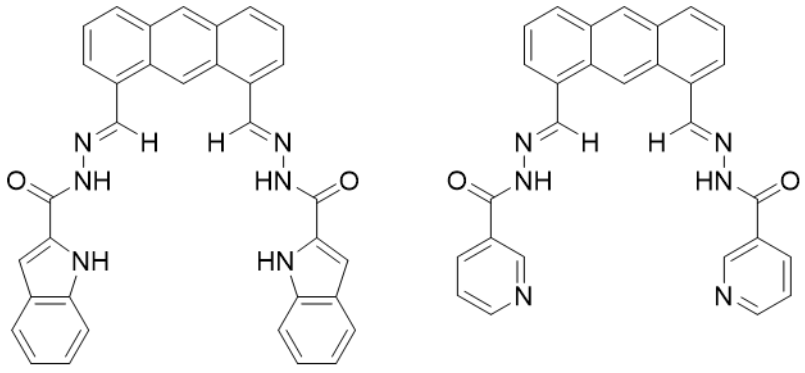

1.30 **1.31**

Both **1.30** and **1.31** contain the same two H-bonding groups: the imine NH, part of the hydrazone, and the NH of the amide. In addition to this, receptor contains **1.30** contains a terminal indole group which can form an additional H-bond to an anion. The terminal pyridyl group of **1.31** can form no such bond to an anion. In order to determine the affinity of the receptors for $H_2PO_4^-$, binding studies were conducted at 298 K in DMSO by titration of the tetrabutylammonium salt and monitored by UV-Vis spectroscopy. Upon the addition of anion to a solution of receptor, characteristic increases and decreases in absorbance through isosbestic points was observed. The presence of isobestic points and subsequent ^{1}H NMR analysis indicated the formation of a H-bonding receptor-anion complex. Receptor **1.31** exhibited broadening and the downfield shift of the binding NH protons, and this was proposed to be the result of the slow binding equilibria upon the addition of anion. Job's plot analysis of the NMR data showed a 1:1 binding stoichiometry with a K_a of 3.3×10^4 and 3.2×10^4 M^{-1} determined from UV-Vis and NMR spectroscopies, respectively. Tetrabutylammonium hydroxide was added in order to probe whether deprotonation of the receptor occurred. Upon addition with hydroxide anions, the receptor solution was seen to change from orange to green, a phenomenon that did not occur upon the addition of $H_2PO_4^-$. Interestingly, UV-Vis and ^{1}H NMR investigation into the binding affinity of **1.31** showed that the receptor had a similar affinity for $H_2PO_4^-$, despite containing one less H-bond donating group: K_a determined to be 3.5×10^4 and 3.6×10^4 M^{-1}, by UV-Vis and NMR spectroscopies, respectively. Modelling calculations undertaken showed that the pyridyl moiety could act as a H-bond acceptor group, further emphasising the directionality of H-bonding systems.

A further example of a colorimetric sensor was demonstrated by Jennings and Son, who designed a chromophore into receptor **1.32**, in order to allow for the naked-eye detection of anion binding.[51] The inclusion of electron-withdrawing groups, such as the included terminal nitro phenyl, which also acts as the chromophore, and the more acidic thiourea (compared to urea), increases the acidity of the receptor and increases the strength of the H-bonding interaction.

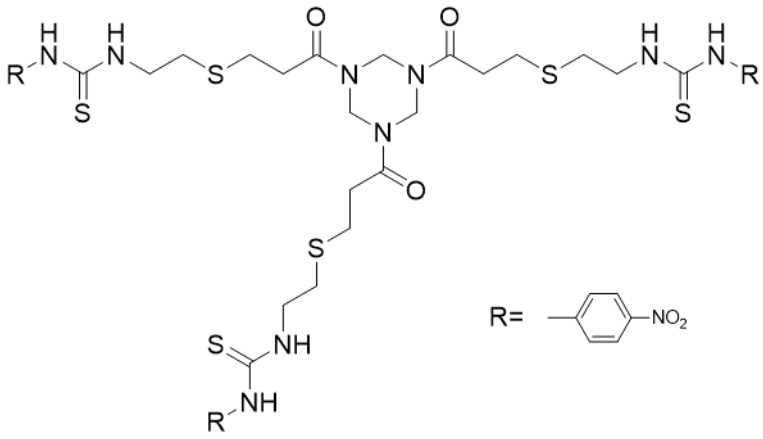

1.32

Receptor **1.32** was synthesised using 1,3,5-triacryloylhexahydro-1,3,5-triazine, which has been shown to be highly reactive in thiol-alkene reactions for the formation of thioethers. The tripodal nature of the core molecule was also determined to be integral to the preorganised structure of the receptor and made **1.32** ideal for the binding of non-spherical anions such as AcO^- and $H_2PO_4^-$, through the reduction of binding disorder. The planar nature of the ring ensured that the binding arms extended on the same side of the ring and caused no overlap. Stoichiometric studies were conducted in d_6-DMSO a using Job's plots and showed a 1:2 receptor-anion stoichiometry upon the addition of non-spherical anions. This showed that not all arms were involved in the H-bonding reaction and was further confirmed upon the addition of the spherical chloride anion, which showed a 1:1 stoichiometry. This was determined to be the result of the large terminal nitrophenyl groups. Affinity constants were determined through both UV-Vis and ^{1}H NMR titrations of the tetrabutylammonium salt and led to slightly different results being obtained. UV-Vis titrations indicated a *log* K_a, for the 1:2 complex with $H_2PO_4^-$, of 6.45. The addition of $H_2PO_4^-$ to the receptor solution caused a shift in the observed absorbances as well a colour change from yellow to orange. This indicated that a H-bonding reaction had occurred. When the *log* K_a was determined through NMR titrations, a drop to 5.62, for the 1:2 complex was obtained. The NMR data obtained showed the signature downfield shift of peaks upon the addition of anion, and as the concentration of anion added increased, the integration of the binding resonances was seen to decrease; this was determined to be the likely result of a deprotonation event occurring. It is this deprotonation that is the likely cause for the difference in calculated affinity values. In the NMR experiments, the concentration of receptor is higher and the propensity for self-complexation is increased and leads to less anion being bound. As a consequence, the affinity for the anion was seen to drop. The much

lower concentrations employed in UV-Vis experiments mean that receptor-receptor complexes were much less likely to form.

Calix[4]arenes have been used extensively in the design of receptors and have been shown to be capable of binding both metal cations and anions. Calix[4]arenes are cyclic oligomers containing four phenol units that are bridged by methylene, CH_2, groups.[52] In 2019, Namor and co-workers designed calix[4]arene derivative based receptors, **1.33** and **1.34**, for the effective removal of fluoride and dihydrogenphosphate from acetonitrile.[53]

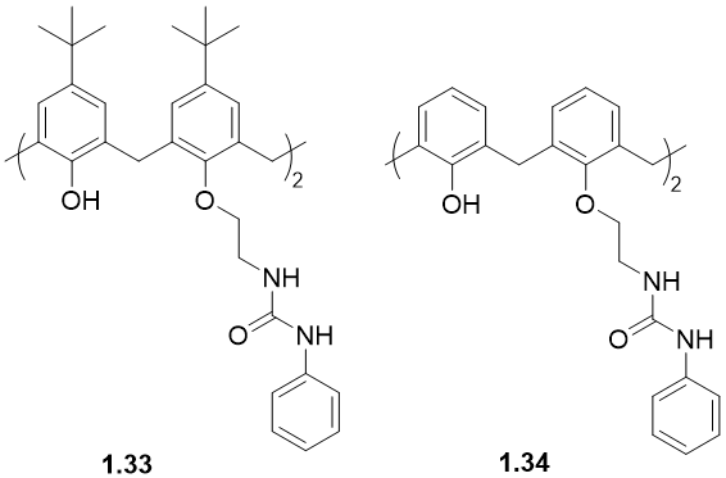

1.33 **1.34**

Proton NMR spectroscopic titrations at 298 K of both receptors with $H_2PO_4^-$ and F^- as their tetrabutylammonium salts in d_3-MeCN showed H-bonding interactions. The observed resonances for both receptors, were seen to shift downfield upon the addition of both anions, however a much more pronounced effect was seen with dihydrogenphosphate. With receptor **1.33** no significant change was observed until 1.0 equivalent of anion was added, at which point a downfield shift was observed that continued until the addition of 2.0 equivalents. The change in proton chemical shift was plotted against $[H_2PO_4^-]$/[28] and was shown to be sigmoidal in nature, with a large increase in the shift centring on 1.0 equivalent. In contrast, upon addition of fluoride anion, a hyperbolic curve is obtained indicating no such cooperative behaviour. This indicated that the receptor had a greater affinity for dihydrogenphosphate over fluoride, which showed no further sequestration after 1.0 equivalent added. Solvent studies performed with CD_3CN showed that the solvent could effectively interact with the receptor by integration into the hydrophobic cavity and cause an allosteric effect, decreasing the binding of the desired anion, as the solvent can better pre-organise. This effect was demonstrated by receptor **1.34**, which does not contain the *tert*-butyl group in the *para* position, which means the receptor -OH proton is more susceptible to solvent interactions. These receptors were designed with the goal of extraction of anion,

however receptor **1.33** was insoluble in water and so extraction studies were done in the solid state. These studies showed that the percentage of anion able to be extracted increases with an increase in receptor and that the removal capacity for dihydrogenphosphate was double that compared to fluoride. This directly correlated with the previously obtained results which showed that receptor-anion complexes were 1:2 and 1:1, for dihydrogenphosphate and fluoride, respectively. These results also suggested that the binding conformation did not change upon changing from solution to the solid state.

Ertul and co-workers also developed a set of H-bonding receptors that relied on the preorganised structure of calixarenes and made use of their relative ease of functionalisation.[52] In their work, they synthesised receptors **1.35** and **1.36**, which both contained two arms with an amide group, which would function as a hydrogen bond donor group, terminated with either 2- or 3-pyridyl, **1.35** or **1.36**, respectively.

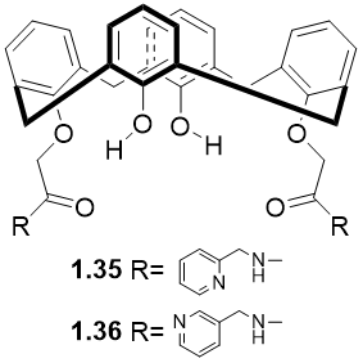

The use of pyridine functionalised calixarenes had not been reported yet at this point. Their studies into the efficacy of the binding of the receptor to phosphate anions- added as disodium hydrogenphosphate- was performed through extraction experiments at different pH values at 25°C. Control experiments demonstrated that no extraction was observed in aqueous solutions of hydrogenphosphate at any pH in the absence of receptor. At the pH levels used, the receptor amine is protonated and can interact strongly with the highly basic $H_2PO_4^-$, this favoured the extraction of the receptor-anion complex into DCM. This binding behaviour can be further tuned through the addition of sodium hydroxide to the organic layer. When base was added, it was determined that the deprotonated receptor species was no longer an effective host for the anion and so the binding affinity can be switched 'off'. The highest extraction values observed for the receptors was determined to be 41% and 44%, for **1.35** and **1.36**, respectively, at pH 1.5. This result is not unexpected, and the extraction values were seen to decrease as pH increased and can be related to the effective protonation of the receptor required for the extraction out of water.

Further work utilising calix[4]arenes was done by Nehra and co-workers who synthesised the highly functionalised phenylenediamine-capped conjugate of calix[4]arene; 5,11,17,23-*tert*-butyl-25,37-bis-{[phenylenebis(azanediyl)]-bis(methylene)-bis-(*tert*-butyl-2-methyl)phenoltriazolylmethoxy}-26,28-dihydroxy-calix[4]arene, **1.37**.[54]

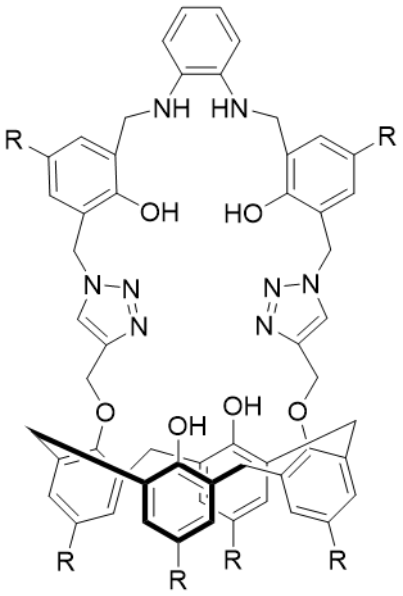

1.37 R= *t*-Bu

Prior to this, limited reports of reduced imine receptors with an affinity for dihydrogenphosphate had been reported. UV-Vis spectroscopy experiments with the free receptor exhibited an absorption band at 290 nm which upon titration with anions, as their tetrabutylammonium salts, led to the emergence of a new peak around 315-320 nm. This was attributed to intermolecular charge transfer between the anion and the amino group of the receptor. Fluorescence spectroscopy was used to determine the affinity of the receptor for a range of anions, such as halides, acetate and carbonate species in acetonitrile. Excitation of the receptor at 290 nm led to an emission band at 315 nm. When $H_2PO_4^-$ was added, this emission was seen to decrease with a concomitant emergence of a new emission at 425 nm. This emission was related to the formation of hydrogen bonding interaction between the dihydrogenphosphate and receptor. Of the other anions tested, only fluoride exhibited similar behaviour but to a much lesser extent. Additional experiments to determine binding stoichiometry and the affinity of the receptor for anion in a competitive MeCN/5% H_2O solution showed that a 1:1 complex was formed, and that the fluorescence band observed was shown to increase by roughly four times upon addition of $H_2PO_4^-$. The affinity constant was determined to be 6.18×10^4 M^{-1} by fluorescence. Subsequent ^1H NMR titrations of the tetrabutylammonium salts at 25°C agreed with the previously obtained fluorescence data and

demonstrated that the receptor showed the highest affinity for dihydrogenphosphate over the other anions tested. Downfield shifts in the salicylic and phenylene protons suggested that the binding of the anion occurred in the 'cap' region of the receptor- no such shifts in the calixarene and triazole protons were observed. This hypothesis was further confirmed through a 'cap-less' control receptor and its titration with $H_2PO_4^-$. This receptor showed no such downfield shifts and demonstrated the cap is the site of anion recognition. Interestingly, it was demonstrated that the fluorescence emission band observed could be turned on and off upon the addition of metal cations, such as Mg^{2+} and Zn^{2+}. This showed that the receptor could act as reversible sensor for the dihydrogenphosphate anion.

Amongst the large array of supramolecular structural scaffolds utilised in the synthesis of hydrogen bonding receptors, sapphyrins presented one of the earliest used. In 1996, Král et al. designed a set of protonated sapphyrins, **1.38** and **1.39**, that were tested for their ability to bind mono- and dibasic phosphate.[55]

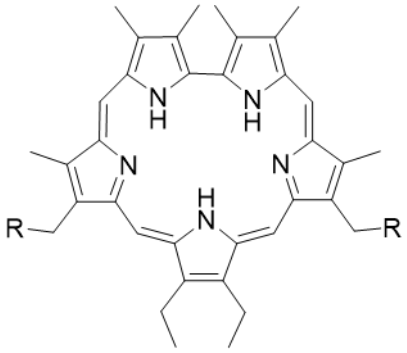

1.38 R= CH_2CH_2OH
1.39 R= CH_3

Sapphyrins are structurally related to porphyrins, containing five pyrrole units as opposed to four. This additional unit increases the number of π-system electrons to 22 and changes the characteristic colour from green, for a porphyrin, to purple. More importantly, the additional pyrrole unit increases the pore cavity size by 25%, meaning that when in its doubly protonated form, the molecule can remain planar, without the internal core being perturbed by interatomic forces such as Van der Waals forces and electrostatic interactions. Král and co-workers showed that both receptors could form complexes with a range of anionic phosphate species including, but not limited to, diphenyl phosphate and monobasic phenylphosphate, along with phosphoric acid. Investigations were undertaken to determine the nature of the binding and to calculate the affinity constant of the binding. Furthermore, the comparison of the interaction in the solution and solid phase was probed. In the latter case, it was shown that both receptors formed 1:1 complexes in solution and 1:2 (receptor:

anion) complexes in the solid state. Proton and ^{31}P-{^{1}H} NMR experiments, at room temperature, were used to determine relative binding constants and affinity of **1.38**. The hypothesis they proposed was that in both the NMR techniques used, a large upfield shift for sapphyrin would be seen when binding to a phosphate species. This was particularly evident in ^{31}P NMR for **1.38**, where in *d*$_4$-CD_3OD, upon the addition of phosphoric acid, upfield shifts of -7 ppm were observed. This upfield shift was further increased to -16 ppm when 2.0 equivalents of tetrabutylammonium dihydrogenphosphate was titrated into a solution of receptor in CD_2Cl_2, this was compared to an analogous porphyrin system which led to an upfield shift of only -0.20 ppm.

The aforementioned sapphyrin and calixarene complexes have relied on groups within the binding cleft of the receptor being susceptible to protonation. The protonation of such groups increases the acidity and strengthens the interaction of receptor with a basic anionic species. In 2015, Zapata and co-workers created a set of triazolium based receptors, **1.40**-**1.43**, which were tested for their ability to bind to a number of different anionic species, such as sulfate, halides, nitrates, and phosphates, all of which were added as their tetrabutylammonium salt, in order for the results to be compared.[16]

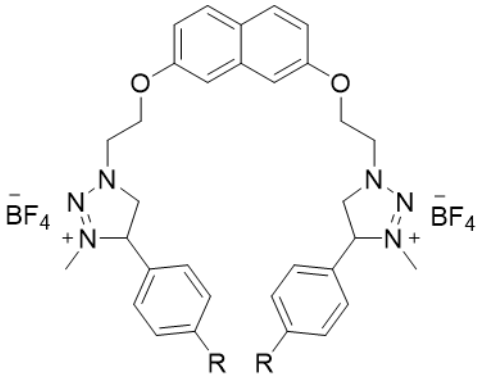

1.40 R= H
1.41 R= OCH_3
1.42 R= NO_2
1.43 R= Ferrocene

Heterocyclic rings, such as triazoles, have been shown to be susceptible to protonation and this can have a drastic effect on the binding ability of a receptor containing such a group. The electronegative N atoms polarise the C-H bond and create a large dipole. Through the generation of the triazolium moiety, Zapata and co-workers proposed that π-anion interactions could dominate and lead to an increase in the binding affinity for the tested anions. The aforementioned π-anion interactions usually arise as a result of an electron-withdrawing group increasing the acidity of an aromatic ring, however by protonating the

triazole Coulombic interactions between the charged ring and anion are much improved. The synthesised receptors were designed so as to include two different non-covalent interactions, H-bonding and electrostatic, with one ring differing from the other. Of the anions tested as their tetrabutylammonium salts, only the phosphate species, $HP_2O_7^{3-}$ and $H_2PO_4^-$, showed any discernible differences in the obtained ^1H NMR spectra at 20°C. The addition of dihydrogenphosphate to solutions of all the receptors led to similar downfield shifts observed in the triazolium C-H and inner naphthalene protons, with a concomitant upfield shift of the outer naphthalene and methylene protons. The largest observed change is with the downfield shifted protons of the triazolium and inner naphthalene indicating these protons are involved in the binding of the anion. Job's plot analysis demonstrated that a 1:2 receptor: anion complex was formed and following this the $K_{a\ 1:2}$ values were calculated as follows for each receptor, 703 ± 50, 926 ± 89, 755 ± 63 and 445 ± 31, for **1.40**-**1.43**, respectively. The symmetry of the signals observed the NMR and mapping models suggested that an '*in-in*' binding mode for dihydrogenphosphate is preferred, Figure 1.10.

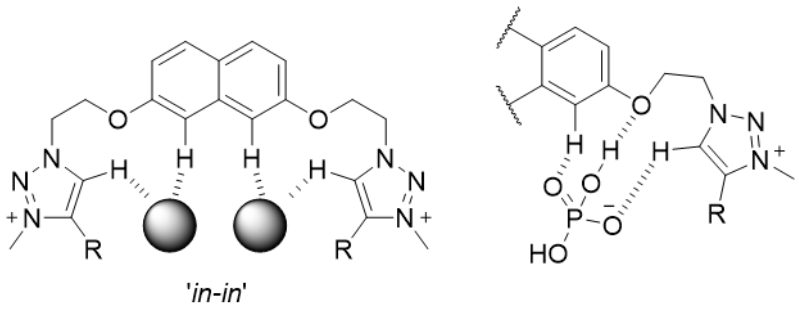

Figure 1.10: The 'in-in' binding mode of **1.40**-**1.43** for 2 anions, with the H-bonding groups shown.

Receptor **1.43** contained ferrocene as a terminal group, and as such, is electroactive. Voltametric experiments on the receptor in CH_3CN/CH_3OH solutions showed strong interaction with the electrode surface when anion was added. Experiments in CH_3OH and with dihydrogenphosphate anion showed no change, even when added in large excess.

As mentioned previously, preorganisation of the receptor and its binding site is integral in order to orientate and maximise the number of H-bonding sites with the binding cleft of a receptor. This preorganisation does not necessarily come as the result of a rigid supramolecular structure or cyclic group, such as indole or naphthalene but can be as a result of restricting the rotation of a molecule around a certain point, i.e., through the use of an alkene, thus reducing the free rotation of the molecule and decreasing the overall entropy of the system. The impact of this effect was demonstrated by Hubertus et al. who showed that the conformation around a double bond can have a large impact on the calculated affinity

constants.[56] In their work, they synthesised three structurally related receptors, **1.44**-**1.46**, which mimic PBP and spermine in their mode of interaction- through a series of electrostatic and H-bonding interactions.

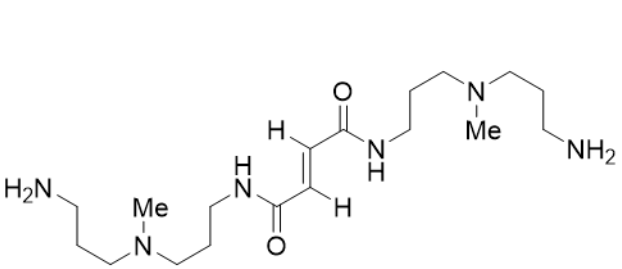

1.44- *trans*

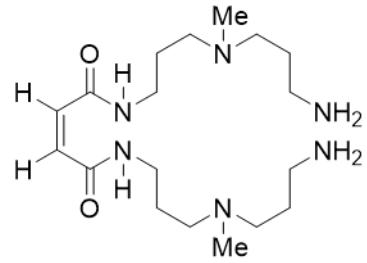

1.45- *cis*

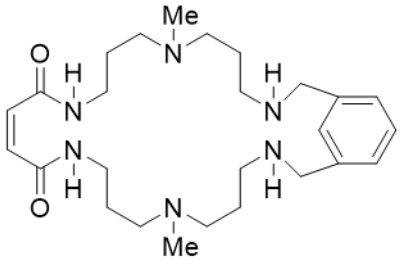

1.46

It can clearly be seen that receptors **1.44** and **1.45** differ in their geometry around the double bond, *trans* versus *cis*. The geometry of the double bond led to different NMR spectra, in both ^{1}H and ^{13}C-{^{1}H}, being obtained. The proton NMR spectrum of **1.44** had a singlet corresponding to both the protons as result of the C_2 centre of symmetry. In contrast, despite being chemically equivalent, **1.45** exhibited a doublet of doublets demonstrating the inequivalence of the protons of the alkene as result of the two hydrogens orientation around the double bond. This was further confirmed through the presence of multiple alkene and carbonyl carbon singlet signals in ^{13}C NMR. Binding affinities for the receptors were determined via two experimental methods. First, a fluorescent phosphate derivative, **1.47**, was used to visually probe the affinity of the synthesised receptors for phosphate, Figure 1.11.

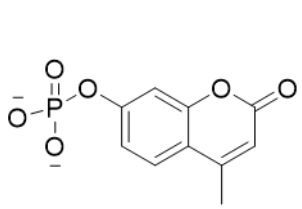

1.47

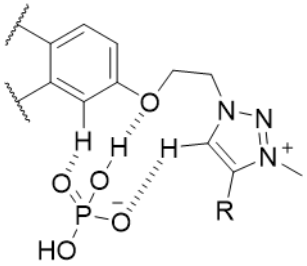

Figure 1.11: Proposed binding of **1.47** to receptor **1.45** and **1.46**.

Upon titration into solutions of receptors **1.45** and **1.46**, the fluorescence emission of the phosphate derivative was quenched, indicating formation of a receptor-anion complex for both. No such quenching was observed upon titration of the open chain *trans* receptor, **1.44**. Fitting of the obtained results to a 1:1 binding model allowed for the calculation of binding constants of *log K* for **1.45** and **1.46**, calculated as 5.15 and 5.30, respectively, at 20°C. Proton NMR investigations into the binding site of **1.45**, showed that there was no change in geometry around the double bond when in the presence of the anion. In addition to this, no shift in the amide proton resonances was observed implying that the amide group played a structural role, organising the structure, as opposed to coordinating to the anion. Further binding studies were performed using potentiometry. The protonation of the receptors was first investigated, and the constants calculated. A spermine, **1.4**, control was used to calibrate the system and the protonation constants calculated for **1.44** were as expected for a polyamine, *trans* alkene receptor, whereby there was only a small change observed upon the addition of subsequent protons. The pseudo-macrocycle, **1.45**, exhibited much more noticeable differences in the consecutive protonations reflecting the conformational rigidity as a result of the alkene and amide bond. The closure of the macrocyclic ring further lowered the observed *log* K_a values for the protonation, emphasising the effect of the increased charge in the small binding cleft. Following this, binding to inorganic phosphate, PO_4^{3-}, was probed and as was expected, the highest affinities for the anion were observed when the charge on the receptor was greatest, indicating a reliance on the Coulombic interactions in the binding cavity. The open-chain receptor, **1.44**, had a *log* K_a = 2.9-3.4 which was comparable to that of other open-chain receptors. Receptors **1.45** and **1.46** exhibited much higher affinity with *log* K_a values of 4.4-8.6 and 7.5-14.2, respectively, at 25°C. Competition experiments between inorganic PO_4^{3-} and organic phosphate, **1.47**, showed that the receptors had a higher affinity for inorganic phosphate over the organic. This was proposed to be as a consequence of the greater charge density and decreased steric repulsion of the significantly smaller molecule.

It can clearly be seen that a large number of hydrogen bonding anion receptors, in this case for phosphate species, have been described in the literature and that their efficacy and selectivity can vary greatly. As the understanding around receptor design and synthesis has improved, so too has the complexity. From **1.12** to **1.18**, the evolution from simple monoindolic receptors with a urea moiety and poorly coordinating amide group to the diindolylurea receptor that was demonstrated to deprotonate the anion in solution, something which had not previously been seen. Zapata and co-workers designed a series of receptors,

1.40-**1.43**, that contained not only H-bonding groups, but contained a charged region that has been shown to increase the acidity of receptors and increase the likelihood and strength of the interaction between host and anionic guest. Receptor design can utilise a large range of predetermined organic scaffolds such as triptycene, **1.19**, calix[4]arenes, **1.33** and **1.34** and sapphyrins, **1.38** and **1.39**. These scaffolds serve as starting building block which can be transformed to tune the affinity of a receptor for a specific target.

1.6 Capacitive Deionisation Systems

The basis of Capacitive Deionisation (CDI) was first described in the 1960's and saw extensive development into the 1970's. [57,58] The process of CDI has seen vast improvements in cell design and setup, which coupled with superior electrode materials, has led to CDI emerging as a promising technique for the desalination of brackish- water with a higher salinity than freshwater but less than sea water- bodies of water. Before looking at the developments of CDI systems, first the overall process and electrochemical theory behind this will be described. Focus on electrode materials and cell setups will not be described in detail.

The process of CDI is two-stage; purification and regeneration, and can be cycled a number of times, in order to improve the overall uptake of ions from a single input stream. A typical CDI system consists of at least a pair of porous carbon electrodes, to which a small potential difference, $\leq \pm 1$ V is applied. Brackish water can then be pumped across the electrodes and ions in the solution are attracted to their oppositely charged electrode, these ions are held electrostatically close to the electrode surface in the electrical double layer (Section 1.6.1). This is the process of purification (Figure 1.12a). Over time the electrodes become saturated, and no more ions can be removed from the stream. Reversal of the polarity across the electrodes, repels the held ions into a new stream and leads to the formation of a concentrated 'waste' stream. This is the regeneration step, Figure 1.12b. The obtained streams can then undergo further processing or can be disposed of, and a new waste stream can be introduced, starting the whole process again.

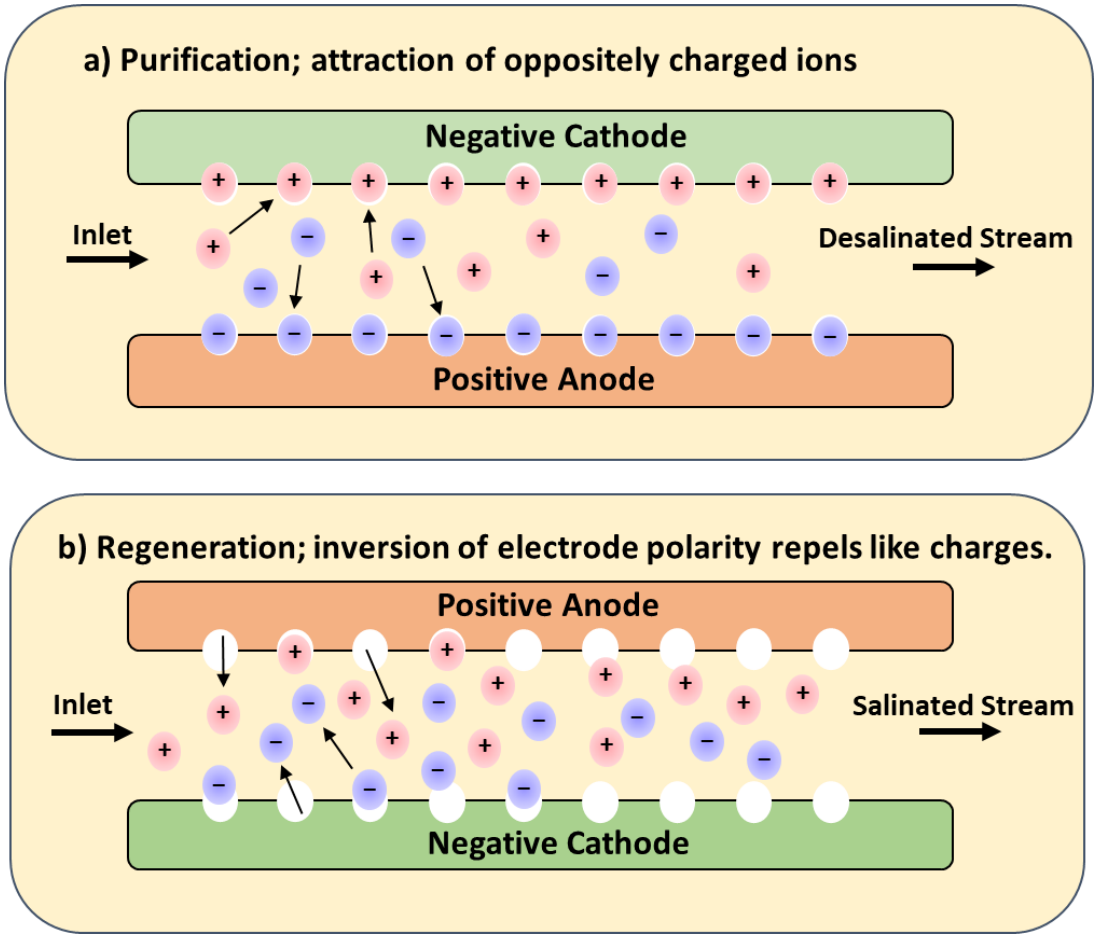

Figure 1.12: Two processes of a CDI system; a) Purification; b) Regeneration

The application of the potential is the driving force for the removal of ions from the salinated, stream. The application of this potential leads to the possibility of two mechanisms for the storage of ions in a CDI system:

1. Non-Faradaic ion storage: this is the primary mode of ion removal in CDI systems and relies on the aforementioned electric double layer formation on/in the porous carbon electrodes. Ions from the solution are held electrostatically within a diffuse double layer close to the electrode surface. In this process, there is a build-up of charge at the electrode surface as the attracted ions cannot leave and no redox reactions occur at the electrode interface. Importantly, there is no direct transfer of electrons from the electrode into the bulk solution and as such, no redox reactions occur.[59] As the primary mechanism of ion storage, significant developments in electrode materials in order to increase the internal surface area, selectivity and the pore distribution within is of great interest. Some examples of carbon-based electrodes employed within CDI include nanotubes, aerogels, graphene sponges and

microporous activated carbon.[60,61] Zuo et al. demonstrated how the synthesis of a polymer coated activated carbon electrode could be used to dramatically increase the removal of sulfate from solution.[62] Their work showed that the electrode could effectively discern between sulfate and other anions, even when present in large excess, such as chloride.

2. Faradaic ion-storage: although less common than non-Faradaic processes, Faradaic processes must still be considered when employing a CDI system. Although initially thought to enhance the process of ion removal, it has since been shown that these processes can have both positive and detrimental effects on the efficacy of a CDI cell, such as, the formation of unwanted by-products, change in the pH and change in electrode performance e.g., degradation or stability issues and overall lifespan.[63] In general, Faradaic reactions constitute the transfer of electrons from one bulk material to the other, in this case, electrode to electrolyte solution or vice versa, depending on the nature of the reaction in question. This is in direct contrast to the previously mentioned non-Faradaic process where no electron transfer occurs. In general, these can be broken down into three separate processes, **type I**, **type II,** and **type III.**
    - **Type I**: these are oxidative reactions occurring at the anode, with the most commonly observed being the oxidation of the carbon electrode itself, however the oxidation of chloride and water have been reported.[63] Landon and co-workers demonstrated that this oxidation of carbon can occur at potentials as low as 0.207 V, and so oxidation of the carbon electrode can occur at the potentials applied within a CDI system.[64] The oxidation of the electrode itself can lead to electrode degradation and blockage of the intra-electrode pores.
    - **Type II**: primarily made up of reduction reactions that take place at the cathode[63]. Like with type I reaction, this has been shown to have a potential lower than those typically employed in CDI systems, 0.815 V, for the reduction of oxygen.[64,65] Principally the reduction of oxygen, these reactions can include the reduction of metal cations, which can be electrodeposited on the electrode. However, He et al. demonstrated that these reductions could have a positive outcome.[66] In their work they showed that the reduction of oxygen could be used to generate H_2O_2 *in situ*, which could be used for water disinfection.

- **Type III**: these reactions can be viewed as 'pseudocapacitive' or intercalation type processes and as such, closely resemble the non-Faradaic processes. Reversible redox reactions at the electrode-electrolyte interface store the ions, rather than being found in the electric double layer[63]. One early example of such an intercalation system is the $Na_2Mn_5O_{10}$ nanorod electrode that was synthesised by Pasta and co-workers.[67,68] In their work, the synthesised electrode was shown to have a high affinity and selectivity for the intercalation of Na^+ over other metal cations, such as Mg^{2+} and Ca^{2+}.

1.6.1 Electric Double Layer

The polarisation of the electrode through the application of a potential generates the non-Faradaic process responsible for the removal of ions from the bulk electrolyte- the electric double layer. Under these conditions, oppositely charged ions, relative to the charge of the electrode, and dipoles are attracted and held close to the surface. At this interfacial region, <1 nm layer, a local potential is generated that differs from the bulk solution. A number of different models have been used to describe the double layer, and over time as understanding has improved, they have evolved in complexity. The following models will indicate a negative potential at the electrode; however, the same models can be applied if the potential was positive.

The first, most simple model was proposed by Helmholtz. In his model, the charge at the electrode surface was balanced by oppositely charged ions directly at the electrode surface (Figure 1.13a). Consequently, the local potential at the surface falls off rapidly as the distance from the electrode increases (Figure 1.13b).

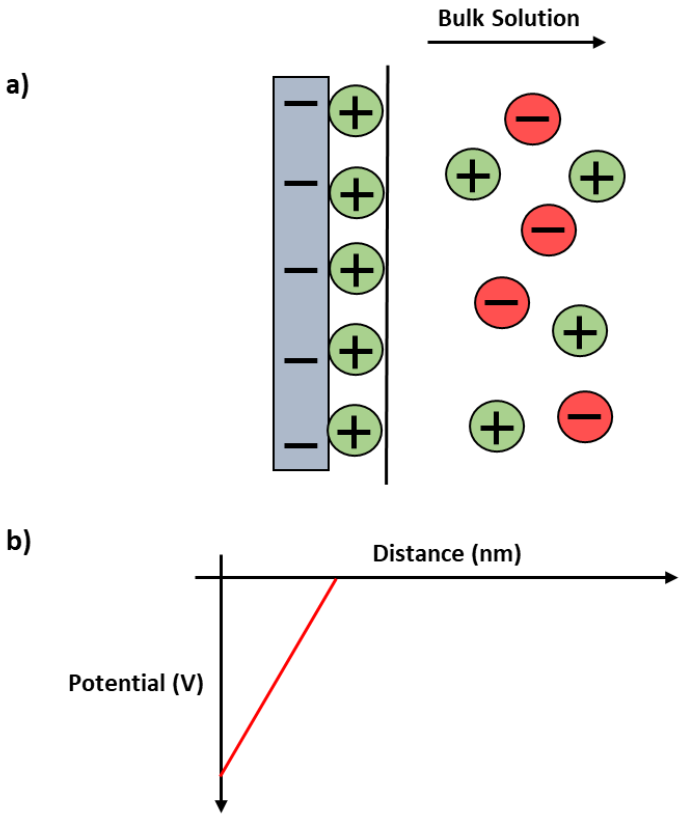

Figure 1.13: a) Helmholtz model of the double layer; b) local potential versus. distance plot for the Helmholtz model. [70]

Outside this layer, the solution behaves as the bulk material, having an equal mix of anions and cations, that are free to diffuse.

This diffusion behaviour led to the development of the second model, the Gouy-Chapman, which allows for the movement of the ionic species. In this model, the charge at the electrode surface is balanced by free moving ions in solution held close to the electrode surface, Figure 1.14a. Within this region, there are a large number of cations relative to anions. As the distance from the electrode is seen to increase, the balance between anion and cation reaches that of the bulk solution. This steady increase in interfacial distance leads to potential change that is steep close to the electrode surface with a decreasing gradient as the distance increases, Figure 1.14b.[69]

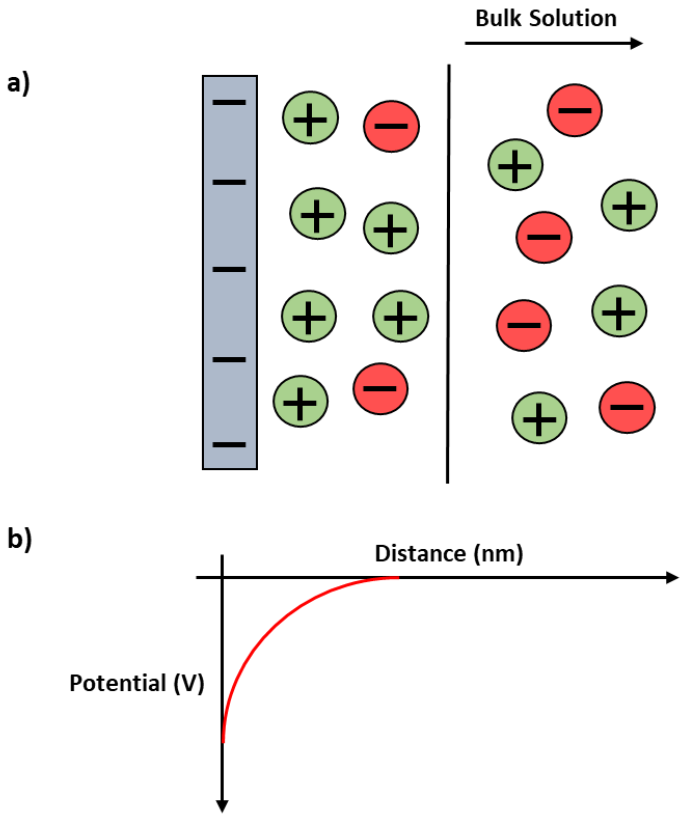

Figure 1.14: a) Gouy-Chapman model of the double layer; b) local potential versus. distance plot for the Gouy-Chapman model. [70]

The final model, the Gouy-Chapman-Stern model, is a combination of the two previous models. In this model, there is a tightly bound layer of cations at the surface, with a diffuse layer of cations and anions- cations once again in excess- bordering the electrode that follows into the bulk solution (Figure 1.15a). In this model, the potential will quickly fall off as distance increases away from the compact surface layer, before becoming more gradual in the diffuse layer and approach the bulk solution (Figure 1.15b).[69]

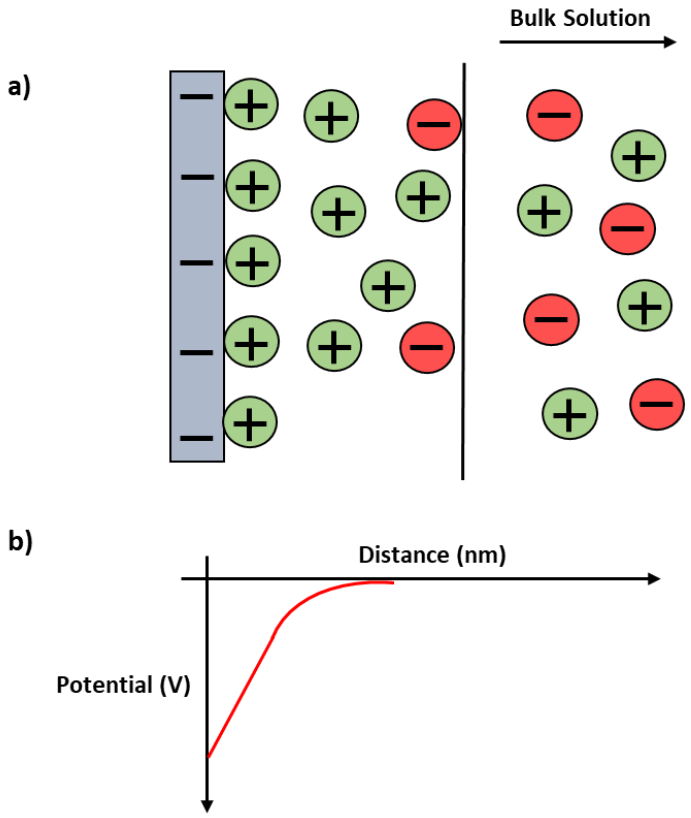

Figure 1.15: a) Gouy-Chapman-Stern model of the double layer; b) local potential versus. distance plot for the Gouy-Chapman-Stern model. [70]

There are a number of factors that should be considered when applying these models, the first of which is the effect of the solvent on the formed double layer. Cations especially, will be hydrated in aqueous solution and increase the distance of the cation from the surface. The second is the increased propensity for anion-electrode reactions to occur. It is likely that if this were to occur, the solvation shell of the anion would be fully removed and some covalent interaction with the electrode may happen. Finally, the dipolar nature of water means that it can interact with and adsorb to the electrode surface. Consequently, there is competition between ions and solvent for sites on the electrode, which can alter the charge distribution. As a result of this, a further updated model is shown in Figure 1.16, where each ionic species is considered as a result of the potential applied across the electrode. In particular, with regards to anions, the increased likelihood of bonding to the surface leads to the formation of two distinct planes of anions. Dehydrated anions, those bound tightly to the electrode surface, form the inner most layer and are found within the inner Helmholtz plane. Conversely, hydrated ions are found further away from the electrode surface and form the outer Helmholtz layer.[69,70]

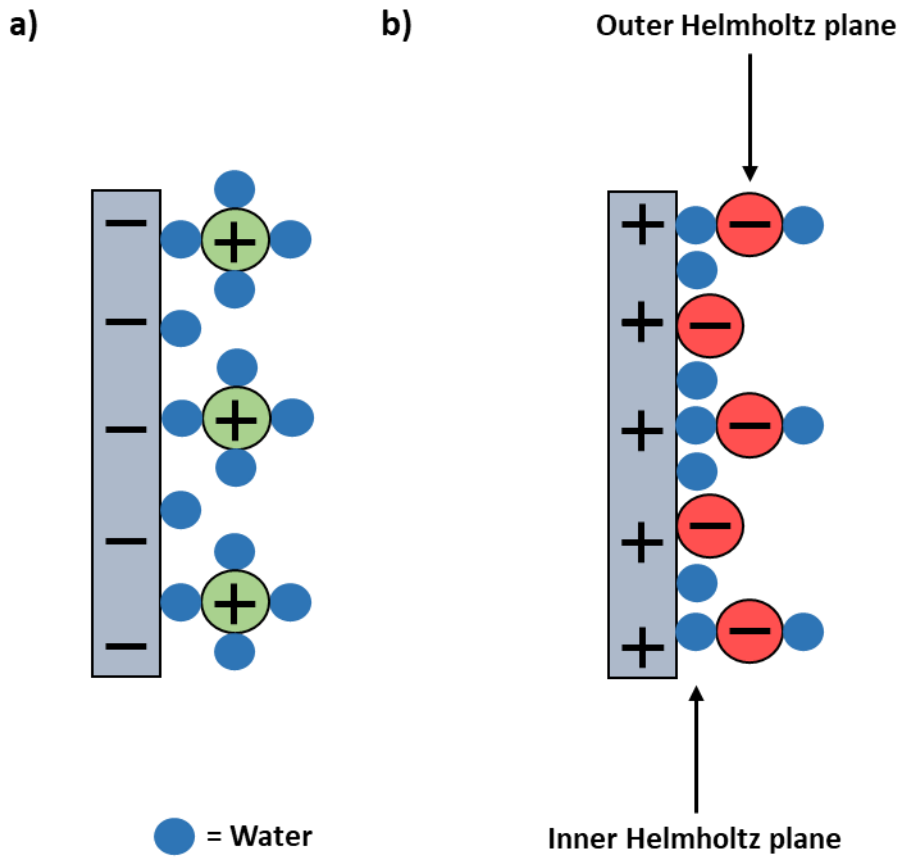

Figure 1.16: Compact double layer model a) at the cathode; b) at the anode. [70]

Consequently, the total capacitance, C, of this interface region, with regards to anions, is sum of the capacitance of the inner compact region, $C_{compact}$, and the more diffuse outer plane, $C_{diffuse}$. Overall, this can be seen in equation 1.1:

$$\frac{1}{C} = \frac{1}{C_{compact}} + \frac{1}{C_{diffuse}} \qquad Equation\ 1.1$$

The overall capacitance of the system will be governed by the smaller of the two capacitance terms: the compact layer on the surface of the electrode.[69] Therefore, increasing the porosity and surface area of electrodes in CDI systems has been of heavy interest in order to maximise the number of ionic species that can be found within this inner layer.

1.6.2 Developments in Capacitive Deionisation systems

Improvements to CDI systems are not just limited to the development of new electrode materials with significant advancement being made to adapting and optimising new cell architectures. A number of cell architectures have been described in the literature including membrane CDI (MCDI)[71] and inverted CDI (ICDI)[72] to name a few.[73,74] Membrane CDI is by far the most well studied and used CDI system and involves the use of ion-exchange membranes. These membranes, often polymeric in makeup, have charge carriers grafted to or embedded within their structure. These structures allow for the selective transport of oppositely charged counterions across the membrane, whilst simultaneously blocking the transport of ions of the same charge (co-ions).[75] The improvement of MCDI over standard flow-by CDI is the result of the movement of the co-ions and counterions. When the counterions are adsorbed into the electrodes pores, in order to balance the overall charge, co-ions are simultaneously desorbed. In a flow-by CDI cell, this desorption process reduces the overall amount of salt that can be removed from the feed stream. In a MCDI cell, as the co-ions are desorbed from the electrode, they become trapped in the layer between the membrane and electrode, Figure 1.17a.

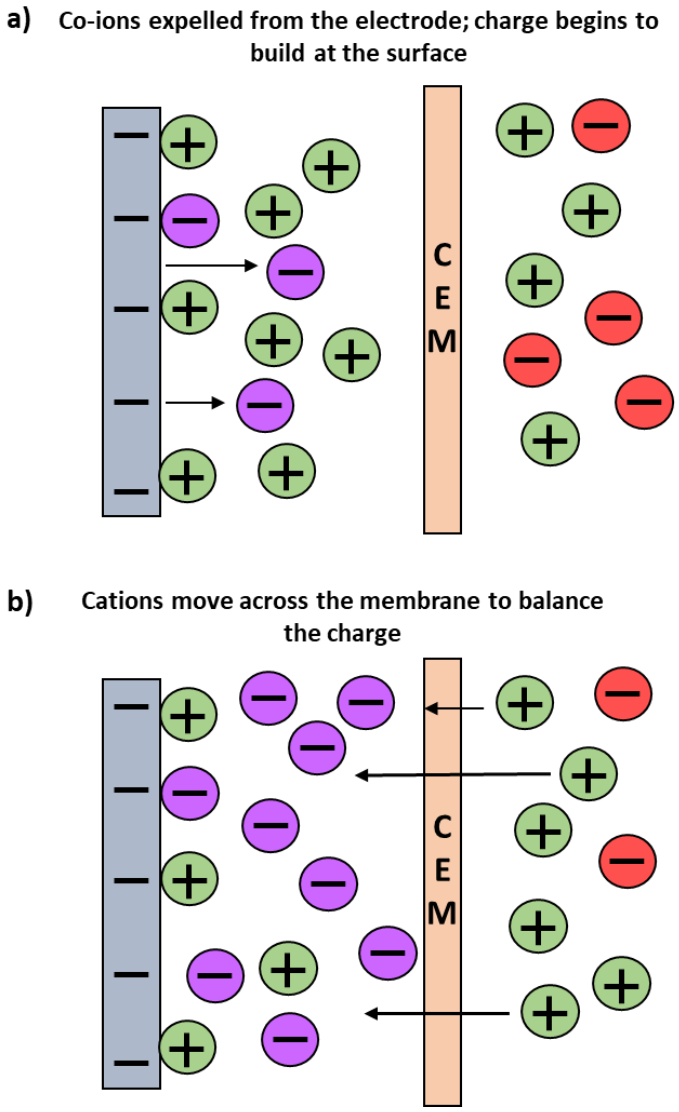

Figure 1.17: MCDI setup a) application of the initial potential and adsorption of cation counterions; b) build-up of co-ions in the interelectrode-membrane layer. CEM = Cation Exchange Membrane

Over time the concentration and subsequent charge within this layer build up and eventually exceeds the concentration of the feed stream itself. In order to balance this excess charge and concentration difference, more counterions are transported across the membrane, Figure 1.17b. Membrane CDI's ability to store and build-up ions within this space between the electrode and membrane means that more salt can be removed per cycle, relative to flow-by CDI alone.[71]

Another alternative cell architecture is ICDI. Gao et al. created an ICDI system with enhanced salt removal capacity through functionalisation of the electrode surface.[72] Inverted CDI systems follow the same electrochemical principles as membrane and flow-by CDI systems where ions are attracted to the electrode of opposite polarity. However, in a ICDI

system, the application of the potential is used to release the ions back into solution, Figure 1.18a, and conversely, the adsorption process occurs when no potential is applied (Figure 1.18b).

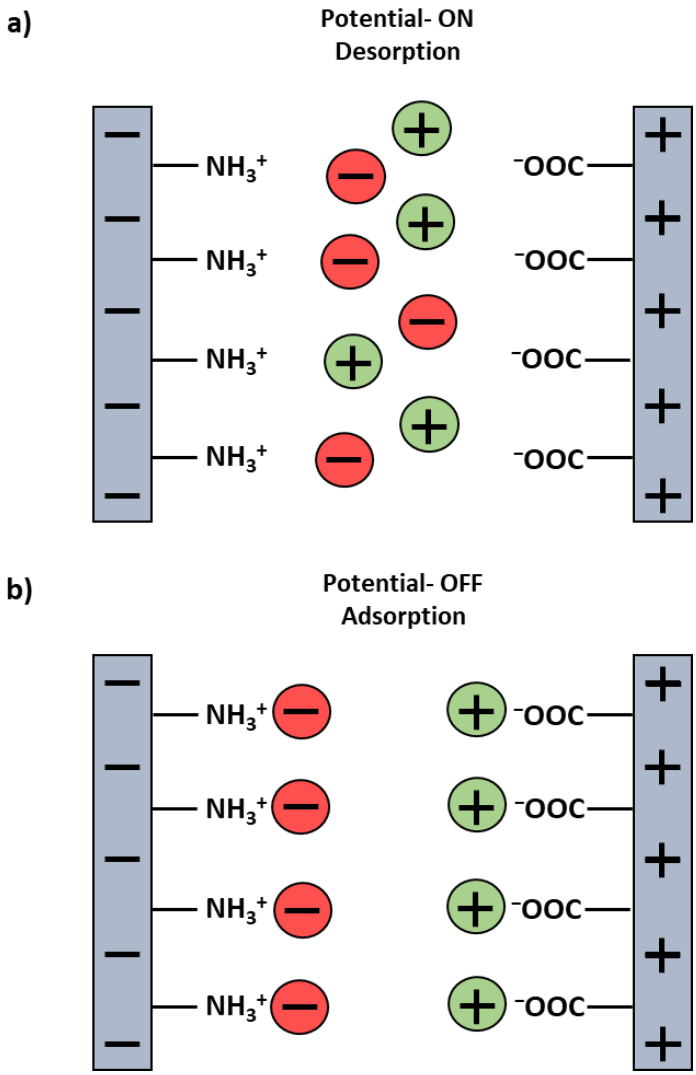

Figure 1.18: a) desorption of ions to charge the ICDI cell.; b) reduction of potential leading to the adsorption of ionic species at the anode and cathode.

Through repeated charge-discharge cycling, it has been shown that the adsorption capacity of the electrodes can decrease over time, and the voltage applied leads to the desorption of ionic species. This was attributed to the oxidation of carbon electrodes over a number of cycles and the subsequent repulsion of the like charges that build up on the oxidised anode surface. Gao and co-workers aimed to exploit this behaviour through the functionalisation of carbon electrodes with positively and negatively charged groups- amine/ammonium and carboxylate moieties, on the cathode and anode, respectively- in order to maximise the number of species that can be removed from the inlet stream, Figure 1.18. The working voltage window of an ICDI system depends on the difference between a property called the potential of zero charge, E_{pzc}, of both the anode and cathode.[72] This is the potential at which

the charge on the surface is zero and no ions are attracted to the surface.[69] In a ICDI system, this E_{pzc} window is the adsorption phase of the process and so having a larger window, with improved salt adsorption capacity is beneficial. A two-fold improvement to the working window can be made; first, by shifting the E_{pzc} of the anode to higher potentials, which has been demonstrated through the functionalisation of the electrode surface with carboxylate groups. A second improvement can be made by shifting the cathode to more negative potentials. This cathodic shift can arise from the treatment of carbon electrodes with gaseous ammonia or ammonia solutions, which can subsequently be protonated. Gao and co-workers' work was the first to successfully address the effect of the cathodic shift on the E_{pzc}. [59]

Commercial efforts to implement CDI systems in real-world situations began as early as 1999. Since then, CDI systems have been used for the removal of a number of different ionic species such as the removal of nitrate from drinking water in a Middle Eastern country. In this system, the average nitrate concentration was 155 mg L^{-1} and after processing using CDI processes, the concentration was reduced to less than 50 mg L^{-1}. Secondly, a CDI process implemented in a harbour water intake system, aimed to reduce calcium and chloride ion concentration to 40 and 60 mg L^{-1}, respectively. Following processing, the concentration of calcium ions was reduced from 55 mg L^{-1} to 5.4 mg L^{-1} and chloride concentration was reduced to 21 mg L^{-1} from 121 mg L^{-1}. Wastewater from a mine in Quebec, after a 4-stage CDI process, led to 90% of the effluent stream being recovered as clean water. Conductivity measurements of the treated water showed a decrease in the overall conductivity from 30 mS cm^{-1} to less than 3.2 mS cm^{-1}.[76]

1.7 Conclusions

The area of hydrogen-bonding receptors has been shown to be hugely varied with a great variation in structure and geometry. These variations lead to receptors with affinities for a number of difference species, in a range of solvents. In the context of this thesis, hydrogen-bonding receptors that have demonstrated a high selectivity for phosphate, in particular dihydrogenphosphate species, have been selected based on their ease of modification and synthesised accordingly, with the end goal of being suitable selective elements in a capacitive deionisation system. It has been shown that a number of organic scaffolds are suitable starting building blocks for functionalisation. Early investigations by Král et al. into sapphyrin based systems that could be protonated and as such improve their affinity for negatively charged anions.[14] Further advances and understanding of hydrogen bonding receptor and guest interactions and the effect of functionalisation lead to the first example of anion deprotonation in solution being observed.[41] Deprotonation in the solid state had previously been observed, but due to competition between the both the ionic guest and solvent molecules, deprotonation in the solution state had yet to be reported in the literature. This further emphasizes the importance and effect that functionalisation can have during complexation processes. The addition of highly electron withdrawing groups, such as -NO_2, can have a huge impact on the acidity of the receptor. This is evidenced by a large number of the aforementioned receptors exhibiting a higher affinity and preferentially binding the tested anions in order of their basicity. [40] Capacitive deionisation is a method that has been demonstrated to be suitable for the desalination of brackish and mid-to-low salt streams and has garnered increased interest in recent years as a result of improvements to electrode materials that are used. Work in this thesis focusses on the functionalisation of electrodes with a selective group or molecule, such as a suitable H-bonding receptor, that will add a selective element to the overall process and allow for the preferential removal of one species over any others in an inlet stream. With this in mind, a series of modified receptors have been synthesised by further functionalising previously reported compounds, with the intention of utilising these modified receptors in a capacitive deionisation system for the removal of both $H_2PO_4^-$ and HCO_3^-. The modifications made to the receptors was done so with the intent of maintaining the receptors selectivity and high affinity for the anion of interest, whilst simultaneously incorporating a labile group, such as a carboxylic acid, azide, or alkyne, that would allow for facile modification of an electrode surface.

Chapter 2 details the techniques used within this thesis, including both proton and carbon NMR, which was used to characterise the synthesised receptors as well as serving as a method for the determination of anion binding, and cyclic voltammetry which was used to electrochemically oxidise or reduce groups that were used to covalently attach the organic compounds to an electrode surface.

Chapter 3 focusses on the first of two H-bonding receptors that have affinity for the dihydrogenphosphate anion. This receptor is based on receptor previously synthesised by Gale et al. and contains two indole scaffolds joined by a central urea.[42] In order to attach to the electrode surface, this receptor was modified to initially include a carboxylic acid which was subsequently changed to alkyne group.

Chapter 4 shifts focus to a second anion of interest, bicarbonate, however the overriding H-bonding principles remain the same. Bicarbonate is the dissolved form of CO_2 and so it was proposed that the removal of bicarbonate could drive the removal of carbon dioxide from the atmosphere. The carbazole-based receptor synthesised is based on work by Hiscock et al.[77] and Sanchez et al.[78], this receptor was modified to contain free amine groups that can subsequently undergo a coupling reaction to a surface bound organic spacer molecule.

Chapter 5 is the second of the dihydrogenphosphate receptors and builds upon work by Kondo and Takai who synthesised a receptor based on the amino acid leucine. Installation of an alkyne on the central core molecule can be used to attach the receptor to the electrode surface directly, or failing that, can be used as a substrate in a 'Click' chemistry type reaction.

1.8 References

1 R. J. Phipps, G. L. Hamilton and F. D. Toste, *Nat Chem*, 2012, **4**, 603–614.

2 Y. Liu, Z. Zhao, R. Huo and Q. Liu, *Sci Rep*, , DOI:10.1038/s41598-018-36916-w.

3 S. H. Hewitt, R. Ali, R. Mailhot, C. R. Antonen, C. A. Dodson and S. J. Butler, *Chem Sci*, 2019, **10**, 5373–5381.

4 Y. Marcus, *Ions in Solution and Their Solvation*, John Wiley & Sons, Inc., 1st edn., 2015.

5 F. and A. O. of the United, *Food and Agriculture Organization of United Nations*, 2017, 38.

6 S. Mukherjee and R. D. Gupta, *J Toxicol*, 2020, **2020**, 1–16.

7 D. Lichosyt, P. Dydio and J. Jurczak, *Chemistry - A European Journal*, 2016, **22**, 17673–17680.

8 S. Y. Wang, Y. L. Lee, Y. H. Lai, J. J. W. Chen, W. L. Wu, J. M. P. Yuann, W. L. Su, S. M. Chuang and M. H. Hou, *PLoS One*, 2012, **7**, 1–12.

9 H. G. Wells, *J Am Med Assoc*, 1927, **88**, 484–485.

10 K. Igarashi and K. Kashiwagi, *International Journal of Biochemistry and Cell Biology*, 2010, **42**, 39–51.

11 L. D'Agostino, M. Di Pietro and A. Di Luccia, *FEBS Journal*, 2005, **272**, 3777–3787.

12 J. E. Rider, A. Hacker, C. A. Mackintosh, A. E. Pegg, P. M. Woster and R. A. Casero, *Amino Acids*, 2007, **33**, 231–240.

13 C. Bejger, J. S. Park, E. S. Silver and J. L. Sessler, *Chemical Communications*, 2010, **46**, 7745–7747.

14 V. Král, H. Furuta, K. Shreder, V. Lynch and J. L. Sessler, *J Am Chem Soc*, 1996, **118**, 1595–1607.

15 G. R. Desiraju, *Acc Chem Res*, 2002, **35**, 565–573.

16 F. Zapata, L. Gonzalez, A. Caballero, I. Alkorta, J. Elguero and P. Molina, *Chemistry - A European Journal*, 2015, **21**, 9797–9808.

17 C. R. Rice, C. Slater, R. A. Faulkner and R. L. Allan, *Angewandte Chemie - International Edition*, 2018, **57**, 13071–13075.

18 Q. He, G. M. Peters, V. M. Lynch and J. L. Sessler, *Angewandte Chemie - International Edition*, 2017, **56**, 13396–13400.

19 Q. He, G. I. Vargas-Zúñiga, S. H. Kim, S. K. Kim and J. L. Sessler, *Chem Rev*, 2019, **119**, 9753–9835.

20 L. Fabbrizzi, P. Pallavicini, L. Parodi and A. Taglietti, *Inorganica Chim Acta*, 1995, **238**, 5–8.

21 V. Amendola, M. Bonizzoni, D. Esteban-Gómez, L. Fabbrizzi, M. Licchelli, F. Sancenón and A. Taglietti, *Coord Chem Rev*, 2006, **250**, 1451–1470.

22 S. J. Park and M. K. Seo, in *Interface Science and Technology*, Elsevier, 2011, vol. 18, pp. 253–331.

23 K. Szalewicz, in *Encyclopedia of Physical Science and Technology*, Elsevier, Third., 2003, pp. 505–538.

24 V. Amendola, M. Bonizzoni, D. Esteban-Gómez, L. Fabbrizzi, M. Licchelli, F. Sancenón and A. Taglietti, *Coord Chem Rev*, 2006, **250**, 1451–1470.

25 J. M. Macleod and F. Rosei, in *Comprehensive Nanoscience and Technology*, Elsevier, 2011, vol. 3, pp. 13–68.

26 D. E. McRee, in *Practical Protein Crystallography*, Elsevier, Second., 1999, pp. 91–269.

27 F. Sommer, Y. Marcus and S. Kubik, *ACS Omega*, 2017, **2**, 3669–3680.

28 J. Qiu, A. Patel and J. M. Stevens, *Org Process Res Dev*, 2020, **24**, 1262–1270.

29 T. B. Gasa, C. Valente and J. F. Stoddart, *Chem Soc Rev*, 2011, **40**, 57–78.

30 S. Bartoli and S. Roelens, *J Am Chem Soc*, 1999, **121**, 11908–11909.

31 D. González-Rodríguez, J. L. J. Van Dongen, M. Lutz, A. L. Spek, A. P. H. J. Schenning and E. W. Meijer, *Nat Chem*, 2009, **1**, 151–155.

32 P. Thordarson, *Chem Soc Rev*, 2011, **40**, 1305–1323.

33 P. Job, *Ann Chim (Paris)*, 1928, **10**, 113–203.

34 F. Ulatowski, K. Dabrowa, T. Bałakier and J. Jurczak, *Journal of Organic Chemistry*, 2016, **81**, 1746–1756.

35 D. Brynn Hibbert and P. Thordarson, *Chemical Communications*, 2016, **52**, 12792–12805.

36 M. Brune, J. L. Hunter, S. A. Howell, S. R. Martin, T. L. Hazlett, J. E. T. Corrie and M. R. Webb, *Biochemistry*, 1998, **37**, 10370–10380.

37 E. A. Katayev, J. L. Sessler, V. N. Khrustalev and Y. A. Ustynyuk, *Journal of Organic Chemistry*, 2007, **72**, 7244–7252.

38 E. A. Katayev, J. L. Sessler, V. N. Khrustalev and Y. A. Ustynyuk, *Journal of Organic Chemistry*, 2007, **72**, 7244–7252.

39 A. Daryl Ariawan, J. E. A. Webb, E. N. W. Howe, P. A. Gale, P. Thordarson and L. Hunter, *Org Biomol Chem*, 2017, **15**, 2962–2967.

40 G. W. Bates, Triyanti, M. E. Light, M. Albrecht and P. A. Gale, *Journal of Organic Chemistry*, 2007, **72**, 8921–8927.

41 C. Caltagirone, J. R. Hiscock, M. B. Hursthouse, M. E. Light and P. A. Gale, *Chemistry - A European Journal*, 2008, **14**, 10236–10243.

42 P. A. Gale, J. R. Hiscock, S. J. Moore, C. Caltagirone, M. B. Hursthouse and M. E. Light, *Chem Asian J*, 2010, **5**, 555–561.

43 J. M. Granda, J. Grabowski and J. Jurczak, *Org Lett*, 2015, **17**, 5882–5885.

44 J. L. Sessler, D. G. Cho and V. Lynch, *J Am Chem Soc*, 2006, **128**, 16518–16519.

45 S. I. Kondo, Y. Hiraoka, N. Kurumatani and Y. Yano, *Chemical Communications*, 2005, **13**, 1720–1722.

46 S. I. Kondo and R. Takai, *Org Lett*, 2013, **15**, 538–541.

47 T. Mizuno, W. H. Wei, L. R. Eller and J. L. Sessler, *J Am Chem Soc*, 2002, **124**, 1134–1135.

48 P. Plitt, D. E. Gross, V. M. Lynch and J. L. Sessler, *Chemistry - A European Journal*, 2007, **13**, 1374–1381.

49 E. A. Kataev and T. A. Shumilova, *Molecules*, 2015, **20**, 3354–3370.

50 T. S. Pandian, S. J. Cho and J. Kang, *Journal of Organic Chemistry*, 2013, **78**, 12121–12127.

51 A. R. Jennings and D. Y. Son, *Tetrahedron Lett*, 2012, **53**, 2181–2184.

52 Ş. Ertul, M. Bayrakci and M. Yilmaz, *J Hazard Mater*, 2010, **181**, 1059–1065.

53 A. F. D. D. de Namor, W. A. Hamdan, O. Webb, R. Bance-Soualhi, B. Howlin and N. al Hakawati, *J Hazard Mater*, 2019, **364**, 733–741.

54 A. Nehra, D. S. Yarramala and C. P. Rao, *Chemistry - A European Journal*, 2016, **22**, 8980–8989.

55 V. Král, H. Furuta, K. Shreder, V. Lynch and J. L. Sessler, *J Am Chem Soc*, 1996, **118**, 1595–1607.

56 H. F. M. Nelissen and D. K. Smith, *Chemical Communications*, 2007, **29**, 3039–3041.

57 J. W. Blair and G. W. Murphy, in *Advances in Chemistry*, 1960, vol. 27, pp. 206–223.

58 A. M. Johnson and J. Newman, *J Electrochem Soc*, 1971, **118**, 510–517.

59 P. M. Biesheuvel, S. Porada and J. E. Dykstra, *arXiv preprint arXiv:1809.02930*, 2018, 1–16.

60 Z. H. Huang, Z. Yang, F. Kang and M. Inagaki, *J Mater Chem A Mater*, 2017, **5**, 470–496.

61 Y. Liu, C. Nie, X. Liu, X. Xu, Z. Sun and L. Pan, *RSC Adv*, 2015, **5**, 15205–15225.

62 K. Zuo, J. Kim, A. Jain, T. Wang, R. Verduzco, M. Long and Q. Li, *Environ Sci Technol*, 2018, **52**, 9486–9494.

63 C. Zhang, D. He, J. Ma, W. Tang and T. D. Waite, *Water Res*, 2018, **128**, 314–330.

64 J. Landon, X. Gao, A. Omosebi and K. Liu, *Curr Opin Chem Eng*, 2019, **25**, 1–8.

65 B. Shapira, E. Avraham and D. Aurbach, *Electrochim Acta*, 2016, **220**, 285–295.

66 D. He, C. E. Wong, W. Tang, P. Kovalsky and T. David Waite, *Environ Sci Technol Lett*, 2016, **3**, 222–226.

67 M. Pasta, C. D. Wessells, Y. Cui and F. la Mantia, *Nano Lett*, 2012, **12**, 839–843.

68 X. Su and T. A. Hatton, *Adv Colloid Interface Sci*, 2017, **244**, 6–20.

69 D. Pletcher, *A First Course in Electrode Processes*, The Royal Society of Chemistry, Cambridge, Second edition., 2009.

70 W. Schmickler, in *Reference Module in Chemistry, Molecular Sciences and Chemical Engineering*, Elsevier, 2014.

71 R. McNair, G. Szekely and R. A. W. Dryfe, *ACS ES&T Water*, 2021, **1**, 217–239.

72 X. Gao, A. Omosebi, J. Landon and K. Liu, *Environ Sci Technol*, 2015, **49**, 10920–10926.

73 W. Xing, J. Liang, W. Tang, D. He, M. Yan, X. Wang, Y. Luo, N. Tang and M. Huang, *Desalination*, 2020, **482**, 1−21.

74 W. Tang, J. Liang, D. He, J. Gong, L. Tang, Z. Liu, D. Wang and G. Zeng, *Water Res*, 2019, **150**, 225–251.

75 S. Porada, R. Zhao, A. van der Wal, V. Presser and P. M. Biesheuvel, *Prog Mater Sci*, 2013, **58**, 1388–1442.

76 Y. Oren, *Desalination*, 2008, **228**, 10–29.

77 J. R. Hiscock, C. Caltagirone, M. E. Light, M. B. Hursthouse and P. A. Gale, *Org Biomol Chem*, 2009, **7**, 1781–1783.

78 G. Sanchez, A. Espinosa, D. Curiel, A. Tarraga and P. Molina, *Journal of Organic Chemistry*, 2013, **78**, 9725–9737.

Chapter 2

Analytical and Electrochemical Techniques

Synopsis

This chapter aims to explain the theoretical background of the techniques- both analytical and electrochemical- used in experimental Chapters 3-5, prior to them being encountered within the text.

2.1 NMR Spectroscopy

2.1.1 Fundamentals of NMR and Chemical Shift

Nuclear Magnetic Resonance (NMR) spectroscopy is an analytical technique commonly used to determine the molecular structure of a compound or material through the analysis of its nuclear spins in a static magnetic field.[1]

In order for NMR to used, the nuclei in question must possess a magnetic moment. This magnetic moment, μ, can be determined through Equation 2.1:

$$\mu = I\gamma\frac{h}{2\pi} \qquad \text{(Equation 2.1)}$$

Where I is the spin quantum number (the result of the number of protons and neutrons in the nucleus), γ is the gyromagnetic ratio (the ratio of the magnetic moment to angular momentum) and h is the Planck's constant, $6.626 \times 10^{-34}\,m^2\,kg\,s^{-1}$. The spin quantum number is an inherent property of the atomic nuclei and as previously stated, must be present in order to be detectable by NMR. This property, I, is determined by the number of mass nucleons- protons and neutrons- within the nucleus. Three possibilities arise for I values. Nuclei with an odd number of nucleons possess fractional spin numbers e.g. I = 1/2 (^{1}H, ^{13}C), 3/2 (^{39}K), and 5/2 (^{17}O). Nuclei with an even number of total mass nucleons but an odd number of protons and neutrons e.g., ^{14}N (7 + 7) and ^{2}H (1+1), have integer spin values. Finally, nuclei with equal numbers of protons and neutrons e.g., ^{12}C and ^{16}O, have zero spin. Nuclei $I \geq 1/2$ are NMR active, however quadrupole nuclei with $I > 1/2$ are more complex due to the asymmetric distribution of charge around the nucleus. For the purpose of this thesis, only ^{1}H and ^{13}C NMR was performed so further discussion shall be limited to nuclei with I = 1/2 only.

In the absence of an external magnetic field, the magnetic moment of the nuclei is randomly oriented. During an NMR experiment, a strong magnetic field, B_0, is applied causing the nuclei to align and begin precessing around B_0. The orientation of the alignment depends on the spin of the nuclei, and for nuclei with I = 1/2, $2I + 1$ 'spin states' exist. These spin states have their own discrete quantum number, m, and have the value ± 1/2, depending on whether they are aligned parallel, α, or antiparallel, β, to B_0 (Figure 2.1).

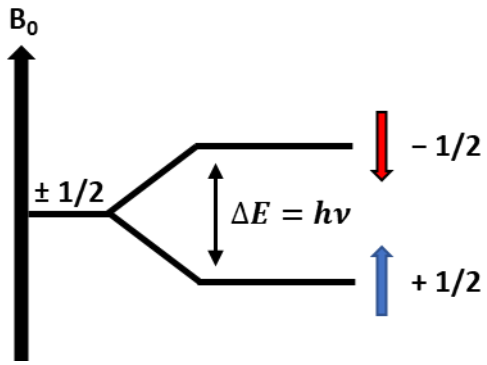

Figure 2.1: Splitting of the energy states of a spin-half nucleus in the presence of an applied magnetic field.

Without the external magnetic field, these spin states are degenerate; however, once a field is applied, the states are split and have discrete energy levels, the difference between which is directly proportional to the strength of the applied magnetic field. Despite the presence of a strong magnetic field, the energy difference between the two states is incredibly small and as such radiowave frequencies are enough to promote the transition from low to high energy states. The frequency required can be obtained by Equation 2.2, the Bohr relation:

$$\Delta E = h\nu \qquad Equation\ 2.2$$

Where ΔE is the energy difference and ν is the frequency applied. This frequency is known as the Larmor frequency and can also be expressed in terms of the gyromagnetic ratio and the applied magnetic field (Equation 2.3):

$$\nu = B_0 \frac{\gamma}{2\pi} \qquad Equation\ 2.3$$

This means that as the field strength increases, so does the frequency and consequently ΔE. This is what makes higher frequency NMR instruments more sensitive. When irradiated with the Larmor frequency, the ΔE between the two energy levels is met, and 'spin-flip' can occur; low energy α spin-state can flip to the higher energy β state. This is called resonance. The absorbed energy is released after excitation allowing the excited nuclei to relax to their original lower energy state. This released energy is in the radiofrequency range and so can subsequently be detected.

In order to better explain the interaction between the nuclei and radiofrequency, a vector model is often used. Figure 2.2 shows that if you consider the sum of the magnetic moments in a sample as a bulk magnet, M_0, the alignment of M_0 is with that of the applied magnetic

field B_0 as a consequence of more nuclei being in the lower energy spin state. This can arbitrarily be assigned to the *z*-axis.

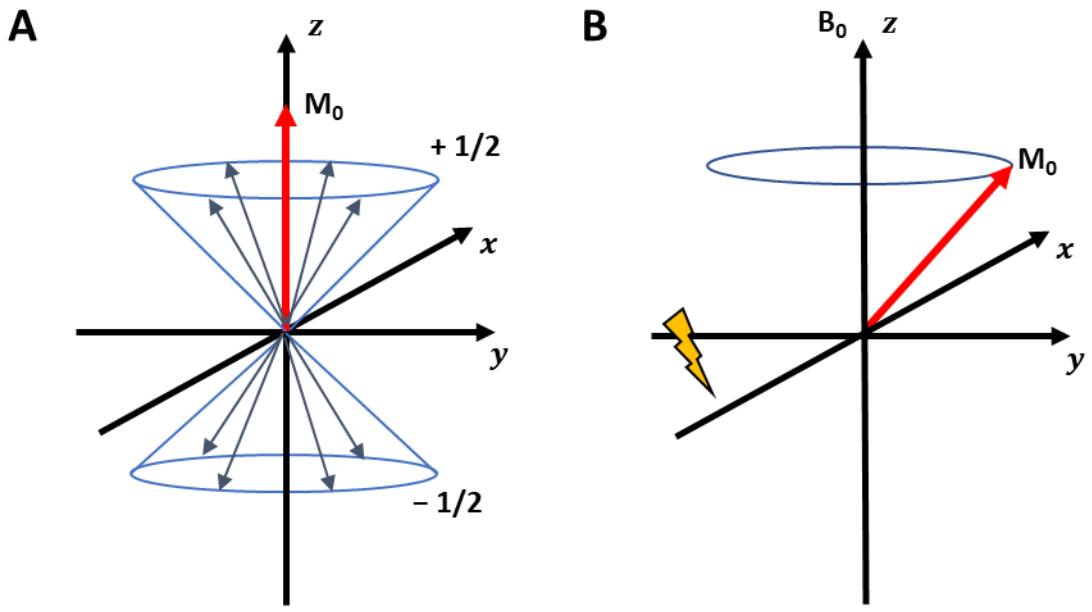

Figure 2.2: A) Alignment of the nuclei with the applied magnetic field B_0 leading to the bulk magnetization vector M_0. B) Tilting of M_0 into the xy-plane upon irradiation with a radiofrequency pulse.

The application of a radiofrequency pulse along the *x*-axis causes the bulk magnetization, M_0, to be tilted into the *xy*-plane as the nuclei absorb the pulse energy. M_0 now precesses around the *z*-axis at a frequency related to the applied B_0 field strength- the Larmor frequency- due to the angular momentum of the magnetic moment. By placing a detector in the *y*-plane, the signal can be observed as an oscillating wave. When the applied radio signal is stopped, the nuclei begin to relax back down to their ground state. At this stage, a radio frequency signal is emitted that, slowly over time, decays as the energy is released. The energy can be released in two ways; spin-spin relaxation, the interaction of spin with the surrounding protons, or spin-lattice relaxation, interaction of spin with surrounding molecules. This signal is known as free induction decay and is transformed into the more useful intensity versus frequency domain using Fourier transformation. The frequency can be obtained from Equation 2.4:

$$\nu = \frac{1}{t} \qquad Equation\ 2.4$$

Where *t* is the time period between two successive crests.

Modern NMR spectrometers maintain a constant magnetic field and the subsequent radio pulse excites all the protons concurrently. The pulse applied spans a large frequency range

and can excite each nucleus into its higher energy spin state. This difference in frequency absorbed means that each nucleus resonates at its own specific frequency and can thus be discerned. This resonating frequency can be affected by the surrounding bonding nuclei. Covalent bonds are the overlap and sharing of electrons and the bonding electrons can interact with an applied magnetic field and induce their own local magnetic field, B_i, which opposes the overall applied B_0. This means that the magnetic field at a given nucleus is reduced (Equation 2.5):

$$B_{eff} = B_0 - B_i \qquad Equation\ 2.5$$

The induction of B_i is said to shield the nucleus, as a larger B_i leads to a smaller B_{eff} being felt by the nucleus. Therefore, if a nucleus is bound to a highly electronegative atom, such as oxygen, it experiences a reduction in the electron density surrounding it and as such, B_i is reduced and the B_{eff} is much larger. This increases the resonance frequency of the nucleus. Nuclei that experience this effect are said to be 'deshielded' and are often found downfield/to the left of an NMR spectrum. Conversely, the opposite case is true, that if a nucleus is next to a less electronegative/electropositive atom, the nucleus experiences a higher electron density and B_i and B_{eff} increase. These variations in the absorbance frequency are what give rise to the different chemical shifts observed in NMR spectra. It is common practice for all signals in an NMR spectrum to be referenced to an internal standard e.g., tetramethyl silane, $Si(CH_3)_4$ in ^1H NMR spectroscopy. Tetramethyl silane is used due to the difference in shielding experienced by the Si centre when NMR experiments are undertaken. This causes a large singlet signal for $Si(CH_3)_4$ to appear upfield as all the protons are in the same environment. For ease of analysis, the signal for $Si(CH_3)_4$ is removed from the NMR spectra and its resonance frequency assigned as 0 Hz. As previously stated, the observed frequencies in NMR are directly related to the strength of the applied magnetic field and this is what makes higher frequency instruments more sensitive. This however creates a problem when comparing NMR data obtained on different instruments with differing strength frequencies. In order to counteract this problem, the relative chemical shift scale is used which is field independent, Equation 2.6:

$$\delta = \frac{\nu_H - \nu_{reference}\ (Hz)}{Spectrometer\ frequency\ (MHz)} \qquad Equation\ 2.6$$

Where ν_H and $\nu_{reference}$ are the frequency of the proton and reference, respectively. This scale is expressed in parts per million (ppm). Commonly, the scale for ^1H NMR is 0-12 ppm and for ^{13}C NMR 0-220 ppm.[2]

2.1.2 Distortionless Enhancement by Polarization Transfer (DEPT)

Distortionless Enhancement by Polarisation Transfer is the 1D ^{13}C technique most commonly used for determining the multiplicities of carbon atoms.[3,4] If DEPT experiments are not decoupled, multiplet patterns corresponding to doublets, triplets etc. are observed in their characteristic ratios. By decoupling the spectra, single peaks are obtained, and this is the origin of the 'distortionless' term. However, in the majority of cases, DEPT spectra are proton decoupled and so multiplet patterns are not seen. Simply, DEPT works through the series of radio frequency pulses that allow the signals of both protons and carbons to mix, this is termed heteronuclear multiple quantum coherence, and this is allowed to develop in both the proton and carbon domains. This coherence cannot be directly observed, and a further pulse decouples the protons and regenerates the observable magnetisation. The differences in this observed outcome depend on the identity of the carbon resonance; methyl, methylene and methine. Quaternary carbons cannot be observed in a DEPT experiment.[3,4]

Variation of the pulse angles can affect the orientation or visibility of the signal e.g., CH and CH_3 oriented in the positive/up direction, whilst CH_2 oriented negative/downwards

2.2 UV-Vis

Ultraviolet-Visible (UV-Vis) spectroscopy is a technique that probes the absorbance or transmittance of electromagnetic radiation of a sample at discrete wavelengths. As the name suggests, the wavelengths used tend to fall between 200–800 nm.[5] The make-up of the sample being analysed, as well as the concentration, can all influence the absorption of a given wavelength. This can be related to the Beer-Lambert law, Equation 2.7:

$$A = \varepsilon c l \qquad Equation\ 2.7$$

Where ε is the molar extinction coefficient of the species, c is the concentration, l is the pathlength and A is absorbance. From Equation 2.7, it can be seen that the concentration of the sample is directly related to the absorbance. The molar extinction coefficient is entirely sample related and gives an indication into how well the sample in question absorbs light of a given wavelength. If the molar extinction coefficient and correct absorbance can be discerned, the concentration of a species in a sample can be calculated.[6]

The absorbance of the electromagnetic radiation can promote the transition of electrons from low energy to higher energy states, which can be subsequently used to identify specific functional groups e.g., nitrates, dienes, which all absorb in specific wavelength ranges.

A single beam spectrometer was used for the work undertaken in this thesis- Chapter 5. A single beam spectrometer can be broken down into six main components (Figure 2.3).

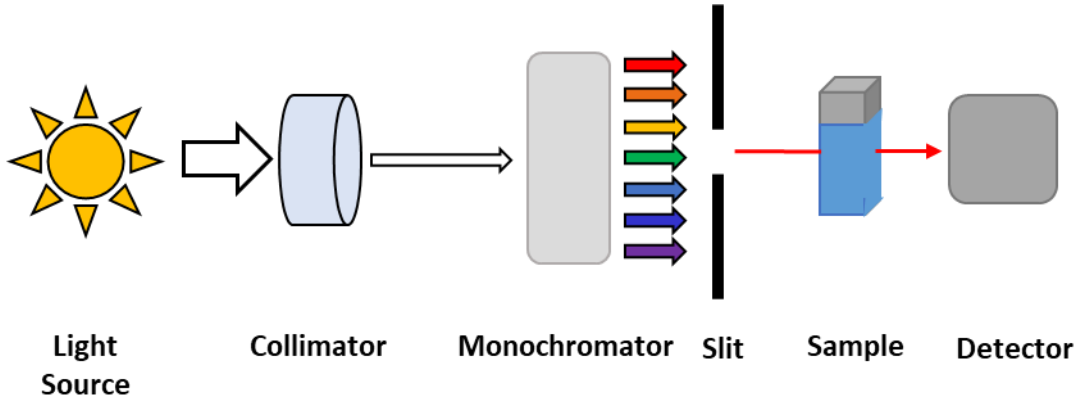

Figure 2.3: Simplified set-up of a single beam UV-Vis spectrometer

First a light source emits a light which is narrowed through the use of a collimator. This narrowed light is then split into its constituent components of light according to wavelength by a monochromator. A mechanical slit can then be used to only allow certain wavelengths of this split light through to the sample. The light passes through the sample and reaches a detector which measures the intensity of the light at the other side. The detector can be used to visualise the absorbance or transmittance of light as a function of its wavelength.[7]

2.3 Infrared Spectroscopy (IR)

As the name suggests, Infrared (IR) spectroscopy uses electromagnetic radiation within the IR range and differs in technique compared to that of UV-Vis and NMR spectroscopy, which use ultraviolet-visible and radio wave radiation, respectively. The IR region can be broken down into three distinct regions: near IR (12500-4000 cm^{-1}), IR (4000-400 cm^{-1}) and far IR (400-10 cm^{-1}). In this body of work, only the mid IR region will be discussed. In this region, only vibrational and rotational modes are able to be detected, not electronic transitions, as in UV-Vis. In order to be IR-active, there must be a net change in the dipole moment during these vibrational modes. Homonuclear species, such as O_2 and N_2, undergo no net change in dipole and so cannot absorb IR radiation and are thus IR-inactive. The molecular vibrations

observed can be classified into two main types: stretching or bending. Stretching is the continuous change in the interatomic distance, out with the normal frequency of vibration.[8,9] Bending is related to the change in angle between two atoms and includes certain characteristic modes. These modes all occur at different frequencies and so give rise to characteristic peaks/ bands in the IR spectrum. Asymmetric groups, such as -NO_2 and -OH are easily identifiable using IR due to the large difference in masses and dipoles. This makes IR particularly useful for discerning the functional groups present in a molecule. The theoretical basis for IR can be related to Hooke's Law and the motion of two objects bound by a spring. For a simple diatomic, the frequency of vibration for the spring can be described by Equation 2.8:

$$\nu = \frac{1}{2\pi}\sqrt{\frac{k}{\mu}} \qquad Equation\ 2.8$$

Where k is the spring constant, which obeys Hooke's law, and μ which is the reduced mass and can be described by a separate equation (Equation 2.9):[2]

$$\mu = \frac{m_1 m_2}{m_1 + m_2} \qquad Equation\ 2.9$$

Where m_1 and m_2 are two masses. In terms of a chemical bond, the frequency term refers to the molecule's vibration and the spring constant is the force constant of the bond between the two atoms. It can therefore be seen that the frequency of the vibrations is directly proportional to the square root of the force constant, and inversely proportional to the root of the effective mass. This means that the stronger a chemical bond or the larger the difference in mass between the two atoms, the larger the vibrational frequency that will be observed. Modern IR instruments, such as Fourier transform IR, work in the time domain, and use an interferometer. The frequency data is obtained using a set of mirrors- one fixed and one movable- and a beam splitter. The beams are split and recombine undergoing interference that depends on the difference in the pathlength the light has taken. This is then decoded by Fourier transform. These IRs are significantly more sensitive than other IR instruments.[8] Unlike in UV-Vis, which often shows the wavelength of the frequency of light, IR conventionally uses wavenumber, measured in cm^{-1}, and bonds/functional groups tend to fall into characteristic regions, Figure 2.4.

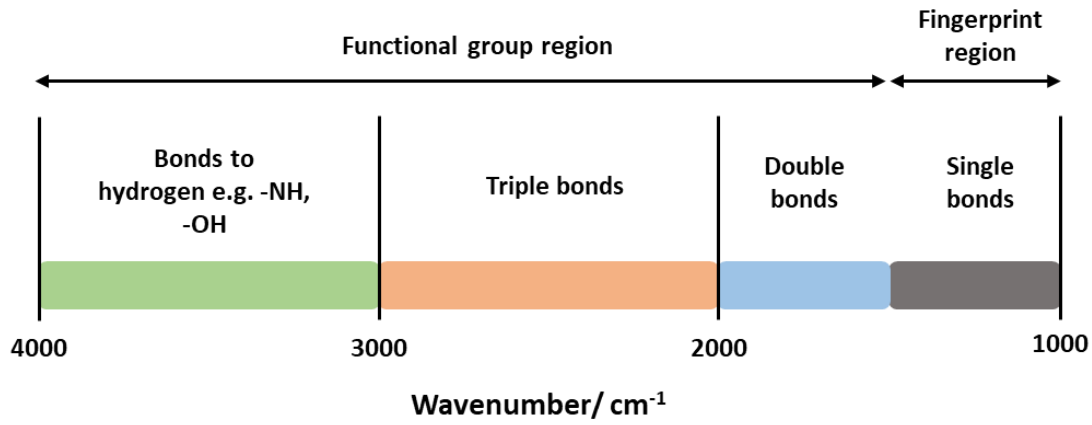

Figure 2.4: Characteristic regions for IR.

The obtained IR spectra can be broken down into two regions: the functional group region (3600-1200 cm^{-1}) and the 'fingerprint' region (1200-600 cm^{-1}). The functional group region can be used to the identify the functional groups present in a compound, based on the frequency at which it absorbs. Commonly identifiable groups include aldehydes, carboxylic acids, esters, ketones, alcohols, amides nitriles and nitro groups.[2] Some C-O bonds and C-Cl bonds are found out with the functional group region so some care should be taken during analysis. The fingerprint region is often unique to the sample in question and small differences in the skeletal structure result in changes to the observed spectra. Computer programs can be used to compare to known existing samples expediting the identification process further, such as the Cambridge Structural Database.

2.4 Mass Spectrometry (MS)

Since its inception in 1912, where it was first described as a parabola spectrograph, mass spectrometry has evolved into one of the main techniques used in the identification of molecules and compounds. A MS system typically consists of four main parts, the first is the ion source whereby the sample to be analysed is ionized, can be done through a number of different methods, but herein only electron ionization and electrospray ionization (ESI) will be mentioned. Once ionized, the sample ions are accelerated towards a mass analyser, which separates the ions based on their mass-to-charge ratio, *m/z*. Once the ions have been separated, they can be detected by a detector that can record the intensities of the *m/z* obtained. This ion signal can then be amplified and digitised by a recording device, to give a more useful form of spectra with intensity versus *m/z*, normalized to the most abundant mass ion[10,11]. An overall, simplified setup is shown in Figure 2.5.

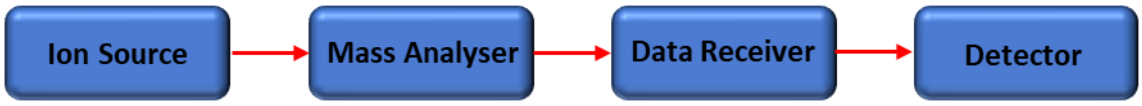

Figure 2.5: Overall set up for a mass spectrometer.

The MS is also generally operated under vacuum as this prevents collisions with unwanted molecules which may complicate the spectra or decrease the overall sensitivity.

2.4.1 Ion source- Electron Ionization

The sample is first volatilised and subsequently bombarded with high energy (around 70 eV) electrons emitted from a heated filament. A magnet placed opposite the filament can be used to increase the likelihood of interaction between an electron and the gaseous sample. The energy of the electrons is sufficient enough to overcome the first ionization potential of the compound, causing the ejection of an electron and forming the molecular ion, $M^{+\cdot}$ (Equation 2.10):

$$M + e^- \rightarrow M^{+\cdot} + 2e^- \qquad Equation\ 2.10$$

The mass ion has a mass nominally equivalent to the mass of the sample molecule. During the ionization process, excess electronic energy can be transferred into the internal bonds of the sample and be of sufficient energy to induce bond cleavage, generating fragment ions that are unique to the sample being ionized. A hypothetical fragmentation pathway can be seen in Equation 2.11:

$$ABCD^{+\cdot} \rightarrow ABC^+ + D^{\cdot} \rightarrow AB^+ + C \rightarrow A^+ + B \qquad Equation\ 2.11$$

An extractor and ion focussing plate, maintained at a negative potential ensures that the positive ions generated are attracted and accelerated towards the mass analyser.[10]

2.4.2 Ion Source- Electrospray Ionization (ESI)

ESI has found extensive use for the identification of involatile, large and polar compounds. In ESI, the sample of interest is dissolved in a suitable solvent and pumped through a capillary with a potential difference of between 1-4 kV at the tip of the capillary, which accumulates charge and generates a cone of charged liquid droplets as the sample is pumped through. A heated gas, such as N_2, is used to disperse the clusters of ions formed, as well as evaporate solvent molecules. The evaporation of solvent means that the droplet size decreases whilst the charge density remains the same. Repulsion of the like charges eventually leads to the formation of smaller and smaller droplets and eventually the release of an ion. These ions are then guided to the mass analyser through a pumped nozzle-skimmer system, Figure 2.6.[11]

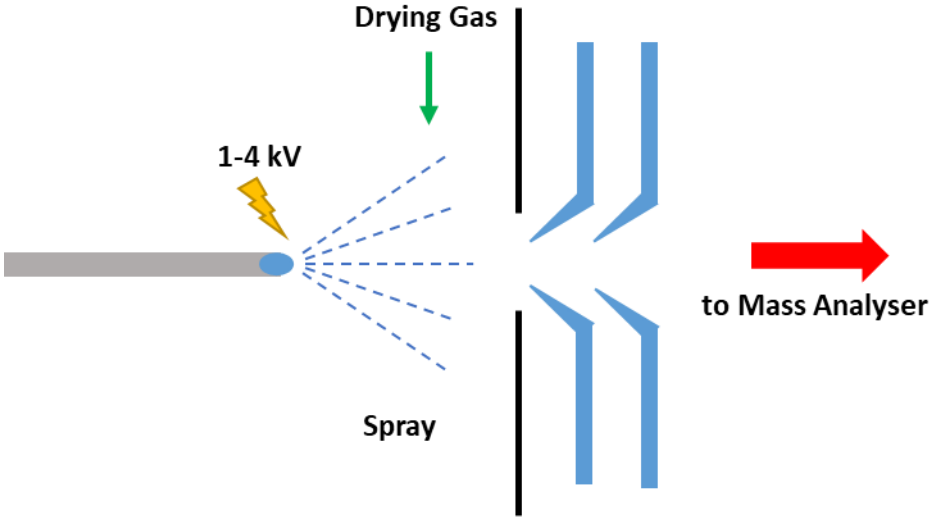

Figure 2.6: Schematic diagram of a mass spectrometer ESI source.

2.4.3 Mass analyser

As previously stated, the mass analyser separates the ionized sample based on the mass-to-charge ratio. There are a number of different ways that ions can be separated, and these vary in their upper detection limit- highest *m/z* that can be detected- and resolution- the analyser's ability to be able to differentiate between two ions of very similar mass. One such analyser is a sector mass analyser which separates ions as they are accelerated through an applied magnetic or electric field. This causes the ions to travel with a curved trajectory towards the

detector, the radius of which is dependent on the applied magnetic field and potential. The motion of the ions can be described by Equation 2.12:

$$m / z = \frac{B^2 r^2 e}{2V} \qquad Equation\ 2.12$$

Where B is the applied magnetic field, r is the radius of the ion path, e is the electronic charge and V is the applied potential. This means that for a given potential or magnetic field, only certain ions with the correct *m/z* value will follow the radius of curvature and reach the detector. Therefore, by varying the either the magnetic field or applied potential, ions of different *m/z* can be detected. Variation of the magnetic field, rather than the applied voltage, is more common, as this leads to more reproducible and sensitive results.[10,11]

2.4.4 Ion Detection

The most common detector utilised in MS is the electron multiplier due to its compact nature and cost effectiveness. The multiplier is a series of dynodes, that are coated in a semi-conductive substance, such as lead oxide or Be-Cu alloy, which readily releases electrons upon impact by high energy particles, such as the ion beam. Figure 2.7 shows a general setup of the dynodes within a MS detector.

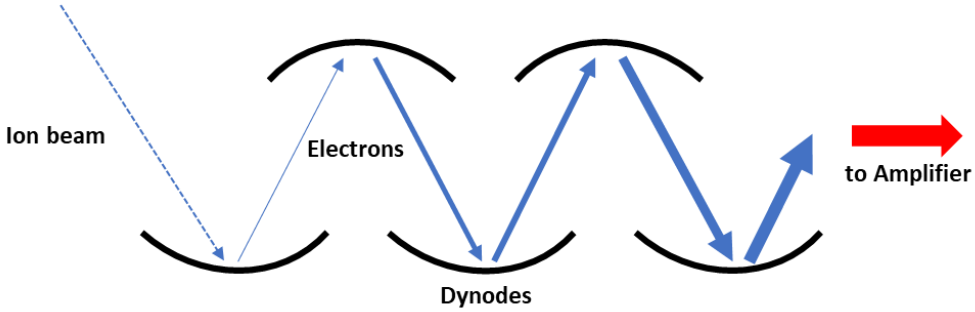

Figure 2.7: Schematic of an electron multiplier in a mass spectrometer.

The first dynode is held at a negative potential in order to attract the positive ion beam towards it. Upon collision with the dynode surface, additional electrons are emitted which travel to a second dynode and collide again. This cascade of electrons allows for signal amplification in the order of 10^6. The current yielded can then be digitized and sent to a recording device.[10,11]

2.4.5 Data Receiver

Typically, the mass spectrometer is connected to a PC which can be used to display the obtained spectra. The same system may also be used to change the acquisition parameters such as the resolution or the scan speed.[10] The plot obtained shows the relative abundance along the *y*-axis and the *m/z* along the *x*-axis. The relative abundance of each peak is set relative to the base peak, which is assigned to the most abundant peak and assigned as 100%.

2.5 Electrochemical Techniques

Over the course of this thesis, a number of electrochemical techniques were employed. Through the monitoring of current, potential, charge and resistance followed by the subsequent analysis, researchers can gain information about compounds/molecules present in an electrochemical system. Electrochemistry can also be used for the formation of new chemical bonds, either to molecules within in the cell or to the electrodes themselves[12,13] or new species entirely, via redox reactions.[14] The following section aims to explain the basics of cell setup and the electrochemical techniques used within this thesis.

2.5.1 Cell Setup

A typical electrochemical reaction is performed using a 3-electrode setup, working, counter and reference electrode. The working electrode is the site of the electrochemical reaction of interest, the counter electrode completes the circuit, passing an equal but opposite current relative to the working and the reference electrode is comprised of a well-established redox couple, that has a half-cell potential that remains constant throughout the electrochemical reaction. Assignation of working or counter electrode depends entirely on the nature of the electrochemical reaction in progress e.g., the anode can function as both the working and counter depending on whether the desired reaction is an oxidation or reduction. One important consideration is the material of choice for the electrodes, both working and counter, as this is integral to the correct functioning of the cell. The material chosen should be stable at the potential/current chosen to ensure that no unwanted side reactions occur. Electrodes used in this thesis were primarily glassy carbon or platinum.

As stated earlier, for an electrochemical cell to function, it requires only the working and counter electrode. In this case, the applied potential is the difference between the working and counter, and is a measure of the overall cell reaction, as opposed to a specific half-reaction. In order to investigate a specific reaction, reference electrodes are utilised. The electrodes contain a well-known redox couple e.g., Ag/AgCl, which has a constant reaction potential under the conditions utilised. These electrodes are placed as close to the working electrode as possible in order to minimise the internal resistance of the cell, which can lead to a drop in the overall applied potential. This potential drop can be described by Equation 2.13:

$$\Delta E_{Ohmic} = iR_{eff} \qquad Equation\ 2.13$$

Where ΔE is the drop in potential, i is the current from the working and R_{eff} is the resistance between the working and reference electrode. R_{eff} is related to the resistivity of the electrolyte, ρ, and the distance between the two electrodes, l, and the area between them, A, as seen in Equation 2.14:

$$R_{eff} = \frac{\rho l}{A} \qquad Equation\ 2.14$$

It is important to compensate for this potential drop in order to get a 'true' value for the potential used in an electrochemical reaction. Most modern potentiostats can do this automatically and all cyclic voltammograms in this thesis have been compensated accordingly. For references in organic solvents, pseudo-reference electrodes, such as $Ag/AgNO_3$, are often employed. The potential of the half-reaction does not remain constant, but changes predictably. In these cases, it is often prudent to add a substance with a well-defined redox couple into the reaction e.g., ferrocene. Within this thesis, both ferrocene and potassium ferricyanide were used when a pseudo-reference was employed.

2.5.2 Cyclic Voltammetry (CV)

Voltametric techniques are utilised extensively in electrochemistry and measure the current response of an electrochemical process as the potential is scanned over a set range. These techniques include, but are not limited to, cyclic voltammetry (CV) and linear sweep voltammetry. Both of these sweep the potential from E_1 to E_2, however in cyclic voltammetry, upon reaching E_2, the potential is reversed and returns to E_1, which may or may not be the end point of the reaction. In this thesis, only cyclic voltammetry was used.

Cyclic voltammetry has many uses, the simplest of which is the determination of the potential at which a redox reaction occurs, however as demonstrated in Chapter 5, it may be used to graft species within the cell to the surface of the electrode. One important aspect of cyclic voltammetry is the reversibility of a redox species which leads to the symmetric peak shape, as seen in Figure 5.8.

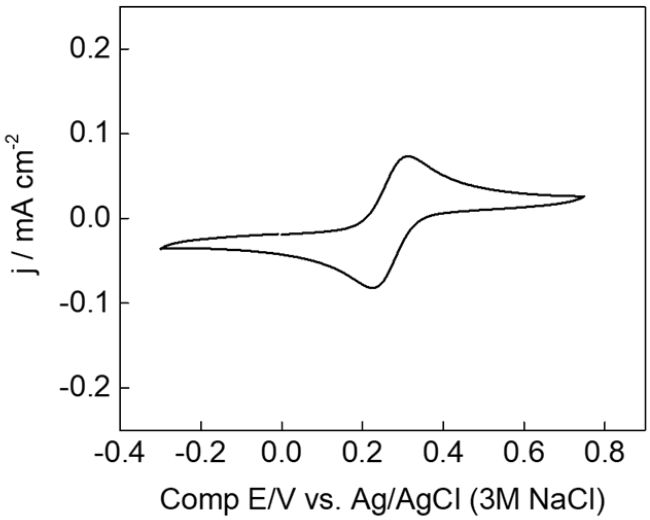

Figure 2.8: Example of a 1 mM potassium ferricyanide redox probe taken at pH 2.

For a redox couple to be described as fully reversible, it must meet a stringent set of criteria:[15]

1. *The potential difference between the peak maxima must fulfil* $\Delta E = \frac{59}{n}\ mV$*, where n is the number of electrons involved in the redox process.*
2. *Peak current proportional to the square root of the scan rate. Increasing scan rate increases the height of the observed peaks.*
3. *Changing scan rate does not change the position at which the peaks are observed.*
4. *Ratio of the observed peaks is 1:1.*

When performing a cyclic voltammogram experiment, in order to determine the reversibility of the cell, mass transport within the cell must be limited. Cyclic voltammetry is a surface sensitive technique, meaning we desire the information that happens at the electrode-electrolyte interface, and not the bulk solution, as in bulk electrolysis (Section 2.5.3). Therefore, cyclic voltammetry experiments are carried out without any mixing. This means that any species that are oxidised or reduced at the electrode are not able to diffuse away and can subsequently be oxidised or reduced on the reverse sweep if the scan rate is fast enough.

2.5.3 Electrolysis

Electrolysis techniques can be divided into two categories; potentiostatic and galvanostatic, in these the potential applied or current applied, respectively, are maintained at a constant set level. The current or potential response versus time is then recorded. For the purpose of this thesis, potentiostatic electrolysis was used and so the following section will focus solely on this. Potentiostatic electrolysis has benefits over galvanostatic electrolysis as it allows for greater reaction control. It is possible to set the potential of the electrolysis to a specific redox process based on a previously obtained cyclic voltammogram. To this end, specific species within an electrochemical cell can be investigated. One important aspect of electrolysis that we can obtain is the charge passed, Q, over the course of the reaction period. By knowing the total amount of charge passed, the theoretical reaction yield can be determined, Equation 2.15:

$$Q = mnF \qquad Equation\ 2.15$$

Where m is the number of moles of the species of interest, n is the number of electrons involved in the process and F is Faraday's constant (96485 C mol^{-1}). This can be used to calculate the Faradaic efficiency of the reaction using Equation 2.16:

$$Faradaic\ Efficiency = \frac{Q_{Reaction}}{Q_{Total}} \qquad Equation\ 2.16$$

Where $Q_{Reaction}$ is the charge required for the reaction of interest and Q_{Total} is the total charge passed.

2.6 References

1 J. Keeler, *Understanding NMR Spectroscopy*, John Wiley & Sons, Ltd, 2005.

2 J. Clayden, N. Greeves and S. Warren, *Organic Chemistry* , Oxford University Press, Second edition, 2012.

3 T. D. W. Claridge, in *High-Resolution NMR Techniques in Organic Chemistry*, Elsevier, 2016, pp. 133–169.

4 Atta-ur-Rahman, M. I. Choudhary and Atia-tul-Wahab, in *Solving Problems with NMR Spectroscopy*, Elsevier, 2016, pp. 133–190.

5 R. J. Anderson, D. J. Bendell and P. W. Groundwater, *Organic Spectroscopic Analysis*, 2004.

6 Y. Guo, C. Liu, R. Ye and Q. Duan, *Applied Sciences (Switzerland)*, 2020, **10**, 1–18.

7 S. Jena, S. Thakur, S. Jena, R. B. Tokas, S. Thakur and N. K. Sahoo, *SMC Bulletin*.

8 T. Tyner and J. Francis, *ACS Reagent Chemicals*, American Chemical Society, Washington, DC, 2017.

9 H. Reddy, S. Ghosh and D. Banji, *Near infra red spectroscopy-An overview Role of an Ethanolic Extract of Crotalaria juncea L. on High-Fat Diet-Induced Hypercholesterolemia View project sydnone derivatives View project*, 2011.

10 F. A. Mellon, in *Encyclopedia of Food Sciences and Nutrition*, 2nd edn., 2003, pp. 3739–3749.

11 R. W. Smith, in *Encyclopedia of Forensic Sciences: Second Edition*, Elsevier Inc., 2013, pp. 603–608.

12 Z. Nazemi, E. Shams and M. K. Amini, *Electrochim Acta*, 2010, **55**, 7246–7253.

13 A. J. Mendonca, M. Inês, A. P. Esteves, D. I. Mendonca and M. J. Medeiros, *Synth Commun*, 2011, **41**, 820–825.

14 A. D. Stergiou and M. D. Symes, *Cell Rep Phys Sci*, 2022, **3**, 100914.

15 D. Pletcher, *A First Course in Electrode Processes*, The Royal Society of Chemistry, Cambridge, Second edition., 2009.

Chapter 3

Diindolylurea Receptors for Anion Recovery

Acknowledgments and Declaration

Calum Hope performed the experimental work and data analysis. Mass spectrometry analysis was conducted by Mr Gangi Ubbara. Mark Symes conceived the idea and assisted with data analysis.

Synopsis

Hydrogen bonding has been demonstrated as an effective means to bind and sequester various anionic species such as fluoride[1]*, hydrogensulfate*[2] *and nitrate*[3]*. The importance of the structural arrangement of the hydrogen bonding motifs is crucial in order for the receptor to be fully effective. To this end, indole has been shown to be one such structural scaffold suitable for use as a receptor due to the presence of a hydrogen bond donating amine and its ease of functionalisation. Phosphate is one of the primary components of fertilizer and is used extensively to maintain food security globally. However, agricultural run-off leads to reduced mineral availability, whilst also leading to large scale eutrophication. Currently, phosphate species can be recovered through precipitation reactions or using biological active organisms. One potential alternative that could be used is capacitive deionisation, which has been shown to be suitable for the desalination of brackish water. Herein, we propose that a capacitive deionisation system, with a selective hydrogen bonding receptor, could be used for the selective recovery of dihydrogenphosphate. Our approach relied on the modification of a diindolylurea-based receptor through the installation of two different organic groups- carboxylic acid and alkyne- that could be used to attach the receptor to an electrode surface. The selectivity of the receptor for the dihydrogenphosphate anion was demonstrated through a series of* ^{1}*H NMR titrations.*

3.1 Introduction

The interest in anion receptors and anion complexation- in their various forms- has been a long running research topic dating back as far as the 1970s,[4,5] and perhaps even further. In recent times, hydrogen bond-based receptors have become increasingly important and are of particular interest- they allow for directional binding from a range of donor or acceptor groups to a variety of different anion geometries. Receptors can be designed that show high affinity and specificity for various oxo-anions, like AcO^-, [6] HSO_4^-, [7] and HPO_4^-, and also halides.[8]

The functionalisation of H-bonding scaffolds such as pyrrole and indole, with such moieties as amides and ureas has provided a large class of receptors with varying affinities, for several different anions. Gale and co-workers demonstrated the evolution of a set of indole-urea based receptors from a single 2,7-substituted indole containing receptor, **3.1**, with three H-bond donating sites, to one of a diindole-diamide symmetric receptor, **3.3**, which contains six H-bond donating sites, Figure 3.1.[9–11]

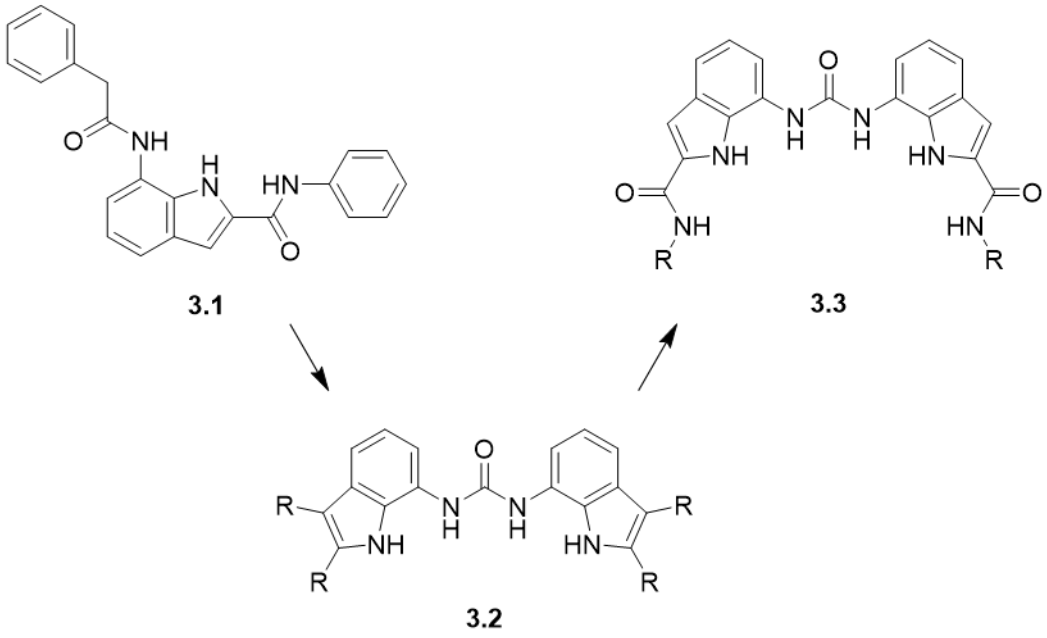

Figure 3.1: Evolution of indole-based receptors.

The addition of the extra indole and amide groups allows for the formation of more hydrogen bonds and subsequently, an increase in the binding affinity. It is this increase in affinity that was shown to promote the deprotonation of the oxo-anions -HCO_3^- and $H_2PO_4^-$ - in solution. During the binding process, the pK_a of the bound anion was postulated to be lowered

sufficiently, that a proton was abstracted from the more basic anion in solution. Proton NMR titrations with $H_2PO_4^-$ showed a slow and fast exchange process.

Herein, we will demonstrate that a receptor based on the aforementioned diindole-diamide symmetric receptor (**3.3**), modified with a terminal alkyne, showed a strong affinity for the dihydrogenphosphate anion in solution. The modification of the receptor with the terminal alkyne would serve as an 'anchor' point for the direct electrochemical surface modification of a glassy carbon electrode.

3.2 Proposed reaction Scheme

The original proposed reaction scheme, Scheme 3.1, modified the synthesis set out by Gale and co-workers in order to attach a labile group that could easily be attached to the surface.[11] The original synthesis contained a *N*-butylamine arm which was subsequently substituted for γ-aminobutyric acid (GABA). The carboxylic acid group was postulated to allow for the formation of an amide bond to the surface- through an already attached surface group (Chapter 5)- using either a coupling reagent, such as CDIm, or through the conversion of the acid to a highly reactive acid chloride.The first step of the reaction was the methyl ester protection of the carboxylic acid. This was necessary to 1) prevent the coupling reaction of the GABA amine with a second molecule of GABA and 2) in order to increase the solubility of the insoluble GABA in organic solvents. Once protected, Me-GABA, **3.4**, was coupled to 7-nitroindole-2-carboxylic acid using 1,1'-carbonyldiimidazole and the resulting nitro product, **3.5**, was reduced using hydrogen over Pd/C to give compound **3.6**. Two indole-amine monomers were coupled using triphosgene, in a 1:1 mix of DCM and sat. $NaHCO_3$ to give the urea coupled dimer, **3.7**. The methyl ester would then be removed using dilute NaOH in order to yield the carboxylic acid, **3.8**. It was also postulated that the acid chloride, **3.9**, could be formed directly from the methyl ester using $SOCl_2$.

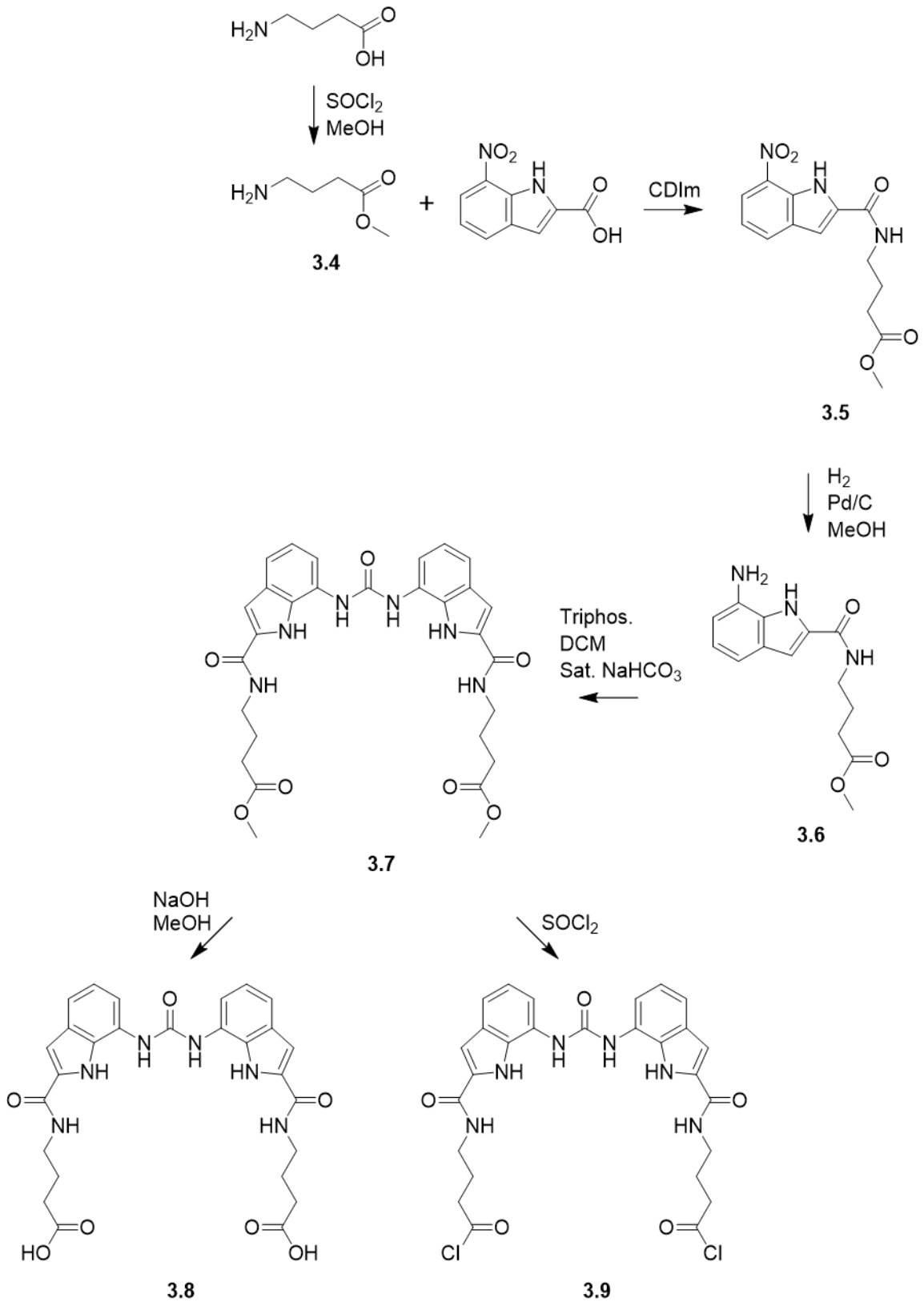

Scheme 3.1: Proposed modified reaction scheme.

3.2.1 GABA esterification

The original synthesis used by Gale et. al, coupled *N*-butylamine and 7-nitroindole-2-carboxylic acid, through an amide bond, using 1,1'-carbonyldiimidazole. In order for the reaction to proceed, it is necessary for all substrates to be dissolved in a suitable aprotic solvent e.g., chloroform. Unlike *N*-butylamine, GABA was determined to be insoluble in most organic solvents- $CHCl_3$, DCM, acetone, THF, MeOH, Et_2O, MeCN and EtOAc. Consequently, a methyl ester 'protecting group' was added to improve the solubility. In addition, due to the nature of GABA, containing both an amine and carboxylic acid group, there is a propensity for GABA to self-react under the coupling conditions used in the subsequent step (Scheme 3.2). The addition of the methyl ester removes one reactive carboxylic acid site and consequently removes the likelihood of the undesired side reaction occurring.

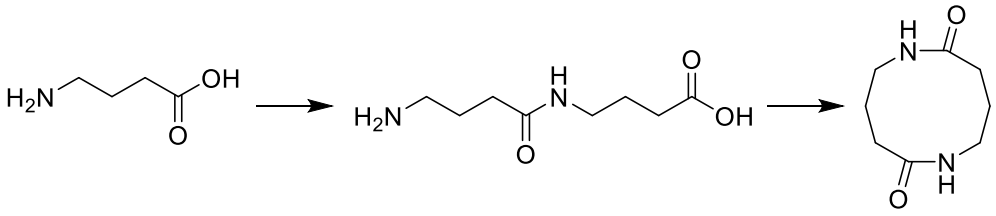

Scheme 3.2: Potential CDIm cyclisation product.

Thionyl chloride has long been used in organic chemistry for the formation of highly reactive acyl chlorides. The use of acyl chlorides is highly important in the fabrication of many polymers and surface bound compounds[12,13] and in drug manufacture.[14] The highly electronegative chlorine creates a large dipole moment, which causes the carbon of the carbonyl to become very electron deficient and as such, it is now susceptible to nucleophilic attack and leads to the formation of several different products (Scheme 3.4).

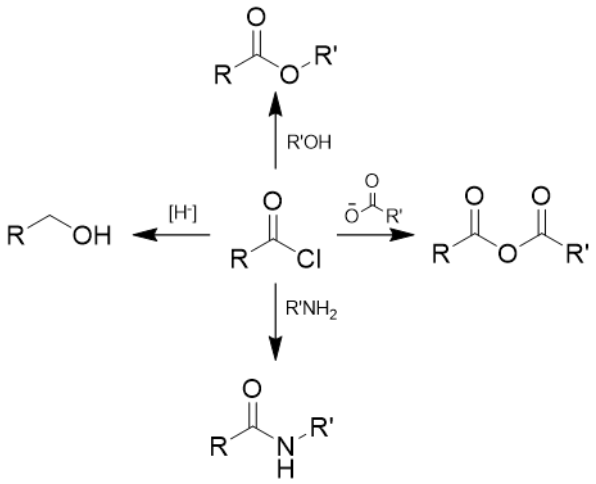

Scheme 3.3: Reactivity of acid chlorides with a range of nucleophiles.

From Scheme 3.3, an acyl chloride reacts with an alcohol and forms the corresponding ester. In the reaction with GABA, the carboxylic acid is first converted into the acyl chloride intermediate that then reacts with methanol and forms the methyl ester. The overall reaction mechanism is detailed in Scheme 3.4.

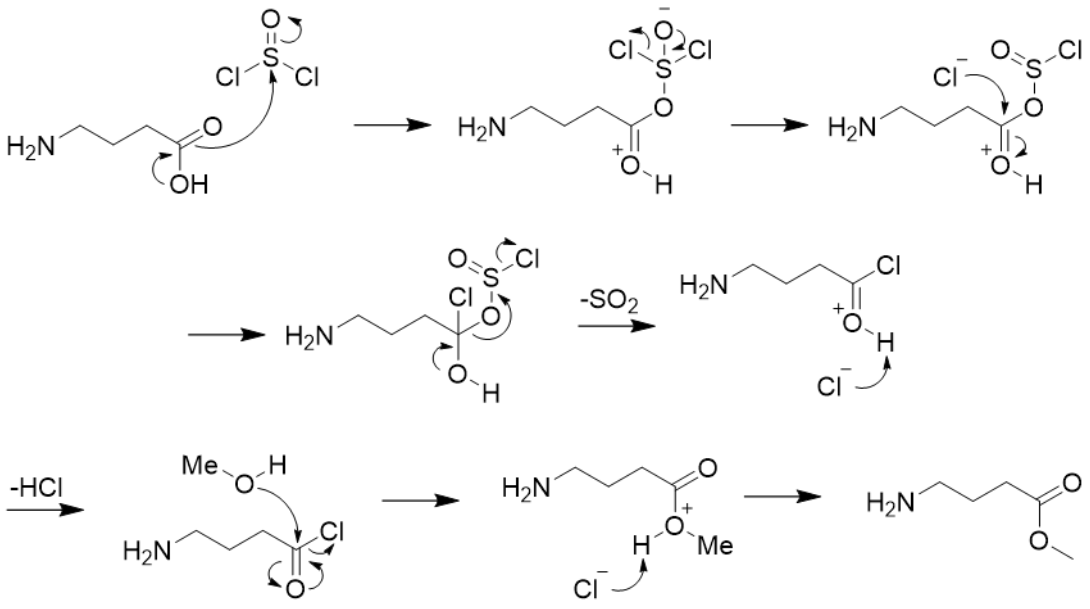

Scheme 3.4: Mechanism for the methyl esterification using $SOCl_2$.

The reaction proceeds via a nucleophilic attack of the carbonyl on the thionyl group of $SOCl_2$. The resulting chloride anion participates in an electrophilic [1,2]-addition reaction to the carbonyl centre. A [1,2]-elimination then occurs liberating sulfur dioxide and hydrochloric acid, giving the acyl chloride intermediate. Nucleophilic methanol is then free to react with

the acyl chloride forming the much more stable ester. The reaction between $SOCl_2$/MeOH and GABA was used successfully to synthesise **3.4** in 100% yield.

3.2.2 CDIm amide coupling

Since its development in the 1960's, 1,1'-carbonyldiimidazole (CDIm) has proven to be a cheap, effective, and easy to use reagent for the coupling of carboxylic acids to a variety of amines. Paul and Anderson developed CDIm as a novel method for peptide coupling when they obtained poor results when coupling the acylated imidazole ring of methyl *N*-benzoyl-1-histidinate and corresponding amine.[15] They found that CDIm was reactive towards carboxylic acids and formed the reactive acyl intermediate that could then react with an amine, forming a peptide in a much-improved yield. CDIm has found large scale use in industry due to the relatively non-toxic side products of the reaction- CO_2 and imidazole. Pfizer produce the drug sildenafil on a huge scale and use CDIm for this reason. In the synthesis, the CDIm acylation reaction is performed concurrently with a nitro reduction and acid activation, greatly reducing solvent waste and the overall environmental impact.[16] The overall mechanism for the coupling of **3.4** with 7-nitroindole-2-carboxylic acid is shown below, Scheme 3.5, and was used to synthesise **3.5** in 73% yield.

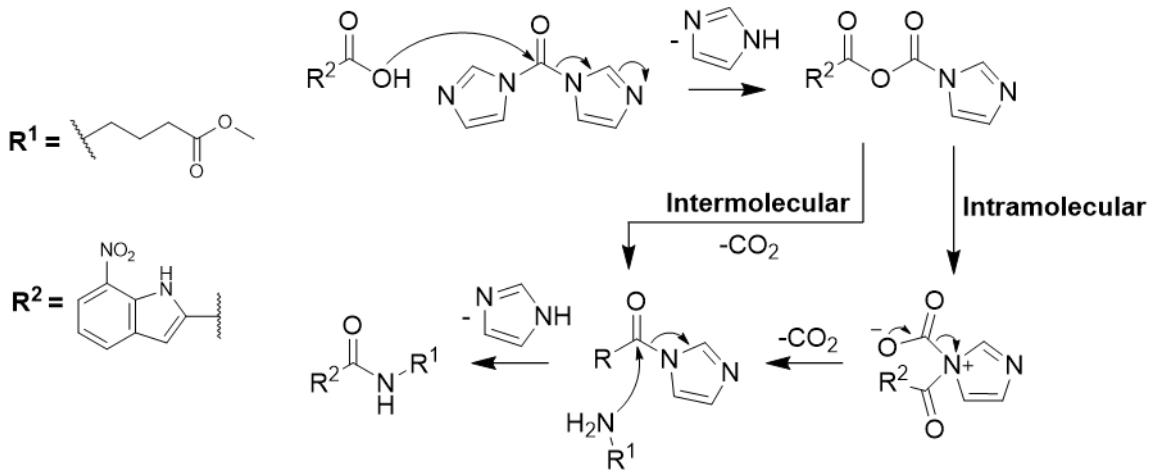

Scheme 3.5: Mechanism of CDIm coupling of 7-nitroindole-2-carboxylic acid and **3.4**.

The first step of the reaction is the reaction of CDIm and the carboxylic acid which forms the reactive acyl imidazole intermediate. The acyl imidazole has a reactivity that is

comparable to that of an acid chloride, however, is much easier to handle and can be isolated, if necessary. CDIm is readily hydrolysed to CO and imidazole, whilst the intermediate has been shown to be stable. In this step, the acidic proton is abstracted by the imidazole, creating a carboxylate that attacks the electrophilic carbonyl centre of CDIm. The acid anhydride derivative formed is attacked by a liberated imidazole- [1,2]-addition- followed by a [1,2]-elimination of CO_2 and imidazole. The release of CO_2 is the driving force of the reaction, and it has been proposed to have a catalytic effect on the rate of the reaction. In 2004, Vaidyanathan et al. postulated the released CO_2, reacts with the amine to produce an alkylammonium *N*-carbamate (Scheme 3.6), which could then proceed through two different acylation routes to yield the corresponding amide.[17]

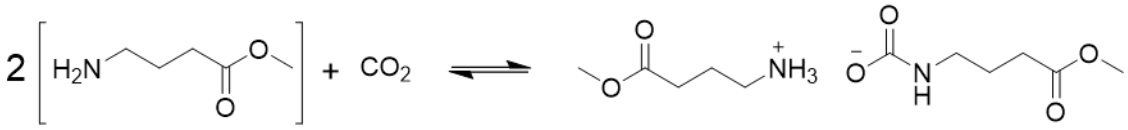

Scheme 3.6: Formation of the alkylammonium *N*-alkyl carbamate.

One proposed mechanism was the *O*-acylation, through the direct attack of the oxygen centre of the carbamate on the imidazolide. The resulting carbonic-carbamic anhydride intermediate can rearrange intermolecularly, releasing CO_2 and forming the desired amide. It was determined, through labelling studies, that the carbonyl present in the amide product, originates from the coupling reagent and not CO_2.[18] A second hypothesis is the *N*-acylation mechanism, through the tautomer of the carbamate, where the nitrogen centre reacts directly with the imidazolide, releasing CO_2 and imidazole and forming the amide directly, Scheme 3.7.

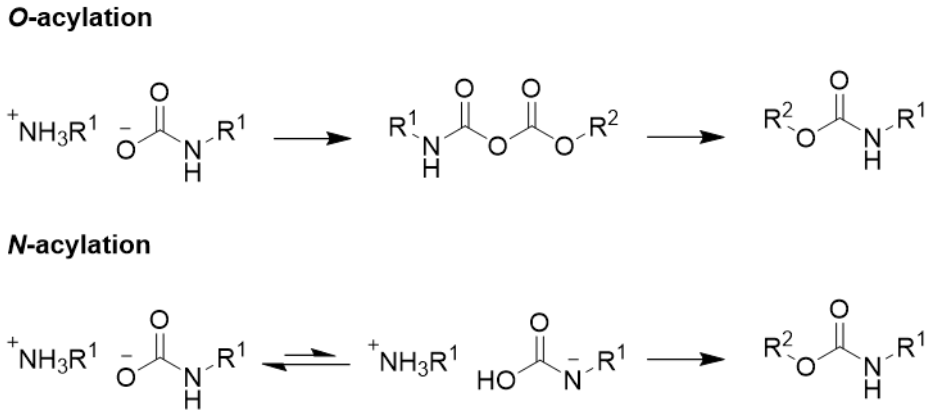

Scheme 3.7: *O*/*N*-acylation pathways for the amide formation from alkylammonium *N*-alkyl carbamate.

3.2.3 Reduction of nitro moiety using Pd/C

Palladium on carbon (Pd/C) has proven to be a highly efficient method for the reduction of nitro groups to amines. Amines are used heavily in the production of pharmaceuticals, dyes and agrochemicals.[19] The reduction of nitro groups is not limited to Pd/C, but can be carried out using other transition metals, like Ni and Pt[20] and electrochemically using a polyoxometalate catalyst mediator.[21] Over the years, mechanistic studies have been conducted in order to determine the species involved in the reduction of the nitro group to the amine. In general, the reduction can proceed through two routes- directly or via a condensation route. Neri and co-workers investigated the reduction of 2,4-dinitrotoluene over Pd/C.[19] Using both GC and HPLC, they determined that 4-hydroxylamine-2-nitrotoluene (4HA2T) decomposed to 4-amino-2-nitrotoluene, a highly reactive nitroso intermediate and 2,2'-dinitro-4,4'-azoxytoluene (DNAT) depending on the reaction conditions. Under ambient conditions, like in HPLC, DNAT is preferentially formed, whereas at the higher temperatures found in GC analysis, a mix of DNAT, the amine and the nitroso compounds were observed. Kinetic studies on the same compound showed that the reaction proceeded through three main intermediates: 4HA2T, 4-amino-2-nitrotoluene (4A2NT) and 2-amino-4-nitrotoluene (2A4NT). Under the conditions used, 283-323 K, 0.1 M dinitrotoluene and under H_2 pressure, the selectivity of the reaction was 65-80% 4HA2T, with the rest being comprised of 4A2NT and 2A4NT. The condensation product, DNAT, was not observed. Baron et al. have also shown that the direct pathway, proceeding through the hydroxylamine, is favoured over the condensation pathway when sonicated, Scheme 3.8.[20]

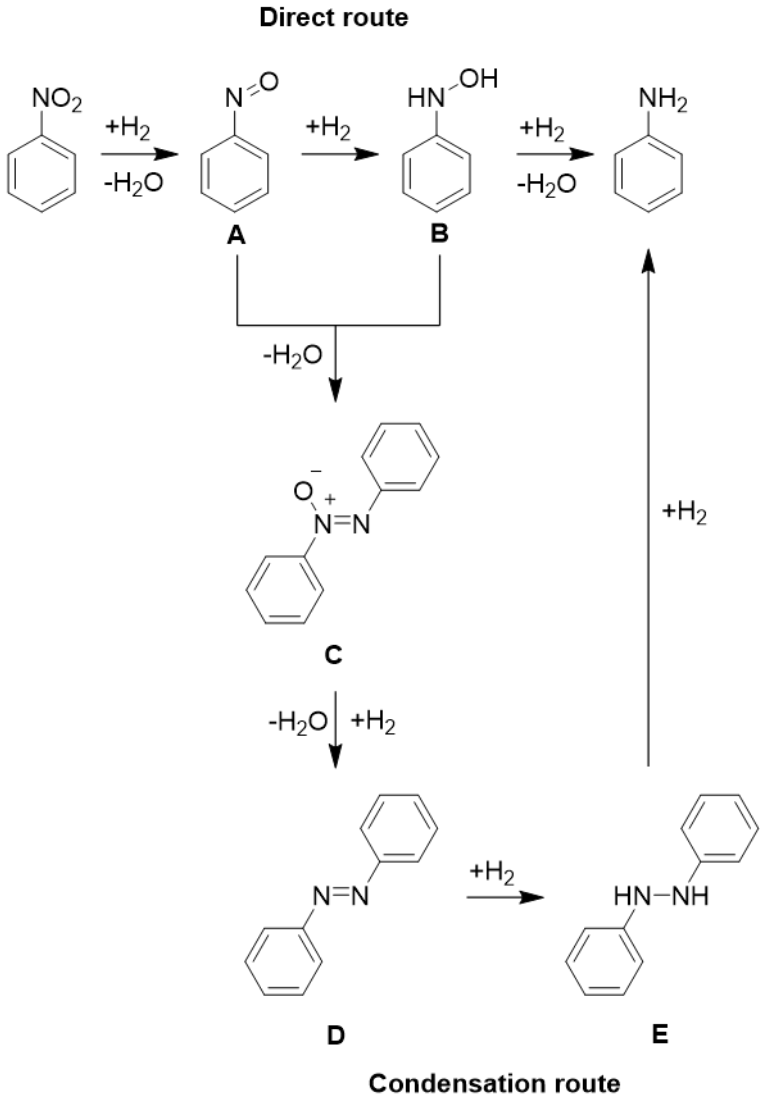

Scheme 3.8: Reduction of nitrobenzene via two alternative pathways; direct or condensation.

By performing reductive studies directly on the postulated intermediates in the reduction of nitrobenzene, Baron and co-workers showed that the direct reduction of nitrosobenzene (**A**) and phenylhydroxylamine (**B**), lead solely to the aniline being detected. The condensation intermediates: azoxybenzene (**C**), azobenzene (**D)** and hydrazobenzene (**E**) lead to trace amounts of aniline product being detected. The rate of reduction of the intermediates in the direct pathway, could explain why no intermediates for the condensation pathway were detected by either Neri or Baron.

Based on these studies, the reduction of methyl 4-(7-nitro-1*H*-indole-2-carboxamido)butanoate, **3.5**, to methyl 4-(7-amino-1H-indole-2-carboxamido)butanoate, **3.6**, can be postulated to proceed via the following direct route, Scheme 3.10. Compound

3.6 was obtained in 50% yield- the poor yield was thought to be the result of the Celite plug used to remove the Pd/C. It was postulated that some material becomes trapped within the Celite and is unable to be removed, even after excess flushing with both methanol and ethyl acetate. The same reaction mechanism can be applied to the reduction of nitro carbazole, compound **4.10**.- Chapter 4.3.1

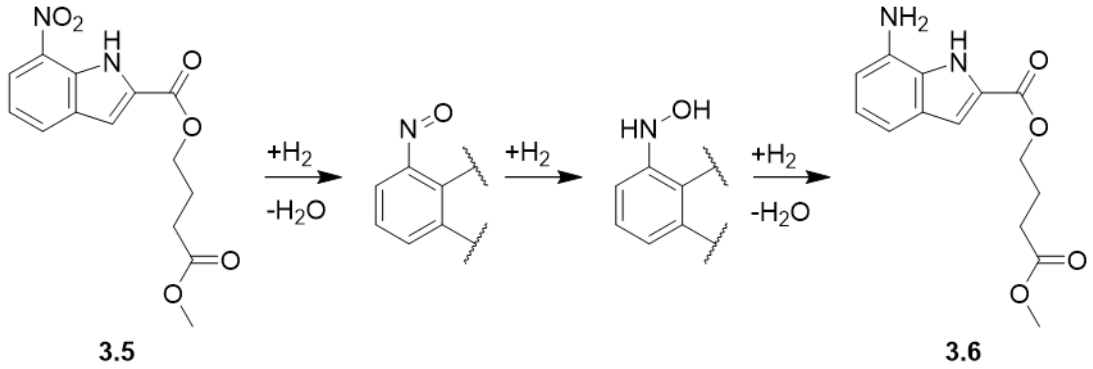

3.5 **3.6**

Scheme 3.9: Proposed route for the reduction of **3.5** using Pd/C.

3.2.4 Urea coupling- Triphosgene

Bis(trichloromethyl) carbonate, also known as triphosgene, is used heavily in research for phosgenation reactions due to its easier to handle physical state, low vapour pressure and availability, compared to gaseous phosgene.[22,23] The reaction of note, in this case, is the formation of a urea via an isocyanate group. The reaction of phosgene-based reagents is normally carried out in the presence of an amine base e.g., triethylamine, however the addition of such is not necessarily required. Charalambides and Moratti demonstrated that the addition of an amine base was not necessary, but in fact complicated the workup. They determined that the acid released only needed to be removed if the substrate of interest was acid sensitive.[23] In section 3.2.1 it was shown that the reaction of an acyl chloride and an amine could be used to produce amides. Scheme 3.10 shows how phosgene, acting as an acyl chloride, reacts with an amine to form a chloroformamide intermediate, which rearranges to the isocyanate, releasing HCl.[24]

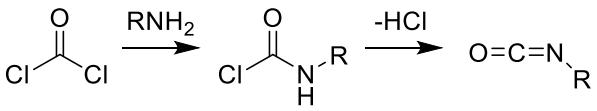

Scheme 3:10: Formation of isocyanate group.

The amine base added removes the released HCl from the reaction mixture through the formation of an ammonium salt and aides in driving the reaction.

In the reaction of indole **3.6** (Scheme 3.11), no amine base was used. Instead, a biphasic solution of 1:1 DCM : Sat. $NaHCO_3$ was used. Such a system was used as the urea product formed is insoluble in both DCM and water, and the $NaHCO_3$ acts to remove the HCl released and prevent potential hydrolysis of the amide. Under these conditions, diindolylurea **3.7**, was obtained in 81% yield.

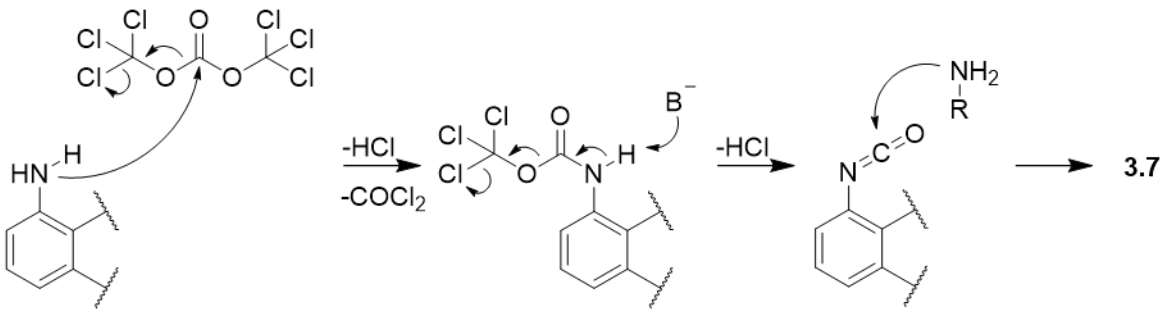

$COCl_2$ Pathway

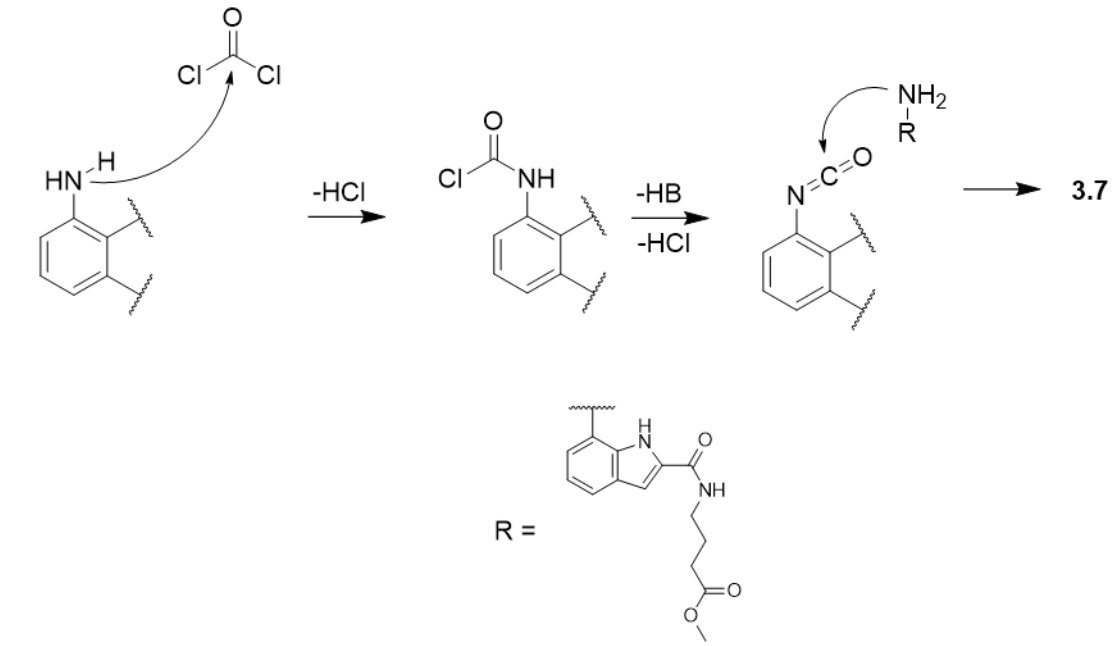

Scheme 3.11: Mechanism of the synthesis of **3.7** using triphosgene.

In the reaction, the amine acts as a nucleophile, attacking the electrophilic carbonyl centre of triphosgene, liberating HCl and phosgene. Unlike in the reaction of phosgene, the intermediate is a carbamate that rearranges to the isocyanate. This highly reactive isocyanate can then undergo nucleophilic addition at the carbonyl to form the desired urea product.

3.2.5 Methyl ester deprotection

The protection of reactive groups with protecting groups, such as methyl esters, allows and prevents the specific functionalisation of a compound during its synthesis. To this end, the methyl ester employed served as a protecting group in order to halt competing side reactions, but concurrently increased the hydrophobicity of the starting material, improving organic solubility. In order to remove the ester, acid or base hydrolysis can be employed however, acidic ester hydrolysis is reversible and would lead to a mix of both product and starting material. There are other ways to deprotect the esters, such as with Me_3SnOH but in this example, the mild and less toxic nature of base hydrolysis, with sodium hydroxide, was preferred, Scheme 3.12.[25,26]

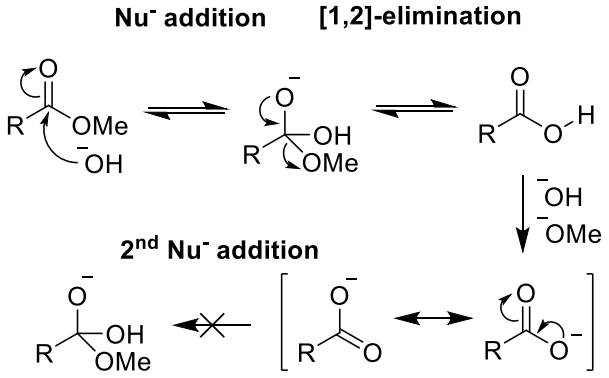

Scheme 3.12: Mechanism for the basic hydrolysis of methyl esters.

The mechanism proceeds firstly, through the nucleophilic attack of the hydroxyl anion on the electrophilic carbonyl centre, leading to a tetrahedral alkoxide intermediate. This intermediate rearranges to eliminate the alkoxide anion, which subsequently abstracts a proton from the carboxylic acid to form the corresponding conjugate acid and base, alcohol and carboxylate, respectively. The formation of the carboxylate, which is less electrophilic than the carboxylic acid, ensures that the alkoxide nucleophile released cannot react at the carbonyl centre.

In the case of the indole deprotection of **3.7**, no product could be obtained or was detected. As the mechanism detailed, the carboxylate is formed and must be protonated in order to obtain the carboxylic acid product. During the acidic workup and extraction, it was postulated that the indole was protonated and could switch from the organic to aqueous phase. Less acidic-more basic workup had a similar effect on the carboxylic acid, whereby deprotonation occurred, and the product could now interact more effectively in the aqueous phase. The resulting gloopy suspension meant that no useable product could be effectively obtained, and alternative methods were investigated. A method was proposed whereby the crude sodium carboxylate of **3.7**, was transformed directly into the reactive acid chloride, **3.9**, directly,[27] Scheme 3.13, using oxalyl chloride, however this was unsuccessful.

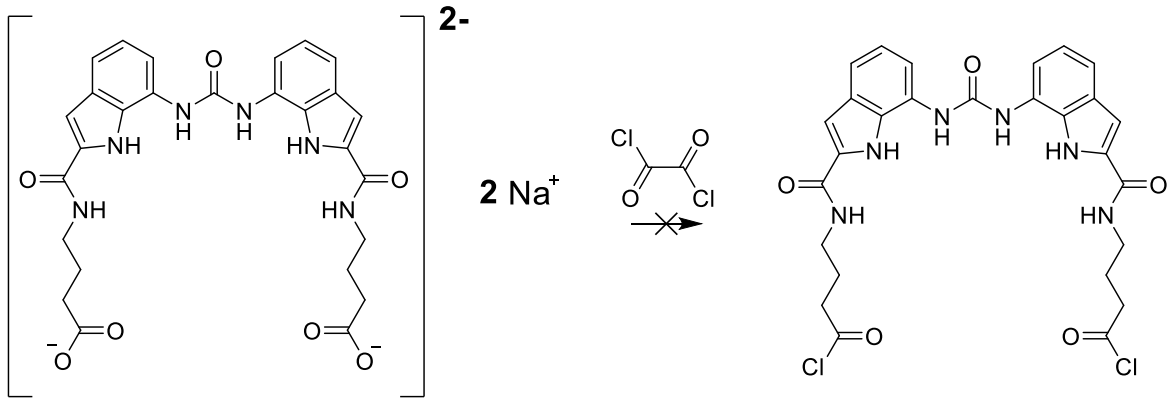

Scheme 3.13: Direct conversion of sodium carboxylate of **3.7** to **3.9** using oxalyl chloride.

3.3 Revised Reaction Scheme

Considering this, the reaction synthesis, in particular, the anchor point for the electrode attachment, was modified. Scheme 3.14 shows that an alkyne starting material was used in place of a carboxylic acid. Alkynes have been shown to be suitable substrates for oxidative electrode modification, and it was proposed that a receptor with a terminal butyl alkyne would allow for flexibility at the point of attachment.[28,29]

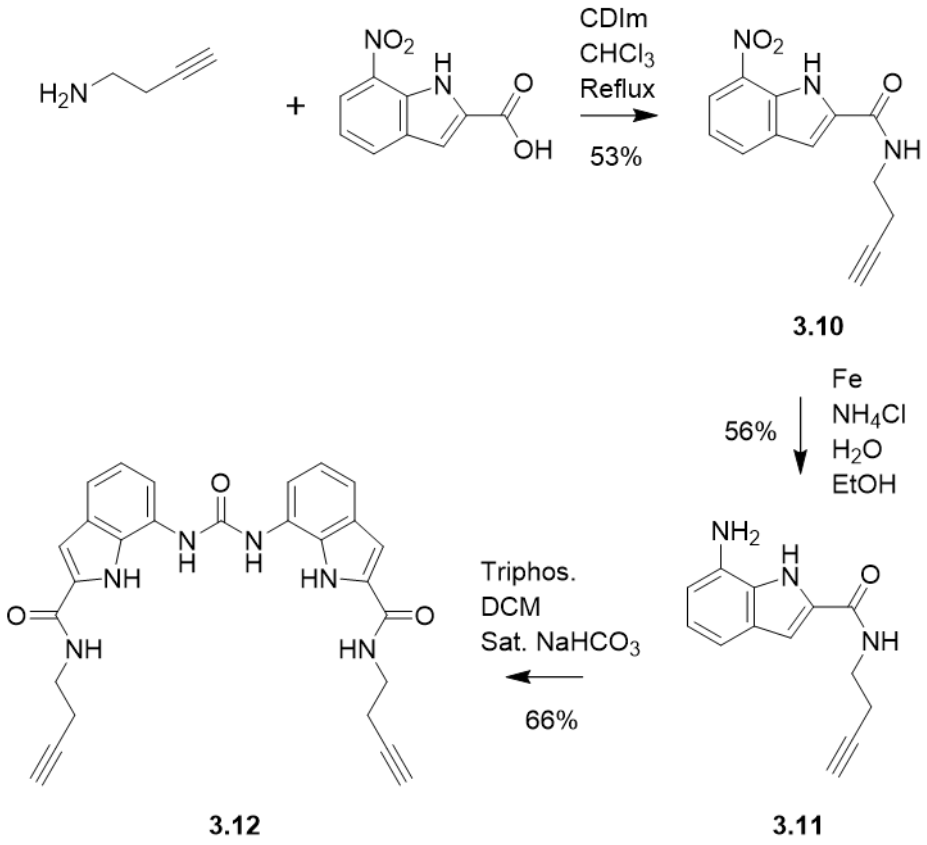

Scheme 3.14: Modified reaction scheme incorporating alkyne moiety.

The modified synthetic route remained like the original one, with only the method of reduction of the nitro group changing. This was necessary as hydrogenation over Pd/C would also cause the reduction of the alkyne group and remove the functional handle for electrode attachment.

3.3.1 Reduction of the nitro moiety- Béchamp reduction

In 1854, Antoine Béchamp first described his methodology for the reduction of nitroarenes to aryl amines using iron and aqueous acid.[30] Unlike other methods for the reduction of nitroarenes which can often stop at the intermediate stages, the Béchamp reduction has been shown to be highly selective for the aryl amine at the cost of overall reaction rate.[31] As a result of this, the large-scale industrial use of the Béchamp reduction has largely been replaced with catalytic hydrogenation, however it is still useful on a batch scale for the production of iron oxides for pigments and also avoids problems such as catalyst impurities and regeneration.[32]

The proposed mechanism is shown in Scheme 3.15.

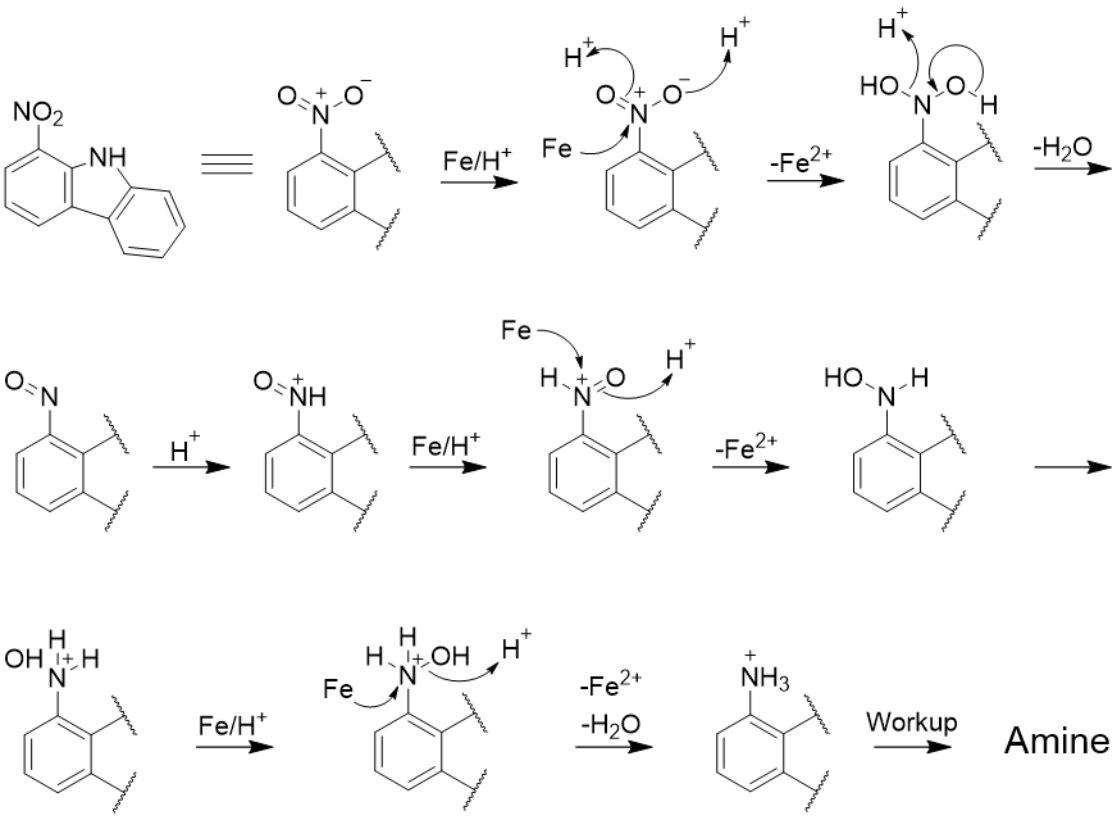

Scheme 3.15: Proposed mechanism for the Béchamp reduction of nitro groups.

In the proposed mechanism, Fe is oxidised to Fe^{2+} with the concomitant reduction of the nitro group to the dihydroxylamine intermediate. This rearranges to the to the nitroso intermediate, through the release of water. Under the acidic conditions, this nitroso group can be protonated, leading to a second redox reaction between Fe and the N-centre. The basic hydroxylamine then undergoes a second protonation, yielding a hydroxylammonium intermediate, that is rapidly reduced by Fe releasing a molecule of water and yields an ammonium product. The desired reduced (amine) product can be obtained through basic workup. The Béchamp reduction was used to synthesise **3.11** with a reasonable yield of 56%.

Once synthesised, compound **3.11** was coupled using triphosgene to successfully synthesise **3.12** with a yield of 66%. The mechanism for the formation of the central urea moiety is analogous to that in Section 3.2.4.

3.4 ^{1}H NMR Titrations of TBA·H_2PO_4

Binding studies of receptor **3.12** were conducted in d_6-DMSO/0.5% H_2O solutions and the NH- proton shifts observed. $H_2PO_4^-$ was added as its TBA salt. By following the downfield shift of the urea, amide and indole proton, the binding constant for the receptor could be determined. Hiscock et al. reported two different processes occurring on the NMR timescale when $H_2PO_4^-$ was added- a fast and slow process.[10] They showed that the first fast process occurred when 0-1 equivalent of anion was added and that a second, slow event on the NMR timescale occurred when more than 1.0 equivalents of anion were added. In their studies, they show that there is a steady downfield shift in the NH-protons involved in the binding of the anion by the receptor. The second slower event that occurred when anion equivalents exceeded 1.0, caused even larger downfield shifts of the binding protons to be observed- in some cases as much as 2.5 ppm (from the signal after 1.0 equiv. added). It was subsequently postulated that this may be the result of deprotonation. Such a large downfield shift would likely be the result of a change of the binding species involved to one that has an even higher affinity for the receptor. The evolution of the receptor, to one that contains six acidic H-bonding sites, was thought to effectively modulate the pK_a of the bound anion, lowering it sufficiently and causing deprotonation by the more basic free anion. The change from a bound monobasic anion to a dibasic one would cause the large downfield shift that was observed. From Figure 3.2, it can be seen that as the concentration of the guest anion increases, the NH-groups involved in the binding of the anion, begin to shift downfield. This occurred through an initial disappearance of the signals before the emergence of new downfield shifted signals.

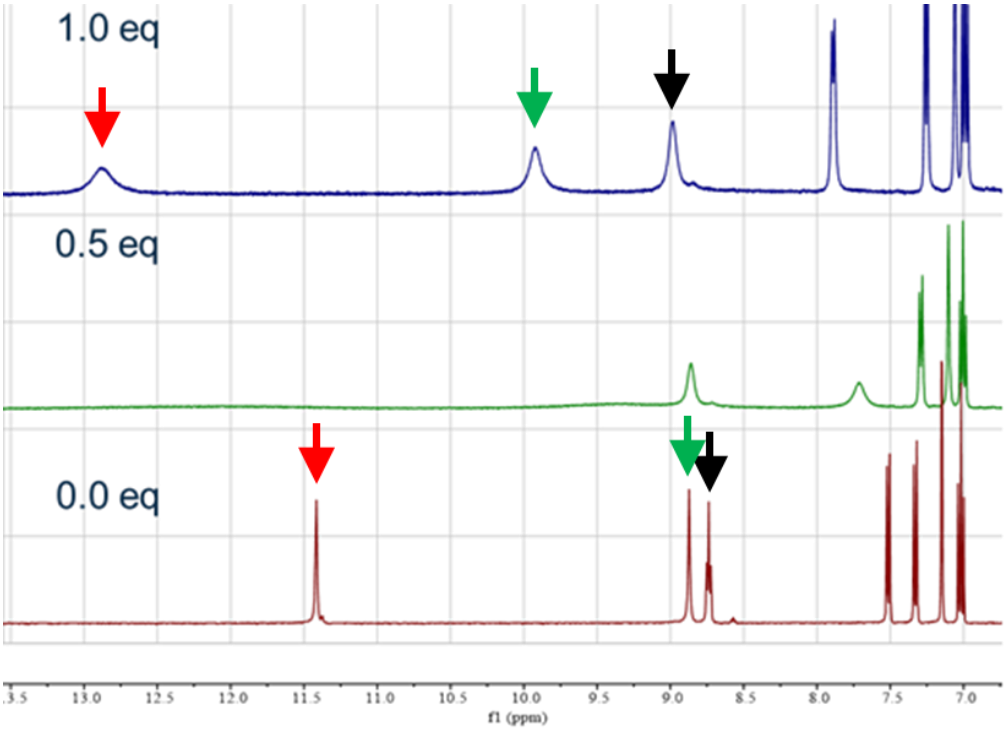

Figure 3.2: ^{1}H NMR spectroscopic titrations of receptor **3.12**, with TBA.H_2PO_4 from 0.0-1.0 equivalents (Arrow Red = Indole; Green = Urea; Black = Amide).

Figure 3.3 shows a proposed binding mode whereby six hydrogen bonds are formed to the anion in the receptor cavity. The H-bond donating groups can be seen shift in the NMR spectra, with the largest observed shift is seen for the NH-indole proton which is shifted downfield by roughly 1.4 ppm (Figure 3.4).

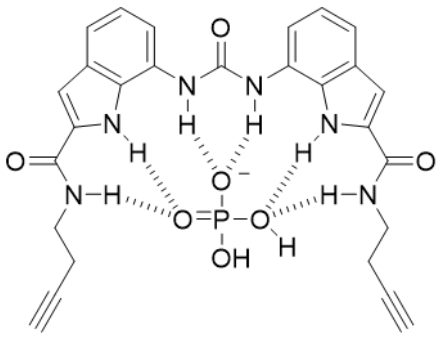

Figure 3.3: Proposed binding mode of **3.12** with $H_2PO_4^-$.

Simultaneously, a relatively large shift is seen for the NH-urea protons and to a lesser extent the NH-amide protons; these are shifted roughly by just over 1.0 and 0.2 ppm, respectively. The mole ratio method can be used to interpret the obtained graph and from analysis of the indole and urea shifts, it can be seen that the largest change in gradient-the break point- is centred on around 1.0 added equivalents, implying a 1:1 binding stoichiometry. The amide protons show no such trend.

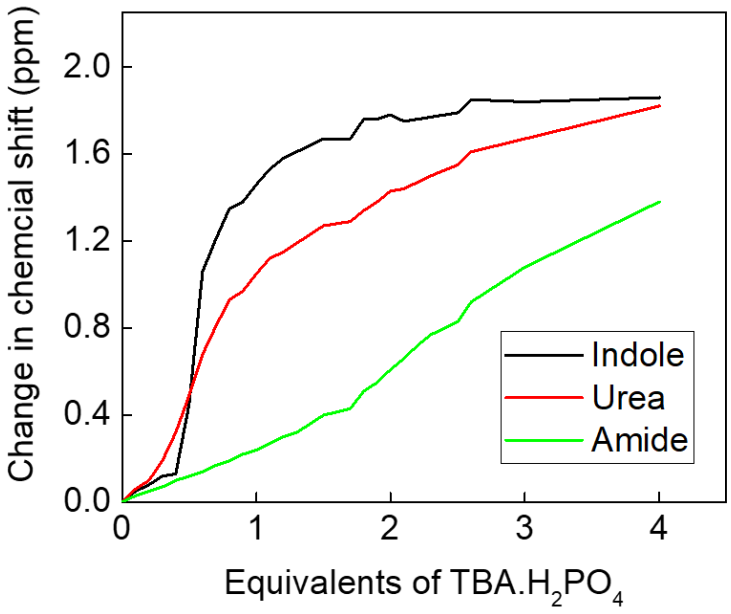

Figure 3.4: Change in the ^{1}H NMR shifts of the NH protons of **3.12** involved in the binding to $H_2PO_4^-$.

The potential for deprotonation was investigated by the continued addition of TBA.H_2PO_4 into the sample, up to 4 equiv. of anion added. From Figure 3.2 it can be seen that deprotonation of the anion did not occur- no further new downfield resonances are observed upon the addition of excess dihydrogenphosphate, as described by Hiscock et. al. Subsequently, it can be postulated that the anion bound by the receptor is the monobasic species. Fitting the obtained date to the Bindfit software generated an association constant for the complexation event. Fitting to a simple 1:1 binding model, as determined from Figure 3.4, gave a K_a = 235.96 M^{-1} ± 14.1829% for a mixed d_6-DMSO/0.5% H_2O solvent system at 298 K. This is substantially lower than expected but shows that there is a binding event occurring. Fitting to 2:1 and 1:2 binding mode also yielded association constants, however the error associated with these was incredibly large and as such it is likely the incorrect binding model (Chapter 7- Appendix).

3.5 Conclusions and Future Work

The neutral H-bonding receptor, **3.12**, was successfully synthesised modifying the original route proposed by Hiscock et al. In order to create a receptor that contained the desired anchor point, one of the starting materials, *N*-butylamine needed to be changed. The proposed substitute, γ-aminobutyric acid, was used as it was postulated that the carboxylic acid moiety could be further used to either 1) create and amide bond to the GCE surface (via

an already bound organic spacer group) using a coupling reagent; or 2) be further functionalised to the highly reactive acid chloride and subsequently make an amide bond. Over the course of our investigations, it was shown that the presence of the methyl ester protecting group caused workup issues- protonation of the indole during the deprotection- led to the need for an alternative synthetic route to be proposed. Replacing γ-aminobutyric acid with 1-amino-3-butyne, eliminated the need for a protecting group entirely and simplified the overall synthesis. Receptor **3.12** was synthesised with an overall yield of 20%. Following the successful synthesis of **3.12**, the affinity for $H_2PO_4^-$ was investigated through a series of ^{1}H-NMR titrations. It was seen that as the concentration of anion increased- up to 1.0 equivalent- the shifts of the NH-protons involved were shifted downfield, indicating an interaction with the receptor. Hiscock et al. reported a second binding event that was slow on the NMR timescale and related to the deprotonation of the bound guest. Further titration of **3.12** with $H_2PO_4^-$, showed no such deprotonation. The shifted signals corresponding to the indole, urea and amide did not disappear and move any further downfield. Consequently, it is likely that the $H_2PO_4^-$ anion is bound in the monobasic form. In order to fully confirm whether deprotonation does occur when the anion is bound, ^{1}H NMR titrations could be carried out with TBA·OH. By adding in HO^-, it is possible to determine the species being effectively deprotonated. It was shown by Hiscock and co-workers that at over 1.0 equivalent of anion added, the second slow process was seen. By adding in basic HO^-, when the equivalents of anion are greater than 1.0, it should be possible to see if the bound anion is deprotonated or not. This would confirm whether in the capacitive deionisation system to be used, the basicity of the phosphate species is sufficient to cause the deprotonation of the receptor. The difference in the valence of the phosphate species would have a substantial impact on the K_a of the interaction. The increased electrostatic charge of the dibasic anion means that there would be increased polarisation of the receptor compared to that of the monobasic form, which may lead to the need for a more positive regeneration potential. This shows that there is both an electrostatic and H-bonding component to the association of the guest and the receptor-host, and that by tuning the acidity of the receptor, you can design in favourable electrostatic interactions that increase the strength of the hydrogen bonding. The deprotonation of the bare receptor would also need to be investigated to confirm that any deprotonation that may occur is the anion. This could be elucidated through any changes to the integration of the proton signals and through visual confirmation of the ^{1}H NMR spectra.

^{1}H NMR titrations of other TBA salts of other anions would also give insight into the affinity of the receptor for other species. By following the same method as described above.

In order to be employed within a CDI system, the electrode surface must be modified with the receptor species. Chapter 5 demonstrated that an organic nitrophenyl could be successfully covalently bound to the GCE surface and subsequently reduced electrochemically to the aniline species (Scheme 3.16).

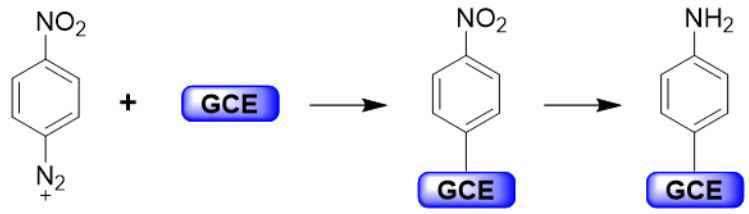

Scheme 3.16: Overall reaction for the covalent attachment and functionalisation of 4-nitrobenzene diazonium salt.

Receptor **3.12** contains a terminal alkyne, and it was postulated that it could be attached to the surface via 'Click chemistry'. Since its inception by Sharpless et al., 'Click chemistry' has become one of the primary methods for the functionalisation of pharmaceutical building blocks.[33] In his initial review on 'Click chemistry' Sharpless and co-workers laid out a stringent set of rules that the reaction must follow in order for it to be deemed a 'Click' reaction. They state the reaction must be:

"modular, wide in scope, give very high yields, generate only inoffensive byproducts that can be removed by nonchromatographic methods and be stereospecific (but not necessarily enantioselective)"

They go on further to state the reaction conditions needed should be increasingly mild, utilising readily available starting materials and reagents that are insensitive to water and oxygen and require the use of no solvent. Should a solvent be required, it must be benign, such as water, or easily removed. The purification of the product, if needed, must be done by using crystallisation, distillation or some other nonchromatographic method. Click reactions also tend to share of lot the following attributes:[33,34]

1. *A large percentage of reagents used in click chemistry contain alkene or alkyne groups. The use of carbon-carbon multiple bond groups is exploited in click reactions, both mechanistically and energetically.*
2. *Most click reactions are highly exothermic as a direct consequence of the stability of the product or the energetic nature of the starting reagents.*

3. *Click reactions tend to be fusion processes, leading to no byproducts, or condensation reactions, liberating only water.*
4. *Click reactions tend to form carbon-heteroatom bonds, especially C-O, C-N and C-S.*
5. *A large percentage of click reactions are tolerant to the presence of water and in some cases, water can accelerate the reaction.*

Click reactions can also be further broken down into different classes of reactions such as:[35]

1. *Nucleophilic ring openings; strained heterocyclic electrophilic systems, such as epoxides, aziridines etc.*
2. *Carbonyl chemistry of the non-aldol type; these reactions include the synthesis of ureas and thioureas, amides and hydrazones, to name a few. Aldol type carbonyl reactions tend to be less thermodynamically favourable, increasing reaction time and leading to the formation of byproducts, therefore they cannot be thought of as a click reaction.*
3. *Additions to carbon-carbon multiple bonds; reactions can include epoxidations, dihydroxylations and nitrosyl halide additions.*
4. *Cycloadditions: can include hetero-Diels-Alder cycloaddition, but primarily relates to [1,3]-dipolar cycloadditions i.e., Huisgen 1,3- dipolar cycloaddition.*

Of particular interest in this case, is the Huisgen 1,3-dipolar cycloaddition (HDC). This reaction is the 'quintessential' click chemistry reaction and leads to the formation of 1,2,3-triazole products. The Cu^{I}-catalysed HDC reaction involves the cycloaddition of an azide and terminal alkyne and fulfils all the required criteria needed in order to be designated a click reaction. The reaction leads to the formation of a regiospecific 1,4-substituted products. The reaction is easy to perform and can be carried out at elevated temperatures, however heating is not always required, can be performed between pH 5-12, is easy to purify and has an increased reaction rate, 10^7, compared to the analogous uncatalyzed reaction. In addition to this, azides and terminal alkynes are easy to install and are stable under the conditions of the reaction. Thermodynamically azides have been shown to be prone to decomposition, but under these conditions they are shown to be stable and remain 'invisible'- they remain unreactive under the reaction unless in the presence of a dipolarophile, such as an alkyne. Generally, 1,3-cycloaddtions can be thought of as proceeding through a concerted mechanism, Scheme 3.17a.[36] However, in contrast to this, Firestone proposed that the actual mechanism proceeded through a spin-paired diradical, Scheme 18b.[37] The latter spin-paired

mechanism was discredited by Huisgen, who suggested that the energy barriers associated with the stepwise mechanism were incorrect. Firestone's diradical intermediate must be in the correct confirmation in order to cyclise otherwise it would revert to the starting material. This would require a change in hybridisation at the A and D positions and significant stretching of the A-D bond.[38] Consequently, the concerted theory has been adopted as the preferred mechanism for the formation.

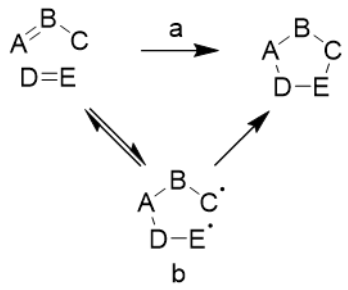

Scheme 3.17: a) concerted Huisgen 1,3-cycloaddition; b) Firestone spin-paired diradical cycloaddition.

Mechanistically, Cu^{I} has been shown to readily insert itself into terminal alkynes e.g., the Sonogashira coupling.[39] Scheme 3.18 details one such way that the triazole product may be formed. Initially, a Cu^{I} dimer forms a π-complex with the alkyne (**I**). The coordination of Cu^{I} drastically lowers the pH of the terminal hydrogen, allowing for the facile deprotonation in aqueous media, without the addition of base, and makes the Cu-acetylide (**II**). The Cu-acetylide formed can then coordinate to the N(1) position of the azide through the second Cu of the dimer. This 'activated' azide species can then attack the electrophilic C(4) centre through the lone pair of the nucleophilic N(3) (**III**). Through a second subsequent nucleophilic attack of N(1) at the C(5) position, a Cu-triazole, 1,4-substituted intermediate (**IV**) is formed. Finally, protonation of this intermediate by an external source i.e., protonated solvent, releases the Cu^{I} catalyst and the final triazole product, **V**.[35] Alternatively, the electron rich alkyne can attack the N(3) position, (**VI**), leading to the formation of metallocycle **VII** (Ligands have been omitted for clarity). Nucleophilic attack of N(1) at the C(5) position gives intermediate **IV** and subsequent elimination of the copper catalyst yields triazole product **V.**[40]

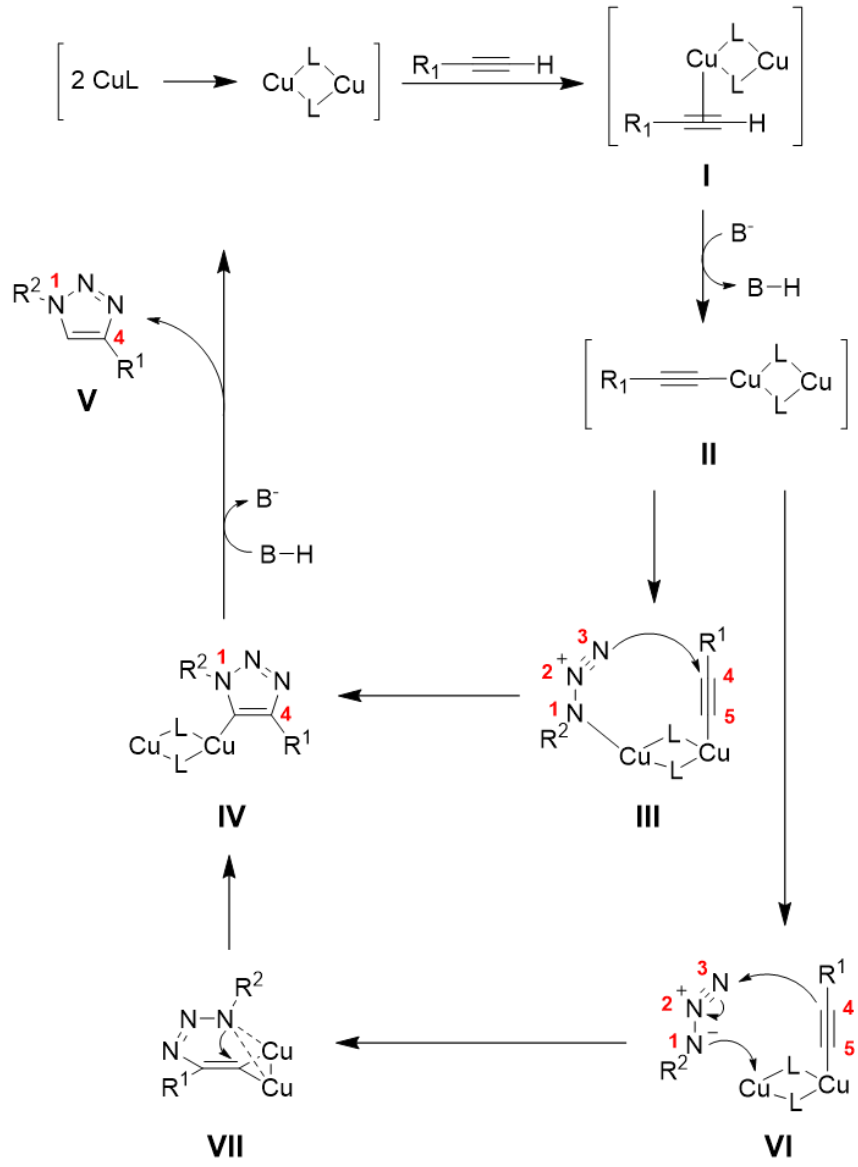

Scheme 3.18: Potential mechanisms of triazole product formation in a Click reaction.

Chapter 5 shows that it is possible to bind an organic nitrophenyl group to an electrode and subsequently reduce the nitro moiety electrochemically. In order to perform the aforementioned click reaction, the free surface bound amine must be transformed into an azide. Mangione and co-workers have shown that it is possible to convert aniline into phenyl azide using sodium nitrite and sodium azide under acidic conditions at 0°C.[41] Once the electrode surface has been fully functionalised, it should be possible to attach receptor **3.12** to the electrode surface and begin to test for functionality in the desired CDI system. Scheme 3.19 details the overall electrode attachment of **3.12** through the triazole linkage.

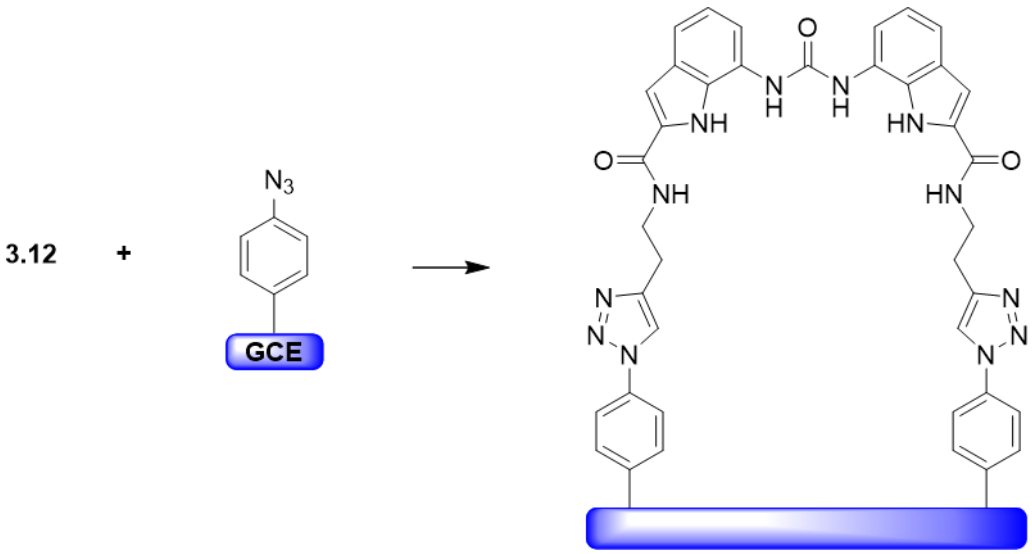

Scheme 3.19: Overall reaction for the Click attachment of **3.12** via a surface bound azide.

3.6 Experimental

3.6.1 Materials and reagents

All chemicals were of analytical reagent grade from Sigma-Aldrich/Merck, Alfa Aesar or Fluorochem and required no further purification.

3.6.2 General synthetic methods

^{1}H NMR spectra were recorded on a Bruker DPX-400 (400 MHz) instrument. The chemical shifts are expressed in parts per million (ppm) referenced to TMS. Data are reported as follows: δ, chemical shift, multiplicity (recorded as b, broad; s, singlet; d, doublet; t, triplet; q, quartet; m, multiplet), coupling constants (J in Hertz, Hz), integration and assignment.

^{13}C NMR spectra were recorded on the same instrument at 100 MHz. The chemical shifts are expressed in parts per million (ppm), proton decoupled and referenced to TMS. Assignments were obtained from 2D-DEPT experiments.

Where applicable, reported NMR data agree with previously reported literature values.

3.6.2.1 NMR Analysis

Synthesis of methyl 4-aminobutanoate hydrochloride (3.4)[42]

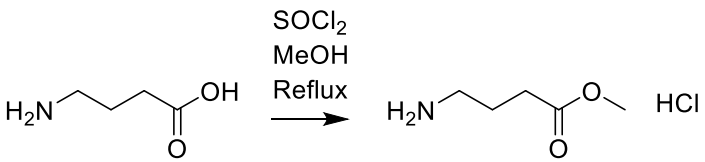

3.4

Thionyl chloride (21.2 mL, 291 mmol) was added dropwise to a stirring solution of γ-aminobutyric acid (10 g, 97.0 mmol) in methanol (39.5 mL) at 0 °C. The resulting solution was then heated to reflux overnight. Volatiles and thionyl chloride removed under reduced pressure. The product was obtained as a white solid (14.81 g, 96.4 mmol, 99%).

^{1}H NMR (400 MHz, $CDCl_3$) δ 3.69 (bs, 3H), 3.15 (bs, 2H), 2.54 (bs, 2H), 2.13 (bs, 2H).

^{13}C NMR (101 MHz, $CDCl_3$) δ 173.2 (CO), 52.0 (CH_3), 41.7 (CH_2), 31.1 (CH_2), 22.8 (CH_2).

Synthesis of methyl 4-(7-nitro-1H-indole-2carboxamido)butanoate (3.5)[10]

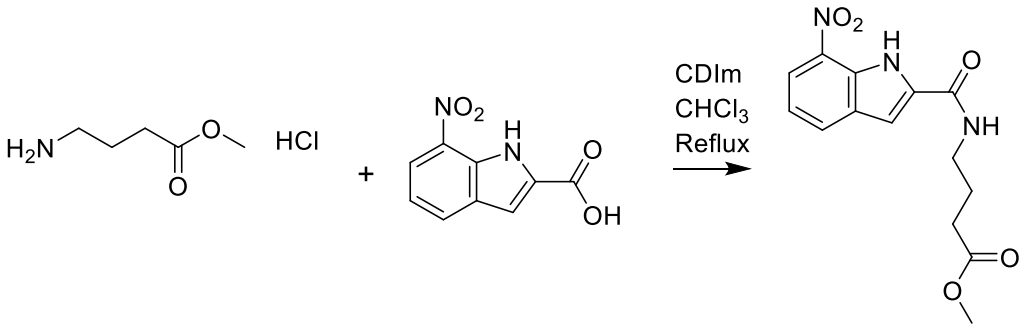

3.5

7-Nitroindole-2-carboxylic acid (1.57 g, 7.28 mmol) and 1,1'-carbonyldiimidazole (2.36 g, 14.6 mmol) were refluxed in $CHCl_3$ (150 mL) for 2 h. Once cooled, the solution was washed with H_2O (2 × 75 mL) and dried over anhydrous MgSO4 and the solid residue filtered off. Most of the solvent was removed under reduced pressure- leaving roughly 30 mL solution. A solution of methyl 4-aminobutanoate hydrochloride (**3.4**) (6.20 g, 40.5 mmol) in $CHCl_3$ (20 mL) was added and the combined solutions were refluxed for 12 h. The solution was allowed to cool, washed with H_2O (3 × 50 mL), dried over $MgSO_4$, filtered, and concentrated under reduced pressure. The product was obtained as a viscous brown oil (1.46 g, 4.45 mmol, 73%).

^{1}H NMR (400 MHz, $CDCl_3$) δ 10.50 (s, 1H), 8.24 (dd, *J* = 8.0, 0.8 Hz, 1H), 8.00 (d, *J* = 7.8 Hz, 1H), 7.22-7.24 (m, 0.80H), 7.02 (d, *J* = 2.2 Hz, 1H), 6.94-7.00 (m, 1H), 3.69 (s, 3H), 3.54-3.60 (m, 2H), 2.51 (t, *J* = 6.7 Hz 2H), 1.97-2.04 (m, 2H).

^{13}C NMR (101 MHz, $CDCl_3$) δ 174.8 (CO), 160.7 (CO), 133.6 (ArC), 133.5 (ArC), 131.5 (ArC), 130.3 (ArCH), 129.4 (ArC), 121.5 (ArCH), 120.1 (ArCH), 103.6 (ArCH), 52.1 (CH_3), 39.8 (CH_2), 32.0 (CH_2), 24.3 (CH_2).

HRMS *m/z*: 328.0901 $[M+Na]^+$ Calculated 328.0898 $[M+Na]^+$; **FTIR (cm^{-1}):** 3431, 1654.

Synthesis of methyl 4-(7-amino-*1H*-indole-2carboxamido)butanoate (3.6)[10]

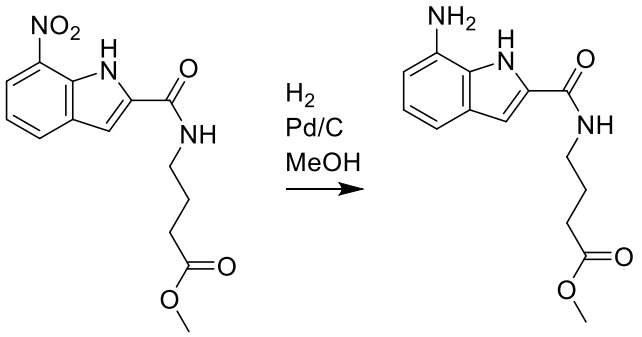

3.6

Methyl 4-(7-nitro-*1H*-indole-2carboxamido)butanoate (**3.5**) (3.40 g, 14.4 mmol) and Pd/C (0.35 g) was added to a stirring solution of dry MeOH (120 mL) at room temperature. H_2 gas, contained within balloons, was initially bubbled through the solution for 30 min before being stirred under a H_2 atmosphere for a further 12 h. The resulting solution was filtered over Celite and activated charcoal to remove the Pd/C. Excess methanol and ethyl acetate was used to flush any remaining organic compounds through. The volatile solvents were removed under reduced pressure to yield a purple solid (3.51 g, 11.8 mmol, 89%).

^{1}H NMR (400 MHz, d_6-DMSO) δ 11.43 (s, 1H), 8.57 (t, *J* = 5.6 Hz, 1H), 7.13 (d, *J* = 7.9 Hz, 1H), 7.10 (d, *J* = 2.0 Hz, 1H), 6.87-6.92 (m, 1H), 6.69 (d, *J* = 7.3 Hz, 1H), 3.53-3.61 (m, 4H), 3.21-3.35 (m, 3H) 2.39 (t, *J* = 7.4 Hz, 2H), 1.76 – 1.85 (m, 2H)

^{13}C NMR (101 MHz, d_6-DMSO) δ 173.1 (CO), 161.0 (CO), 131.5 (ArC), 128.4 (ArC), 127.4 (ArC), 121.0 (ArC), 120.6 (ArCH), 113.8 (ArCH), 110.2 (ArCH), 102.8 (ArCH), 51.2 (CH_3), 38.1 (CH_2), 30.7 (CH_2), 24.6 (CH_2).

HRMS *m/z*: 298.1161 $[M+Na]^+$ Calculated 298.1198 $[M+Na]^+$; **FTIR (cm^{-1}):** 3433, 1733, 1652.

Synthesis of Methyl 4-(((7-(((2-((4-methoxy-4-oxobutyl)carbamoyl)-*1H*-indol-7-yl)carbamoyl)amino)-*1H*-indol-2-yl)carbonyl)amino)butanoate (3.7)[10]

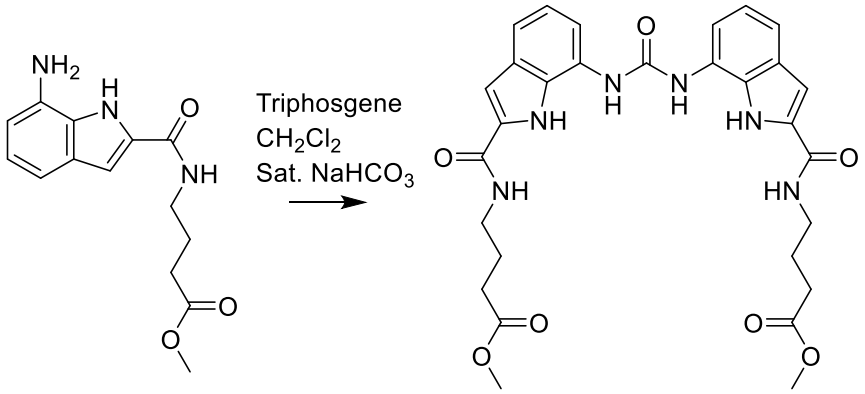

3.7

Methyl 4-(7-amino-*1H*-indole-2carboxamido)butanoate (**3.6**) (0.260 g, 0.94 mmol) was dissolved in a two-phase (1:1) solution of CH_2Cl_2 and $NaHCO_3$ (40 mL each). The solution was stirred vigorously at room temperature and triphosgene (0.280 g, 1.09 mmol) added. The solution was stirred overnight at room temperature. The resulting two-phase solution was first filtered, and the precipitate sonicated in water for 30 min. The dispersed solid was collected by Buchner filtration and washed with excess CH_2Cl_2 and Et_2O and left to filter further until dry. The solid was collected and further dried under vacuum. Product obtained as a blue-grey solid (0.087g, 0.15 mmol, 32%).

^{1}H NMR (400 MHz, d_6-DMSO) δ 11.39 (s, 2H), 8.90 (s, 2H), 8.57 (t, *J* = 5.1 Hz, 2H), 7.53 (d, J = 7.2 Hz, 2H), 7.32 (d, J = 8.1 Hz, 2H), 7.15 (s, 2H), 6.98-7.05 (m, 2H), 3.59 (s, 6H), 2.40 (t, J = 7.2 Hz, 4H), 1.78-1.86 (m, 4H) (Signal for CH_2 masked by water peak in DMSO).

^{13}C NMR (101 MHz, d_6-DMSO) δ 173.2 (CO), 161.0 (CO), 153.1 (CO), 131.5 (ArC), 128.6 (ArC), 128.0 (ArC), 124.9 (ArC), 120.2 (ArCH), 116.0 (ArCH), 113.8 (ArCH), 102.9 (ArCH), 51.2 (CH_3), 38.1 (CH_2), 30.8 (CH_2), 24.6 (CH_2).

HRMS *m/z*: 599.2205 $[M+Na]^+$ Calculated 599.2198 $[M+Na]^+$; **FTIR (cm^{-1}):** 3294, 1731, 1631.

Synthesis of *N*-(but-3-yn-1-yl)-7-nitro-*1H*-indole-2-carboxamide (3.10)[10]

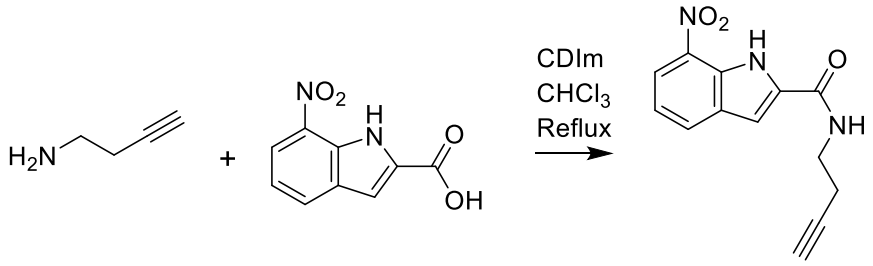

3.10

7-Nitroindole-2-carboxylic acid (0.373 g, 1.81 mmol) and 1,1'-carbonyldiimidazole (CDI) (0.590 g, 3.62 mmol) was refluxed in $CHCl_3$ (40 mL) for 2 h. Once cooled, solution was with H2O (2 × 75 mL), dried over $MgSO_4$, filtered and, volatiles partly removed under reduced pressure- leaving roughly 20 mL solution. Solution of but-3-yn-1-amine (0.500 g, 7.23 mmol) in $CHCl_3$ (20 mL) was added and the combined solutions were refluxed for 12 h. The solution was allowed to cool before being washed with H_2O (3 × 50 mL), dried over $MgSO_4$, filtered, and concentrated under reduced pressure. Product obtained as viscous brown oil (0.245 g, 0.95 mmol, 53%).

^{1}H NMR (400 MHz, $CDCl_3$) δ 10.51 (s, 1H), 8.28 (dd, *J* = 8.1, 0.9 Hz, 1H), 8.02 (d, J = 7.9 Hz, 1H), 7.27 (s, 0.51H), 7.25 (s, 0.25H), 7.00 (d, J = 2.3 Hz, 1H), 6.53 (bs, 1H), 3.66-3.70 (m, 2H), 2.54-2.60 (m, 2H), 2.09 (t, J = 2.6 Hz, 1H)

^{13}C NMR (101 MHz, d_6-DMSO) δ 159.5 (CO), 134.5 (ArC), 133.0 (ArC), 130.9 (ArC), 130.6 (ArCH), 128.7 (ArC), 121.1 (ArCH), 119.9 (ArCH), 106.4 (ArCH), 82.2 (C), 72.3 (CH), 38.1 (CH_2), 18.7 (CH_2).

HRMS *m/z*: 258.0879 $[M+H]^+$ Calculated 258.0878 $[M+H]^+$; **FTIR (cm^{-1}):** 3466, 3246, 1643, 1506.

Synthesis of 7-amino-N-(but-3-yn-1-yl)-1H-indole-2-carboxamide (3.11)[10]

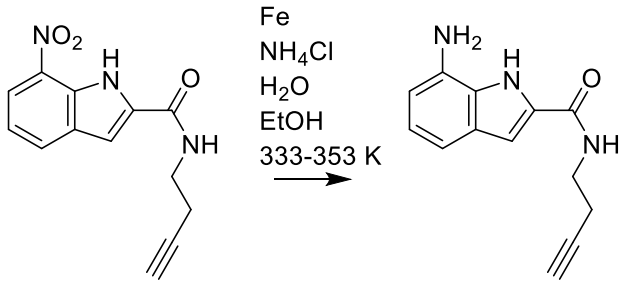

3.11

Iron powder (0.340 g, 5.98 mmol) and NH_4Cl (0.320 g, 5.98 mmol) were added to a 1:1 H_2O: EtOH solution and stirred at 60 °C for 0.5 h. *N*-(but-3-yn-1-yl)-7-nitro-*1H*-indole-2-carboxamide (**3.10**) (0.263 g, 0.92 mmol) was added to the stirred iron solution and the temperature was raised to 80 °C and stirred for a further 45 min. The reaction was cooled in an ice bath and basified, using 1 M NaOH, to around pH 12 and filtered over Celite to remove the iron powder. The resulting filtrate was concentrated under reduced pressure and the residue extracted with EtOAc (2 × 50 mL). The organic phase was separated and dried over $MgSO_4$. The solid was filtered off and the organic phase was concentrated under reduced pressure once more. The crude product was purified by column chromatography using 6:4 Petroleum ether: EtOAc. Product obtained as brown solid (0.118 g, 0.52 mmol, 56%).

^{1}H NMR (400 MHz, $CDCl_3$) δ 10.48 (s, 1H) 7.11 (d, J = 8.0 Hz, 1H), 6.95-7.00 (m, 1H), 6.88 (d, J = 2.2 Hz, 1H), 6.58-6.64 (m, 2H), 4.52 (s, 2H), 3.64-3.69 (m, 2H), 2.57 (td, J = 6.6, 2.6 Hz, 2H), 2.11 (t, J = 2.6 Hz, 1H)

^{13}C NMR (101 MHz, $CDCl_3$) δ 162.9 (CO), 133.1 (ArC), 129.8 (ArC), 128.7 (ArC), 128.0 (ArC), 121.9 (ArCH), 112.1 (ArCH), 108.8 (ArCH), 103.6 (ArCH), 81.2 (C), 71.0 (CH), 38.6 (CH_2), 19.8 (CH_2).

HRMS *m/z*: 228.1134 $[M+H]^+$ Calculated 228.1178 $[M+H]^+$; **FTIR (cm^{-1}):** 3393, 3350, 3287, 1628.

Synthesis of *N*-(but-3-yn-1-yl)-7-(((2-(but-3-yn-1-ylcarbamoyl)-*1H*-indol-7-yl)carbamoyl)amino)-*1H*-indole-2-carboxamide (3.12)[10]

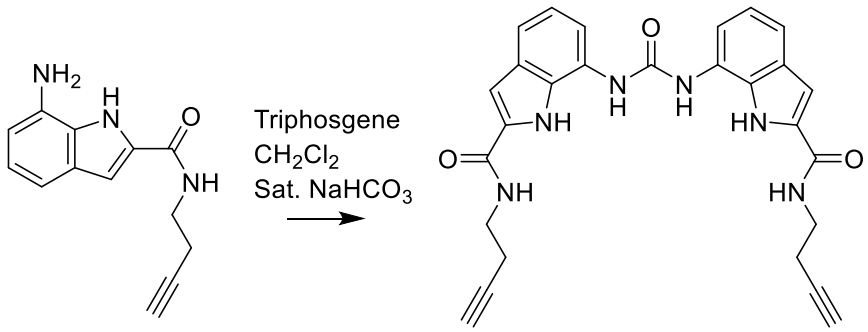

3.12

7-amino-N-(but-3-yn-1-yl)-1H-indole-2-carboxamide (**3.11**) (0.118 g, 0.52 mmol) was dissolved in a two-phase (1:1) solution of CH_2Cl_2 and $NaHCO_3$ (15 mL each). Solution stirred vigorously and triphosgene (0.172 g, 0.52 mmol) added and stirred overnight at room temperature. The two-phase solution was filtered, and the precipitate sonicated in water for 30 min. Solid was collected by filtration and washed with CH_2Cl_2. Product obtained as a grey solid (0.082g, 0.17 mmol, 66%).

^{1}H NMR (400 MHz, d_6-DMSO) δ 11.42 (s, 2H), 8.88 (s, 2H), 8.73 (t, J = 5.8 Hz, 2H), 7.52 (dd, *J* = 7.6, 0.6 Hz, 2H), 7.33 (d, J = 7.9 Hz, 2H), 7.15 (d, J = 2.0 Hz, 2H), 6.99-7.04 (m, 2H), 3.40-3.46 (m, 4H), 2.85 (t, J = 2.6 Hz, 2H), 2.46 (td, *J* = 7.2, 2.7 Hz, 4H).

^{13}C NMR (101 MHz, d_6-DMSO) δ 161.0 (CO), 153.1 (CO), 131.3 (ArC), 128.5 (ArC), 128.1 (ArC), 124.9 (ArC), 120.2 (ArCH), 116.0 (ArCH), 113.8 (ArCH), 103.3 (ArCH), 82.2 (C), 72.2 (CH), 38.1 (CH_2), 18.8 (CH_2).

HRMS *m/z*: 481.1987 $[M+H]^+$ Calculated 481.1978 $[M+H]^+$; **FTIR (cm^{-1}):** 3285, 1636, 1602.

3.6.3 ^{1}H NMR Titrations

10 mL of a 0.01 M solution of receptor **3.12** was prepared. 0.5 mL was added to a new, dry NMR tube and capped. 1 mL of 0.01 M receptor solution was used to make a 0.15 M solution of TBA·H_2PO_4. The receptor-anion solution was titrated into the NMR tube in 0.1 equivalent aliquots. This method allows for the concentration of the anion to increase, while

maintaining a constant concentration of receptor. Chemical shifts for each ^{1}H-NMR spectrum were recorded in ppm and calibrated to the solvent peak; d_6-DMSO = 2.50 ppm.

3.7 References

1 R. Montis, A. Bencini, S. J. Coles, L. Conti, L. Fusaro, P. A. Gale, C. Giorgi, P. N. Horton, V. Lippolis, L. K. Mapp and C. Caltagirone, *Chemical Communications*, 2019, **55**, 2745–2748.

2 C. Deng, J. P. Bard, J. A. Lohrman, J. E. Barker, L. N. Zakharov, D. W. Johnson and M. M. Haley, *Angewandte Chemie*, 2019, **131**, 3974–3978.

3 M. M. Watt, L. N. Zakharov, M. M. Haley and D. W. Johnson, *Angewandte Chemie International Edition*, 2013, **52**, 10275–10280.

4 D. N. Hague and M. S. Zetter, *Role of Metals in Enzymatic Reactions Part 2.-Kinetics of Complex Formation in Model Systems Involving Manganese(I1) and 8-Hydroxyquinoline*, 1970, vol. 3.

5 P. W. Taylor and A. S. v Burgen, *Biochemistry*, 1971, **10**, 3859–3866.

6 Y. Wang, H. Lin, J. Shao, Z. S. Cai and H. K. Lin, *Talanta*, 2008, **74**, 1122–1125.

7 K. Chun Nam, S. Ok Kang, H. Sang Jeong and S. Jeon, *TETRAHEDRON LETTERS Pergamon Tetrahedron Letters*, 1999, **40**, 7343–7346.

8 J. Kang and J. Kim, *Tetrahedron Lett*, 2005, **46**, 1759–1762.

9 G. W. Bates, Triyanti, M. E. Light, M. Albrecht and P. A. Gale, *Journal of Organic Chemistry*, 2007, **72**, 8921–8927.

10 C. Caltagirone, J. R. Hiscock, M. B. Hursthouse, M. E. Light and P. A. Gale, *Chemistry - A European Journal*, 2008, **14**, 10236–10243.

11 P. A. Gale, J. R. Hiscock, S. J. Moore, C. Caltagirone, M. B. Hursthouse and M. E. Light, *Chem Asian J*, 2010, **5**, 555–561.

12 P. D. Mines, D. Thirion, B. Uthuppu, Y. Hwang, M. H. Jakobsen, H. R. Andersen and C. T. Yavuz, *Chemical Engineering Journal*, 2017, **309**, 766–771.

13 Y. Qin, Y. Zhu, X. Luo, S. Liang, J. Wang and L. Zhang, *Int J Energy Res*, 2019, **43**, 1000–1011.

14 C. R. Sagandira and P. Watts, *J Flow Chem*, 2019, **9**, 79–87.

15 R. Paul, *J Am Chem Soc*, 1960, **82**, 4596–4600.

16 D. J. Dale, P. J. Dunn, C. Golightly, M. L. Hughes, P. C. Levett, A. K. Pearce, P. M. Searle, G. Ward and A. S. Wood, *Org Pro Res Dev*, 2000, **4**, 17–22.

17 R. Vaidyanathan, V. G. Kalthod, D. P. Ngo, J. M. Manley and S. P. Lapekas, *Journal Organic Chemistry*, 2004, **69**, 2565–2568.

18 M. Aresta and E. Quaranta, *Tetrahedron*, 1991, **47**, 9489–9502.

19 G. Neri, M. G. Musolino, C. Milone, A. M. Visco and A. di Mario, *J Mol Catal A Chem*, 1995, **95**, 235–241.

20 M. Baron, E. Métay, M. Lemaire and F. Popowycz, *Green Chemistry*, 2013, **15**, 1006–1015.

21 A. D. Stergiou and M. D. Symes, *Cell Rep Phys Sci*, 2022, **3**, 100914.

22 L. Cotarca, T. Geller and J. Répási, *Org Process Res Dev*, 2017, **21**, 1439–1446.

23 Y. C. Charalambides and S. C. Moratti, *Synth Commun*, 2007, **37**, 1037–1044.

24 M. B. Smith, *March's Advanced Organic Chemistry: Reactions, Mechanisms and Structure*, John Wiley & Sons, Inc, 2013, 1213–1214.

25 G. M. Salamończyk, *Tetrahedron Lett*, 2011, **52**, 155–158.

26 V. Theodorou, K. Skobridis, A. G. Tzakos and V. Ragoussis, *Tetrahedron Lett*, 2007, **48**, 8230–8233.

27 R. Srinivasan, L. P. Tan, H. Wu, P. Y. Yang, K. A. Kalesh and S. Q. Yao, *Org Biomol Chem*, 2009, **7**, 1821–1828.

28 M. V Sheridan, K. Lam and W. E. Geiger, *Supporting Information Covalent Attachment of Porphyrins and Ferrocenes to Electrode Surfaces through Direct Anodic Oxidation of Terminal Ethynyl Groups**, .*

29 M. V. Sheridan, K. Lam and W. E. Geiger, *Angewandte Chemie - International Edition*, 2013, **52**, 12897–12900.

30 M. A. Béchamp, *Annales de chimie et de physique*, 1854, **42**,186–195.

31 Z. Wang, in *Comprehensive Organic Name Reactions and Reagents*, 2010, pp. 284–287.

32 V. Popat and N. Padhiyar, *International Journal of Chemical Engineering and Applications*, 2013, 401–405.

33 H. C. Kolb, M. G. Finn and K. B. Sharpless, *Angewandte Chemie - International Edition*, 2001, 40, 2004–2021.

34 P. Thirumurugan, D. Matosiuk and K. Jozwiak, *Chem Rev*, 2013, 113, 4905–4979.

35 C. D. Hein, X. M. Liu and D. Wang, *Pharm Res*, 2008, 25, 2216–2230.

36 R. Huisgen, *Angewandte Chemie*, 1963, **75**, 604–637.

37 R. A. Firestone, *J Org Chem*, 1968, **3**, 2285–2290.

38 R. Huisgen, *J Org Chem*, 1968, **33**, 2291–2297.

39 K. Sonogashira, *J Organomet Chem*, 2002, **653**, 46–49.

40 S. P. Shirame and R. B. Bhosale, in *Green Chemistry*, InTech, 2018, pp. 171–180.

41 M. I. Mangione, R. A. Spanevello and M. B. Anzardi, *RSC Adv Supporting Information EFFICIENT AND STRAIGHFORWARD CLICK SYNTHESIS OF STRUCTURALLY RELATED DENDRITIC TRIAZOLES*, 2017, 8.5

42 P. K. Mandal and J. S. McMurray, *Journal of Organic Chemistry*, 2007, **72**, 6599–6601.

Chapter 4

Bis-carbazolylurea Receptor for Anion Recovery

Acknowledgements and Declaration

Calum Hope performed the experimental work and data analysis. Mass spectrometry analysis was conducted by Mr Gangi Ubbara. Mark Symes conceived the idea and assisted with data analysis.

Synopsis

Since the Industrial Revolution the levels of carbon dioxide in the Earth's atmosphere have increased dramatically. Before this, the levels of CO_2 present in the atmosphere never exceeded 280 ppm and according to the National Oceanic and Atmospheric Administration, the levels present in the atmosphere in 2021 were 414.72 ppm.[1] *As a consequence, the development of new technologies or methods for the removal of CO_2 have been of increased interest to scientists globally. Oceanic sinks for carbon dioxide are responsible for the removal of large amount of carbon dioxide from the atmosphere and it's storage as different carbonate species. The equilibrium of the dissolution of carbon dioxide could potentially be exploited, through the selective removal of bicarbonate from oceanic sources, to drive the removal of CO_2 from the atmosphere. One potential method for the removal of bicarbonate, is a capacitive deionisation system containing electrodes decorated with a selective element, such as a hydrogen bonding receptor. To this end, our work endeavoured to synthesise and characterise the suitability of a bis-carbazolylurea based receptor for use within such a system.*

4.1 Introduction

Since the Industrial Revolution, the level of carbon dioxide in our atmosphere has continued to grow as a result of the continued reliance on the combustion of fossil fuels, however of this released CO_2, it is estimated that only 50% remains in the atmosphere as a result of the uptake by terrestrial and aquatic systems.

Oceanic sinks for carbon dioxide are estimated to have removed 118 petagrams from the atmosphere. When CO_2 dissolves in water, it exists predominantly in three main forms: free $CO_{2\,(aq)}$, HCO_3^- and CO_3^{2-} (Scheme 4.1).

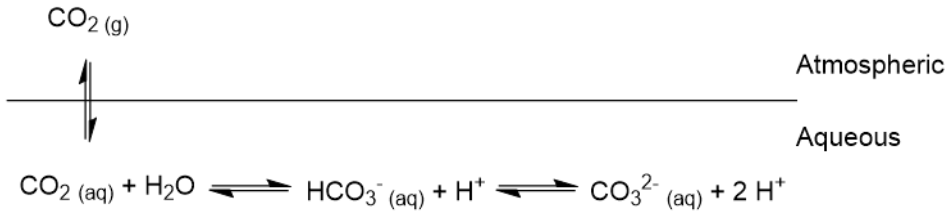

Scheme 4.1: Equilibrium of CO_2 in an aquatic system.

The fourth form carbonic acid, H_2CO_3, is not considered due to its incredibly low concentration. The distribution of dissolved CO_2 in the ocean is not uniform; predominantly the upper ocean contains the highest concentration of dissolved CO_2 and as this level has increased, the effect on the upper ocean layer's carbonate chemistry has been affected- a reduction in pH and CO_3^{2-} concentration. Typically, bicarbonate, HCO_3^-, makes up roughly 90% of the dissolved carbonate species, with carbonate making up only 9% of the dissolved species. Therefore, the efficient removal of bicarbonate could be of significant environmental importance by driving the equilibrium in the forward direction and effective and sustainable methods of removal continue to be of great interest.[2,3] The most well-known and utilised methods for carbon dioxide capture occur in the gas phase, with limited examples occurring in the solution phase, or from the removal of carbon dioxide containing species, such as bicarbonates/carbonates. The materials used for the capture of CO_2 need to finely balance the affinity of the material for carbon dioxide against the energy cost associated with the regeneration of said material. A high affinity for CO_2 is essential in order to remove carbon dioxide from the flue stream, however if this interaction is too strong, the energy costs associated with the desorption of carbon dioxide are greatly increased and sustainability becomes the prevailing factor. Conversely, if the material's affinity is low, the associated energy costs for the removal are substantially lowered, but this weak interaction may influence the selectivity of the material and as such other components of the flue stream

may be adsorbed/sequestered. These materials must also be highly stable towards the conditions used to capture and regenerate CO_2 in order to keep overhead costs to a minimum. Due to the volume of gaseous CO_2 likely released by a plant, the density of carbon dioxide uptake should be maximised so that the volume of material required is kept to a minimum.[2] Currently, one of the favoured methods for CO_2 capture is the use of aqueous alkanolamine solutions.[4] Under these conditions, the carbonyl centre of CO_2 is attacked by the nucleophilic amine leading to the formation of a C-N bond. Depending on the initial type of alkanolamine used, the CO_2 is either trapped as a carbamate or bicarbonate, Scheme 4.2.

The affinity of the amine towards carbon dioxide can be controlled by tuning the substituents around the amine. This must be considered as there may be a high energy cost associated with formation of the carbamate due to the strong orbital overlap. Monoethanolamine (MEA) is the most well studied alkanolamine for carbon dioxide capture.

From Scheme 4.2, two equivalents of MEA react with CO_2 to form the carbamate species and associated monoethanolammonium species. If a secondary or tertiary amine e.g., triethanolamine (TriEA), is added to a solution of CO_2, then a 1:1 reaction is observed whereby the bicarbonate product is formed. This is the result of the steric bulk surrounding the nucleophilic N-centre.

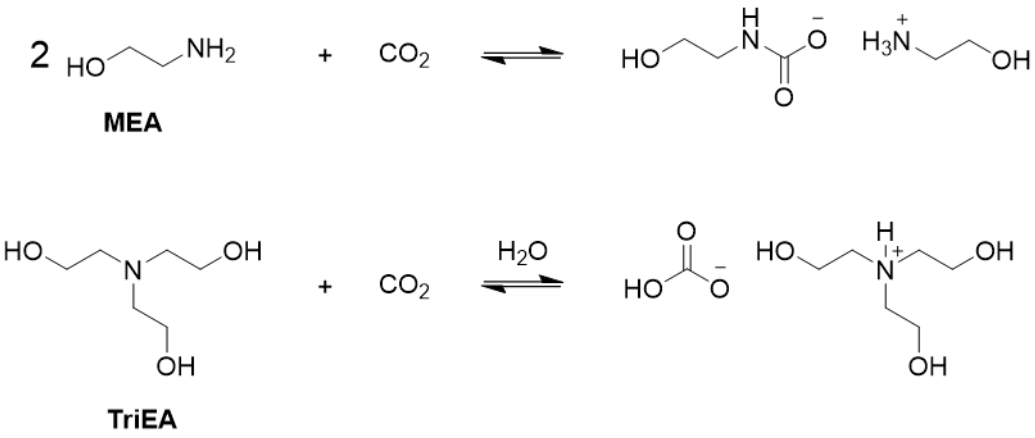

Scheme 4.2: Reaction of top) MEA and CO_2 to form a carbamate; bottom) TriEA and CO_2 to form a bicarbonate.

In terms of the energy cost associated with the release of the sequestered CO_2, bicarbonates are less stable than carbamates and consequently the energy required for the reversal of the CO_2-alkanolamine adduct is 1° > 2° > 3°. There are also other limitations to consider when using alkanolamines such as the effective working load. Typically, 20-30 wt% MEA in water

is used, however the actual working capacity of the solution is much lower- 2.1-5.5 wt% for a 30 wt% solution suggesting that incomplete regeneration, side reactions or decomposition are occurring. It has been shown that the amine solutions are unstable towards heating meaning incomplete regeneration is likely, and at higher temperatures, decomposition is likely to occur further negatively impacting the overall efficiency of the process. A second issue is the highly corrosive nature of the solutions at concentrations above 40 wt%, this is generally avoided as working conditions are 20-30 wt%, which means that larger volumes of water are required that must be heated in order to regenerate alkanolamine. This increases the energy penalty of regeneration and means that the heat capacity for both a 20 and 40 wt% solution is close to that of water- 4.18 J K^{-1} g^{-1}.

Recently, hypercrosslinked polymers (HCPs), a class of porous materials, have been shown to have potential applications in gas sequestration. HCPs can be made simply by through the crosslinking of aryl subunits, often using Lewis acid metal-based catalysts, with acetals often serving as the external crosslinking agent. The versatility of HCPs stems from the functionalisation of the utilised starting materials, this leads to HCPs having large surface areas and high thermal stability, making them suitable for a small gas molecule capture and the removal of small toxic molecules.[5] In order to make HCPs effective for the removal of CO_2, they often utilise polar groups, such as -OH or -NH_2, or contain heteroaromatic subunits. Ansari and co-workers developed a triptycene based HCP that contained no such polar group or heterocycle.[5] Triptycene, with its unique paddlewheel like structure, is an ideal molecule for an HCP for the capture of small gases due to the internal free volume that is created. The synthesised HCP, **4.1**, was synthesised from triptycene and 2,4,6-tris(bromomethyl)mesitylene using a Friedel-Crafts alkylation.

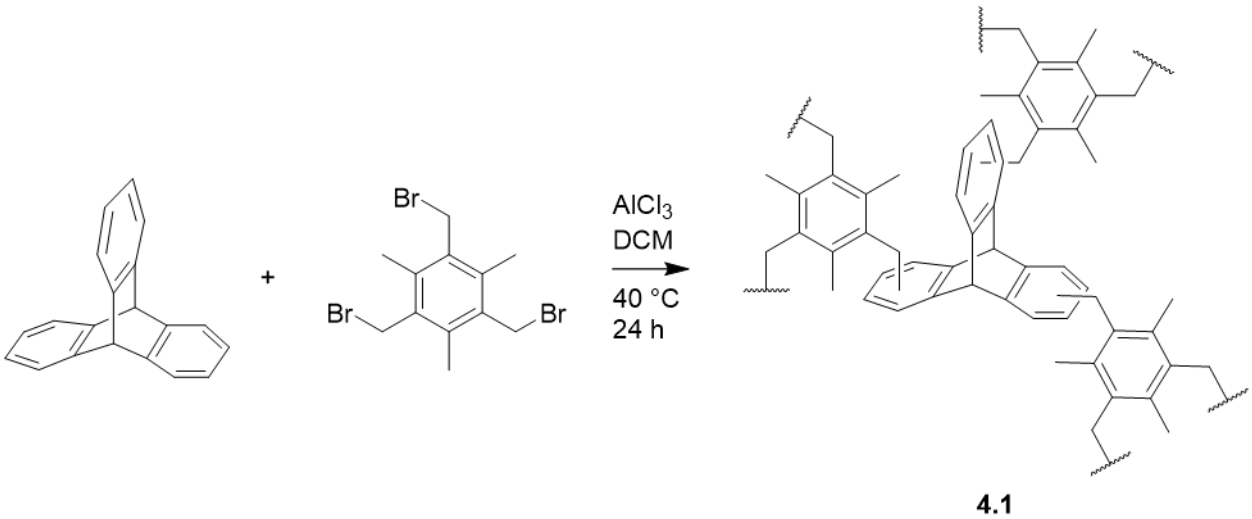

4.1

Scheme 4.3: Synthesis of triptycene based HCP.

One such synthesised HCP, **4.1** was shown to have a high surface area and as such was further explored for its ability to capture CO_2. Adsorption-desorption isotherms were recorded at different temperatures- 273 and 298 K- and 1 bar pressure and showed that **4.1** could reversibly capture carbon dioxide. This reversible behaviour means that the energy cost associated with the regeneration would be lowered significantly. The carbon capture capability of the HCP was demonstrated to be 132 mg g^{-1} at 273 K and 1 bar; with good selectivity for carbon dioxide. Qian et al. have shown that etherified glycerol derivatives have potential as CO_2 capture solvents whilst also making use of the main by-product of biodiesel production- glycerol.[6] They subsequently built upon this work and introduced a third ether moiety in place of the central alcohol group. During their investigation, Qian and co-workers identified two potential triethers, **4.2** and **4.3**, as potential solvents for carbon dioxide capture.

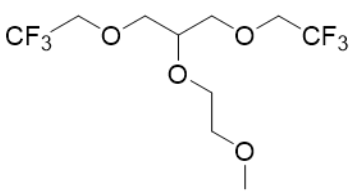

4.2

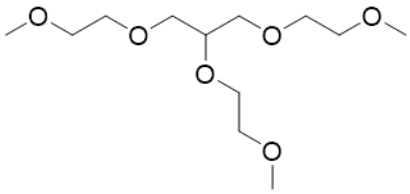

4.3

The studies indicated that that **4.2** and **4.3** had the highest and second highest affinity for CO_2, respectively. The enhanced CO_2 removal capability of **4.2** over **4.3**, can be attributed to the presence of the fluorine atoms. Fluorinating compounds has been demonstrated to improve the gas dissolving ability whilst also having very weak intermolecular interactions.[7] It was postulated that the increase in affinity for CO_2, over the previously identified diethers, was as a result of the decrease in potential H-bond formation. By removing the central hydroxyl moiety, it was thought that there would be fewer intermolecular interactions between the solvent molecules and increase the likelihood of interaction with carbon dioxide. During their investigations they also synthesised several glycerol-based ketones, such as **4.4**, which also showed a high affinity for CO_2 but not to the same extent as the triethers. This was thought to be as a result of the increase in the free volume of the triethers compared to the ketones due to the increased sterics.

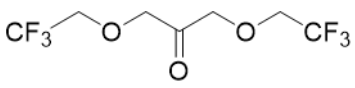

4.4

In this body of work, we aim to show that a simple, neutral H-bonding receptor is capable of binding bicarbonate, HCO_3^-, with the end goal of driving the dissolution of CO_2 equilibrium in the forward direction. Modifying the work of Hiscock and Sanchez, the synthesised receptor will bear amine moieties that would allow it to be grafted to a glassy carbon electrode, via a urea coupling.[8,9] The grafted receptor can then be employed within an electrochemical system to allow for the selective removal of bicarbonate from ocean water.

4.2 Proposed Reaction Scheme

The original proposed reaction scheme (Scheme 4.4) modified the original synthesis proposed by Hiscock et al. in order to install a suitable group for the electrode attachment, in this case an amine was chosen as this could be used to make the stable urea coupling to the electrode surface but also simplified the synthetic process.[9] It was thought that once the initial 'bare'-unfunctionalized receptor had been synthesised, applying the same nitration and reduction methods that were used in the synthesis, would successfully install the desired amine group at the 8-position of the carbazole ring.

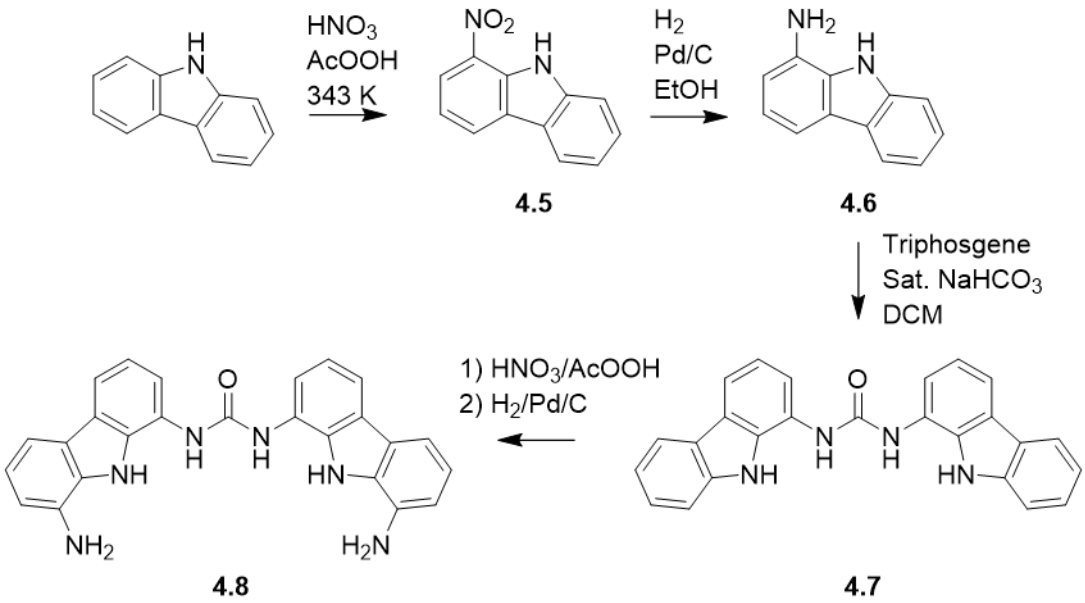

Scheme 4:4: Proposed reaction scheme for synthesis of receptor **4.8**

The first step is the synthesis of 1-nitro-9*H*-carbazole, **4.5**, by refluxing carbazole in concentrated nitric acid and acetic acid. The reduction of the nitro group over Pd/C using H_2 would yield the amino carbazole product, **4.6**. Using triphosgene, two aminocarbazole

monomer units are joined together through a urea bond. This reaction proceeds first through the formation of an isocyanato group, that subsequently reacts with the amine of a second molecule. This yields the 'bare' receptor, **4.7**, that was subjected to the first nitration reaction, followed by the hydrogenation of the nitro group over Pd/C, to yield the complete receptor **4.8**.

4.2.1 Synthesis of 1-nitrocarbazole (4.5)

4.2.1.1 Nitration with HNO_3

The nitration of carbazole, Cbz, has long been of interest because of how the products, and ratios thereof, can be affected by the reagent conditions.[10] The mechanisms for such reactions are not fully understood, and as previously stated, can vary greatly based on the conditions used. Kyziol and Daszkiewicz's work on both acetanilide and carbazole compounds showed that the ratio of the *ortho* to *para* products varied greatly depending on the substrate and conditions[10]. For both cases, they postulated that the nitro compounds can be formed through two independent reactions. The first, is the direct nitration of the of the aromatic ring, leading preferentially to the para product. The second, is the formation *N*-nitro intermediates that rearrange and form predominantly ortho products. For carbazole, the ratio of *o*/*p*-products formed is 3:7 and led to two different mechanisms being proposed; the nitrosation of the pyrrole followed by a Fischer-Hepp rearrangement (Scheme 4.5) and oxidation of 3-nitrosocarbazole or the formation and rearrangement of 9-nitrocarbazole.

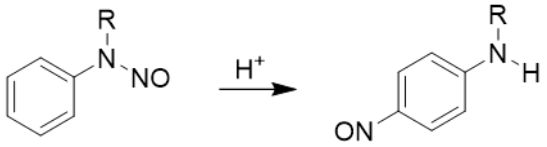

Scheme 4.5: Fischer-Hepp rearrangement.

The first pathway was initially proposed by Drake et al. and led only to the para-position being nitrated- in relatively poor yields.[11] The mechanism for the Fischer-Hepp rearrangement is not well understood but has been shown to be intramolecular in nature by Morgan and Williams, who investigated the rearrangement in the presence of urea. If nitrite were released, it would have been quenched by the urea.[12]

In order to validate the second pathway, a 9-nitrocarbazole derivative needed to be formed under the conditions used, without any rearrangement to the ortho- or para-product. This was successfully performed using a 1,3,6,8- tetrachlorocarbazole. The direct formation of 9-nitrocarbazole proved difficult, however 9-nitrosocarbazole could be oxidised using peracetic acid to give the protonated form of 9-nitrocarbazole, Scheme 4.6 (middle). This *N*-nitroamine product rapidly rearranges into the ortho and para forms in the same ratio that is observed with carbazole.[10] Two mechanisms have been suggested for how the *N*-nitroamine rearranges in acid, the first is the cyclic attack by the oxygen of the nitro group at the ortho position, and the alternative being a radical and radical cation held together in a solvent cage. Support for the second pathway is evidenced by the large amount of nitrous acid and non-nitrated amine that is produced when radicals are able to escape the cage, Scheme 4.6.[13]

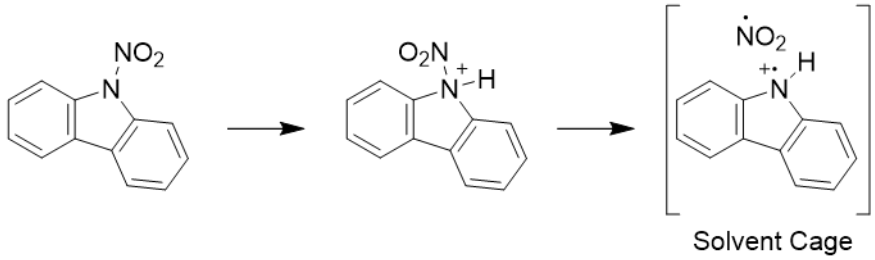

Scheme 4.6: Rearrangement of 9-nitrocarbazole.

It can be postulated that through resonance with the ring, the ortho and para positions are activated and as such, are susceptible to attack by the nitro group. Both ortho and para products were synthesised in an overall crude yield of 91% using HNO_3 in acetic acid. Efforts to purify the crude material using column chromatography- eluting solvent $CHCl_3$- proved to be unsuccessful with only the para-regioisomer being successfully isolated. An isolated yield for the ortho-isomer could not be effectively obtained and efforts to purify using column chromatography, led to a product which contained both the desired ortho-isomer and the carbazole starting material. As a result, an alternative method for the synthesis of the ortho-isomer was investigated.

4.2.1.2 Buchwald-Hartwig cross-coupling

The Buchwald-Hartwig cross-coupling is the palladium-catalysed cross-coupling of an aryl halide, typically aryl bromides, with an aniline, forming a C-N bond.

Typically, the classical method for the formation of C-N bonds is through either nucleophilic substitution or reductive elimination. Methods utilising aryl halide have been shown to be

limited by the functional groups involved, often requiring energetic activation e.g., the presence of strongly electro withdrawing moieties in the ortho or para position, in particular nitro. It has been shown that without such activation, aryl halides, such as bromo and chloro, have similar reactivities to their alkyl counterparts.[14] In 1901, Ullmann described the copper-catalysed cross-coupling of a variety of nitrophenyl halides.[15] These substrates contained the highly electron withdrawing nitro group and were further activated by the addition of catalytic copper. This cross-coupling type reaction between aryl halides, phenols and anilines with a copper catalyst became known as the Ullmann coupling and is an early example of activation of a halide for C-N cross-coupling, Scheme 4.7.

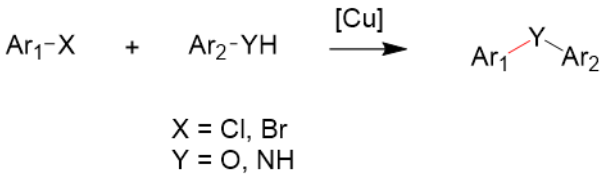

Scheme 4.7: Biaryl ether and amine coupling.

In 1983, Migita and co-workers first described the Pd-catalysed aromatic amination of bromobenzene and an aminostannane, (*N*,*N*-diethylamino)tributyltin (Scheme 4.8)[16].

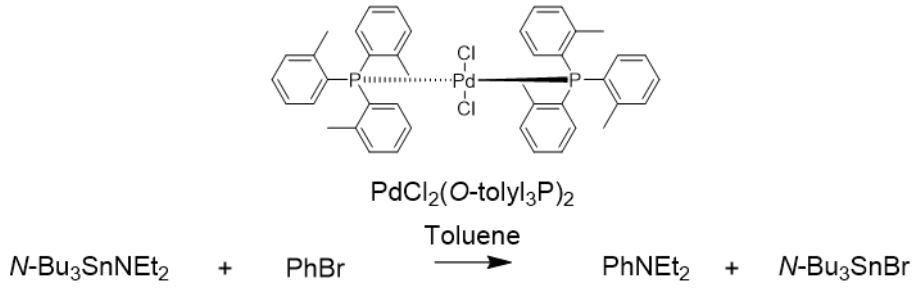

Scheme 4.8: Aminostannane catalysed amination

Their investigations showed that the Pd-catalyst used gave drastically improved yields, compared to the other palladium catalysts tested. They also showed that the reaction was highly substrate dependent with no reaction occurring with iodo- or chlorobenzene starting materials and only a select few substituted bromobenzenes proving to be suitable substrates. They postulated that the reaction mechanism did not proceed through an aryne or $S_{RN}1$ mechanism. This was evidenced by the lack of isomers that would likely be observed in the aryne mechanism and that no product was observed in the reaction of iodobenzene, the most favourable substrate for an $S_{RN}1$ reaction. They proposed that the likely cross-coupling occurred through oxidative-addition, transmetallation and reductive elimination.

Further work by Guram and Buchwald aimed to improve the scope of the reaction by the in-situ generation of a range of aminostannane reagents.[17] They suggested that the limited initial reaction proposed by Migita and co-workers was as the result of the unstable and highly reactive nature of the aminostannanes. During the course of investigations, they showed that the ligand -P(*o*-tolyl)$_3$ and higher temperatures were favourable. The *in-situ* generation of aminostannanes via the reaction of lithium amides with tributyltin chloride in ether proved to be unsuccessful- likely the result of deactivation by excess BuLi, ether or the formation of the LiCl salt. To circumvent this, the transamination of aminostannanes was performed using aminostannanes generated from volatile amines and a higher boiling amine, whilst simultaneously removing the generated volatile amine. This first step, coupled with the Pd-catalysis, lead to a range of arylamine products. Like Migata and co-workers, they suggested the reaction is initiated by the reduction of the Pd^{II} complex to Pd^0, followed by oxidative-addition, transmetallation and reductive-elimination. Further work by Buchwald and Wolfe showed the effect that the ligand has on the rate and efficacy of the amination reaction.[18] The most utilised ligand for this is BINAP, 2,2′-bis(diphenylphosphino)-1,1′-binaphthalene.

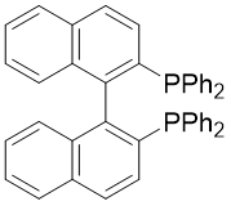

BINAP

BINAP is a large, bulky, electron-rich phosphine chelating ligand that has been demonstrated to have good reactivity in the presence of caesium carbonate base, allowing for a broad range of substrate functional groups to be used, in comparison to the strong base sodium *tert*-butoxide, NaO-*t*-Bu. Other catalytic ligands allow for a range of functional groups to be tolerated when potassium carbonate is used as a base, however BINAP appears to still give better results in the reaction of primary amines. Comparing the results obtained when 5-bromo-*m*-xylene and *N*-hexylamine were coupled using Pd(BINAP) and Pd(P*o*-tolyl)$_3$ systems, showed that not only did BINAP lead to an improved yield, 88% vs. 35%, but it also requires lower catalyst loading, 0.5 mol % vs 2 mol %. Investigations into the reaction rate showed that electronically neutral and electron-deficient aryl bromides reacted fastest compared to electron-rich bromides, often requiring longer reaction times and higher temperatures. As previously mentioned, the choice of base used can affect the type of initial substrate used. The strong base, NaO-*t*-Bu, was only tolerated by aryl halides that contained acetals, nitriles and *tert*-butyl esters. Their amine counterparts that contained acetals, alkenes

or tertiary amine moieties were also stable under these conditions. In addition, the strong base was shown to decrease the catalytic loading required as well as increase the reaction rate. However, not all functional groups can be tolerated, for example, methyl and ethyl esters can react to form amides and enolizable ketones can be deprotonated. By using the weaker Cs_2CO_3 base, these groups are tolerated and able to undergo the cross-coupling.

The catalytic cycle proposed by Buchwald, was very similar to that proposed by Hartwig,[19] and is very similar to that of other Pd-catalysed C-C cross-couplings, Scheme 4.9.[18]

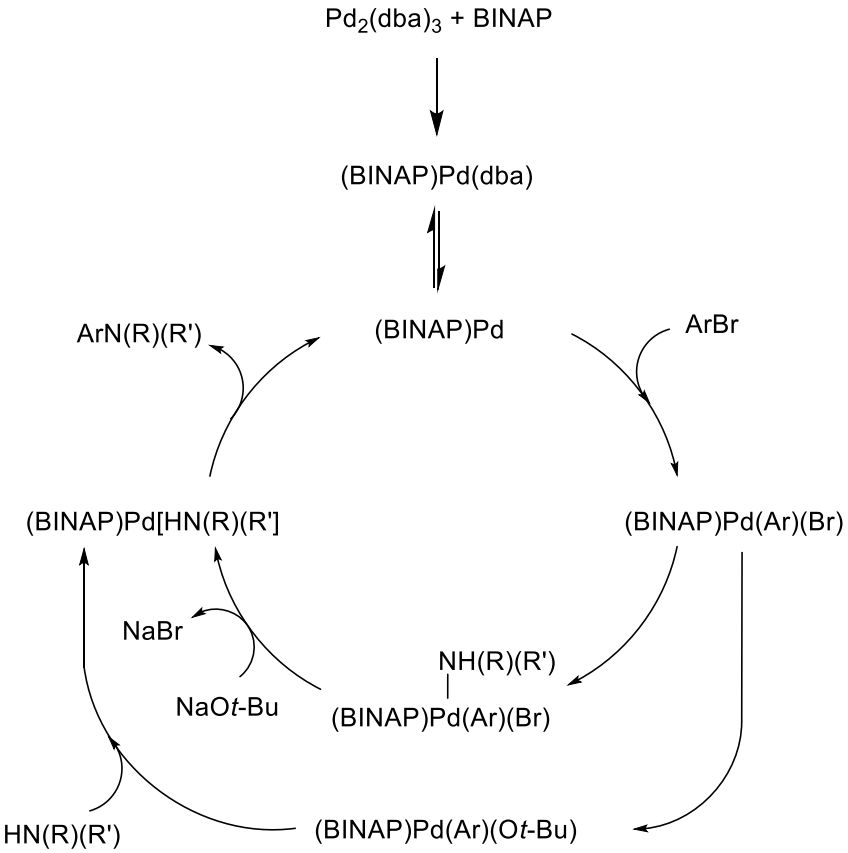

Scheme 4.9: Proposed catalytic route of Pd-catalysed coupling using NaOt-Bu and BINAP.

The initial ligand exchange between $Pd_2(dba)_3$ and BINAP leads to the reactive Pd(BINAP) complex before the subsequent oxidative addition of the aryl bromide and formation of the Pd^{II}(BINAP)(Ar)(Br) complex. Buchwald suggests that coordination of the amine to the palladium centre, followed by deprotonation leads to the amido complex. Reductive-elimination then occurs to release the desired C-N cross-coupled product and regenerate the Pd^0(BINAP) catalyst. Hartwig and co-workers suggested an alternative route, whereby a Pd^{II}(BINAP)(O-*t*-Bu) complex is formed before the amido complex is formed and reductive elimination takes place.

In this scheme of work, a Buchwald-Hartwig 'double-coupling' of 2-bromo-2-nitrobenzene and 2-bromoaniline was demonstrated to yield 1-nitro-9*H*-carbazole in very good yields.[20] These double couplings proceed through an initial Pd-catalysed heteroatom bond forming step- the Buchwald-Hartwig coupling- followed by a second Pd-catalysed C-H activation electrophilic ring closing step and have been shown to be successful in the synthesis of carbazoles and dibenzofurans[21]. A proposed catalytic cycle, Scheme 4.10, shows the likely method for how 1-nitro-9*H*-carbazole may be synthesised.

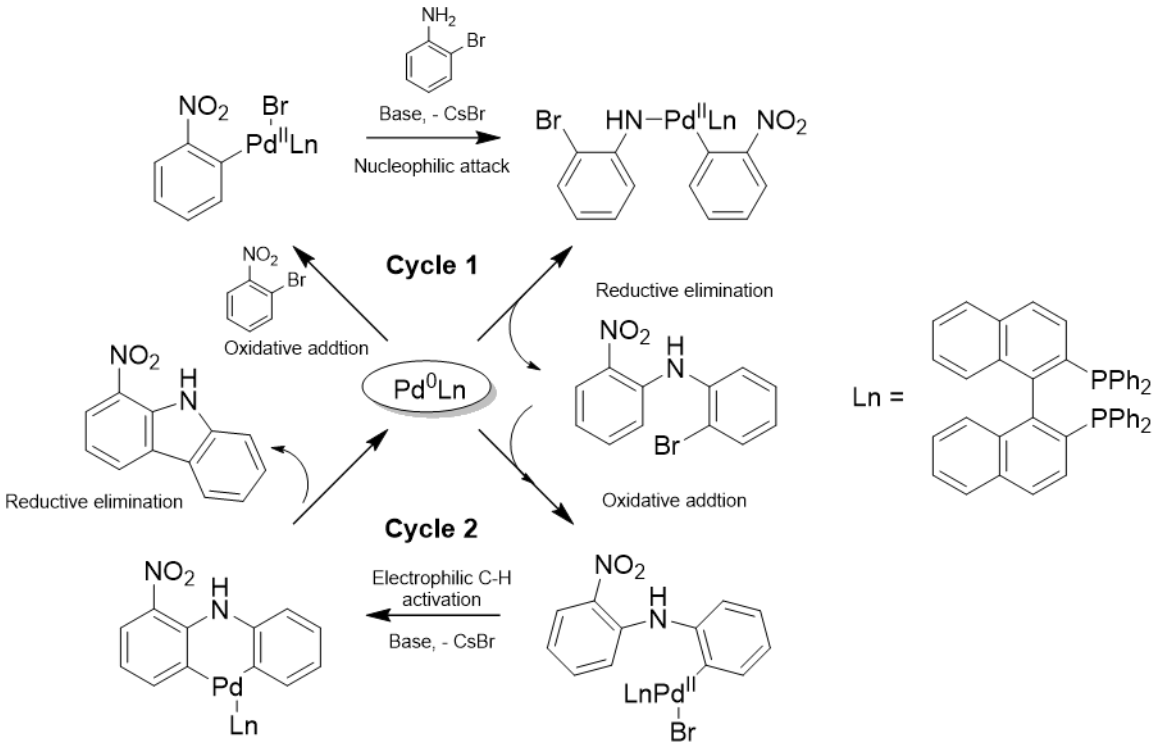

Scheme 4.10: Proposed catalytic Buchwald-Hartwig based double-coupling.

In order for effective C-H activation, the rate of oxidative addition of the C-N forming step must be far greater than the oxidative addition in the C-H activation step. Bedford and Cazin suggested that this could be achieved through altering the halide at each stage, for example, Br for the heterocoupling and Cl for C-H activation. For the reaction of 2-bromo-2-nitrobenzene and 2-bromoaniline, the addition of only 2-bromo-2-nitrobenzene initially and allowing the Pd^{II} complex to form before the addition of the 2-bromoaniline circumvents this problem. This method also ensures that the highly electro-withdrawing nitro moiety is meta to the C-H involved in the next step, making this site more electrophilic. This reaction was used to successfully synthesise 1-nitro-9*H*-carbazole in 35% yield. This was significantly lower than those reported by Beifuss and may have been the result of incomplete reaction or perhaps catalyst oxidation. Consequently, an alternative method for the synthesis of 1-nitro-9*H*-carbazole was found that would have a greater yield.

4.3 Revised Reaction Scheme

In order to improve the yield and reaction selectivity, a reaction scheme, Scheme 4.11, was proposed that would effectively lead to the 1-nitrocarbazole product exclusively.

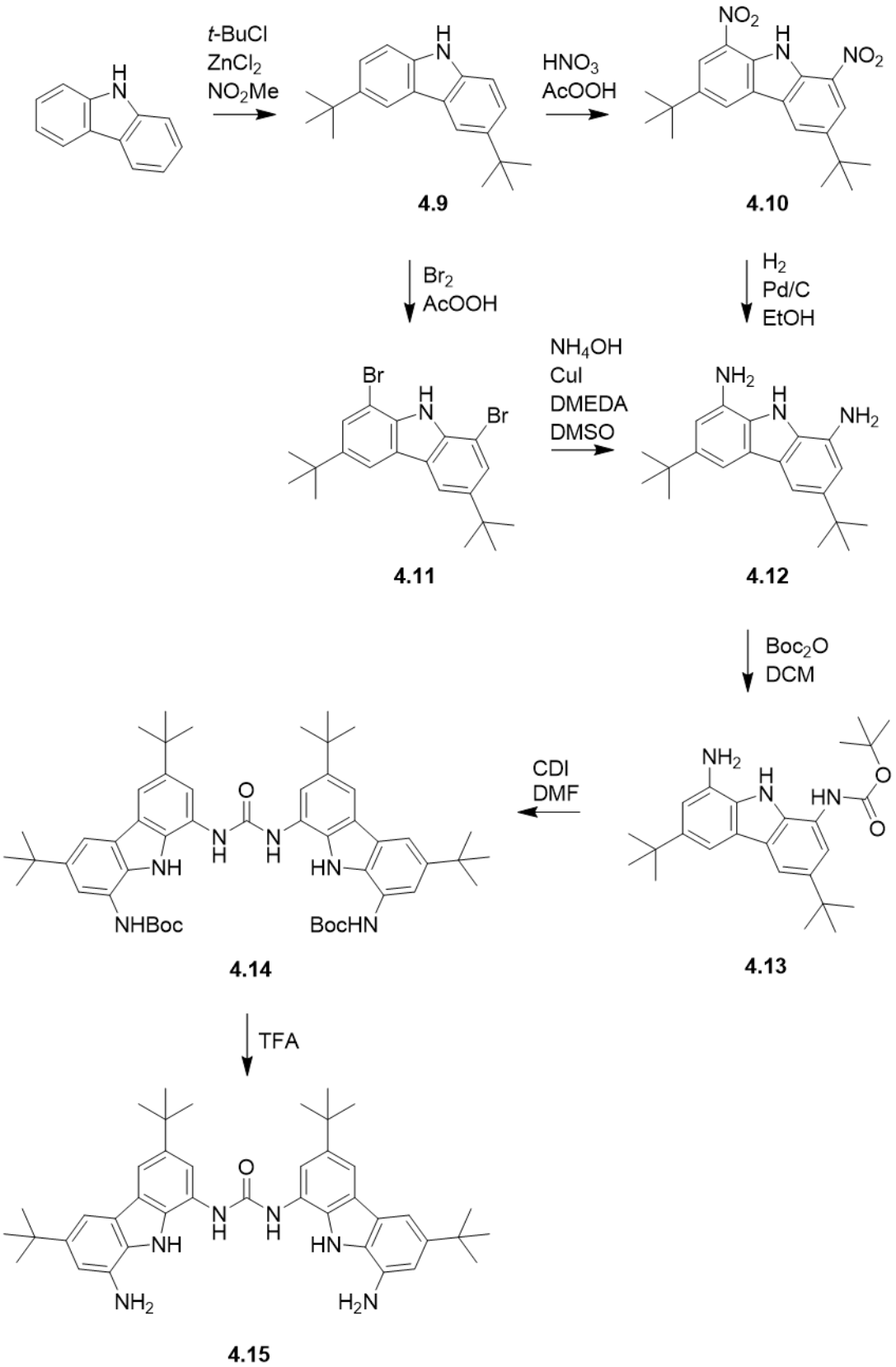

Scheme 4.11: Revised reaction scheme for the synthesis of receptor **4.15.**

Rüütel and co-workers designed a biscarbazolylurea synthesis, that is related to the initially proposed synthesis, and begins with a Friedel-Crafts alkylation of carbazole to yield **4.9** that blocks any reactions at the 3- and 6-positions.[22] The aminated product, **4.12**, can then be obtained through two routes 1) nitration with HNO_3 (**4.10**) followed by hydrogenation over Pd/C; 2) bromination at the 1-position (**4.11**) and subsequent amination. Rüütel report that the latter bromination route gave improved yields as the highly acidic nature of the HNO_3 pathway led to potential cleavage of the *tert*-butyl groups. In this body of work, both methods were attempted, with varying success and will be discussed further in this chapter. Following the successful synthesis of the diaminocarbazole product, **4.12**, one amine moiety was boc-protected, **4.13**, leaving the free amine to undergo a urea-bond forming reaction using 1,1'-carbonyldiimidazole, **4.14**. Finally, the boc group was removed using trifluoracetic acid to afford the final amine receptor product, **4.15**.

4.3.1 Friedel-Crafts alkylation of carbazole (4.9)

In 1877, Friedel and Crafts developed a series of reactions for the alkylation or acylation of an aromatic ring and is an example of electrophilic aromatic substitution.[23] In their original paper, they demonstrated the alkylation of benzene using amyl chloride, in the presence aluminium strips.[23,24] These reactions typically require large amounts of a Lewis acid catalyst, traditionally $AlCl_3$, but BF_3 and $TiCl_4$, to name a couple, have also been shown to be effective Lewis acids for the catalysis. Alkyl halides are employed as the alkylating agents. The reaction is not without drawbacks, often requiring large excesses of the Lewis acid catalyst and toxic alkyl halides that lead large amount of salt by-products.[25] The addition of alkyl moieties makes the formed product more nucleophilic than the starting material and as such, overalkylation can occur. This can be reduced through the employment of sterically large alkyl groups, such as *tert*-butyl. Despite these drawbacks, the alkylation reaction is still widely used today. In 2022, Krusenbaum et al. demonstrated the mechanochemical Friedel-Crafts alkylation (FCA) as an effective method of cross-linking in microporous polymers.[26] In their work, they successfully performed a FCA to generate a series of porous organic polymers (POPs) from 1,3,5,-triphenylbenzene (TPB), cross-linked with either CH_2Cl_2 or $CHCl_3$ (Scheme 4.12).

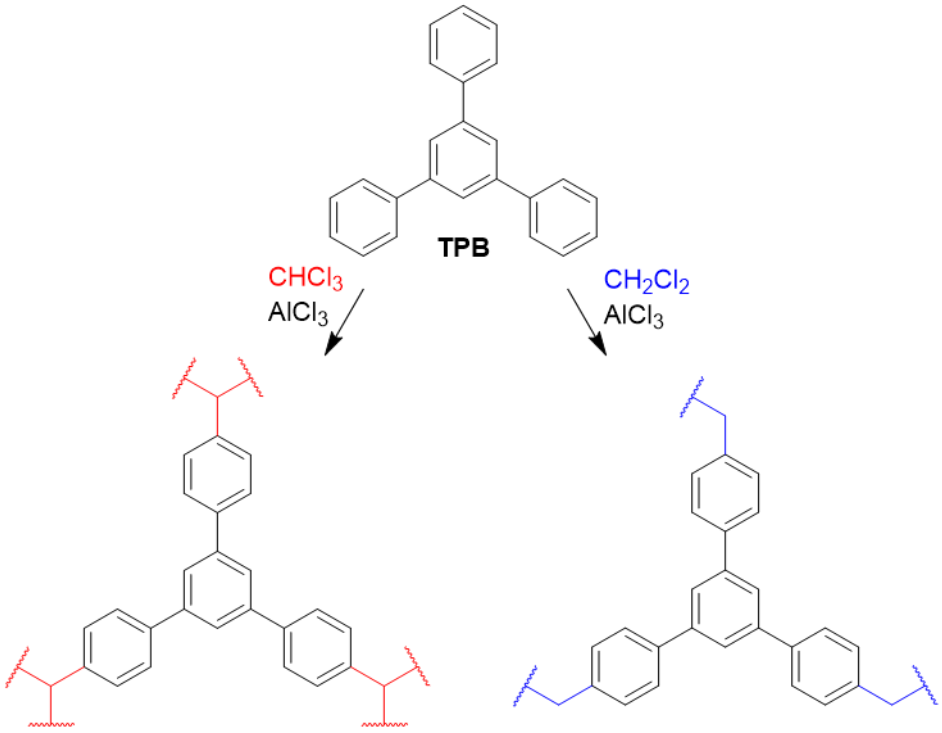

Scheme 4.12: TPB based POPs functionalised through FCA and organohalides.

POPs are of increased interest as they combine the properties of both polymers and porous materials. Interestingly, the synthesis of the generated POPs was performed mechanochemically, without the use of solvents, in a high-speed ball mill. In this reaction the collision of the milling balls with the wall, the material and the balls themselves, transfers the kinetic energy required to initiate a chemical reaction. This method reduces the associated drawbacks of a solvated FCA POP system, such as rapid precipitation of polymer and the need for solubilizing groups which may require further synthetic steps or expensive starting materials, as well as eliminating solvent waste. Jiang and co-workers also used a FCA to generate an anionic POP using potassium tetraphenylborate, $FeCl_3$ and dimethoxymethane.[27] The synthesised polymer contained tetraphenylborate subunits, cross-linked by methylene groups and is an example of an FCA with a less toxic alkylating agent. The charged anionic POP was demonstrated to have a large surface area and was able to effectively differentiate between ethylene and acetylene, making it of potential use in the industrial production of ethylene. Kader at al. used a FCA in the functionalisation of indolo[3,2,1-*jk*]carbazole, ICbz, in order to improve solubility.[28] ICbz has been shown to be integral to the function of phosphorescent OLEDs, however these ICbz-based OLEDs suffer from poor solubility and as such cannot be manufactured efficiently in solution. To improve this, *tert*-butyl and *N*-hexyl groups were successfully added to the ICbz scaffold by FCA in

good yields. The *tert*-butyl substituted ICbz derivative was synthesised in one-step using 2-chloro-2-methylpropane and $ZnCl_2$ as the Lewis acid catalyst. Similarly, functionalisation with *N*-hexyl groups was achieved using $AlCl_3$ and hexanoyl chloride, followed by reduction of the carbonyl moiety with $LiAlH_4$. This is an example of a Friedel-Crafts acylation reaction, the mechanism can be seen in Scheme 4.13, and first requires the pre-activation of alkyl halide species by the Lewis acid ($AlCl_3$) to form the acylium cation.

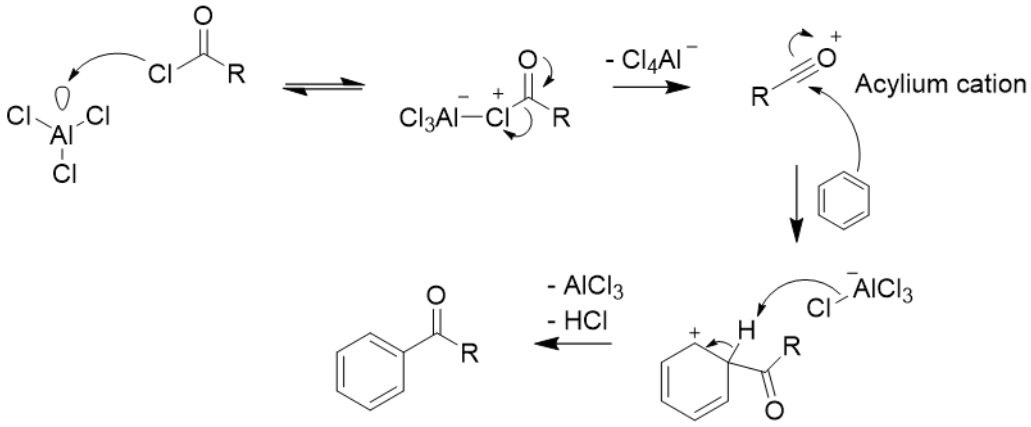

Scheme 4.13: Friedel-Crafts acylation mechanism.

The carbonyl formed is a weak Lewis base and can further coordinate to the Lewis acid, meaning that stoichiometric addition of the Lewis acid is often required. The alkylation of carbazole was performed in order to function as a 'pseudo' protecting group. As previously shown in section 4.2.1.1, the nitration of Cbz yielded a mix of the ortho- and para-substituted products. In order to maximise the yield of the 1-nitro substituted product obtained, it was thought that by effectively blocking the para-position the ortho-nitro product could be preferentially obtained. Liu et al. successfully demonstrated the synthesis of the di-*tert*-butyl substituted Cbz.[29] The formation of the di-alkylated product over the mono-alkylated is advantageous for later stage transformations. The mechanism for the alkylation is shown in Scheme 4.14.

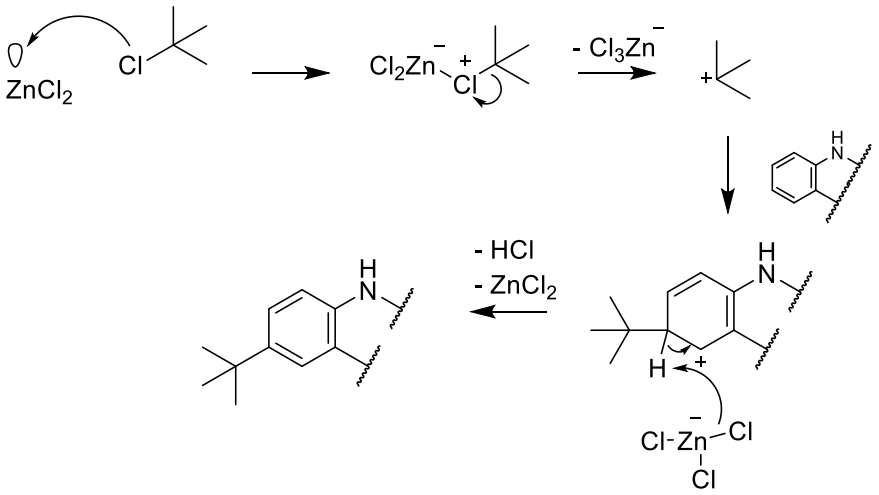

Scheme 4.14: Friedel-Crafts alkylation mechanism.

The alkylated product, 3,6-di-*tert*-butyl-*9H*-carbazole, **4.9**, was synthesised from carbazole using a $ZnCl_2$ catalyst in nitromethane, to which 2-chloro-2-methylpropane was added. 3,6-di-*tert*-butyl-*9H*-carbazole was isolated in 51% yield after purification by column chromatography using 7:3 CH_2Cl_2: Pet. Ether.

1,8-dinitro-3,6-di-*tert*-butyl-*9H*-carbazole (**4.10**) was successfully synthesised using the same methodology as in section 4.2.1.1. The crude product was purified by recrystallisation in DMF to give **4.10** in 23% yield. The dinitrocarbazole **4.10** was reduced to the amine **4.12** using Pd/C with a yield of 99%- overall yield of the two-steps was 23%. Due to the relatively poor yield of the first step, an alternative pathway was explored that would improve the overall yield of the transformation.

4.3.2 Bromination of 3,6-di-*tert*-butyl-*9H*-carbazole (4.11)

One method proposed in the synthesis of receptor *N*-bis(8-amino-3,6-di-*tert*-butyl-*9H*-carbazol-1-yl)carbamic amide, **4.15**, was the bromination of the *tert*-butyl substituted carbazole, **4.9**. The installation of bromine at the 1- and 8-position, via electrophilic aromatic substitution, Scheme 4.15, would allow for the facile amination transformation, eliminating the need for a nitration and subsequent reduction step entirely.

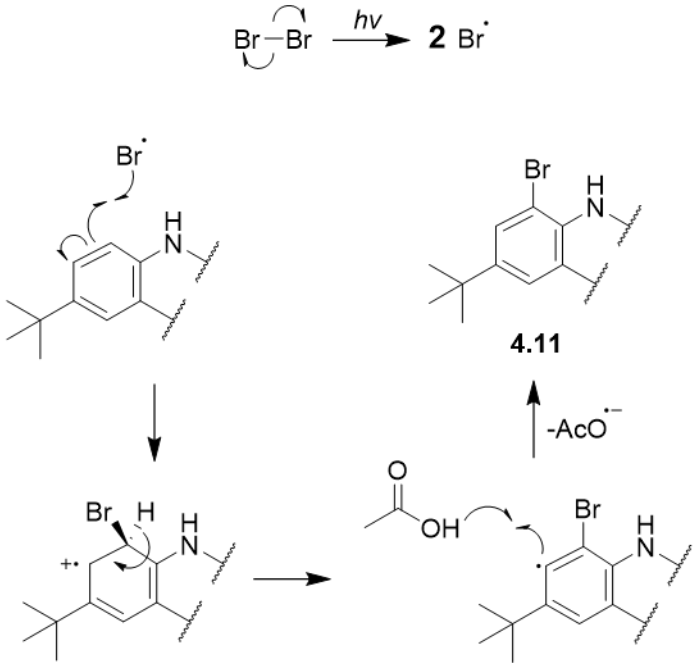

Scheme 4.15: Proposed radical substitution mechanism for the bromination of **4.9**.

In 1957, Brown and Stock investigated the relative reaction rates for the bromination of benzene and methylbenzenes.[30] They showed that the rate of the reaction relied upon numerous factors including the concentration of the initial aromatic, the presence of HBr and how concentrated the acetic acid solvent was. They determined that, in the case of the lower methylbenzenes (and benzene), pure acetic acid was reacting the bromine electrophile and decreasing the rate and so consequently, the acid solvent was diluted to 85% v/v with water. In the reaction of 3,6-di-*tert*-butyl-*9H*-carbazole, **4.9**, and Br_2, the desired product, **4.11**, was obtained in 99% yield. The *tert*-butyl group at the 3- and 6-position effectively blocked the substitution reaction at the *para* position, thus promoting the substitution at the *ortho* position, relative to -NH. The steric bulk of the electron-donating *tert*-butyl group meant that no addition at the *ortho* position was seen.

4.3.3 Amination of 1,8-dibromo-3,6-di-*tert*-butyl-*9H*-carbazole (4.12)

Copper has been shown to be an effective catalysis for numerous organic transformations and is finding use as a substitute for palladium. When compared to palladium, copper has a lower overall efficiency and thus requires a higher catalyst loading, however there are a number of benefits. The abundance of copper is significantly higher than palladium and with a much lower associated toxicity. Complexes of copper are easier to handle and more stable,

being less prone to oxidative deactivation.[31] The activity of copper can be further tuned through the coordination of different ligand systems around the metal. These ligands can modulate the electron density at the metal centre but also direct the site of the reaction through steric hinderance. Traditional reactions for the synthesis of C-N bonds, like Ullmann couplings (Section 3.2.1.2), often require stoichiometric amounts of Cu-catalyst and high reaction temperatures and by introducing coordinating ligands, it has been shown that the conditions required for amination can be made less intensive, requiring less than stoichiometric amounts of catalyst.[29] In 2008, Kim and Chang demonstrated the amination of electron-deficient aryl halides with ammonium salts in DMSO.[32] They showed that at 20 mol % CuI loading and 40 mol % L-proline ligand, aniline derivatives could be obtained in yields up to 97% at room temperature. Further developments of coordinating ligands led to Jung et al. developing a 1,2-dimethylethylenediamine (DMEDA) ligand/CuI system that required only 10 mol % catalyst and 15 mol % ligand loading, Scheme 4.16.[31] Their system used ammonium hydroxide as the ammonia source in DMSO and allowed for the amination of electron-rich aromatic substrates. The system also did not require the addition of any further inorganic base, such as Cs_2CO_3 or K_2CO_3, which is often seen in Cu amination reactions.

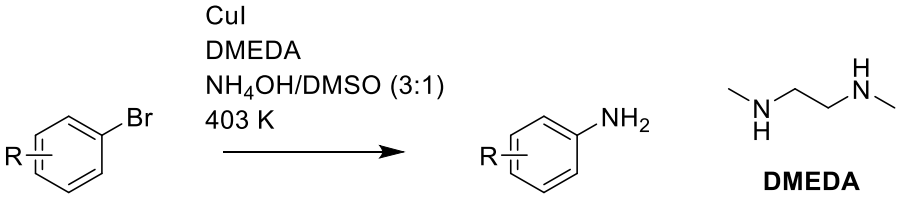

Scheme 4.16: Copper/DMEDA catalysed reaction for the formation of anilines.

Yields for the reaction ranged from 82-99%, showing excellent yields can be obtained at lower catalyst loadings. A tentative reaction mechanism can be proposed based on the related Pd-catalysed amination mechanism, Scheme 4.17.

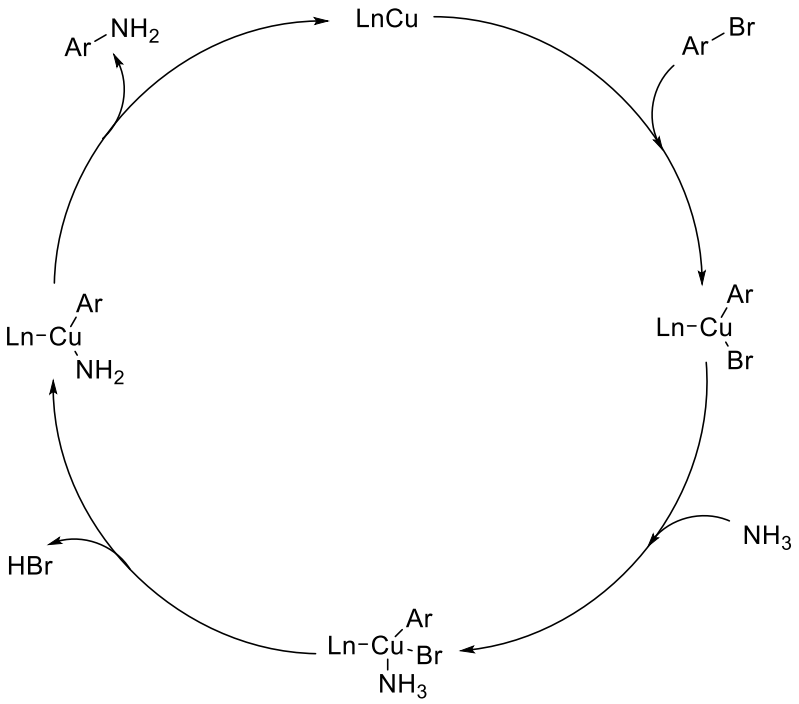

Scheme 4.17: Proposed Cu-catalysed amination mechanism.

This work by Jung and co-workers was the basis for the amination of the bromocarbazole yielding compound, **4.12**. In this reaction 1,8-dibromo-3,6-di-*tert*-butyl-*9H*-carbazole, **4.11**, was successfully converted to the corresponding diamine product, **4.12**, in 69% yield. This reaction was intended to reduce the reported problem of *t*-butyl group cleavage and eliminate the need for nitration-reduction steps, however reproducibility of this reaction proved troublesome. Although contained within a suitable pressure-vessel, the high reaction temperature and use of aqueous ammonia caused issues. It was thought that at the temperature used- 130 °C- both water and ammonia are gaseous, and the highly corrosive nature of ammonia appeared to react with the O-ring used to seal the vessel. This led to gaseous components escaping from the reaction and subsequently no aniline products were observed when the reaction was repeated. Based on this, the nitration-reduction route was used preferentially.

4.3.4 Mono-Boc protection of 3,6-di-*tert*-butyl-*9H*-carbazole-1,8-diamine (4.13)

Di-*tert*-butyl carbonate, or Boc anhydride, is one of the primary groups used in the protection of amines in both peptide and organic synthesis. Boc shows stability to a range of nucleophiles and is stable under basic hydrolysis, with the primary method of removal being

hydrolysis in strong acid, such as TFA. This leads to the release of isobutylene and carbon dioxide.[33] It is this release of CO_2 that drives the reaction. Yamaberi and co-workers used the Boc protecting group extensively during their synthesis of the cyclic α,α-disubstituted α-amino acid (*S*)(−)-Cucurbitine, **4.16** (shown with carboxybenzyl protecting group in red).[34]

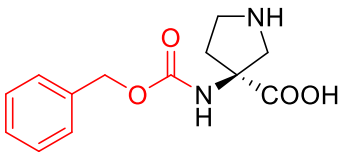

4.16

Cucurbitine has been shown to be an antiparasitic for schistosomiasis and inhibitory for the conversion of histidine to histamine. Cyclic disubstituted amino acids, like cucurbitine, have be shown to stabilize helical peptide structures. Homopeptides of these building blocks have been shown to have a preference for either right- or left-handed helical screws. In Yamaberi et al's experiments, they endeavoured to synthesise the (*S*)-(−)-enantiomer and characterise the helical screw of various lengths of homopeptides composed of cucurbitine. In order to effectively increase the chain length and prevent the cross-reaction with the pyrrolidine sidechain, a Boc protecting group was installed. During the synthesis, the terminal amine was protected using a carboxybenzyl group, which has a method of deprotection that is orthogonal to Boc- H_2 over Pd/C- allowing for the selective reaction-deprotection at each particular site. Morita et al. investigated the directing ability of the carbamate Boc group during the rhodium catalysed alkenylation of *N*-acylanilines.[35] It is well known that the C-H functionalisation can be catalysed by various metal catalysts such as palladium and rhodium, however these reactions can be further improved through the addition of directing groups, promoting the regioselective reaction. N-acylanilines have been shown to undergo ortho-selective alkenylation with the aforementioned metal catalysts, however limited work on carbamate directing groups, like Boc, had been investigated. Boc is easier to install and remove compared to acyl groups giving it potential as a traceless directing protecting group. In their investigation, Morita and co-workers successfully showed that using a Rh-catalyst ligand system, the ortho position could be alkenylated. Following this, they demonstrated that the Boc group could be readily removed, allowing for the further reaction of the free amine and the successful synthesis of a range of heterocyclic systems.

In this body of work, Boc was used to prevent the coupling of both the free amine moieties which would lead to the macrocycle being formed removing the reactive group for electrode attachment. The mechanism of protection is shown in Scheme 4.18.

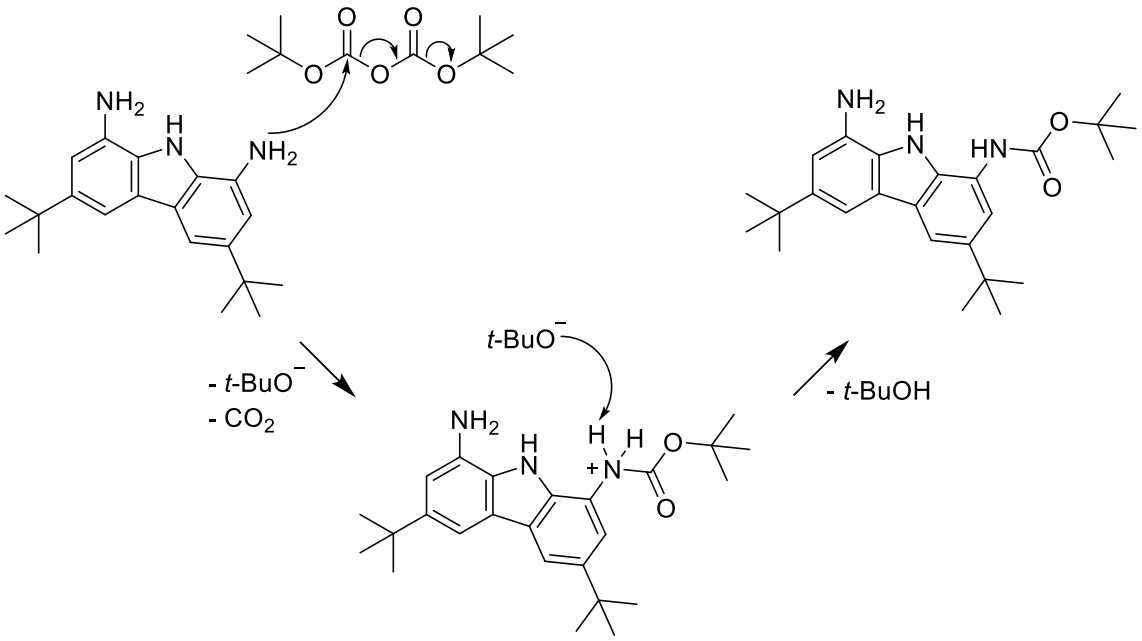

Scheme 4.18: Mechanism of Boc_2O protection.

The first step is the nucleophilic attack of -NH_2 at the electrophilic carbonyl carbon centre. This leads to the release of CO_2 and *t*-BuO^-. Secondly, deprotonation of the ammonium centre by either the released *t*-BuO^- or an added base, such as $NaHCO_3$, leads to the carbamate product. The group was successfully installed using Boc_2O and the mono-protected product, *tert*-butyl (8-amino-3,6-di-*tert*-butyl-*9H*-carbazol-1-yl)carbamate, **4.13**, was obtained in in 46% yield after purification by column chromatography.

4.3.5 CDIm coupling; synthesis of 1,3-Bis(3,6-di-*tert*-butyl-8-(*tert*-butoxycarbonylamino)-*9H*-carbazol-1-yl)urea (4.14)

1,1'-carbonyldiimidazole (CDIm) is a highly useful reagent capable of coupling a number of different functional groups. CDIm found use primarily as a peptide coupling reagent, responsible for the formation of the amide bond, however its use is not limited to such. CDIm can effectively be used to makes esters, and in the case of this work, urea groups. Danilov et al. showed the versatility of CDIm during their synthesis of adamantane-based ureas.[36] In their investigations, they attempted to form 2-(adamantan-1-yl)ethyl isocyanate, **4.17**, using two different synthetic methods.

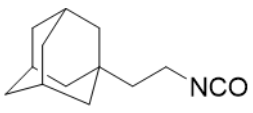

17

The first method involved the formation of an acid chloride and subsequent Curtius rearrangement using NaN_3. This method had two major drawbacks: the availability of the initial carboxylic acid and the use of the highly explosive sodium azide. An alternative synthesis was proposed that used a one-pot synthesis starting from an amine and its reaction with CDIm. This method used the more readily available amine starting material and requires less demanding conditions. The imidazole intermediate formed could also be isolated from the reaction mixture if needed. Pitushkin and co-workers used CDIm to create a range of asymmetric 1,3-disubstituted ureas.[37] They used CDIm in order to eliminate the inherent risks associated with using isocyanates, like toxicity and propensity for homocoupling and reaction with moisture. In their work, they used CDIm and two amines with different basicity and structure in order to effectively control the reaction. The formation of symmetric amine by-products is controlled by the basicity (nucleophilicity) of the starting amine. In order to prevent the homo-coupling, the amine introduced second must be more basic than the starting amine and react preferentially with the isocyanate formed. The coupling of two amine moieties using CDIm, to form a urea bond, is closely related to the amide forming reaction using CDIm, shown in 3.2.2. Scheme 4.19 shows the mechanism for the urea bond formation. The initial step is nucleophilic attack of the amine at the electrophilic carbonyl centre. This liberates imidazole and forms an imidazole containing urea. Subsequently, thermal rearrangement and decomposition of this urea liberates a second imidazole and forms the highly reactive isocyanate. The isocyanate is highly reactive and prone to nucleophilic attack by a second amine. This leads to the formation of the desired urea product, 1,3-Bis(3,6-di-*tert*-butyl-8-(*tert*-butoxycarbonylamino)-*9H*-carbazol-1-yl)urea, **4.14**, in 54% yield.

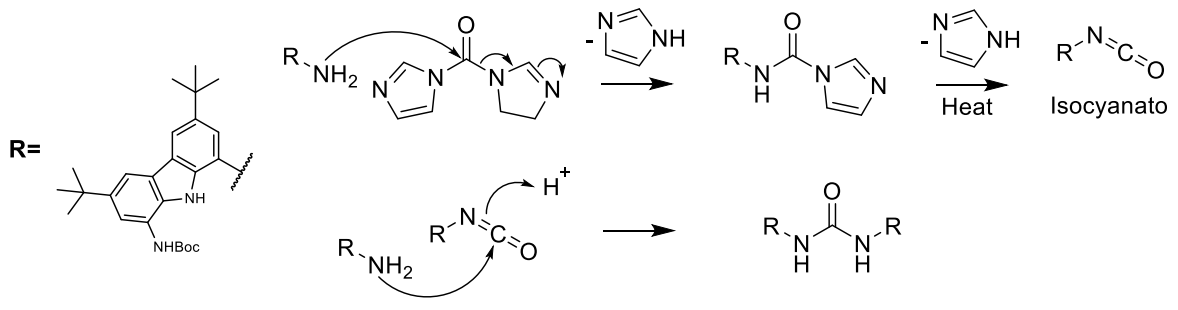

Scheme 4.19: CDIm coupling for the formation of urea mechanism.

4.3.6 Deprotection of 1,3-Bis(3,6-di-*tert*-butyl-8-(*tert*-butoxycarbonylamino)-*9H*-carbazol-1-yl)urea (4.15)

As shown in section 4.3.4, the Boc protecting group is incredibly important in the synthesis of a range of molecules due to its easy installation, relative stability to a range of nucleophiles and facile method of removal. The primary method for the removal is using trifluoroacetic acid, TFA, and the mechanism of removal, from a mono-Boc protected carbazole, is shown in Scheme 4.20. This same mechanism can be applied in the deprotection of **4.14**. Initially, the carbonyl of the carbamate can be protonated by the TFA. Subsequently, a rearrangement can occur whereby a *t*-butyl cation is liberated, and a carboxylic acid derivative is formed. These two species, the acid and cation, can undergo a further deprotonation by the TFA carboxylate conjugate base. The carboxylic acid will then release a molecule of CO_2. The carboxylate can also abstract a hydrogen from the cation and release isobutylene.

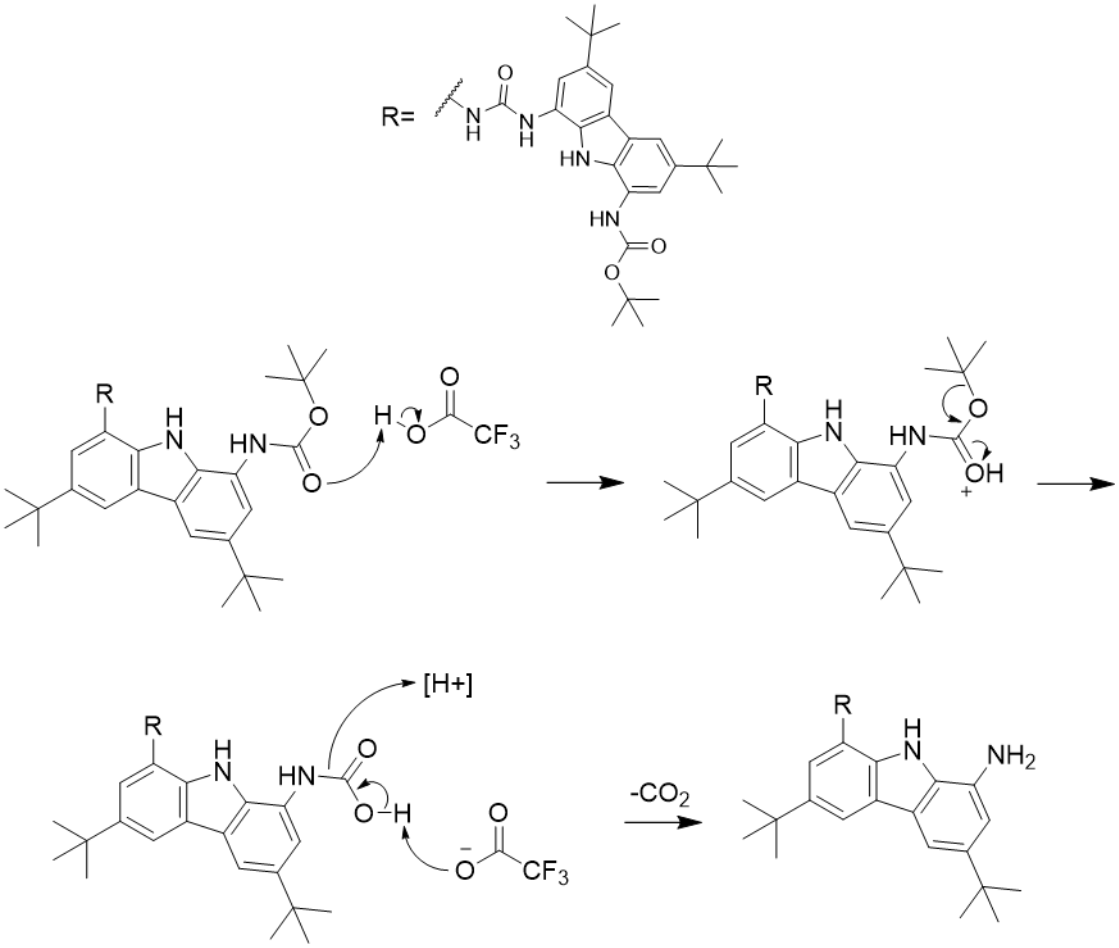

Scheme 4.20: Mechanism of deprotection of Boc using TFA.

Following the addition of TFA, **4.15**, was successfully obtained in excellent yield, 94%.

4.4 ^{1}H NMR Titrations of TEA·HCO_3

Binding studies of receptor **4.15** were conducted in d_6-DMSO/0.5% H_2O solutions and the NH- proton shifts observed. Bicarbonate was added as its TEA salt. By following the downfield shift of the urea and carbazole protons, the binding constant for the receptor could be determined. The addition of HCO_3^- anion causes the downfield shift of the NH-proton signals. Figure 4.1 shows this observed shift for up to 1.0 equivalent of anion added. As the concentration of anion increases, new signals in the spectra are observed. Integration of the signals show that these are not the result of deprotonation of the receptor as no change was observed in the integration.

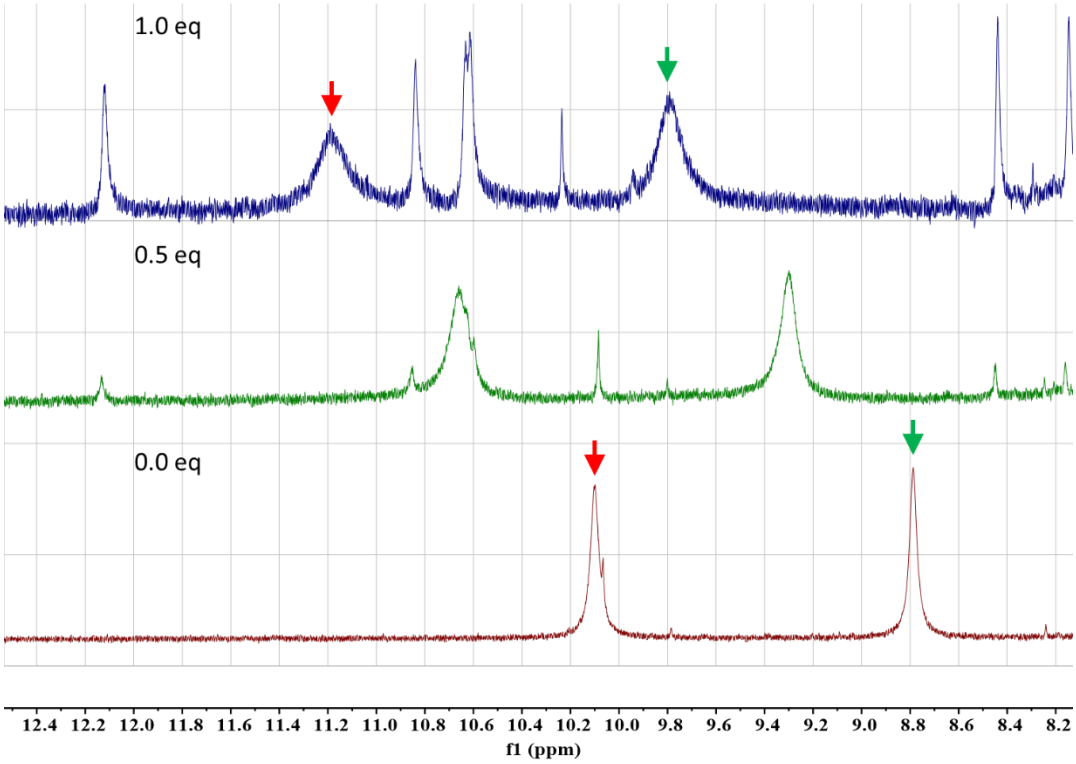

Figure 4.1: ^{1}H NMR of receptor **4.15** with TEA.HCO_3. Red arrow = carbazole; Green arrow = urea

The large shift is the result of the interaction of the H-bond donating NH-sites coordinating to the bicarbonate guest, proposed methods of which can be seen in Figure 4.2. It is proposed that the receptor donates four H-bonds to the anionic guest, as in Figure 4.2a, however it is plausible that the terminal amines are also involved and as such, six hydrogen bonds are formed between the receptor and the bicarbonate during complexation, Figure 4.2b.

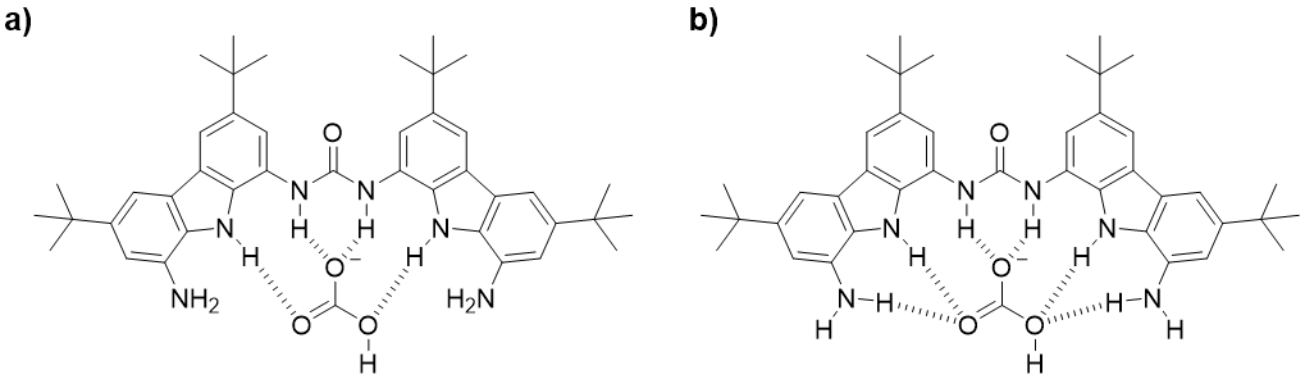

Figure 4.2: Proposed a) 4 H-bond; b) 6 H-bond binding mode of **4.15** and HCO_3^-.

From Figure 4.3, it can be seen that there is a reasonably large shift of just over 1.0 ppm observed for both the carbazole and urea NH-protons, indicating that it is likely that they are involved in the coordination of the anion. No such change in chemical shift was observed for the terminal amines and as such are unlikely to be involved in the complexation. The downfield shift that is seen is characteristic of the interaction of receptor and anion. From the graph, it can be seen that a break point is observed at around 1.0 equivalent of anion added, indicating a 1:1 binding stoichiometry. Fitting of the obtained data to a 1:1 binding model using Bindfit gave a K_a = > 10,000 M^{-1} for a mixed *d*$_6$-DMSO/0.5% H_2O solvent system at 298 K, Appendix-Chapter 4.[38] In order to gain a more accurate value for the K_a, a more sensitive technique should be used i.e., UV- Vis or fluorescence.

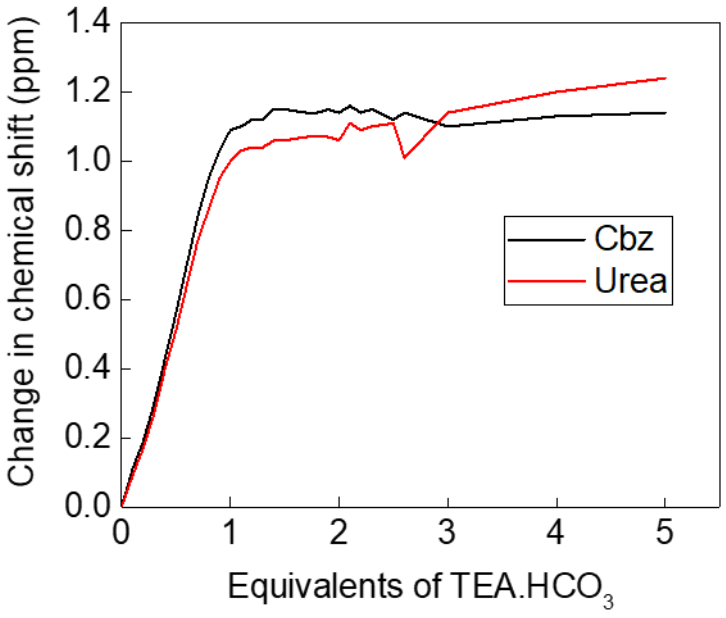

Figure 4.3: Change in ppm upon the addition of $TEA.HCO_3$ to receptor **4.15**.

4.5 Conclusions and Future Work

A bis-carbazolylurea receptor was synthesised modifying the work of Hiscock et al. and following closely the work of Sanchez and co-workers. This receptor had previously been shown to have high affinity for the bicarbonate anion and this formed the basis for this current body of work. Initially the synthetic route followed the one previously described by Hiscock and co-workers, but purification and poor yields at the start of the reaction led to a need for the change of synthetic route. The route proposed by Sanchez et al., installed *tert*-butyl at the carbazole para-position which aided the following synthetic step; the nitration reaction, by effectively blocking the most activated position of the carbazole ring and allowing for the desired 1-substituted product to be synthesised. Subsequent reactions followed those set out by Sanchez et al. and allowed for the synthesis of receptor **4.15** with an overall yield of 5%. The troublesome purification of the nitrocarbazole product was made much more facile through the addition of the *t*-Bu groups and utilisation of recrystallisation of the desired product from DMF. Proton NMR titrations of $TEA{\cdot}HCO_3$ were be performed in order to confirm the affinity of the receptor for the anion. It was demonstrated that receptor **4.15** showed affinity for the bicarbonate anion. Significant signal shifting was observed upon the addition of anion into solution of the receptor, indicative of a positive receptor-anion interaction. In addition to this, the titration of the receptor against other anions, such as NO_3, halides and AcO^-, would serve as a comparison and show the extent of the selectivity, if any, for HCO_3^-. It should be noted that direct comparison of the anion binding can only be done if the experimental conditions are the same e.g., same counterion, solvent etc., as previously discussed in Section 1.2. Following this the electrode attachment would be the next step. Glassy carbon electrodes (GCEs) have been shown to be able to form covalent bonds to a variety of different organic moieties- this can be the result of the reduction of a diazonium salt or the oxidation of an alkyne (Chapter 5.5). For receptor **4.15**, which bears free amine groups, the use of the diazonium salt would be employed. From Scheme 4.21, it can be seen how the functionalised GCE can be decorated with the synthesised receptor through a urea bond.

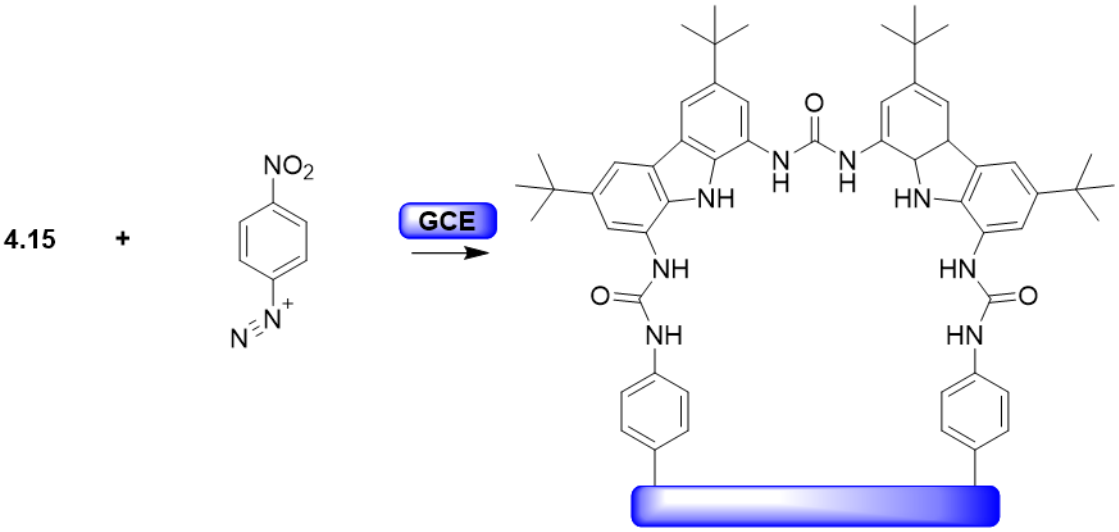

Scheme 4.21: Functionalisation of a GCE using a diazonium based linker and **4.15**.

The formation of this urea bond could be promoted through the use of coupling reagents, which include CDIm, triphosgene and DCC(/HOBt). By employing a urea as the coupling group, an extra H-bonding group has been introduced into the receptor's binding pocket, which may have a positive effect on the affinity of the receptor. Subsequently, the effectiveness of the functionalised electrode would be investigated in an electrochemical system.

4.6 Experimental

4.6.1 Materials and Reagents

All chemicals were of analytical reagent grade from Sigma-Aldrich/Merck, Alfa Aesar or Fluorochem and required no further purification.

4.6.2 General Synthetic methods

^{1}H NMR spectra were recorded on a Bruker DPX-400 (400 MHz) instrument. The chemical shifts are expressed in parts per million (ppm) referenced to TMS. Data are reported as follows: δ, chemical shift, multiplicity (recorded as b, broad; s, singlet; d, doublet; t, triplet; q, quartet; m, multiplet), coupling constants (J in Hertz, Hz), integration and assignment.

^{13}C NMR spectra were recorded on the same instrument at 100 MHz. The chemical shifts are expressed in parts per million (ppm), proton decoupled and referenced to TMS. Assignments were obtained from 2D-DEPT.

All NMR agree with literature data, where applicable.

4.6.2.1 NMR Analysis

Synthesis of 1-nitro-*9H*-carbazole (4.5)[21]

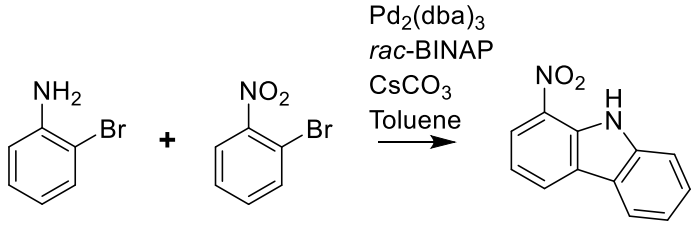

4.5

2-bromo-2-nitrobenzene (2.00 g, 9.90 mmol), $Pd_2(dba)_3$ (0.453 g, 0.495 mmol, 5 mol %), *rac*-BINAP (0.462 g, 0.743 mmol, 7.5 mol %) and Cs_2CO_3 (6.45 g, 19.8 mmol) were added to a 3-neck flask containing toluene (65 mL), through which N_2 gas was bubbled whilst stirring the solution for 15 min. 2-bromoaniline (1.08 mL, 9.90 mmol) was added dropwise and the resulting solution heated to reflux for 19 h. The resulting solution was filtered over

Celite and activated charcoal to yield a deep yellow solution. Volatiles were removed under reduced pressure and the crude product was purified using column chromatography using $CHCl_3$. The product **4.5** was obtained as yellow solid (0.728 g, 3.43 mmol 35%).

^{1}H NMR (400 MHz, d_6-DMSO) δ 12.17 (s, 1H), 8.63 (d, *J* = 7.5 Hz, 1H), 8.33 (d, *J* = 8.2 Hz, 1H), 8.26 (d, *J* = 7.8 Hz, 1H), 7.77 (d, *J* = 8.2 Hz, 1H), 7.50-7.55 (m, 1H), 7.34-7.39 (m, 1H), 7.28-7.34 (m, 1H).

^{13}C NMR (101 MHz, d_6-DMSO) δ 140.7 (ArC), 132.9 (ArC), 131.7 (ArC), 128.1 (ArCH), 127.3 (ArCH), 127.1 (ArC), 121.7 (ArCH), 121.5 (ArC), 120.7 (ArCH), 120.6 (ArCH), 118.4 (ArCH), 112.6 (ArCH).

Nominal MS *m/z*: 212 [M^+] Calculated 212.06 [M^+]

Synthesis of 3,6-di-*tert*-butyl-*9H*-carbazole[29] (**4.9**)

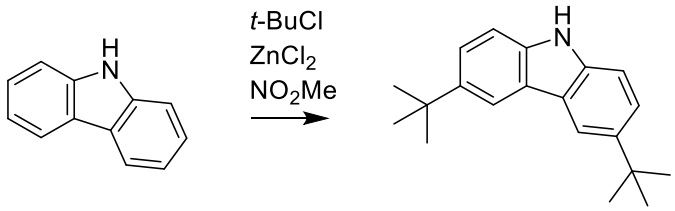

4.9

9H-carbazole (3.30 g, 20 mmol) and $ZnCl_2$ (8.10 g, 60 mmol) were added to 100 mL nitromethane and N_2 was bubbled through the solution for 15 min. 2-Chloro-2-methylpropane (6.5 mL, 60 mmol) was added dropwise under stirring and an N_2 atmosphere. The mixture was stirred at room temperature for 5 h and then hydrolysed with 100 mL water. The product was extracted with CH_2Cl_2 (3 × 60 mL). The organic layer was washed with H_2O (2 × 150 mL), dried over $MgSO_4$ and filtered to remove the solid. The organic solvent was removed under reduced pressure and the crude product was purified by column chromatography using 7:3 CH_2Cl_2: Pet. Ether as the eluting solvent. Product **4.9** was obtained as an off-white solid (2.86 g, 9.46 mmol 51%).

^{1}H NMR (400 MHz, $CDCl_3$) δ 8.09 (d, *J* = 1.8 Hz, 2H) 7.84 (bs, 1H), 7.48 (dd, *J* = 8.5, 1.9 Hz, 2H), 7.33 (d, *J* = 8.5 Hz, 2H), 1.46 (s, 18H)

^{13}C NMR (101 MHz, $CDCl_3$) δ 142.5 (ArC), 138.3 (ArC), 123.7 (ArCH), 123.4 (ArC), 116.4 (ArCH), 110.2 (ArCH), 34.9 (C), 32.2 (CH_3).

HRMS *m/z*: 302.1879 [M+Na]$^+$ Calculated 302.4198 [M+Na]$^+$.

Synthesis of 1,8-dinitro-3,6-di-*tert*-butyl-*9H*-carbazole[8] (**4.10**)

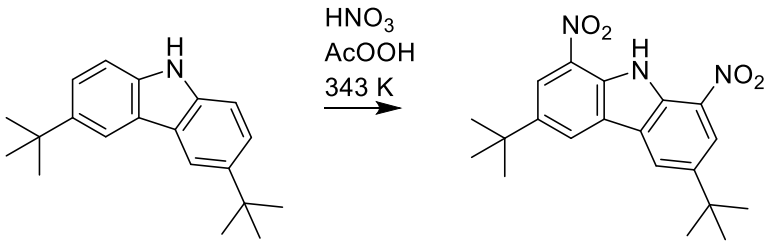

4.10

3,6-di-*tert*-butyl-*9H*-carbazole (**4.9**) (1.496 g, 5.36 mmol) was dissolved in acetic acid (35 mL) and stirred at 70 °C for 20 min. 0.360 mL (8.00 mmol) conc. HNO_3 added dropwise to the solution and stirred for a further 20 min. A further 0.360 mL HNO_3 was added, and the solution refluxed for 3 h. Solvent removed under reduced pressure. Product purified by crystallization in DMF. Insoluble product obtained by filtration to yield **4.10** as a yellow solid (0.441 g, 1.19 mmol, 23%).

^{1}H NMR (400 MHz, $CDCl_3$) δ 11.21 (s, 1H) 8.48 (d, *J* = 1.7 Hz, 2H), 8.45 (d, *J* = 1.6 Hz, 2H), 1.52 (s, 18H)
^{13}C NMR (101 MHz, $CDCl_3$) δ 144.8 (ArC), 132.8 (ArC), 132.6 (ArC), 126.3 (ArC), 124.8 (ArCH), 121.0 (ArCH), 35.4 (C), 31.9 (CH_3).
HRMS *m/z*: 370.1762 $[M+H]^+$ Calculated 370.1778 $[M+H]^+$.

Synthesis of 1,8-dibromo-3,6-di-*tert*-butyl-*9H*-carbazole[22] (**4.11**)

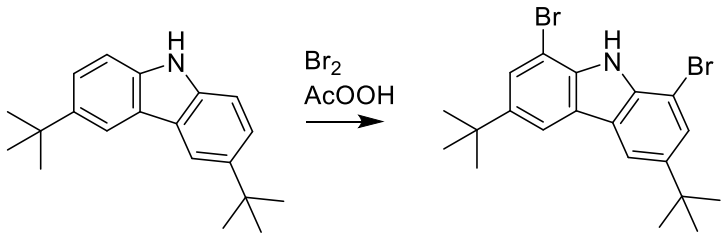

4.11

3,6-di-*tert*-butyl-*9H*-carbazole (**9**) (1.5 g, 5.4 mmol) was dissolved in glacial acetic acid (150 mL). At room temperature and with the exclusion of light, Br_2 (0.6 mL) was added dropwise. The mixture was stirred for 60 min, the volatiles were removed by rotary evaporation. The residue was dissolved in EtOAc (100 mL) and first washed with 1 M aqueous NaOH (3 × 30 mL) followed by $NaHCO_3$ (1 × 50 mL). Organic phase was dried over $MgSO_4$, filtered,

and concentrated under reduced pressure. Product **4.11** obtained as a yellow solid (2.32 g, 5.07 mmol, 99%).

^{1}H NMR (400 MHz, $CDCl_3$) δ 8.14 (s, 1H), 7.98 (d, *J* = 1.2 Hz, 2H), 7.64 (d, *J* = 1.6 Hz, 2H), 1.44 (s, 18H).
^{13}C NMR (101 MHz, $CDCl_3$) δ 145.0 (ArC), 136.5 (ArC), 126.8 (ArCH), 125.0 (ArC), 116.1 (ArCH), 104.2 (ArC), 35.1 (C), 32.1 (CH_3).
HRMS *m/z*: 458.0086 $[M+Na]^+$ Calculated 458.0098 $[M+Na]^+$.

Synthesis of 3,6-di-*tert*-butyl-*9H*-carbazole-1,8-diamine[22] (**4.12**)

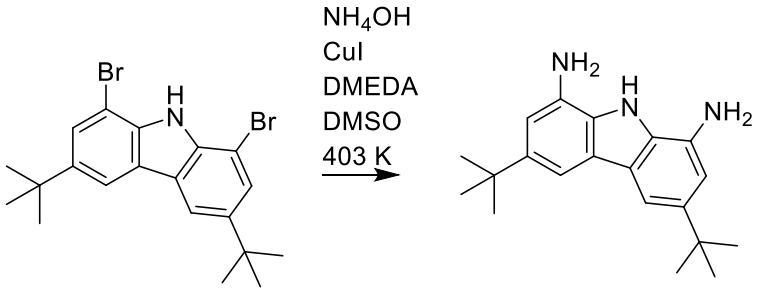

4.12

A 100 mL pressure (withstanding a maximum pressure of 10 bar at 120 °C was charged with a stirring bar, 1,8-dibromo-3,6-di-*tert*-butyl-*9H*-carbazole (**4.11**) (2.00 g, 4.57 mmol) and CuI (261 mg, 1.37 mmol). DMSO (24 mL) was added, and Ar gas bubbled through the solution for 5 min under stirring. Under Ar counterflow, *N*,*N'*-dimethyethylenediamine (226 μL, 2.06 mmol) was added and Ar bubbled through the mixture for a further minute. Ar flow stopped and the tube capped and stirred at room temperature for 20 min and then cooled in a water bath (10-15 °C). Stirring was stopped and the cap removed and under Ar counterflow, 16 mL 25% aqueous NH_3 was added by the sidewalls as to not disturb the contents. Ar flow was removed, and the tube was capped tightly with a screwcap. The mixture was vigorously stirred in an oil bath at 130 °C for 18 h. After heating, the tube was cooled to roughly 15 °C and the contents diluted with 100 mL EtOAc. The mixture was filtered, and brine (250 mL) was added to the filtrate. Phases were separated and the aqueous phase was extracted with EtOAc (3 × 50 mL). Combined organic phases were washed with brine, dried over $MgSO_4$, filtered and concentrated under reduced pressure. Resulting residue was dissolved in 10 mL CH_2Cl_2 and 100 mL hexane added, and the mixture cooled in an ice bath. The precipitate was filtered and washed three time with cold CH_2Cl_2:Hexane (1:10). Product **4.12** obtained as a grey powdery solid (0.98 g, 3.18 mmol, 69%).

^{1}H NMR (400 MHz, DMSO) δ 10.09 (s, 1H), 7.25 (d, *J* = 1.6 Hz, 2H), 6.70 (d, *J* = 1.7 Hz, 2H) 4.84 (s, 4H), 1.34 (s, 18H)

^{13}C NMR (101 MHz, DMSO) δ 141.6 (ArC), 132.5 (ArC), 127.5 (ArC), 123.4 (ArC), 107.5(ArCH), 104.8 (ArCH), 34.2 (C), 32.0 (CH_3).

HRMS *m/z*: 308.2135 $[M-H]^-$ Calculated 308.2122 $[M-H]^-$.

Synthesis of 3,6-di-*tert*-butyl-*9H*-carbazole-1,8-diamine[8,22] (**4.12**)

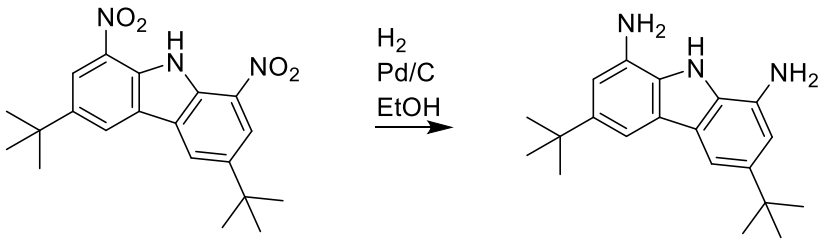

4.12

1,8-dinitro-3,6-di-*tert*-butyl-*9H*-carbazole (**4.10**) (0.441 g, 1.19 mmol) and Pd/C (0.100 g) was added to a stirring solution of dry EtOH (300 mL). H_2 gas was bubbled through the solution for 30 min before being stirred under a H_2 atmosphere for 12 h. The resulting solution was filtered over Celite and activated charcoal and EtOAc flushed through. Volatiles were removed under reduced pressure to yield **4.12** as a purple/grey solid (0.364 g, 1.18 mmol, 99%).

^{1}H NMR (400 MHz, DMSO) δ 10.09 (s, 1H), 7.25 (d, *J* = 1.6 Hz, 2H), 6.70 (d, *J* = 1.7 Hz, 2H) 4.84 (s, 4H), 1.34 (s, 18H)

^{13}C NMR (101 MHz, DMSO) δ 141.6 (ArC), 132.5 (ArC), 127.5 (ArC), 123.4 (ArC), 107.5(ArCH), 104.8 (ArCH), 34.2 (C), 32.0 (CH3).

Synthesis of *tert*-butyl (8-amino-3,6-di-*tert*-butyl-*9H*-carbazol-1-yl)carbamate[8] (**4.13**)

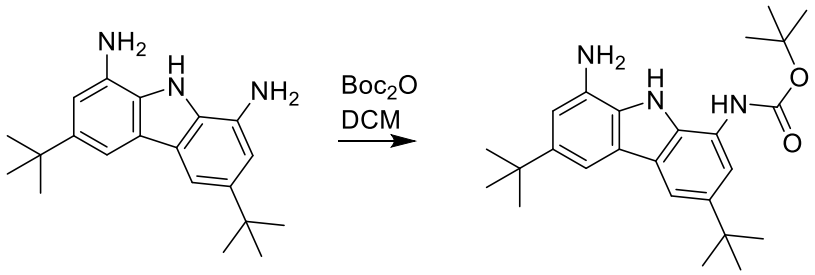

4.13

Di-*tert*-butyl bicarbonate (200 mg, 0.91 mmol) was added dropwise to a solution of 3,6-di-*tert*-butyl-*9H*-carbazole-1,8-diamine (**4.12**) in CH_2Cl_2 at 0 °C. Mixture stirred for 15 h at room temperature. H_2O (25 mL) added, and the biphasic mixture was extracted with CH_2Cl_2, dried over $MgSO_4$, filtered and concentrated under reduced pressure, yielding a purple-grey solid. Crude product was purified by column chromatography using initially, 3:1 Hexane: EtOAc, followed by 1:1 Hexane: EtOAc, for elution of the doubly protected and mono-protected amine, respectively. Product **4.13** obtained as pale grey solid (0.172 g, 0.42 mmol, 46%).

^{1}H NMR (400 MHz, d_6-DMSO) δ 10.16 (s, 1H), 8.87 (s, 1H), 7.74 (d, *J* = 1.6 Hz, 1H), 7.60 (bs, 1H), 7.35 (d, *J* = 1.6 Hz, 1H), 6.74 (d, *J* = 1.6 Hz, 1H), 5.01 (s, 2H), 1.52 (s, 9H), 1.37 (s, 9H), 1.35 (s, 9H)

^{13}C NMR (101 MHz, d_6-DMSO) δ 153.3 (CO), 142.2 (ArC), 140.8 (ArC), 132.7 (ArC), 127.4 (ArC), 124.3 (ArC), 122.9 (ArC), 122.4 (ArC), 122.3 (ArC), 115.3 (ArCH), 111.6 (ArCH), 108.1 (ArCH), 104.7 (ArCH), 79.0 (C), 34.4 (C), 34.3 (C), 31.9 (CH_3), 31.9 (CH_3), 28.2 (CH_3).

HRMS *m/z*: 410.2792 $[M+H]^+$ Calculated 410.2778 $[M+H]^+$.

Synthesis of 1,3-Bis(3,6-di-*tert*-butyl-8-(*tert*-butoxycarbonylamino)-*9H*-carbazol-1-yl)urea[8] (**4.14**)

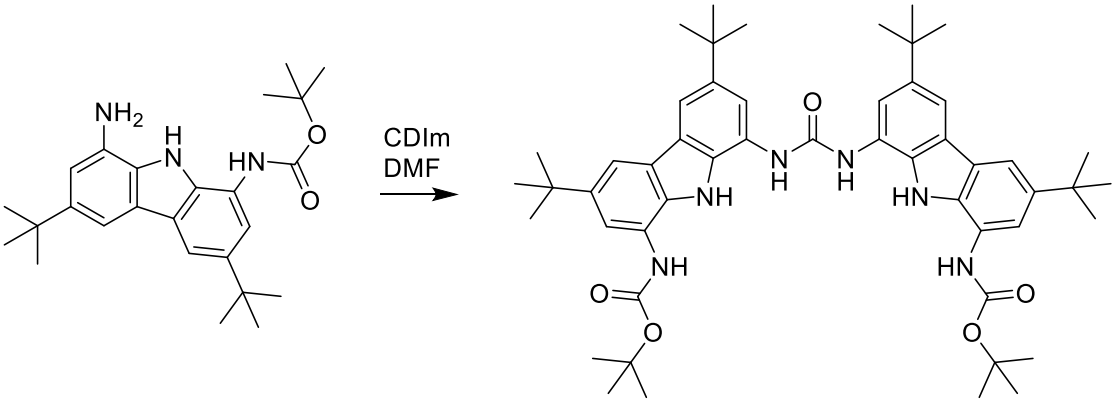

4.14

CDIm (0.120 g, 0.74 mmol) and *tert*-butyl (8-amino-3,6-di-*tert*-butyl-*9H*-carbazol-1-yl)carbamate (**4.13**) (0.172 g, 0.42 mmol) were dissolved in dry DMF (30 mL), under an N_2 atmosphere, and the resulting solution stirred for 15 h at 60 °C. Once cooled, the reaction was quenched with aqueous NaCl to yield a pale white precipitate which was isolated by filtration. Precipitate was dissolved in CH_2Cl_2 (20 mL) and washed with H_2O. Organic layers combined, dried over $MgSO_4$ and concentrated under reduced pressure. Product obtained as a brown solid (0.096 g, 0.11 mmol 54%).

^{1}H NMR (400 MHz, d_6-DMSO) δ 10.26 (s, 2H), 9.28 (s, 2H), 8.79 (s, 2H) 7.92 (d, J = 1.6 Hz, 2H) 7.86 (d, J = 1.6 Hz, 2H), 7.79 (bs, 2H), 7.50 (d, J = 1.1 Hz, 2H), 1.45 (s, 18H), 1.41 (s, 18H), 1.39 (s, 18H)

^{13}C NMR (101 MHz, d_6-DMSO) δ 153.7 (CO), 153.2 (CO), 141.6 (ArC), 141.5 (ArC), 131.6 (ArC), 129.8 (ArC), 124.2 (ArC), 123.9 (ArC), 122.9 (2 × ArC), 117.0 (ArCH), 114.8 (ArCH), 112.1 (ArCH), 111.2 (ArCH), 79.2 (C), 34.5 (C), 34.4 (C), 31.9 (2 × CH_3), 28.1 (CH_3).

HRMS *m/z*: 867.5145 $[M+Na]^+$ Calculated 867.5198 $[M+Na]^+$.

Synthesis of *N*-bis(8-amino-3,6-di-*tert*-butyl-*9H*-carbazol-1-yl)carbamic amide[8] (4.15)

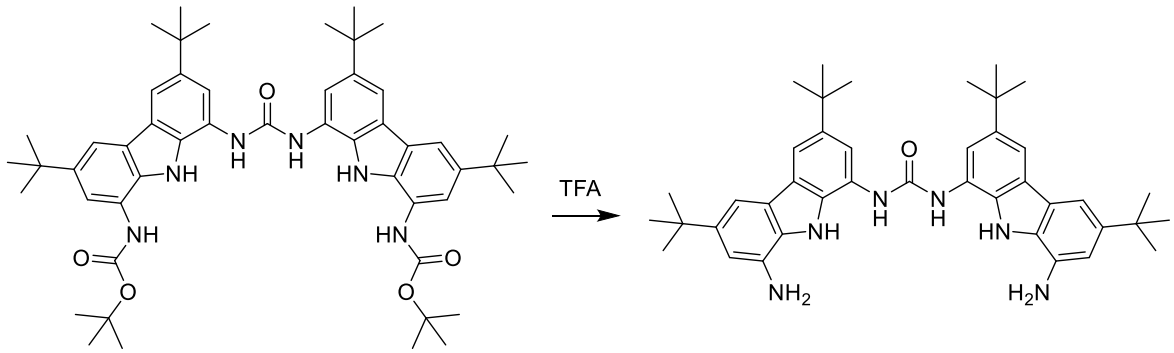

4.15

1,3-Bis(3,6-di-*tert*-butyl-8-(*tert*-butoxycarbonylamino)-*9H*-carbazol-1-yl)urea (**4.14**) (0.272 g, 0.322 mmol) was dissolved in TFA (40 mL) and stirred at room temperature for 2 h. Solution was concentrated under reduced pressure and the viscous oil obtained was partitioned between CH_2Cl_2 and sat. $NaHCO_3$. The organic phases were combined, dried over $MgSO_4$, filtered, and concentrated under reduced pressure. Product obtained as a pale purple/grey solid (0.098g, 0.15 mmol, 94%).

^{1}H NMR (400 MHz, d_6-DMSO) δ 10.02 (s, 2H), 8.72 (s, 2H), 7.82 (d, *J* = 1.4 Hz, 2H), 7.37 (d, *J* = 1.5 Hz, 2H), 7.35 (d, *J* = 1.7 Hz, 2H), 6.75 (d, *J* = 1.7 Hz, 2H), 5.17 (bs, 4H), 1.41 (s, 18H), 1.36 (s, 18H).

^{13}C NMR (101 MHz, d_6-DMSO) δ 153.9 (CO), 142.2 (ArC), 140.9 (ArC), 132.8 (ArC), 131.8 (ArC), 127.3 (ArC), 124.8 (ArC), 123.0 (ArC), 122.7 (ArC), 116.5 (ArCH), 112.1 (ArCH), 107.9 (ArCH), 104.4 (ArCH), 34.4 (C), 34.3 (C), 32.0 (CH_3), 31.9 (CH_3).

HRMS *m/z*: 645.5304 $[M+H]^+$ Calculated 645.4278 $[M+H]^+$.

4.7 References

1 R. Lindsey, Climate Change: Atmospheric Carbon Dioxide, https://www.climate.gov/news-features/understanding-climate/climate-change-atmospheric-carbon-dioxide#, (accessed 20 March 2023).

2 K. Sumida, D. L. Rogow, J. A. Mason, T. M. McDonald, E. D. Bloch, Z. R. Herm, T. H. Bae and J. R. Long, *Chem Rev*, 2012, **112**, 724–781.

3 P. R. Edwards, J. R. Hiscock and P. A. Gale, *Tetrahedron Lett*, 2009, **50**, 4922–4924.

4 R. E. Zeebe and D. Wolf-Gladrow, , in *CO_2 in Seawater: Equilibrium, KInetics and Isotopes*, Gulf Professional Publishing 2001, 2–3.

5 M. Ansari, R. Bera and N. Das, *J Appl Polym Sci*, 2022, **139**, 1–9.

6 S. Qian, X. Liu, C. H. Turner and J. E. Bara, *Chem Eng Sci*, , DOI:10.1016/j.ces.2021.117150.

7 M. Pagliaro and R. Ciriminna, *J Mater Chem*, 2005, **15**, 4981–4991.

8 G. Sánchez, A. Espinosa, D. Curiel, A. Tárraga and P. Molina, *Journal of Organic Chemistry*, 2013, **19**, 9725-9737.

9 J. R. Hiscock, C. Caltagirone, M. E. Light, M. B. Hursthouse and P. A. Gale, *Org Biomol Chem*, 2009, **7**, 1781–1783.

10 J. B. Kyziol and Z. Daszkiewicz, *Tetrahedron*, 1984, **40**, 1857–1861.

11 N. L. Drake, H. J. S. Winkler, C. M. Kraebel and T. D. Smith, 1961, **27**, 1026–1030.

12 T. D. B. Morgan and D. L. H. Williams, *Journal of the Chemical Society, Perkin Transactions 2*, 1972, **1**, 74–78.

13 M. B. Smith, *March's Advanced Organic Chemistry: Reactions, Mechanisms and Structure*, John Wiley & Sons, Inc, 2013, 1213–1214.

14 Weygand and Hilgetag, *Preparative Organic Chemistry*, John Wiley & Sons, Inc, 4th edn., 1972, 461.

15 F. Ullmann and J. Bielecki, *Berichte der deutschen chemischen Gesellschaft*, 1901, **34**, 2174–2185.

16 M. Kosugi, M. Kameyama and T. Migita, *Chem Lett*, 1983, 927–928.

17 A. S. Guram and S. L. Buchwald, *J. J. Am. Chem. Soc*, 1994, **116**, 7901–7902.

18 J. P. Wolfe and S. L. Buchwald, *Journal of Organic Chemistry*, 2000, **65**, 1144–1157.

19 G. Mann and J. F. Hartwig, *Journal American Chemical Society* , 1996, **118**, 13109–13110.

20 E. Merişor and U. Beifuss, *Tetrahedron Lett*, 2007, **48**, 8383–8387.

21 R. B. Bedford and C. S. J. Cazin, *Chemical Communications*, 2002, **2**, 2310–2311.

22 A. Rüütel, V. Yrjänä, S. A. Kadam, I. Saar, M. Ilisson, A. Darnell, K. Haav, T. Haljasorg, L. Toom, J. Bobacka and I. Leito, *Beilstein Journal of Organic Chemistry*, 2020, **16**, 1901–1914.

23 C. Friedel and J.-M. Crafts, *Sur une nouvelle méthode générale de synthèse d'hydrocarbures, d'acétones, etc.*, Paris, 1877, vol. 84.

24 N. Calloway, *Chem. Rev*, 1935, **17**, 327–382.

25 M. Rueping and B. J. Nachtsheim, *Beilstein Journal of Organic Chemistry*, 2010, **6**, 1−24.

26 A. Krusenbaum, J. Geisler, F. J. L. Kraus, S. Grätz, M. V. Höfler, T. Gutmann and L. Borchardt, *Journal of Polymer Science*, 2022, **60**, 62–71.

27 L. Jiang, P. Wang, Y. Wang, Y. Wang, X. Li, Q. Xia and H. Ren, *J Colloid Interface Sci*, 2021, **582**, 631–637.

28 T. Kader, G. Jin, M. Pletzer, D. Ma, J. Fröhlich, J. Chen and P. Kautny, *Org Electron*, , DOI:10.1016/j.orgel.2021.106215.

29 Y. Liu, M. Nishiura, Y. Wang and Z. Hou, *Journal American Chemical Society*, 2006, **128**, 5592–5593.

30 B. C. Herbert Brown and L. M. Stock, *J. Am. Chem. Soc*, 1957, **79**, 1421–1425.

31 H. S. Jung, T. Yun, Y. Cho and H. B. Jeon, *Tetrahedron*, 2016, **72**, 5988–5993.

32 J. Kim and S. Chang, *Chemical Communications*, 2008, **26**, 3052–3054.

33 P. G. M. Wuts and T. W. Greene, in *Greene's Protective Groups in Organic Synthesis*, John Wiley & Sons, Inc., 2006, pp. 696–926.

34 Y. Yamaberi, R. Eto, T. Umeno, T. Kato, M. Doi, H. Yokoo, M. Oba and M. Tanaka, *Org Lett*, 2021, **23**, 4358–4362.

35 T. Morita, T. Satoh and M. Miura, *Org Lett*, 2017, **19**, 1800–1803.

36 D. v. Danilov, V. v. Burmistrov and G. M. Butov, *Russian Journal of Organic Chemistry*, 2020, **56**, 1132–1139.

37 D. A. Pitushkin, V. v. Burmistrov, M. H. A. Saeef, A. A. Vernigora and G. M. Butov, *Russian Journal of Organic Chemistry*, 2020, **56**, 1893–1904.

38 D. Brynn Hibbert and P. Thordarson, *Chemical Communications*, 2016, **52**, 12792–12805.

Chapter 5

1,3-dicarboxamide Receptor for Anion Recovery and Electrochemical methods for electrode attachment

Acknowledgements and Declaration

Calum Hope performed the experimental work and data analysis. Mass spectrometry analysis was conducted by Mr Gangi Ubbara. Mark Symes conceived the idea and assisted with data analysis.

Synopsis

Capacitive deionisation has been demonstrated to be a promising method for the removal of ionic species, such as nitrate,[1] fluoride,[2] and sulfate,[3] from low-to-medium salinity water inlet streams. The addition of a selective element, such as a hydrogen bonding receptor, to such a system would hopefully allow for the preferential removal of one specific species over others within the stream. In order to be applicable within a capacitive deionisation system, the receptor must contain a group which can be used to attach the receptor to the electrode surface. There are a number of different groups that have been shown to allow organic groups to be covalently attached to an electrode surface, such as diazonium salts and alkyne groups. Within this chapter, a hydrogen bonding receptor was devised that had been modified to contain one of two potential groups that would allow for immobilisation on the electrode surface-a carboxylic acid or an alkyne. UV-Vis spectroscopy was used to determine the alkyne functionalised receptor's ability to bind to a number of different anionic species. The synthesised receptor was shown to be selective for dihydrogenphosphate, showing no affinity for any of the other anions tested.

5.1 Introduction

Anion receptors, particularly hydrogen bond accepting, have been shown to be highly effective in the sequestering of various anions. Fluorescent anion receptors have garnered heavy interest due to their low detection limit and high sensitivity.[4,5] The design of fluorescent receptors relies on effective integration of binding motifs that can accept or donate bonds to the anion, being successfully coupled to a fluorophore. During the binding process, the emission of the fluorophore is modified and leads to a specific anion-receptor emission spectrum. Development of simple to synthesise anion receptors has focussed on implementing moieties such as ureas (and their derivatives), indoles,[6,7] pyrroles[8] and various others. In 2005, Kang and co-workers synthesised two anion receptors, **5.1** and **5.2**, that had a 2-aminobenzimidazole as the recognition site, joined to an anthracene fluorophore via a methylene.[9]

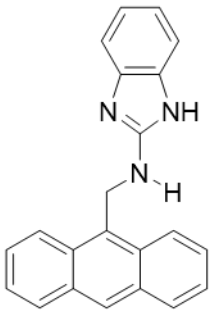

5.1

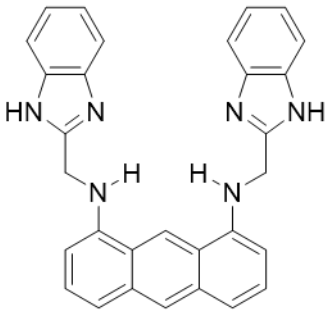

5.2

This was the first example of a 2-aminobenzimidazole based receptor. The binding constants for both receptors were determined through fluorescence titrations in CH_3CN at 25°C and showed fluorescence quenching as the concentration of halide anions- F^-, Cl^- and Br^- - increased. The decrease in emission and no change to the spectral absorption indicated a photoinduced electron transfer as a result of the formation of a receptor-anion complex. Receptor **1** showed the greatest affinity for fluoride with K_a determined to be 2.06 ± 0.32 $\times 10^5$ M^{-1}. The binding constants for the halides follow the diameter and basicity of the ions, with the smaller, more basic fluoride having the largest affinity as a result of the better fit into the binding cleft. Consequently, the affinity for **5.1** was 42 times more for fluoride than chloride. Fluorescence titrations of **5.1** with anions of a different geometry, tetrahedral $H_2PO_4^-$ and trigonal planar AcO^-, showed affinity for AcO^- with the association constant determined to be 1.00 ± 0.26 $\times 10^5$ M^{-1}. Stoichiometric investigations showed that for all the halides and carboxylate anions tested, the associated Job's plot showed a 1:1 binding stoichiometry. During the investigations of $H_2PO_4^-$, the asymmetric Job's plot observed

implies that a mixed stoichiometry is responsible for the binding and subsequently, an accurate binding constant could not be calculated. Investigation into the binding affinity of receptor **5.2** under the same conditions used, showed a slight increase in the affinity for the halides. A much larger increase in binding affinity was observed for the non-spherical acetate and dihydrogenphosphate anion. Job's plots for all the anions showed a 1:1 stoichiometry. The large increase was determined to be the result of the increase in the number of the H-bonding motifs involved in the binding process. The association constants for **5.2** were similar to those observed for urea/thiourea based receptors.

Zaleskaya-Hernik et al. developed a squaramide receptor, **5.3**, that contained an anthracene fluorophore and was shown to be highly sensitive to sulfate with the ability to extract sulfate anions from the aqueous phase into the organic phase.[10]

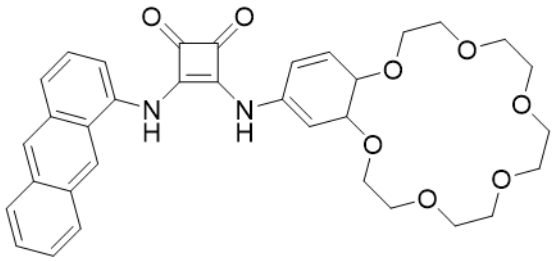

5.3

This was the first example of a fluorescent receptor for the extraction of the extremely hydrophilic sulfate anion. Initial mass spectrometry experiments showed a complex binding model when TBA·SO_4 was added showing that a 4:1 receptor-anion complex was formed. They showed that the presence of the crown-ether and fluorophore ensure that the ion-pair receptor can interact sufficiently with the anions whilst also ensuring solubility in organic solvents, such as $CHCl_3$. They consequently showed a 17.6% extraction for K_2SO_4. Fluorescence experiments showed almost complete quenching of the observed spectra when 100 equivalents of sulfate anion were added. Interestingly, they showed that in the presence of water, the fluorescence intensity of **5.3** was quenched as a result of the water molecules interacting with the binding squaramide binding site. Fluorescence titrations of sulfate into receptor solutions - 2.4 mM **5.3** in acetonitrile containing 1% water at 298 K – initially led to an increase in the fluorescence intensity up to a point, before a decrease was observed. The increase in intensity is attributed to the changing of **5.3**-water complexes to complexes with sulfate. These properties were utilised in order to create a system whereby sulfate anions could be detected in dry organic solvents and could be extracted from wet acetonitrile and chloroform.

5.1.1 Capacitive Deionisation

Since its inception in the late 1960s and early 1970's, the CDI process has been extensively studied and the technology implemented within such systems has been hugely improved. Developments to electrode materials e.g., porosity, cell design and operational conditions have led to CDI showing enhanced promise for the desalination of low-medium salinity waterbodies.[11,12] Capacitive deionisation (CDI) systems have been shown to be effective in the desalination of brackish wastewater systems through the formation of the electric-double layer. In these systems a small electrical potential is applied across a porous, normally carbon, electrode pair, attracting oppositely charged ions in solution, towards the electrode surface and a desalinated solution is obtained. Over time, the electrode surface becomes saturated, and no further ions can be removed from the solution and held electrostatically on (or close) to electrode surface. By reversing the polarity across the electrodes, ions held at the surface are repelled into a new flue stream leading to a concentrated 'waste' solution of ions that can be disposed of or undergo downstream processing. This two-stage process is known as purification (Figure 5.1a) and regeneration (Figure 5.1b), respectively.

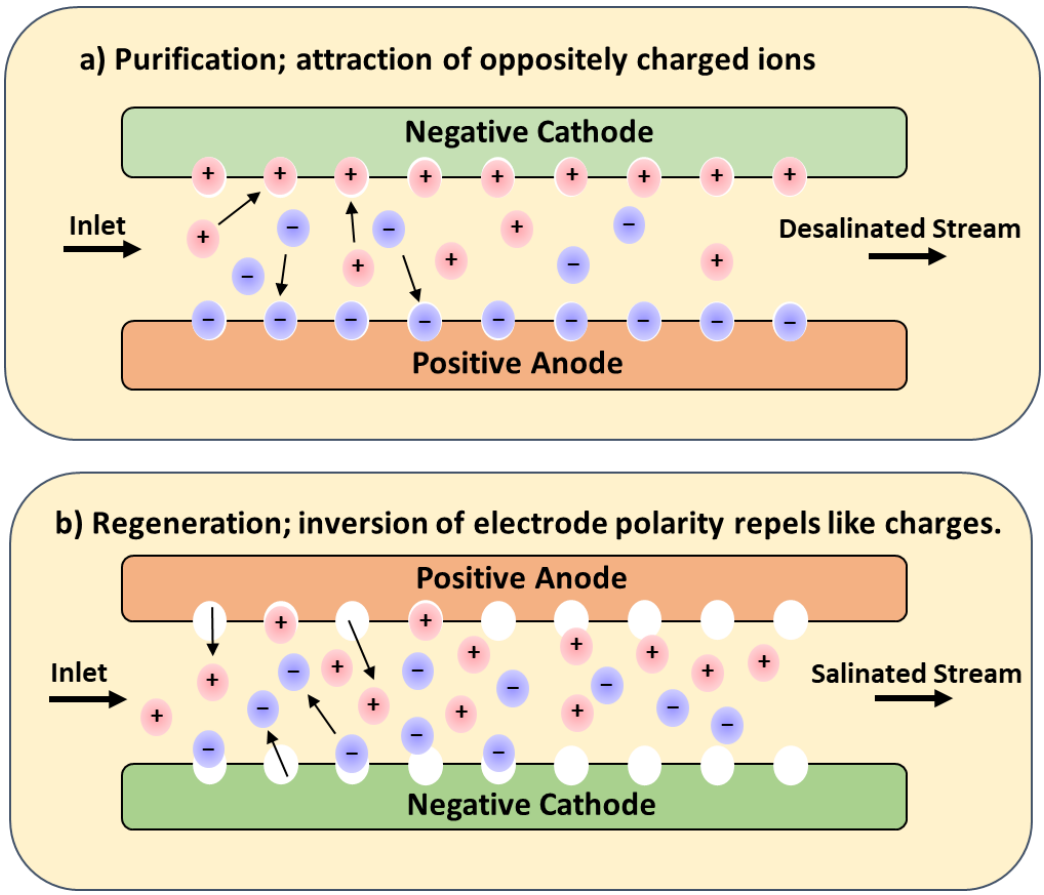

Figure 5.1: Two-stage CDI process a) purification; b) regeneration

$H_2PO_4^-$, and phosphoric acid in its other forms, are used heavily in fertilizers and agricultural run-off leads to elevated concentrations of phosphate in bodies of water such as rivers and lakes. Herein, we show that a capacitive deionisation system could potentially be created in which an anion, in this instance $H_2PO_4^-$, could be selectively removed by means of a H-bonding receptor that is covalently bound to the surface, via an organic spacer group, of a carbon electrode. UV-Vis spectroscopic titrations with a range of anions, show that the synthesised receptor showed high affinity for $H_2PO_4^-$, with minimal to no binding observed upon the addition of NO_3^-, I^-, Br^- and AcO^-. Job's plot analysis of this binding with the dihydrogenphosphate anion, showed the receptor-anion binding stoichiometry was 1:1.

5.2 Proposed Reaction Scheme

In 2012, Kondo and Takai designed two tetra-amide based receptors, **5.4** and **5.5**, which both contained different fluorophore groups, 1-isoquinolyl and 2-quinolyl, respectively, an amino acid and an isophthaloyl central spacer.[13]

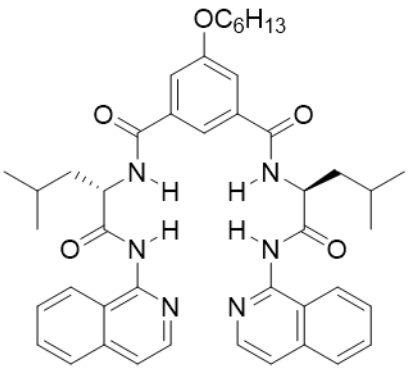

5.4

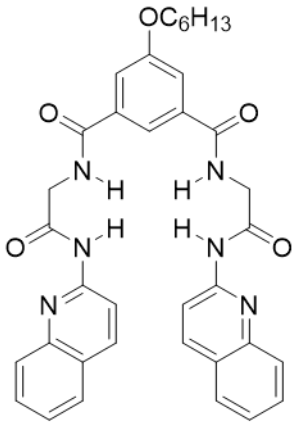

5.5

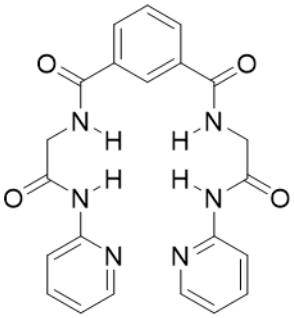

5.6

This work built upon a previously synthesised receptor, **5.6**, which was also tetra-amide based and terminated with a pyridyl moiety. This receptor was shown to be able to discriminate between the structurally similar $H_2PO_4^-$ and AcO^- anions, in favour of $H_2PO_4^-$

as the result of the formation of additional H-bonds formed from the terminal pyridine groups.[14] The lack of fluorophore in receptor **5.6** prompted the substitution of the pyridyl end group with one of isoquinoline or quinoline in order to be able to apply fluorescent detection techniques to show anion binding. The synthetic scheme for the synthesis of **5.4** or **5.5** is seen in scheme 1. Both receptors were synthesised with an overall yield of 47% and 34%, respectively.

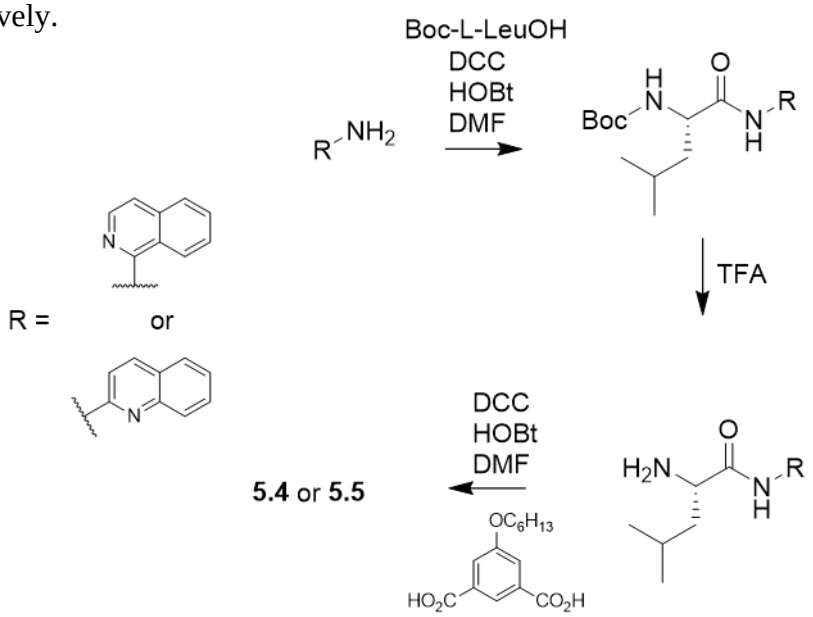

Scheme 5.1: Synthetic route for the synthesis of **5.4** and **5.5.**

Their work showed that receptor **5.5**, which bore the 2-quinolyl terminal fluorophore, was shown to have high affinity for $H_2PO_4^-$; K_a, at 298 K, was determined to be $(5.41 \pm 0.40) \times 10^6$ by UV-Vis and $(2.76 \pm 0.10) \times 10^6$ by fluorescence, making it suitable as a fluorescence sensor. **5.5** was also shown to have a much greater selectivity for $H_2PO_4^-$ over AcO^-. Competition studies showed that the selectivity of **5.5** was 27.8 times greater in favour of dihydrogenphosphate. They proposed that the nitrogen group in the quinolyl moiety was integral in discerning the difference between the two anions. The four amide groups act as H-bond donors and bind to the oxygen atoms in both $H_2PO_4^-$ and AcO^-, however the isoquinolyl nitrogen is able to act as a H-bond acceptor for the $H_2PO_4^-$ hydroxyl groups. These groups are not present in the acetate anion and so a higher selectivity is observed for the phosphate species. In order to synthesise a receptor that can be employed within a CDI system, the receptor must be modified to include a group that can be used to graft the electrode to the surface. Based on the synthesis first described by Kondo and Takai, the isophthaloyl group could be modified to include such a moiety. Receptor **5.7** was proposed and substituted the hexyl ether for a carboxylic acid. The carboxylic acid could then be

coupled to the electrode through an amide moiety via an organic spacer molecule, using coupling reagents or further transformation to a highly reactive acid chloride.

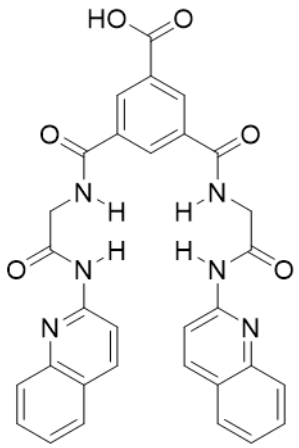

5.7

Scheme 5.2 shows the initial proposed synthesis. The initial work undertaken was to ensure that the isophthaloyl spacer molecule could be synthesised. The first step is the mono deprotection of **5.10** using dilute NaOH in methanol. The dimethyl ester-carboxylic acid, **5.11**, can then subsequently have a benzyl ester installed using Boc_2O, benzyl alcohol and catalytic DMAP. The installation of the orthogonal benzyl ester protecting group (PG) allows for the selective removal of the methyl ester groups in the following step. By repeating the initial reaction, deprotection of the methyl esters using NaOH, the dicarboxylic acid, **5.13**, could be obtained. Intermediate **5.9** could be synthesised following the synthetic route set out by Kondo and Takai. The coupling of **5.9** and **5.13** using DCC as the coupling reagent, catalysed by HOBt, would yield the benzyl protected receptor, **5.14**, which can be deprotected under mild conditions using H_2 over a Pd/C catalyst.

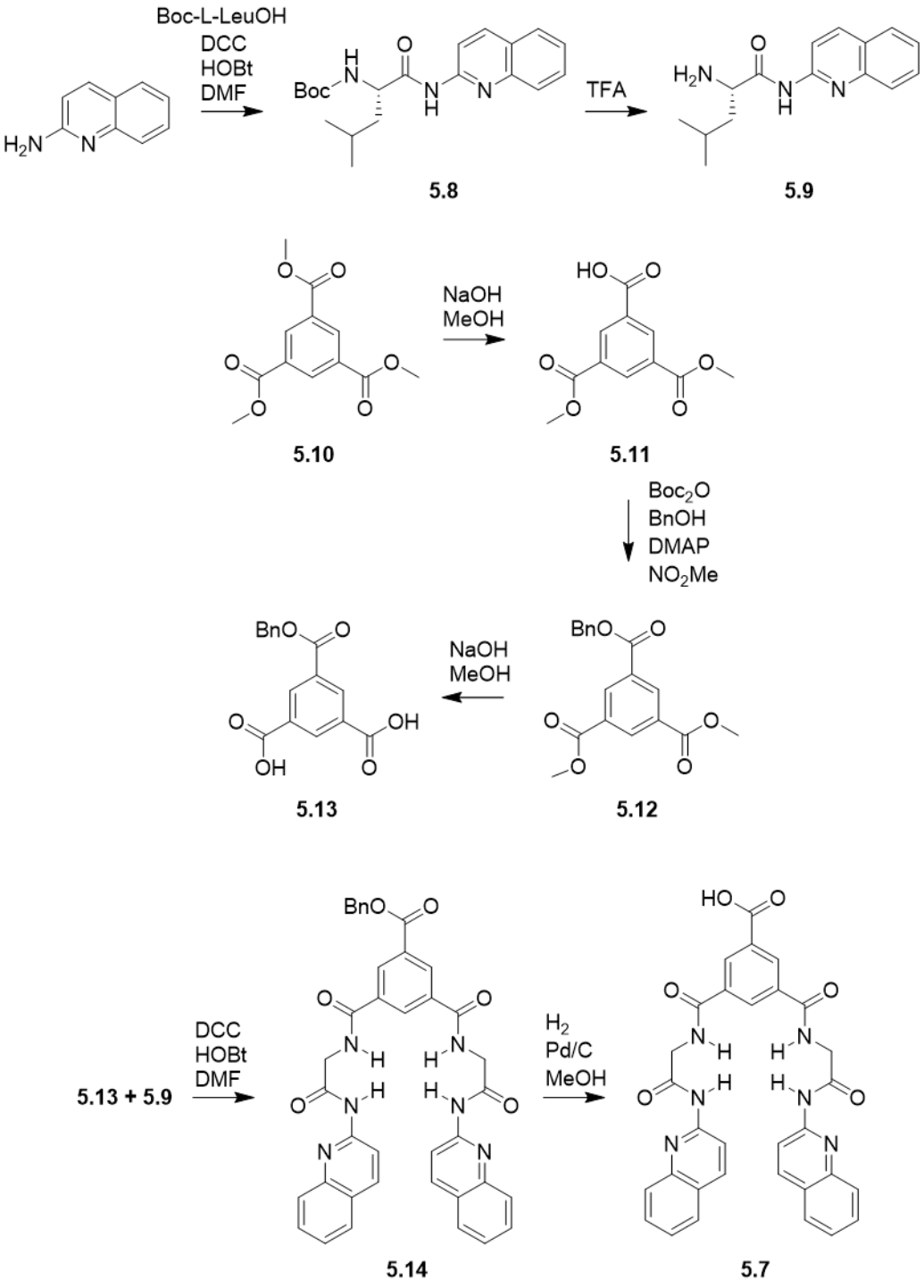

Scheme 5.2: Proposed synthesis of receptor **5.7**.

5.2.1 *N*-boc-*L*-leucine and 2-aminoquinoline coupling using *N,N'*-dicyclohexylcarbodiimide (5.8)

Since its advent in 1955 by Sheehan and Hess, *N,N'*-dicyclohexylcarbodiimide has evolved into one of the primary coupling reagents for the formation of amide bonds.[15] In their initial studies they showed that high yields could be obtained selectively as demonstrated by the use of substrates containing hydroxyl groups. They further went on to show that the coupling reagent was insensitive to moisture and the urea by-product of the reaction could easily be separated from the reaction mixture. The mechanism for the formation of the amide bond involves the formation of an *O*-acylisourea active intermediate. This intermediate is highly reactive and hard to isolate, reacting rapidly with any nucleophiles present, meaning it is preferential to perform the coupling reaction in aprotic solvents, such as $CHCl_3$ and dimethylformamide[16]. One problem associated with the use of dicyclohexylcarbodiimide is the possibility of the rearrangement of the active *O*-acylisourea into the inactive *N*-acylurea, Scheme 5.3.

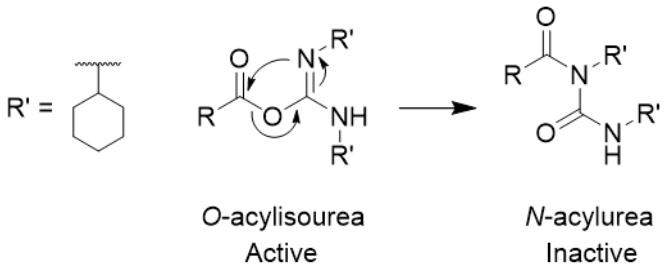

Scheme 5.3: Formation of the inactive N-acylurea from the *O*-acylisourea.

In order to avoid the formation of the inactive urea species, the addition of a select nucleophile that can react faster with the active intermediate than acyl transfer can occur, but still allow for the reaction with the amine can be utilised. One such nucleophile is hydroxybenzotriazole which can be added into the reaction mix to form an activated ester that prevents the conversion to the inactive urea species and side reactions, while also being reactive to the addition of amine.[17] In the course of this body of work, a *N,N'*-dicyclohexylcarbodiimide and hydroxybenzotriazole system was utilised for the synthesis of compound **5.8** in 69% yield. Scheme 4 details the overall mechanism for the formation of **5.8** from 2-aminoquinoline and *N*-boc-*L*-leucine.

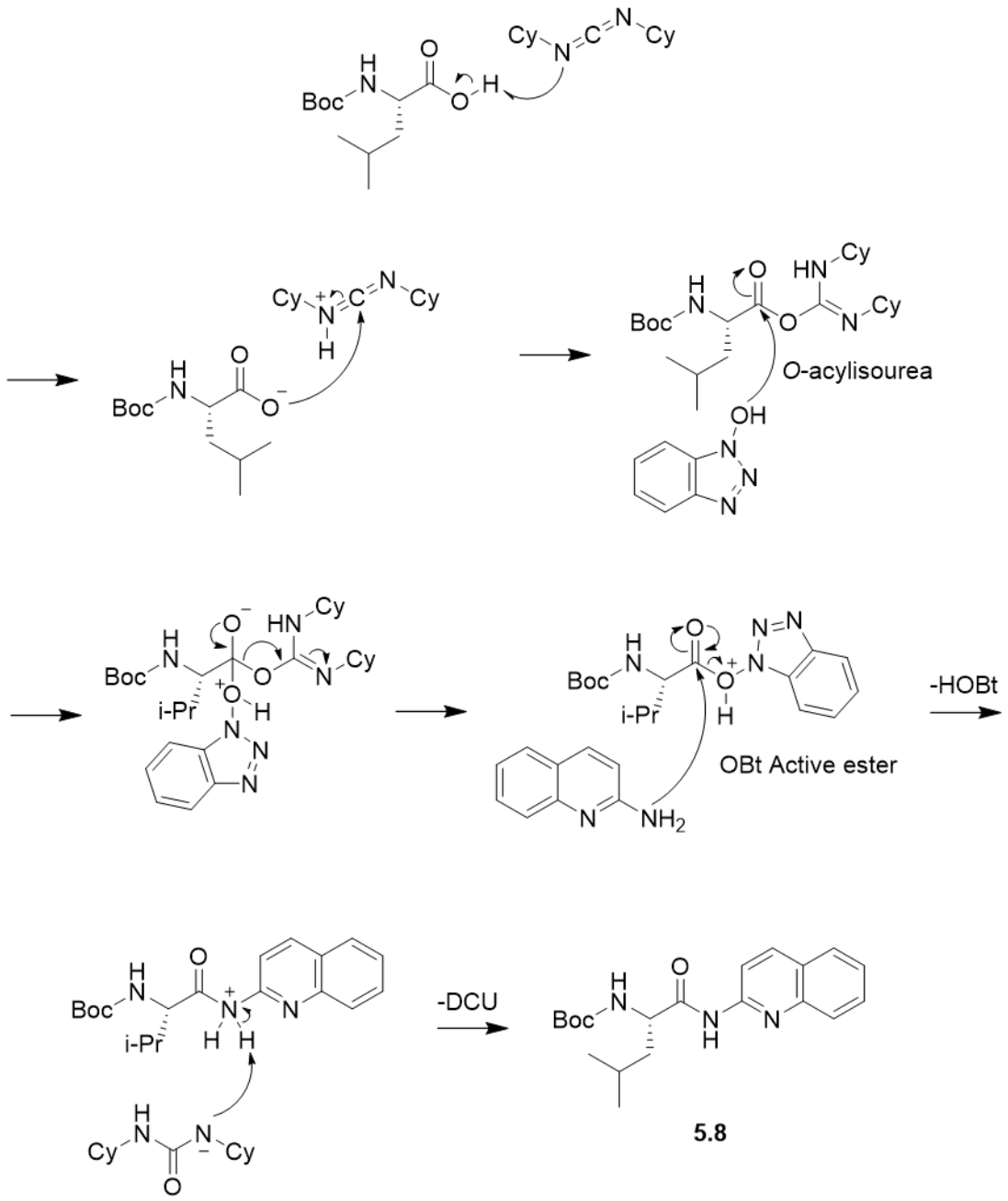

Scheme 5.4: Mechanism of amide coupling using *N*,*N'*-dicyclohexylcarbodiimide and hydroxybenzotriazole.

The initial step is the formation of the *O*-acylisourea intermediate. This can subsequently react with the hydroxybenzotriazole catalyst and form the active ester species, which undergoes a nucleophilic substitution with the 2-aminoquinoline. This regenerates the hydroxybenzotriazole catalyst which can undergo a second reaction with the *O*-acylisourea. The ammonium species is then deprotonated by the dicyclohexylcarbodiimide to yield the desired product **5.8** and the dicyclohexylurea by-product.

5.2.2 Deprotection of trimethyl-1,3,5-benzenetricarboxylate (5.11)

Methyl esters have been demonstrated to be an incredibly important protecting group used in chemical synthesis due to their stability to a wide range of chemical conditions and their ease of removal. Mayato and co-workers demonstrated that the methyl ester protecting group, which had previously been overlooked, could be used in the synthesis of *O*-glycosyl amino acid building blocks.[18] Their work focussed on the need to be readily able to synthesise the building blocks for glycopeptide synthesis- the α-glycosidic linkage between various substituted sugars and *L*-amino acids bearing hydroxyl groups, such as threonine and serine (Figure 5.2).

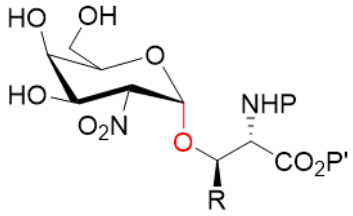

Figure 5.2: Example of an α-glycosidic linkage (red) between 3,4,6-tri-*O*-benzyl-2-nitro-D-galactal and an amino acid e.g., serine or threonine. R = H or Me; P and P' = orthogonal PGs

The methyl esters of amino acids are readily available, easy to prepare and stable, however due to the methods employed in the deprotection they are underutilised. Epimerization of the α-carbon of the amino acid can occur, as well as the cleavage of other PGs, such as acetyl, can occur under basic hydrolysis. To avoid this issue, Mayato et al. used LiI as a means of deprotection and demonstrated that the free carboxylic acid could be obtained, in excellent yields, >90%, in the presence of other PGs such as acetyl and N-protecting groups. Nicolaou et al. also demonstrated the need for a facile, mild, and selective method for the hydrolysis of esters during their synthetic route towards a highly complex antibiotic.[19] They detailed the same problems as Mayato and co. when using standard hydrolysis conditions; epimerization of stereocentres and the hydrolysis at unwanted positions, in addition to potential elimination reactions that may occur. In order to combat these issues, they employed a Me_3SnOH system based on the work by Mascaretti et al. which was shown to be effective in the cleavage of resin bound amino acid esters and hydrolysis of methyl esters to the corresponding acids.[20] Nicolaou and co-workers demonstrated that the methyl esters in sensitive and precious materials could be selectively cleaved in the presence of 1-10 equivalents of Me_3SnOH with heating, without epimerization being observed. They also showed that the other PGs, like Fmoc, were not labile under these conditions. Investigations

using LiOH on Fmoc protected substrates showed the partial cleavage of the Fmoc group by the time the methyl group had been removed. There are a number of additional methods for the deprotection of methyl groups which can be used depending on the substrate in question including, but not limited to:[21]

- LiOH, MeOH:H_2O (3:1), 5 °C, 15 h
- $NaBH_4$, I_2, 3 h, RT
- $CuCO_3$, $Cu(OH)_2$; H_2S workup, 50-60 °C
- Cs_2CO_3, PhSH, DMF, 85 °C, 3 h

For the deprotection of **5.10**, standard hydrolysis conditions using alkali metal hydroxide in aqueous/organic solvent was used as a result of the readily available nature of the starting material and the lack of epimerizable centres or propensity for the unwanted cleavage of other PGs[22]. The mechanism for the deprotection can be seen in Section 3.2.5.

Carboxylic acid, **5.11**, was successfully synthesised in 86% yield using the aforementioned method. The product was used without further purification in the next step.

5.2.3 Benzylation of dimethyl-1,3,5-benzenetricarboxylate (5.12)

In addition to methyl esters as protecting groups, benzyl esters also find extensive use within synthetic chemistry due to the exceedingly mild conditions used for their cleavage, hydrogenation over Pd/C being the most common. In the context of this work, they were intended to be used due to the orthogonal nature of removal relative to the methyl ester groups. Benzyl esters can be installed in a variety of different ways, the most classical being the base catalysed reaction of an acid chloride or anhydride in the presence of a benzyl alcohol. Under these conditions, benzyl alcohol is stable and sterically unhindered and generally yields are good, however, these conditions cannot be applied to all substrates due to stability or functional group tolerance.[21] This has led to the development of alternative methods for the installation of benzyl groups. Mevan Dissanayake and co-workers developed a method for the amidation of acid anhydrides that improved the overall atom economy through the simultaneous treatment of the carboxylate ‘waste’ with benzyl bromide yielding high-value, useful benzyl ester co-products, Scheme 5.5.[23]

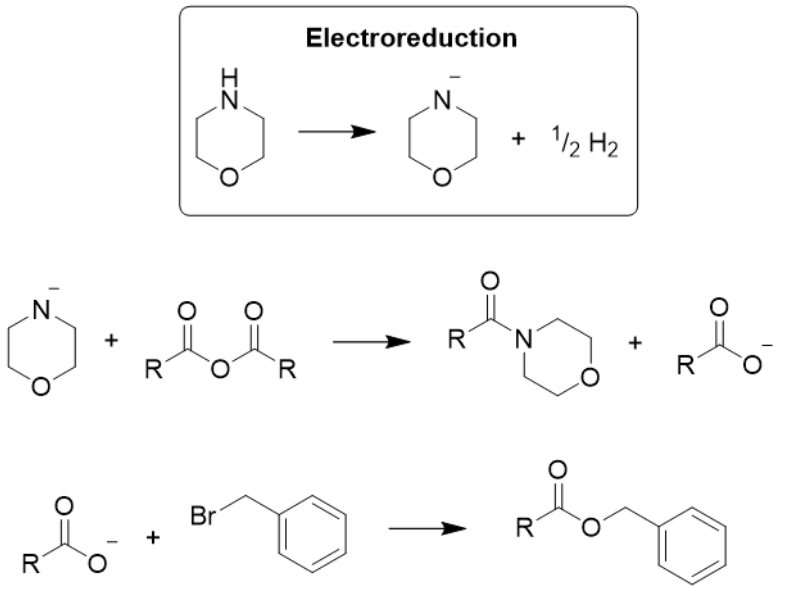

Scheme 5.5: Overall amidation reaction, with morpholine, showing formation of the amide and subsequent esterification of the carboxylate 'waste'.

Using acetonitrile as the solvent and reticulated vitreous carbon electrodes, by alternating the current applied between 8 mA- amine reduction- and 0.5 mA- addition of the acid anhydride they developed a base, catalyst, and precious-metal free method for amidation and concurrent esterification. They subsequently showed that the method could tolerate a variety of amine and acid chloride substrates e.g., primary and secondary amines and aromatic and aliphatic acid chlorides. 2-Benzyloxy-1-methylpyridinium triflate, **5.15**, has emerged as an effective method for the benzylation of alcohols due to the formation of an electrophilic benzyl species when heated. **5.15** is pre-activated and therefore does not require the addition of acid or base, is stable under ambient conditions and serves solely as a benzyl transfer reagent.

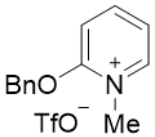

5.15

Tummatorn et al. endeavoured to optimise the conditions used for the benzylation of carboxylic esters using **5.15**.[24] Although base was not required for the reaction to proceed, they demonstrated that the addition of triethylamine led to high yields of the ester being obtained but also the complete suppression of benzyl ether formation. They suggested that the triethylamine base activates the carboxylic acid for reduction and acts a scavenger for

the phenylcarbenium species once the carboxylic acid has been completely consumed- Scheme 5.6.

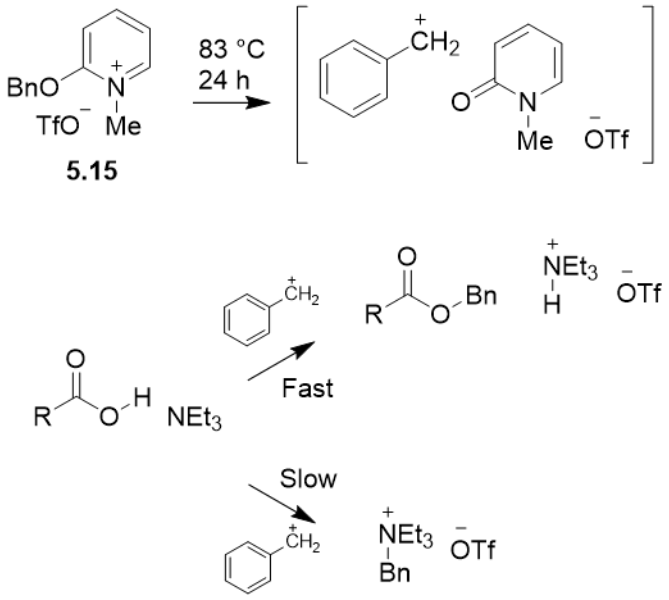

Scheme 5.6: Reaction of **5.15** with carboxylic acid; fast step) reaction of the phenylcarbenium with carboxylic acid; slow step) excess triethylamine scavenges phenylcarbenium.

Further work showed the effectiveness of **5.15** in the benzylation of a range of chemical substrates including strained 3-membered cycles, alkynes, and alkenes. They further showed that the more complex compounds could be benzylated effectively- aspirin, nicotinic acid and Boc-protected amino acids were all obtained with yields in excess of 81%.

The benzyl group of **5.12** was installed using a procedure set out by Gooβen and Döhring, which allowed for the facile installation of benzyl groups using benzyl alcohol in the presence of di-*t*-butyl dicarbonate and catalytic N,N'-dimethylaminopyridine.[25] The design of this method eliminates some of the problems with other alternative methods used for the esterification of carboxylic acids such as functional group tolerance e.g., acid-catalysed esterification and some protecting groups and the variety of alkyl halides available compared to alcohols. This makes the use of alcohols and coupling reagents the preferred method for esterification of carboxylic acids. However, these reactions themselves require the use of further downstream workup in order to remove the waste by-products. The method developed by Gooβen and Döhring produces solely volatile by-products that can be easily removed- residual dicarbonate can be removed using dilute acid and *t*-butyl alcohol and CO_2 are volatile. They showed that di-*t*-butyl dicarbonate reacted with carboxylic acids to form a carbonic carboxylic anhydride and one equivalent of the corresponding alkyl alcohol i.e., *t*-butyl alcohol. The addition of dimethylaminopyridine promotes the deprotonation of the

alcohol, which can react at the electrophilic centre of the anhydride and releases CO_2. The steric bulk of the *t*-butyl group was demonstrated to retard the reaction rate and subsequently it was proposed that the addition of a primary or secondary alcohol would preferentially react with the carbonic carboxylic anhydride intermediate, Scheme 5.7.

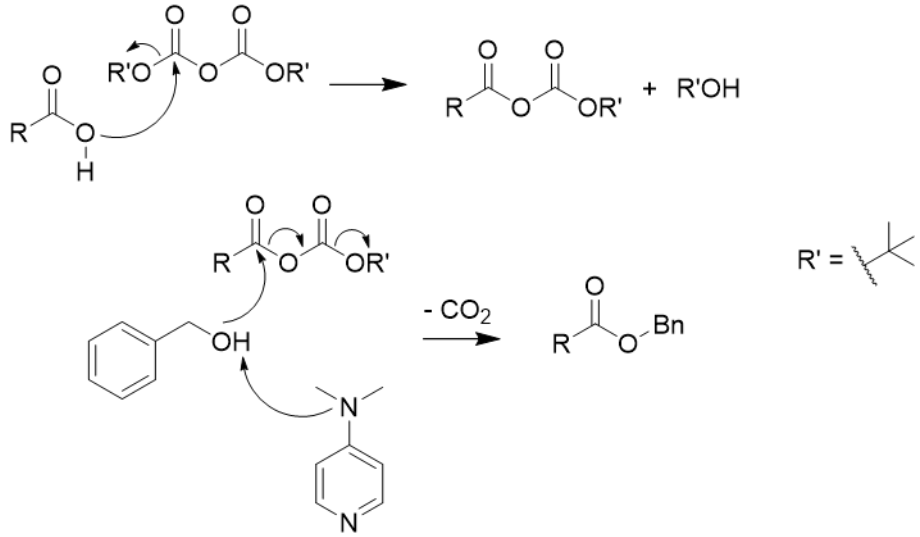

Scheme 5.7: Decarboxylative esterification of carboxylic acids using dialkyl dicarbonates and benzyl alcohol.

They demonstrated that this was the case as reactions with benzyl alcohol and di-*t*-butyl dicarbonate showed only trace amounts of the *t*-butyl ester were formed. This method was used to successfully synthesise **5.12** in 32% yield.

Once synthesised, the isophthaloyl derivative was subjected to the same conditions as employed in Section 5.2.2- the deprotection of the methyl esters using dilute sodium hydroxide. However, this reaction proved to be unsuccessful and led to all the ester groups being cleaved and trimesic acid being the sole product. Consequently, a revised reaction scheme was employed that used an alternative isophthaloyl spacer group with appropriate moiety for the electrode attachment.

5.3 Revised Reaction Scheme

In order to simplify the synthesis further, a spacer group that did not require a protecting group was hypothesised as being the most likely successful candidate. As a result, 5-ethynylbenzene-1,3-dioic acid, **5.17**, was chosen as the central spacer molecule. The reaction

conditions did not alter from those used by Kondo and Takai, Scheme 5.1. The modified, alkyne containing reaction scheme is shown in Scheme 5.8.

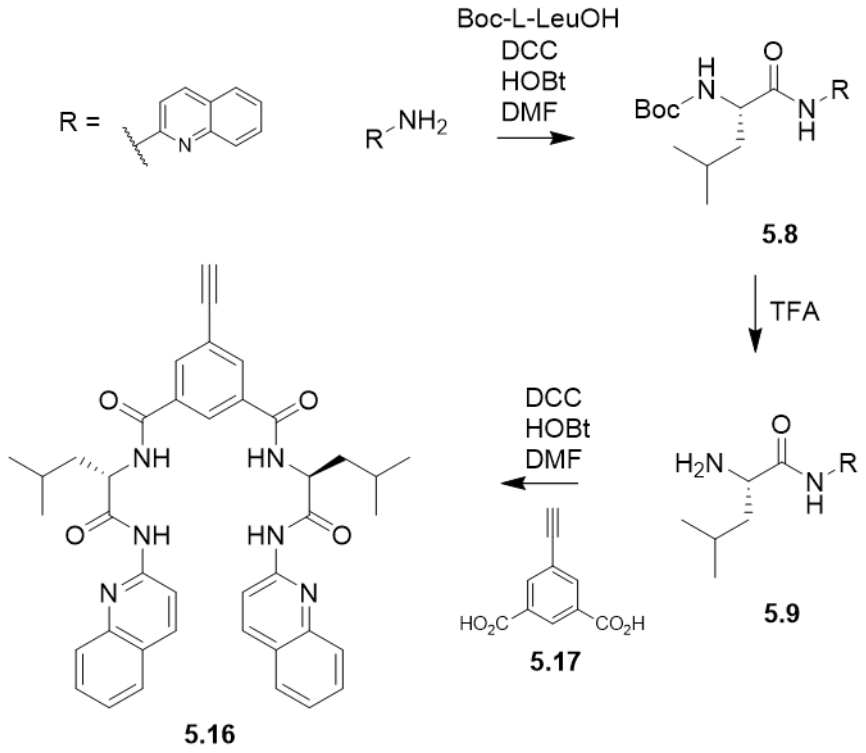

Scheme 5.8: Revised reaction scheme for the synthesis of **5.16**.

Compound **5.8** was synthesised according to the procedure laid out in section 5.2.1 in 69% yield. Following this, compound **5.9** was obtained from the deprotection of **5.8** following the same method in Section 4.3.6., **5.9** was used immediately in the next step due to its relative instability. The coupling of **5.9** and 5-ethynylbenzene-1,3-dioic acid was performed using the same conditions for the synthesis of **5.8**. Receptor **5.16** was synthesised with an overall reaction yield of 39%.

5.4 Binding Studies- UV-Vis Titrations

Following the successful synthesis of receptor **5.16**, the binding of a range of anions, as their tetrabutylammonium salts, was tested by means of UV-Vis titrations in acetonitrile at 298 K. The titration of the **5.16** with $H_2PO_4^-$ as its tetrabutylammonium salt, up to 1.5 eq. is shown in Figure 5.3.

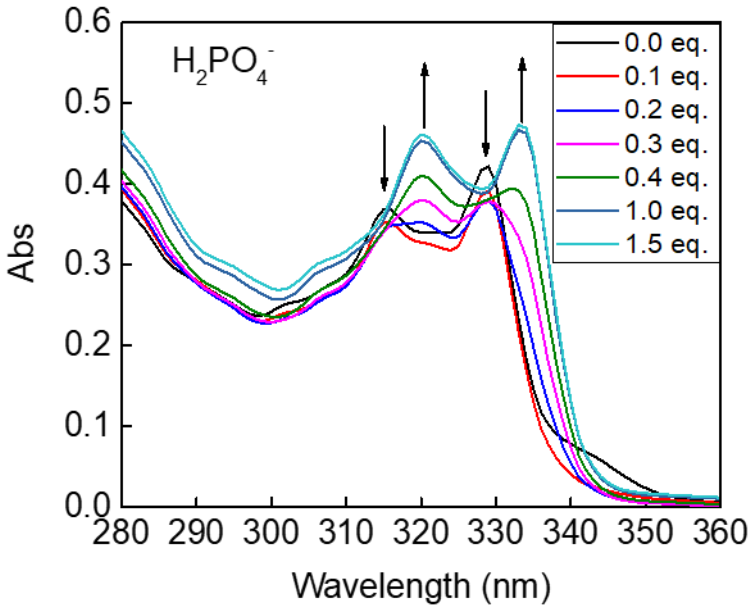

Figure 5.3: UV-Vis titration of **5.16** with TBA·H_2PO_4, up to 1.5 equivalents at 298 K.

It can be seen that there is a clear decrease in the absorbance peaks at 315.0 and 328.5 nm along with the simultaneous increase of absorbance at 320.0 and 333.5 nm. The values for the absorbance obtained are analogous to those of Kondo and Takai, indicating that the modification of the isophthaloyl spacer has not altered the receptor's binding cleft. Kondo and Takai, indicate that these spectral changes occur through isosbestic points at 318.0, 328.5 and 330.0 nm. Isosbestic points occur when the molar absorption coefficients of two species- in this case **5.16** and **5.16**·$H_2PO_4^-$ - are the same. At this point in the equilibrium, the absorbance of the species is the same and does not depend on the relative proportions of each within the sample.[26] The presence of two isosbestic points indicates that the change in the observed spectra is the result of the interaction of the two species. Figure 5.3 indicated that there may be isosbestic points around those previously described by Kondo and Takai, however further investigations need to be performed in order to clarify this. The small deviations centred around what could be isosbestic points could be due to changes to the solvent e.g., temperature. Alternatively, these differences could be accounted for by the presence of a third UV-Vis active species i.e., the presence of a second binding mode, although unlikely, or experimental inaccuracy.[27] In addition to titrations with $H_2PO_4^-$, titrations with AcO^-, Br^-, I^- and NO_3^- were performed. The results of these can be seen in Figures 5.4 -5.7 and show that minimal spectroscopic changes are observed upon the addition of each anion. Only acetate shows a slight shift in the observed peaks, however this is negligible. These results suggest that receptor **5.16** is selective for dihydrogenphosphate over all the other anions tested.

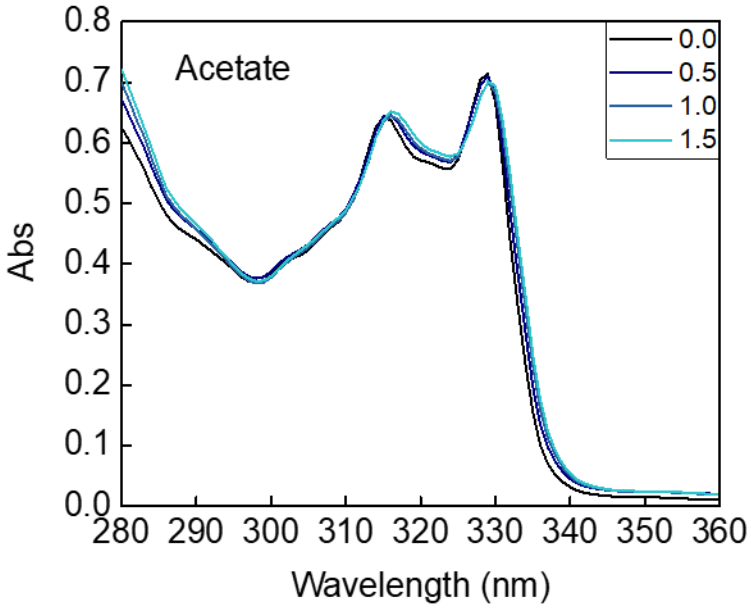

Figure 5.4: UV-Vis titration of **5.16** with TBA·AcO up to 1.5 equivalents at 298 K.

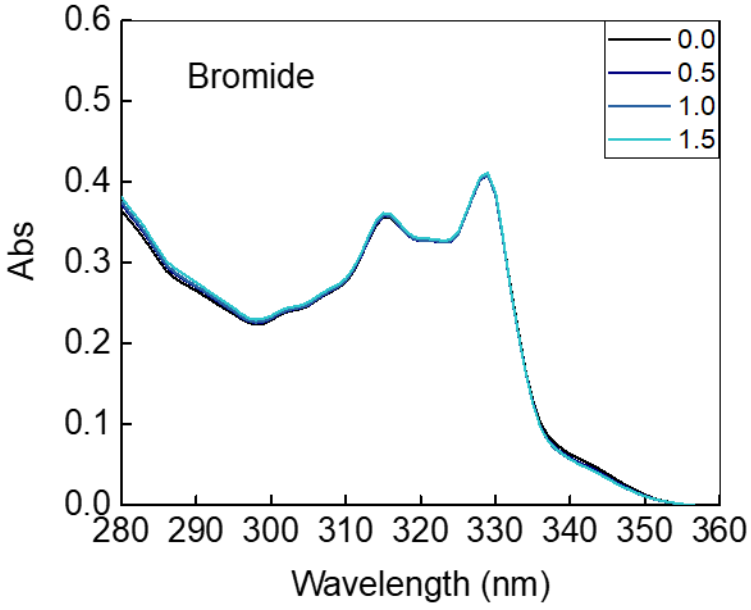

Figure 5.5: UV-Vis titration of **5.16** with TBA·Br up to 1.5 equivalents at 298 K.

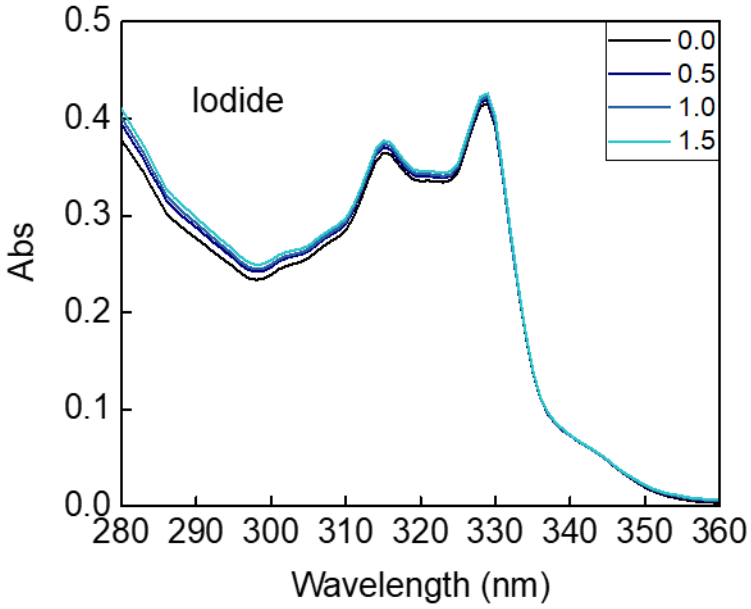

Figure 5.6: UV-Vis titration of **5.16** with TBA·I up to 1.5 equivalents at 298 K.

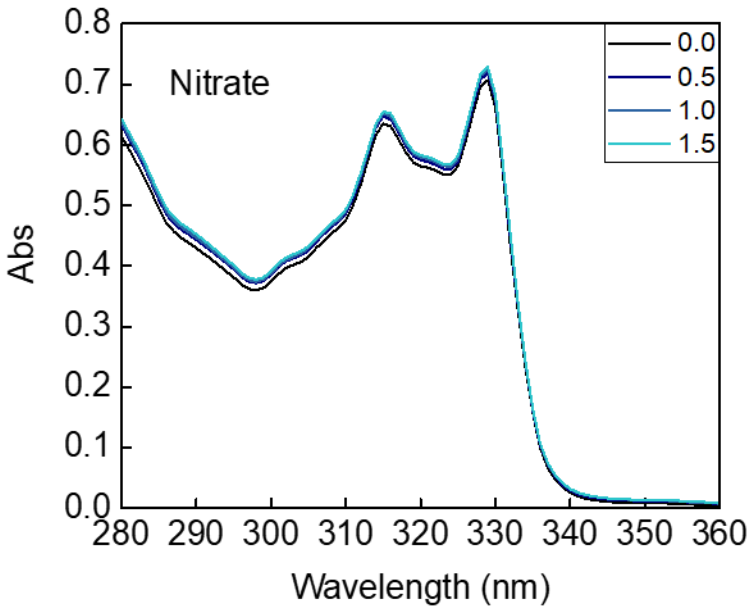

Figure 5.7: UV-Vis titration of **5.16** with TBA·NO_3 up to 1.5 equivalents at 298 K.

Investigations into the binding stoichiometry were performed using Job's method of continuous variation. In this method, the total concentration of two species i.e., **5.16** and $H_2PO_4^-$, is kept constant whilst the ratio of each of the species involved is varied.[28] Figure 5.8 shows that AcO^- shows limited interaction with **5.16** and as such no binding stoichiometry can be calculated. $H_2PO_4^-$ was shown to strongly interact with

the receptor and consequently the Job's plot showed a maximum at 0.5 mole fraction of anion added. This indicated that a 1:1 receptor: anion complex is formed, however as previously discussed alternative methods, such as the mole ratio method, should be applied to confirm the accuracy of this data. Fitting of the obtained data to a 1:1 binding model using Bindfit gave a K_a = 4142268.66 M^{-1} in MeCN at 298 K (Appendix- Chapter 4).[29]

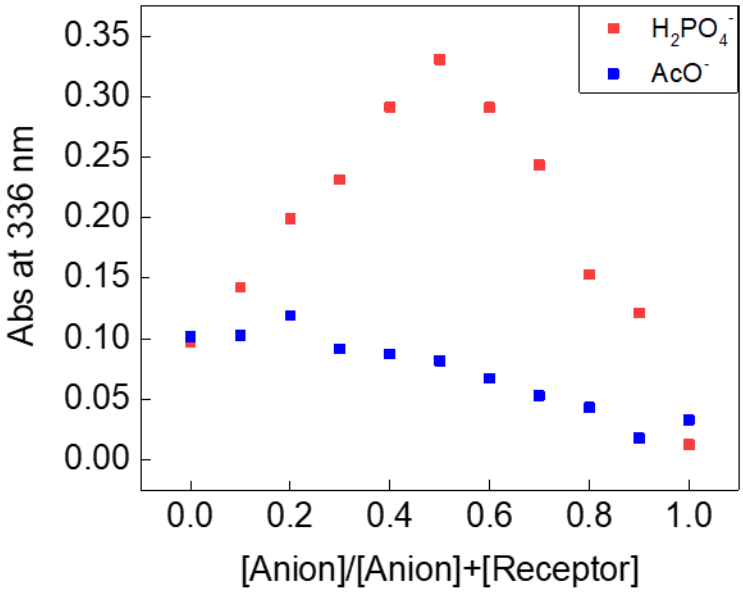

Figure 5.8: Job's plot of **5.16** and TBA·H_2PO_4.

5.5 Electrode Attachment

In order for any receptor synthesised in Chapters 3-5 to be applied within a capacitive deionisation system, the receptors must be effectively grafted to the electrode surface- glassy carbon for this body of work- via a covalent bond to the surface. There have been a number of developments for the functionalisation of electrode surfaces, the most widely utilised being the electrochemical reduction of alcohols[30] and amines.[31] In addition, the electrochemical reduction of diaryliodonium[32] and aryldiazonium salts[33,34] has proven to be effective for surface modification. In this work, the electroreduction of the diazonium salts proved to be most effective as the radicals generated directly attack the electrode surface and form a highly stable covalent bond.

5.5.1 Electroreduction of 4-nitrobenzene diazonium salt

Nazemi et al. demonstrated that 4-nitrobenzene diazonium tetrafluoroborate could be effectively grafted to the surface of a glassy carbon electrode and then subsequently functionalised once bound, Scheme 5.9.[34] This method is the basis for the work carried out in the following section and was chosen preferentially over the aforementioned methods due to the thermal and electrochemical stability of the formed monolayer, in addition to the ease of functionalisation of the layer. However, there are drawbacks associated with the use of a radical mechanism for the electrode functionalisation such as the propensity to form multilayers as well as the formation of side products. It is also reported that the conductivity of the electrode can be reduced and subsequently electrochemical reactions at the surface can be slowed or stopped completely.

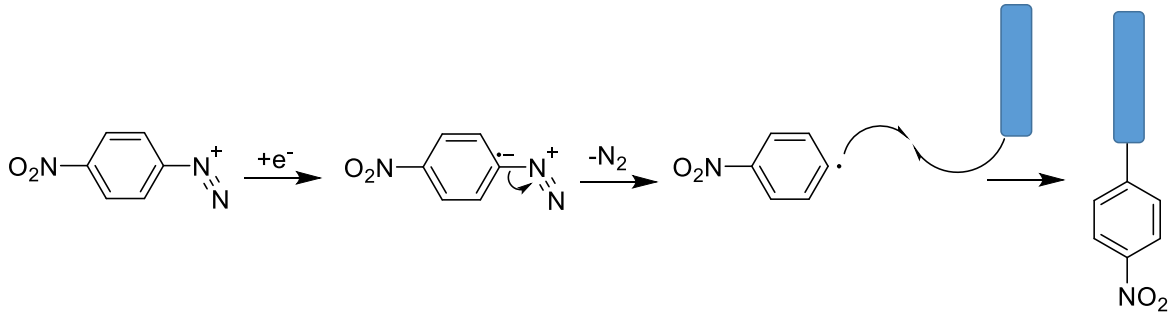

Scheme 5.9: Proposed mechanism for the electroreduction of 4-nitrobenzene diazonium salt via a radical pathway.

The first step of the electrode modification was the attachment of the 4-nitrophenyl group via the reduction of its corresponding diazonium salt in acetonitrile, Figure 5.9. It can clearly be seen that there is a large irreversible wave at around −0.30 V in the first scan and subsequent further additional scans do not show the same behaviour. This large irreversible wave is attributed to the electron transfer from the electrode to the diazonium species, leading to the radical anion, followed by the cleavage of the C-N bond and formation of the 4-nitrobenzene radical. The decrease in the current density observed in the CVs can be attributed to the blocking of the electrode surface by the electro-inactive 4-nitrophenyl species. Potentiostatic electrolysis at −0.40 V ensures that the diazonium species was effectively reduced.

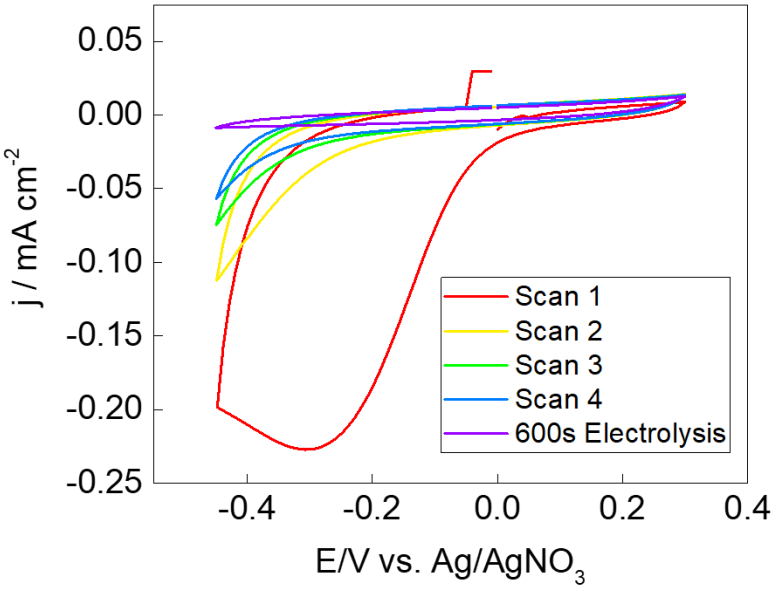

Figure 5.9: CV of the modification of GCE with 1 mM 4-nitrobenzenediazonium tetrafluoroborate in CH_3CN, with 0.1 M TBA.TFB as supporting electrolyte.

The surface bound nitrophenyl group was reduced electrochemically through repetitive cycling between −1.50 and −0.70 V in 9:1 ethanol: water, with 0.1 M potassium chloride as supporting electrolyte, Figure 5.10. The reduction of the nitro group electrochemically is likely to proceed to in the same manner as demonstrated in Section 3.2.3.[35]

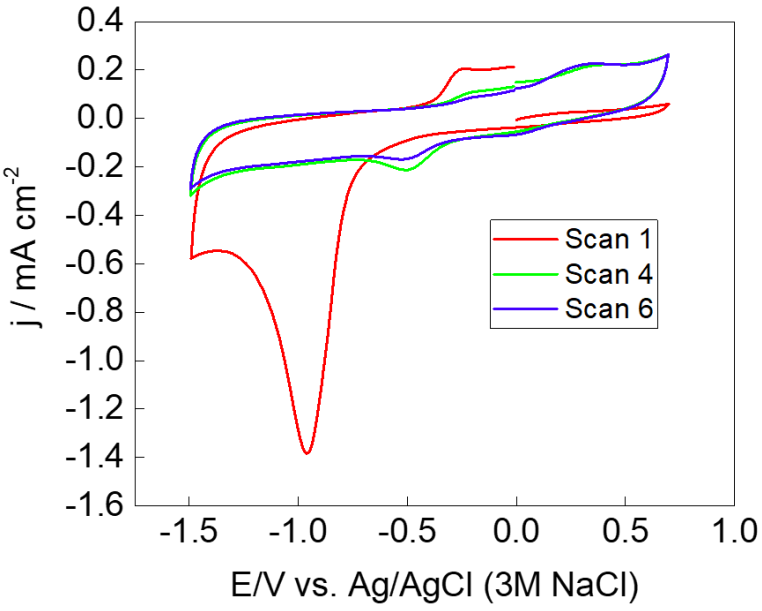

Figure 5.10: CV of the reduction of surface bound 4-nitrophenyl. 6 scans −1.50 to −0.70 V in 9:1 ethanol: water with 0.1 M potassium chloride as supporting electrolyte.

The species that were surface bound are electro-inactive and so the progression of the reaction was followed by the use of a well-defined redox probe- $K_3Fe(CN)_6$. The CV of the 'bare' electrode can be seen in Figure 5.11. It clearly shows the redox couple associated with the ferrocyanide-ferricyanide couple.

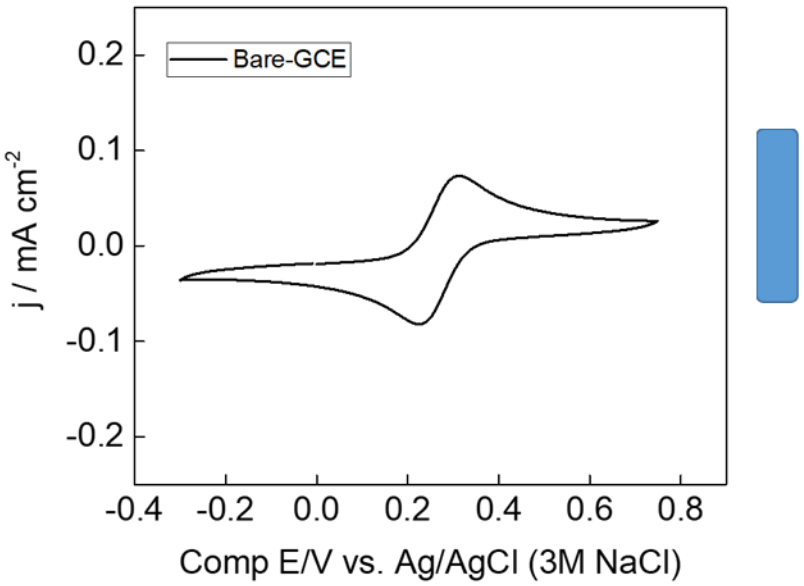

Figure 5.11: CV of 1 mM $Fe(CN)_6^{3-/4-}$ at a bare GCE.

Once modified with 4-nitrophenyl, the redox couple is now no longer observed. This is the result of the electro-inactive organic group blocking the surface preventing the redox of the electroactive probe, Figure 5.12.

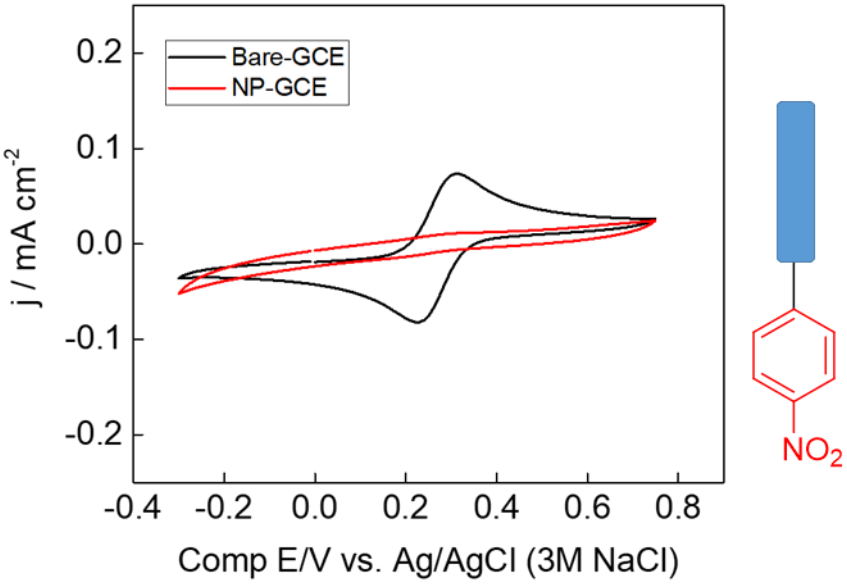

Figure 5.12: CV of 1 mM $Fe(CN)_6^{3-/4-}$ at a 4- nitrophenyl modified GCE (NP = Nitrophenyl).

The reduction of the nitro group to amine can be monitored using the same $Fe(CN)_6^{3-/4-}$ probe at pH 2. At acidic pH, the basic amine group is protonated and forms the ammonium species. The ammonium species can effectively interact with the anionic probe in solution and consequently, the redox of the activity of the probe returns, and the current density is seen to increase dramatically, Figure 5.13.

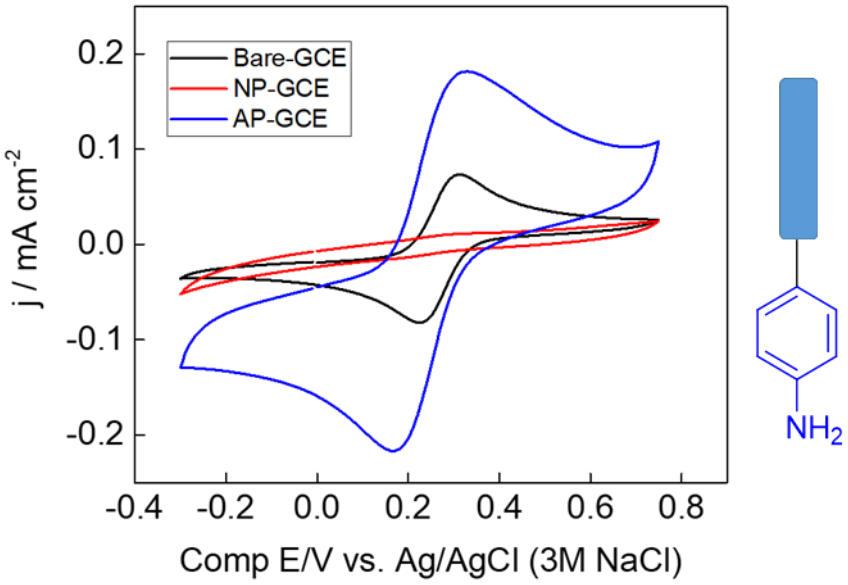

Figure 5.13: CV of 1 mM $Fe(CN)_6^{3-/4-}$ at a 4- aminophenyl modified GCE (AP = Aminophenyl).

Finally, the reactivity of the amine functionality was investigated through the use of an aldehyde. Glutaraldehyde was shown to react with the amine groups on the surface of the electrode and led once again to a decrease in the current density observed, Figure 5.14. The decrease seen is less prominent than that seen when the nitrophenyl group is attached, this is likely due to the incomplete coupling of the glutaraldehyde to the surface bound amine.

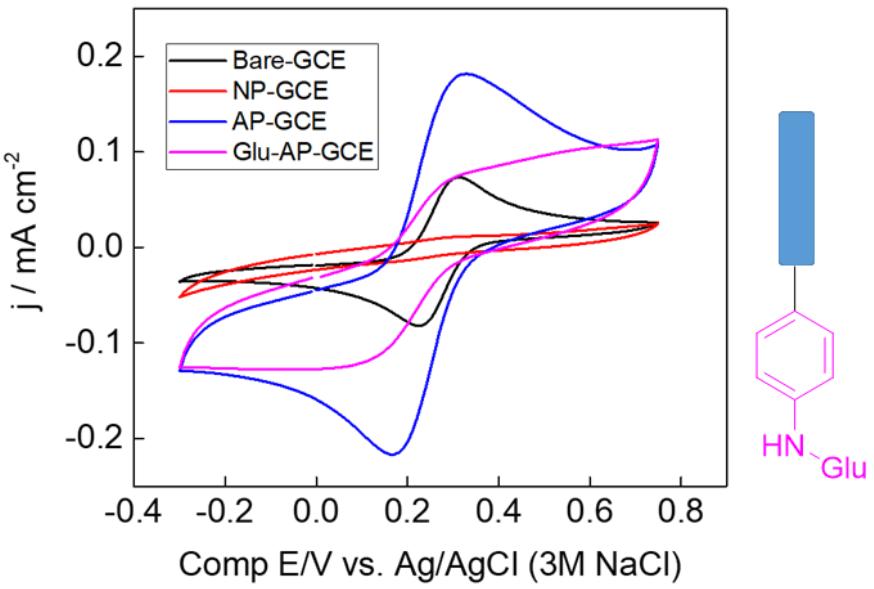

Figure 5.14: CV of 1 mM $Fe(CN)_6^{3-/4-}$ at a 4- amino-Glu-phenyl modified GCE (Glu = glutaraldehyde).

5.6 Conclusions and Future Work

Receptor **5.16** was successfully synthesised with an overall yield of 39% with modification of the procedure set out previously by Kondo and Takai. The initial modification proposed was the substitution of the original alkyl chain group of the central isophthaloyl for a carboxylic acid moiety, which would act as the binding point to the electrode. This was attempted through a mono methyl ester deprotection of trimethyl 1,3,5-benzenetricarboxylate, followed by the benzyl ester protection of the free carboxylic acid group. The final step, the deprotection of the remaining methyl ester groups, proved to be problematic and led to the cleavage of all the installed protecting groups, both benzyl and methyl. As a result, an alternative isophthaloyl group containing an alkyne was used. The affinity of **5.16** for a number of different anions, as their tetrabutylammonium salts, was determined through the use of UV-Vis experiments. These results showed that only $H_2PO_4^-$ showed any affinity for the receptor. All the other anions tested- acetate, iodide, bromide, and nitrate- showed little to no affinity for the receptor. Based on this, receptor **5.16** was shown to be selective for dihydrogenphosphate. Further investigations using Job's plots gave insight into the binding stoichiometry of **5.16** and $H_2PO_4^-$. Through these investigations, the binding stoichiometry was proposed to be 1:1. The surface of a glassy carbon electrode was modified through the covalent attachment of an organic spacer molecule. 4-nitrobenzene

diazonium, as its tetrafluoroborate salt, was successfully grafted to the electrode surface using a combination of cyclic voltammetry and potentiostatic electrolysis using the same method as Nazemi et al. The nitro group was shown to be susceptible to electrochemical reduction, and afforded an amine-modified electrode that was shown to be reactive to other groups, such as aldehydes. The surface modification at all stages was followed through the use of a potassium ferricyanide probe. Through analysis of the probe's activity, the functional group on the organic spacer could be determined.

The use of the alkyne moiety of **5.16** allows for two potential methods for the attachment to the electrode. Firstly, Click chemistry, as outlined in Chapter 3.5, could be utilised if the surface bound amine can be successfully transformed into an azide group, Scheme 5.10.

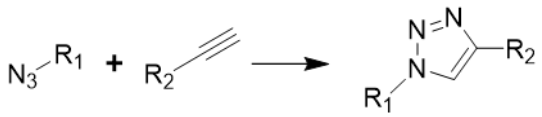

Scheme 5.10: Overall click chemistry reaction of an azide with an alkyne.

A second and more facile approach through the direct oxidation of the ethynyl group would eliminate the need for any further organic transformation reactions. Sheridan et al. have shown that ethynyl groups can be successfully oxidised and subsequently attached directly to an electrode.[36] They demonstrated that an ethynyl ferrocene can be effectively attached to the surface of the electrode using a single CV scan. They propose that the method of attachment proceeds through an alkynyl radical as the result of a one-electron oxidation of the ethynyl group- Scheme 5.11.

Scheme 5.11: Radical oxidation of an alkyne.

The success of the attachment of the ethynyl ferrocene can be tracked through the ferrocene subunit which itself acts as surface bound electrochemical probe. If successful, a modified electrode in a solution of electrolyte only, should show the characteristic redox couple of the ferrocene unit. Based on the success of these experiments, this same method could be applied for the attachment of **5.16** to a glassy carbon electrode and optimised for use within a capacitive deionisation system.

5.7 Experimental

5.7.1 Materials and Reagents

All chemicals were of analytical reagent grade from Sigma-Aldrich/Merck, Alfa Aesar or Fluorochem and required no further purification.

5.7.2 General synthetic methods

^{1}H NMR spectra were recorded on a Bruker DPX-400 (400 MHz) instrument. The chemical shifts are expressed in parts per million (ppm) referenced to TMS. Data are reported as follows: δ, chemical shift, multiplicity (recorded as b, broad; s, singlet; d, doublet; t, triplet; q, quartet; m, multiplet), coupling constants (J in Hertz, Hz), integration and assignment. Assignments were based on obtained from DEPT, HMBC and HSQC experiments.

^{13}C NMR spectra were recorded on the same instrument at 100 MHz. The chemical shifts are expressed in parts per million (ppm), proton decoupled and referenced to TMS. Assignments were obtained from 2D-DEPT.

All NMR agree with literature data, where applicable

5.7.2.1 NMR Analysis

Synthesis of *N*-boc-*L*-leucyl-2-aminoquinoline (5.8)[13]

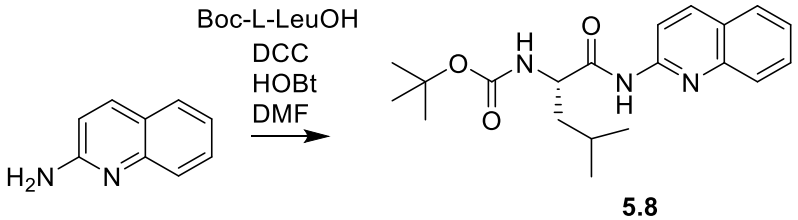

5.8

N-boc-*L*-leucine (4.64 g, 20 mmol), 2-aminoquinoline (1.04 g, 7.24 mmol) and 1-hydroxybenzotriazole (2.38 g, 17.6 mmol) was dissolved in DMF (80 mL). Into this was added a solution dicyclohexylcarbodiimide (3.15 g, 15.3 mmol) in DMF (40 mL) and stirred for 19 h at room temperature, under a N_2 atmosphere. The crude product was concentrated under reduced pressure and the crude residue dissolved in 300 mL EtOAc and the organic

layer washed consecutively with 0.1 M citrate, 1 M NaOH and brine (400 mL each). The resulting organic layer was separated and dried over $MgSO_4$, filtered to remove the solid residue and concentrated under reduced pressure. The crude product was purified by columnchromatography using CH_2Cl_2 as the eluent. The product was obtained as a flaky white solid (2.27 g, 6.34 mmol, 69%).

^{1}H NMR (400 MHz, d_6-DMSO) δ 10.74 (s, 1H), 8.35 (d, *J* = 9.0 Hz, 1H), 8.27 (d, *J* = 8.9 Hz, 1H), 7.91 (dd, *J* = 8.1, 0.8 Hz, 1H), 7.81 (d, *J* = 8.5 Hz 1H), 7.68-7.74 (m, 1H), 7.46-7.52 (m, 1H), 7.12 (d, *J* = 8.0 Hz, 1H), 4.29 (bs, 1H), 1.63-1.76 (m, 1H), 1.46-1.59 (m, 2H), 1.38 (s, 9H), 0.91 (s, 3H), 0.89 (s, 3H).

^{13}C NMR (101 MHz, d_6-DMSO) δ 173.4 (CO), 155.5 (CO), 151.6 (ArC), 146.3 (ArC), 138.3 (ArCH), 130.0 (ArCH), 127.8 (ArCH), 126.9 (ArCH), 125.6 (ArC), 124.9 (ArCH), 114.2 (ArCH), 78.1 (C), 53.6 (CH), 28.2 (CH_3), 24.4 (CH_3), 23.1 (CH_3), 21.3 (CH_3).

HRMS *m/z*: 358.2134 $[M+H]^+$ Calculated 358.2178 $[M+H]^+$.

Synthesis of dimethyl-1,3,5-benzenetricarboxylate (5.11)[22]

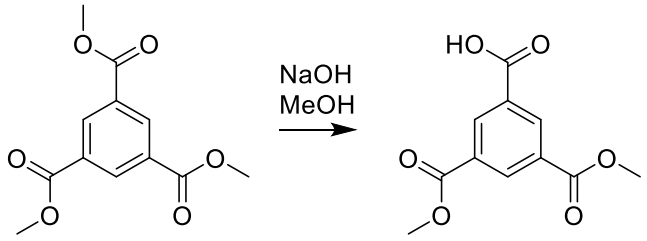

5.11

Trimethyl 1,3,5-benzenetricarboxylate (1.58g g, 6.25 mmol) was added to MeOH (140 mL). Aqueous NaOH (5.36 mL of 1.0 M, 5.63 mmol, 0.9 eq.). The suspension was stirred, with the solid dissolving over time. After 18 h, solvent was removed under reduced pressure and the residue dissolved in CH_2Cl_2 (50 mL). The organic phase was washed with saturated $NaHCO_3$, dried over $MgSO_4$ and concentrated at reduced pressure to give unreacted starting material. Aqueous washings were acidified (pH 2.0) with concentrated HCl, yielding a white suspension that was washed with EtOAc (2 × 50 mL). The combined organic phases were washed with brine (50 mL), dried over $MgSO_4$, filtered and concentrated under reduced pressure. Product obtained as a white powdery solid (1.28 g, 5.40 mmol, 86%)

^{1H} NMR (400 MHz, $CDCl_3$) δ 8.91-8.95 (m, 3H), 4.00 (s, 6H).

^{13}C NMR (101 MHz, $CDCl_3$) δ 170.0 (CO), 165.5 (CO), 135.7 (ArCH), 135.4 (ArCH), 131.7 (ArC), 130.5 (ArC), 52.7 (CH_3).

HRMS *m/z*: 237.0403 $[M-H]^-$ Calculated 237.0422 $[M-Na]^-$.

Synthesis of 1-benzyl-3,5-dimethylbenzene-1,3,5-tricarboxylate (5.12)[25]

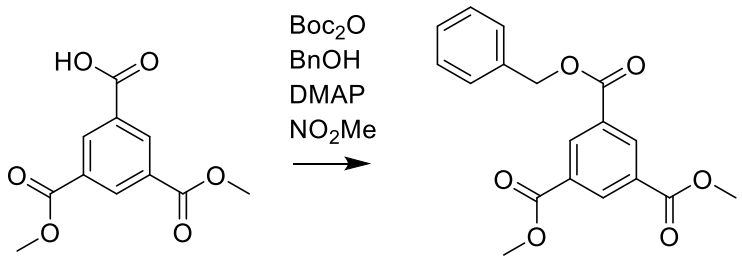

5.12

A flask was charged with dimethyl-1,3,5-benzenetricarboxylate, **5.11**, (1.00 g, 4.2 mmol), di-tert-butyl bicarbonate (1.20 g, 5.5 mmol), benzyl alcohol (0.435 mL, 4.2 mmol and DMAP (26 mg, 0.21 mmol), to which 10 mL of nitromethane was added. The reaction was stirred for 12 h at 50 °C. Once cooled, EtOAc (20 mL) was added and the organic layer was washed consecutively with 2 M HCl, sat. $NaHCO_3$, H_2O and brine. Organic layers combined, dried over MgSO4, filtered and concentrated under reduced pressure. Crude product was purified by column chromatography using toluene : EtOAc (7:3). Product obtained as a white solid (0.435 g, 1.33 mmol, 32%).

^{1H} NMR (400 MHz, d_6-DMSO) δ 8.64-8.66 (m, 3H), 7.37-7.52 (m, 5H), 5.42 (s, 2H), 3.92 (s, 6H).

^{13}C NMR (101 MHz, d_6-DMSO) δ 164.5 (CO), 164.0 (CO), 135.6 (ArC), 133.6 (ArCH), 133.5 (ArCH), 131.0 (ArC), 131.0 (ArC), 128.6 (ArCH), 128.4 (ArCH), 128.3 (ArCH), 67.0 (CH_2), 52.8 (CH_3).

HRMS *m/z*: 327.1019 $[M-H]^-$ Calculated 327.0822 $[M-Na]^-$.

Synthesis of *L*-leucyl-2-aminoquinoline and 5-ethynyl-*N1,N3*-bis((2*S*)-4-methyl-1-oxo-1-(quinoline-2-ylamino)pentan-2-yl)benzene-1,3-dicarboxamide (5.16)[13]

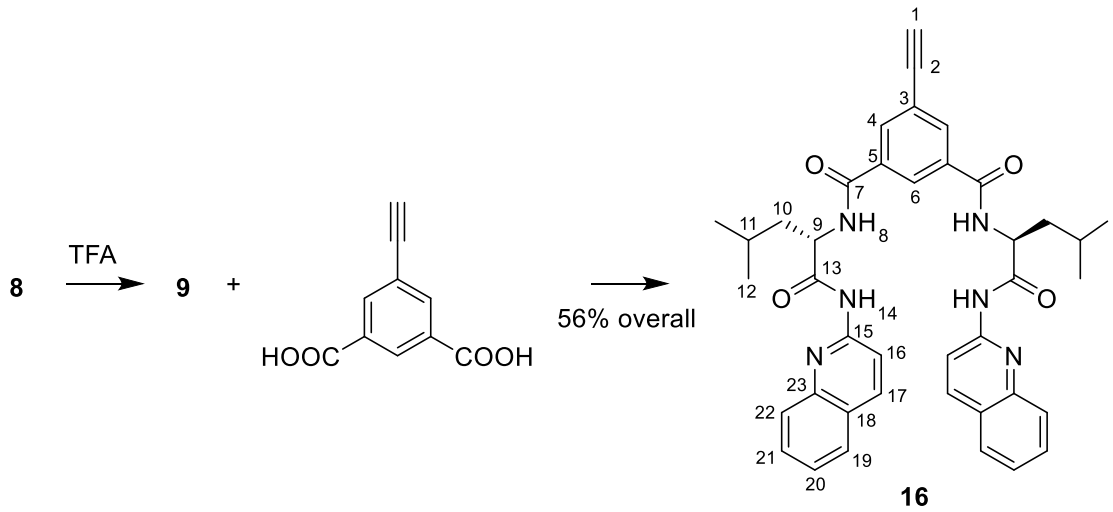

N-boc-*L*-leucyl-2-aminoquinoline, **5.8** (572 mg, 1.6 mmol) was added to trifluoroacetic acid (80 mL) and stirred for 2 h at room temperature, after which the solvent was removed under reduced pressure. To the residue was added saturated K_2CO_3 solution (80 mL) and the mixture extracted with Et_2O (2 × 60 mL). The combined organic layer was dried over $MgSO_4$, filtered and concentrated under reduced pressure to give 183 mg of *L*-leucyl-2-aminoquinoline as a pale orange solid- this product was used without further purification due to relative instability. Into a mixture of 5-ethynylbenzene-1,3-dioic acid (90 mg, 0.47 mmol), *L*-leucyl-2-aminoquinoline (183 mg, 0.71 mmol) and 1-hydroxybenzotriazole (142 mg, 10.5 mmol) in 40 mL DMF, was added a solution of dicyclohexylcarbodiimide (280 mg, 1.36 mmol) in 20 mL DMF. The mixture was for 19 h at room temperature, under a N_2 atmosphere. The solution was concentrated under reduced pressure and the residue dissolved in EtOAc (100 mL) and the organic layer was washed with H_2O and saturated $NaHCO_3$ (60 mL each), dried over $MgSO_4$, filtered and concentrated under reduced pressure. The crude residue was purified by column chromatography using Pet. Ether : EtOAc (1:1). Product obtained as an off-white/beige solid (0.177 g, 0.26 mmol, 56%)

^{1H} NMR (400 MHz, d_6-DMSO) δ 11.02 (s, 2H), 8.91 (d, *J* = 7.6 Hz, 2H), 8.44 (t, *J* = 1.6 Hz, 1H), 8.36 (d, *J* = 9.0 Hz, 2H), 8.28 (d, *J* = 8.8 Hz, 2H), 8.21 (d, *J* = 1.6 Hz, 2H), 7.92 (dd, *J* = 8.1, 0.8 Hz, 2H), 7.83 (d, *J* = 8.5 Hz, 2H), 7.69-7.75 (m, 2H), 7.48-7.53 (m, 2H), 4.84 (bs, 2H), 4.45 (s, 1H), 1.77-1.90 (m, 4H), 1.61-1.69 (m, 2H), 0.93-0.99 (m, 12H).

^{13}C NMR (101 MHz, d_6-DMSO) δ 172.7 (CO), 165.3 (CO), 151.5 (ArC), 146.3 (ArC), 138.3 (ArCH), 134.7 (ArC), 133.0 (ArCH), 130.0 (ArCH), 127.8 (ArCH), 127.6 (ArCH), 126.9 (ArCH), 125.6 (ArC), 125.0 (ArCH), 121.8 (ArC), 114.3 (ArCH), 82.3 (C), 82.2 (CH), 53.2 (CH), 24.6 (CH), 23.2 (CH_3), 21.2 (CH_3)

HRMS *m/z*: 669.3187 [M+H$^+$] Calculated 669.3178 [M+H]$^+$; **FTIR (cm^{-1}):** 3323, 2116, 1660, 1623.

5.7.3 UV-Vis titrations

Two solutions were made for the UV-Vis titrations. Firstly, 10 mL of a 1×10^{-5} M solution of receptor **16** was prepared in acetonitrile. Secondly, 100 mL of 1×10^{-3} M solutions of each of the corresponding tetrabutylammonium anions in acetonitrile were made. The anion solution was then titrated into the receptor solution in suitable aliquots e.g., 0.1 equivalent aliquots up to 2.0 equivalents and then 1.0 equivalents thereafter, up to a total of 6.0 equivalents. Readings were then taken after each addition.

5.7.4 Electrode attachment

The modified glassy carbon electrode was prepared accordingly to previously reported literature methods[34,37].

Before the modification of the electrode surface, glassy carbon electrodes were polished three times with 1 μm alumina slurries on microcloth pads, rinsed with water and sonicated in acetonitrile for 5 min. Surface modification was carried out with a 1 mM 4-nitrobenzenediazonium tetrafluoroborate and 0.1 M tetrabutylammonium tetrafluoroborate in acetonitrile solution. Repetitive scanning from 0.30 to −0.40 V versus Ag/$AgNO_3$ reference, at a scan rate of 200 mVs^{-1} was used for the initial reduction of the diazonium species. Potentiostatic electrolysis was then performed at −0.40 V for 600 s to further reduce the diazonium salt. The glassy carbon electrodes were then rinsed thoroughly with acetonitrile and sonicated for 10 min, in order to remove loosely bound species. 1 mM potassium ferricyanide in an aqueous 0.1 M phosphate buffer at pH 2 was used as a redox probe for the cyclic voltammetry. 4 repeat scans from 0.30 to −0.40 V versus Ag/AgCl reference, at a scan rate of 100 mVs^{-1} were used for the electrochemical probe.

5.8 References

1 Y. J. Kim and J. H. Choi, *Water Res*, 2012, **46**, 6033–6039.

2 J. Pan, Y. Zheng, J. Ding, C. Gao, B. Van Der Bruggen and J. Shen, *Ind Eng Chem Res*, 2018, **57**, 7048–7053.

3 K. Zuo, J. Kim, A. Jain, T. Wang, R. Verduzco, M. Long and Q. Li, *Environ Sci Technol*, 2018, **52**, 9486–9494.

4 J. Kang and J. Kim, *Tetrahedron Lett*, 2005, **46**, 1759–1762.

5 J. Kang, H. S. Kim and D. O. Jang, *Tetrahedron Lett*, 2005, **46**, 6079–6082.

6 J. L. Sessler, D. G. Cho and V. Lynch, *J Am Chem Soc*, 2006, **128**, 16518–16519.

7 G. W. Bates, Triyanti, M. E. Light, M. Albrecht and P. A. Gale, *Journal Organic Chemistry*, 2007, **72**, 8921–8927.

8 A. Abebayehu, R. Dutta, S. J. Kim, J. H. Lee, H. Hwang and C. H. Lee, *European J Org Chem*, 2016, **2016**, 3959–3963.

9 J. Kang, H. S. Kim and D. O. Jang, *Tetrahedron Lett*, 2005, **46**, 6079–6082.

10 J. Vicente, J.-A. Abad, B. Rink, F.-S. Hernández and M. C. R. de Arellano, *Organometallics*, 2002, **16**, 5269–5282.

11 J. Landon, X. Gao, A. Omosebi and K. Liu, *Curr Opin Chem Eng*, 2019, **25**, 1–8.

12 A. Kalfa, B. Shapira, A. Shopin, I. Cohen, E. Avraham and D. Aurbach, *Chemosphere*, 2020, 241, 1−12.

13 S. I. Kondo and R. Takai, *Org Lett*, 2013, **15**, 538–541.

14 S. I. Kondo, Y. Hiraoka, N. Kurumatani and Y. Yano, *Chemical Communications*, 2005, **13**, 1720–1722.

15 John. Sheehan and G. P. Hess, *J Am Chem Soc*, 1955, **77**, 1067–1068.

16 T. R. Shah and A. Misra, in *Challenges in Delivery of Therapeutic Genomics and Proteomics*, Elsevier Inc., 2011, pp. 387–427.

17 C. A. G. N. Montalbetti and V. Falque, *Tetrahedron*, 2005, **61**, 10827–10852.

18 C. Mayato, R. L. Dorta and J. T. Vázquez, *Tetrahedron Lett*, 2008, **49**, 1396–1398.

19 K. C. Nicolaou, A. A. Estrada, M. Zak, S. H. Lee and B. S. Safina, *Angewandte Chemie*, 2005, **117**, 1402–1406.

20 R. L. E. Furlán, E. G. Mata and O. A. Mascaretti, *J. Chem. Soc., Perkin Trans. 1*, 1998, 355–358.

21 P. G. M. Wuts and T. W. Greene, in *Greene's Protective Groups in Organic Synthesis*, John Wiley & Sons, Inc., 2006, pp. 533–646.

22 S. M. Dimick, S. C. Powell, S. A. McMahon, D. N. Moothoo, J. H. Naismith and E. J. Toone, *J Am Chem Soc*, 1999, **121**, 10286–10296.

23 D. M. M. Mevan Dissanayake, A. D. Melville and A. K. Vannucci, *Green Chemistry*, 2019, **21**, 3165–3171.

24 J. Tummatorn, P. A. Albiniak and G. B. Dudley, *Journal of Organic Chemistry*, 2007, **72**, 8962–8964.

25 L. J. Gooßen and A. Döhring, *Synlett*, 2004, **2**, 263–266.

26 P. L. Geissler, *J Am Chem Soc*, 2005, **127**, 14930–14935.

27 R. S. Drago, in *Physical Methods for Chemists*, Surfside Scientific Publishers, Gainesville, 1st edn., 1977, pp. 81–96.

28 E. J. Olson and P. Bühlmann, *Journal of Organic Chemistry*, 2011, **76**, 8406–8412.

29 D. Brynn Hibbert and P. Thordarson, *Chemical Communications*, 2016, **52**, 12792–12805.

30 H. Maeda, T. Kitano, C. Z. Huang, K. Katayama, Y. Yamauchi and H. Ohmori, *Analytical Sciences* , 1999, **15**, 531–536.

31 R. S. Deinhammer, M. Ho, J. W. Anderegg and M. D. Porter, *Langmuir*, 1994, **10**, 1306–1313.

32 K. H. Vase, A. H. Holm, K. Norrman, S. U. Pedersen and K. Daasbjerg, *Langmuir*, 2007, **23**, 3786–3793.

33 P. A. Brooksby and A. J. Downard, *Langmuir*, 2004, **20**, 5038–5045.

34 Z. Nazemi, E. Shams and M. K. Amini, *Electrochim Acta*, 2010, **55**, 7246–7253.

35 A. D. Stergiou and M. D. Symes, *Cell Rep Phys Sci*, 2022, **3**, 100914.

36 M. V. Sheridan, K. Lam and W. E. Geiger, *Angewandte Chemie - International Edition*, 2013, **52**, 12897–12900.

37 L. M. Santos, J. Ghilane, C. Fave, P. C. Lacaze, H. Randriamahazaka, L. M. Abrantes and J. C. Lacroix, *Journal of Physical Chemistry C*, 2008, **112**, 16103–16109.

Chapter 6

Final Conclusions and Future Work

Final Conclusions and Future Work

In this thesis, we successfully synthesised a group of modified hydrogen bonding receptors that showed specificity for either the dihydrogenphosphate or bicarbonate anion.

Chapter 3 developed upon the class of indole-based receptors previously described in the literature[1–3], through modification with either a carboxylic acid or alkyne group. Initial synthesis to include the carboxylic acid group proved to be unsuccessful. During the synthetic process it was necessary to protect the free carboxylic acid, with a methyl ester, in order to prevent cross-reaction during the coupling stages, as well as improving the initial solubility of the starting material- γ-aminobutyric acid. In order to be attached to the electrode surface, the methyl group needed to be removed in order to yield the carboxylic acid. However, the deprotection, under basic conditions, with and without heat, proved to be troublesome and no useable receptor was obtained. It was postulated that during the acidic workup, necessary in order to protonate the obtained carboxylate and extract into organic solvent, the basic indole groups of the receptor were also protonated, and as such the receptor was able to move back into the aqueous phase. This led to a gloopy, emulsion like mix whereby no product was obtained. In order to circumvent such a problem, a second related receptor was devised that did not contain a readily protonatable group, such as an alkyne. This receptor was successfully synthesised with an overall yield of 20% over 3 steps. ^{1}H NMR titrations of the receptor with the tetrabutylammonium salt of dihydrogenphosphate in 0.5% H_2O/d_6-DMSO indicated that a receptor-anion complex was formed. From the obtained spectra it could clearly be seen that upon addition of increasing amounts of dihydrogenphosphate, the resonances for the indole, urea and amide were seen to shift downfield by up to 1.4 ppm, for the indole proton. Smaller changes were observed for the urea and amide protons. These changes in chemical shift are evidence of hydrogen bonds being formed between the receptor and anion. It had previously been shown that the addition of the basic dihydrogenphosphate could lead to a deprotonation event occurring[3]. This was proposed to be the result of the pK_a of a bound anion being lowered sufficiently by the receptor, that it could be deprotonated by the more basic 'free' anion in solution. Further studies, using basic tetrabutylammonium hydroxide could be used in order to confirm whether a deprotonation event occurs with the synthesised receptor, be it the deprotonation of the anion, as previously described, or the receptor. In our studies, addition of anion, up to 7 equivalents did not cause such a deprotonation event. However, this should be further investigated through the aforementioned method, as a bound dibasic

monohydrogenphopshate would be more tightly bound and as such could potentially require a more positive potential when utilised within a capacitive deionisation system. Additionally, a range of further anions would be tested for their ability to interact and form hydrogen bond to the receptor. This would confirm the suitability of the receptor for use within a dihydrogenphosphate specific capacitive deionisation system.

In Chapter 4, a carbazole-based receptor was synthesised and tested for its ability to bind to the bicarbonate anion. A first initial synthesis was proposed that followed a previously described literature procedure to synthesise a bis-carbazolylurea receptor[4]. The synthesised receptor could then be subjected to the same reaction conditions- nitration, reduction of the nitro group and isocyanate formation- which would allow for the receptor to be grafted to an electrode surface (via a surface bound organic group). However, nitration of carbazole led to two main products being obtained- 1-and 3-nitrocarbazole. Purification of the desired 1-nitrocarbazole proved to be troublesome with a useable isolated yield not being obtained. A Buchwald-Hartwig cross coupling was used in order to improve the separation process by eliminating the formation of the 3-nitrocarbaozle altogether. The coupling reaction was successful and 1-nitrocarbazole was obtained, however the reaction yield was significantly lower than expected. Consequently, a third method was proposed that installed *tert*-butyl group in the 3,6-positions on the carbazole ring[5]. This allowed for the nitration solely in the 1,8-positions. Subsequently, a *tert*-butyl substituted bis-carbazolylurea receptor was synthesised over 5 steps with an overall yield of 5%. ^{1}H NMR titrations with the tetraethylammonium salt of bicarbonate in 0.5% H_2O/d_6-DMSO indicated the formation of a receptor-anion complex. Addition of the anion, up to 1 equivalent, caused a large downfield shift in the observed resonances for both the carbazole and urea NH-protons. In order to further confirm the suitability of the receptor for its use within a capacitive deionisation system, further investigations into the potential interaction of the receptor with other anions needs to be investigated. Ideally, this should be with the same counter-ion, e.g., tetraethylammonium, in order to allow for the direct comparison of the affinity of the receptor for each anion.

Chapter 5 synthesised a receptor, based on the amino acid leucine, that demonstrated affinity for dihydrogenphosphate[6]. The isophthaloyl core proposed contained three carboxylic acid groups (protected as the methyl ester)- which would allow for the attachment of the two leucine-based receptor arms, as well as serving as an attachment point for the electrode. Mono-deprotection of one of the esters and its subsequent benzylation proved to be successful, however deprotection of the remaining methyl ester groups, under basic

conditions, led solely to the benzene-1,3,5-tricarboxylic acid being obtained. Consequently, an alternative core molecule was used. This core contained the required carboxylic acid moieties and an alkyne group as the point of electrode attachment. The receptor, containing the alkyne, was successfully synthesised with an overall yield of 39% over 3 steps. UV-Vis titrations of the receptor with various anions, as their tetrabutylammonium salts, showed that the receptor solely had affinity for dihydrogenphosphate, over all the other anions tested. Chapter 5 also showed that it is possible to electrochemically modify a glassy carbon electrode through the electroreduction of a diazonium salt. 4-nitrobenzene diazonium salt was shown to be successfully reduced and covalently bound to the electrode surface. This modified surface layer was then subsequently transformed to the amine through the electrochemical reduction of the nitro group. Finally, it was shown that this amine could react with a suitable electrophilic centre, such as an aldehyde, to form an amide bond. This surface bound amine was proposed as the principle point of attachment for all the receptors described in Chapters 3-5, either through the formation of a urea linkage, specifically the bicarbonate receptor in Chapter 4, or, after further transformation of the amine moiety into and azide, a click chemistry type reaction with the alkyne could be performed. Additionally, the direct attachment of the two dihydrogenphosphate receptors, via the alkyne bond could function as an alternative method of attachment. It has been shown that the alkyne group can be oxidised and can be directly bound to the electrode surface[7].

It was possible to determine an association constant, K_a, for the synthesised receptors. The association constants for each of the receptors for a range of anions should be determined, in order to conclusively show the extent of receptor-anion interaction and determine whether or not the receptor could be used in a capacitive deionisation system. Due to time constraints, it was not possible to obtain repeat data for in order to corroborate the calculated association constants. It would be beneficial to repeat the previously mentioned UV-Vis and NMR spectroscopic titrations, in particular NMR titrations as no other anionic species were tested. The UV-Vis data obtained gave a clear picture that the receptor was selective for $H_2PO_4^-$ over all of the other anions tested. As discussed above, no other anions were tested for their affinity for receptors **3.12** and **4.16** and further experiments should be conducted in order to confirm the selectivity of the receptors before being utilised in a CDI system.

Further time should be invested in finding a reliable method for the functionalisation of the electrode surface. As demonstrated, this can be done using diazonium species and reductive potentials and monitored using an electrochemical probe. This provides a qualitative method

for following the reaction at the different stages but gives no indication of the uniformity of the layer on the electrode surface. It would therefore be prudent to determine if a mono- or multilayer is formed on the electrode surface. This could potentially be done through the use of infrared spectroscopy or scanning electron microscopy. With regards to the alkynyl moiety, the oxidation described by Sheridan et al.[7] provides a facile option for electrode attachment. It would be beneficial to invest more time investigating the oxidation of the alkynyl moiety and the conditions that could be utilised to attach both **3.12** and **5.16** to the surface without the need for further chemical modification, as would be required if a click reaction was to be performed.

As the chemical space of receptors continues to increase it becomes more important to find real world applications that can benefit from their incorporation. CDI systems and the underlying ideas have been around for a number of years now, and yet it is still an emerging technology that is still to be fully optimised. It has been shown to be highly versatile and can successfully and effectively remove both anionic and cationic species from a range of sources,[8] however large scale, widespread operation is some time away yet.

References

1 J. R. Hiscock, *BINDING ANIONS USING SIMPLE NEUTRAL MOLECULES*, Southampton, 2010.

2 C. Caltagirone, J. R. Hiscock, M. B. Hursthouse, M. E. Light and P. A. Gale, *Chemistry - A European Journal*, 2008, **14**, 10236–10243.

3 P. A. Gale, J. R. Hiscock, S. J. Moore, C. Caltagirone, M. B. Hursthouse and M. E. Light, *Chem Asian J*, 2010, **5**, 555–561.

4 J. R. Hiscock, C. Caltagirone, M. E. Light, M. B. Hursthouse and P. A. Gale, *Org Biomol Chem*, 2009, **7**, 1781–1783.

5 G. Sanchez, A. Espinosa, D. Curiel, A. Tarraga and P. Molina, *Journal of Organic Chemistry*, 2013, **78**, 9725–9737.

6 S. I. Kondo and R. Takai, *Org Lett*, 2013, **15**, 538–541.

7 M. V. Sheridan, K. Lam and W. E. Geiger, *Angewandte Chemie - International Edition*, 2013, **52**, 12897–12900.

8 Y. Oren, Desalination, 2008, 228, **1-3**, 10–29.

Appendix

NMR Spectra

Compounds- Chapter 3

Compound **3.4**

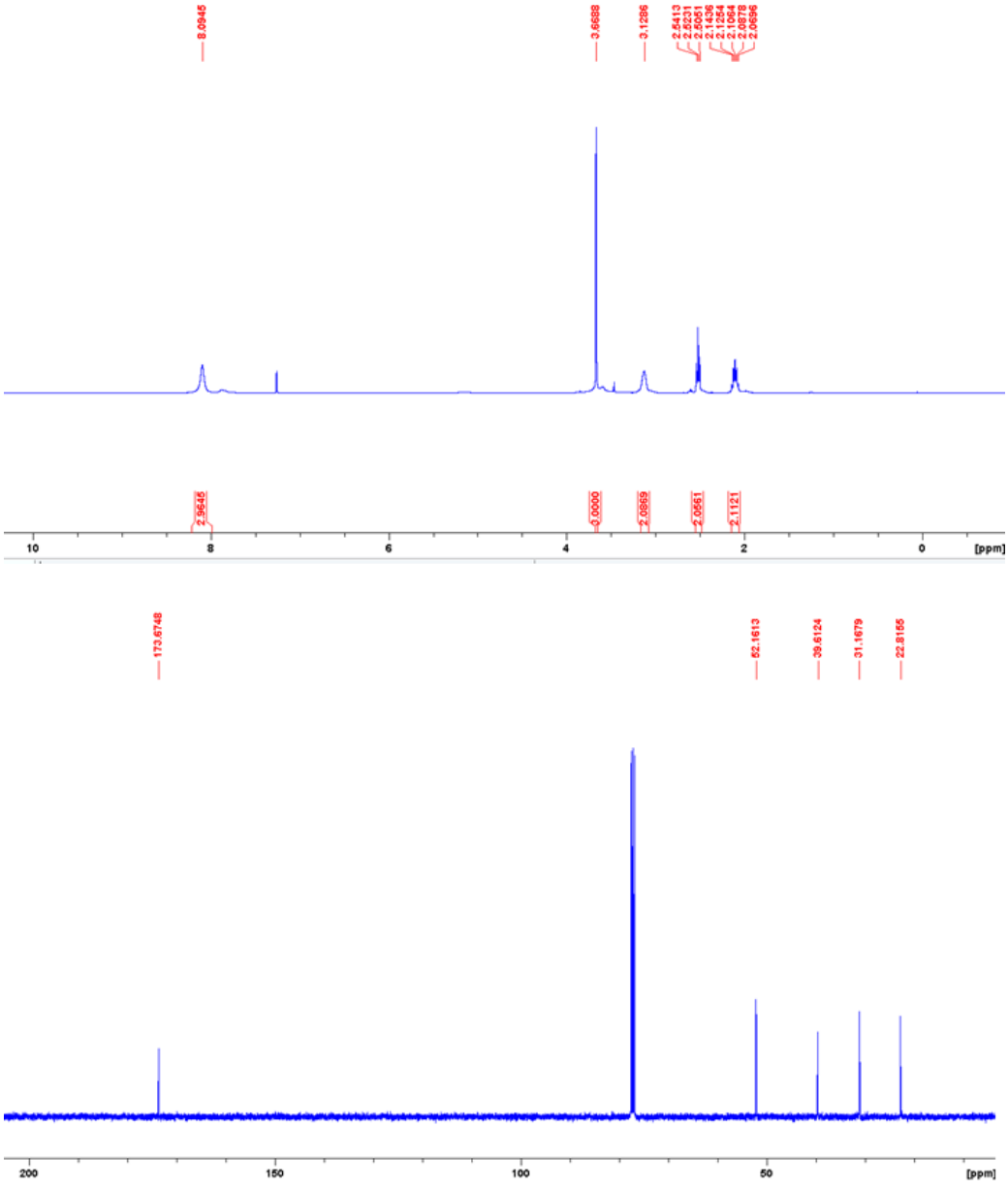

Appendix 1: Top) ^{1}H; Bottom) ^{13}C NMR spectra of compound **3.4** in $CDCl_3$ at 298 K.

Compound **3.5**

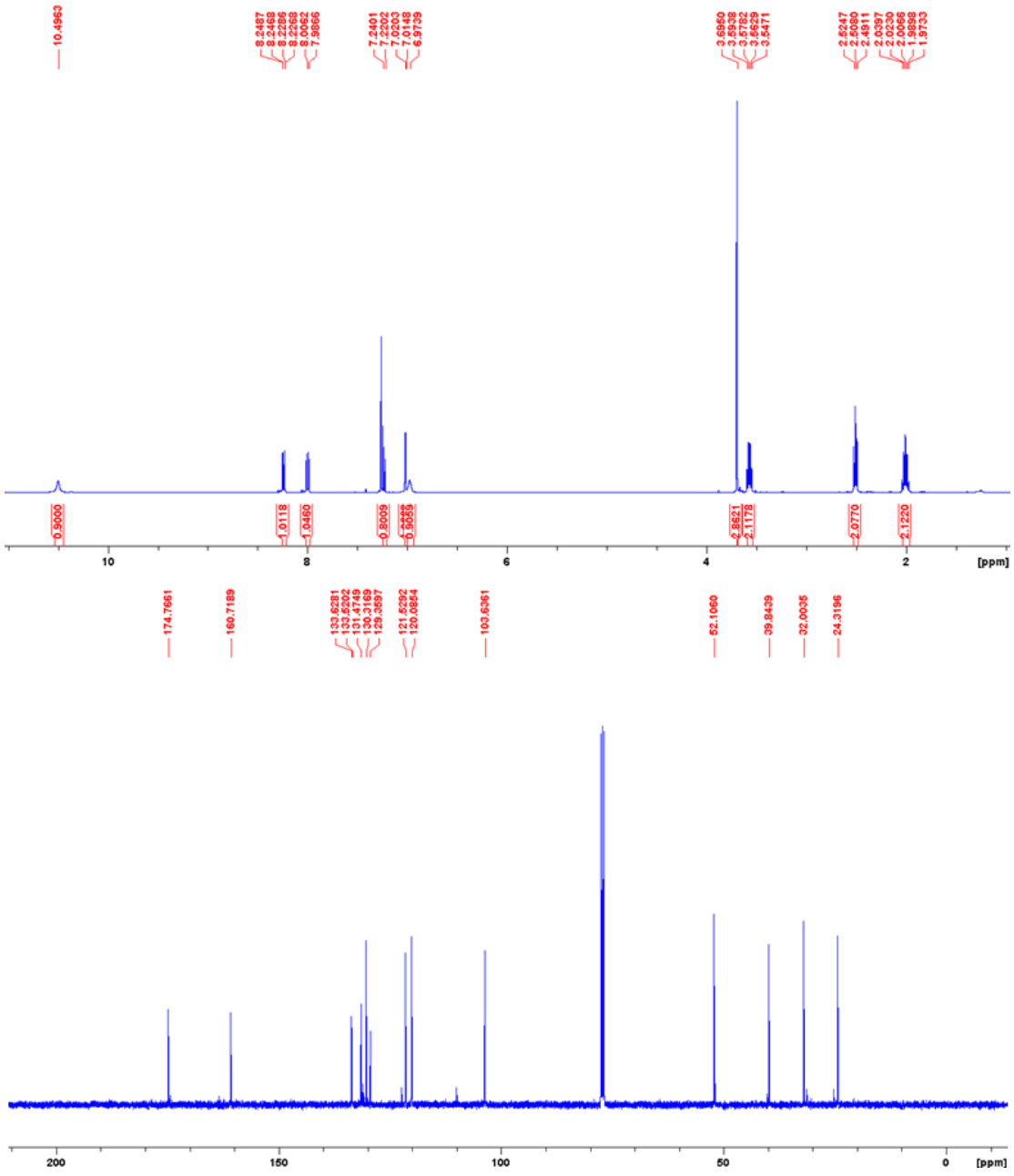

Appendix 2: Top) ^{1}H; Bottom) ^{13}C NMR spectra of compound **3.5** in $CDCl_3$ at 298 K.

Compound **3.6**

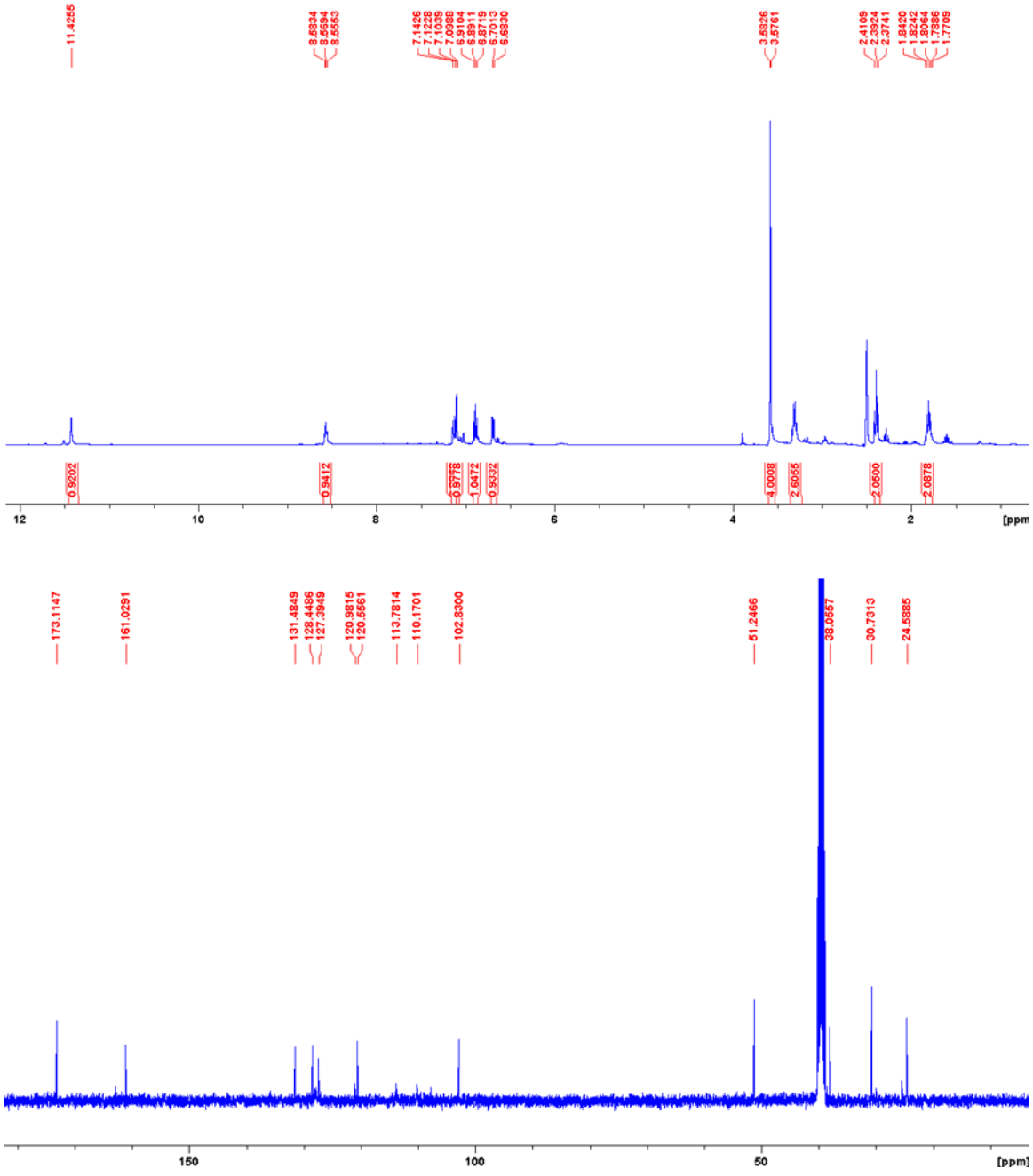

Appendix 3: Top) ^{1}H; Bottom) ^{13}C NMR spectra of compound **3.6** in d_6-DMSO at 298 K.

Compound **3.7**

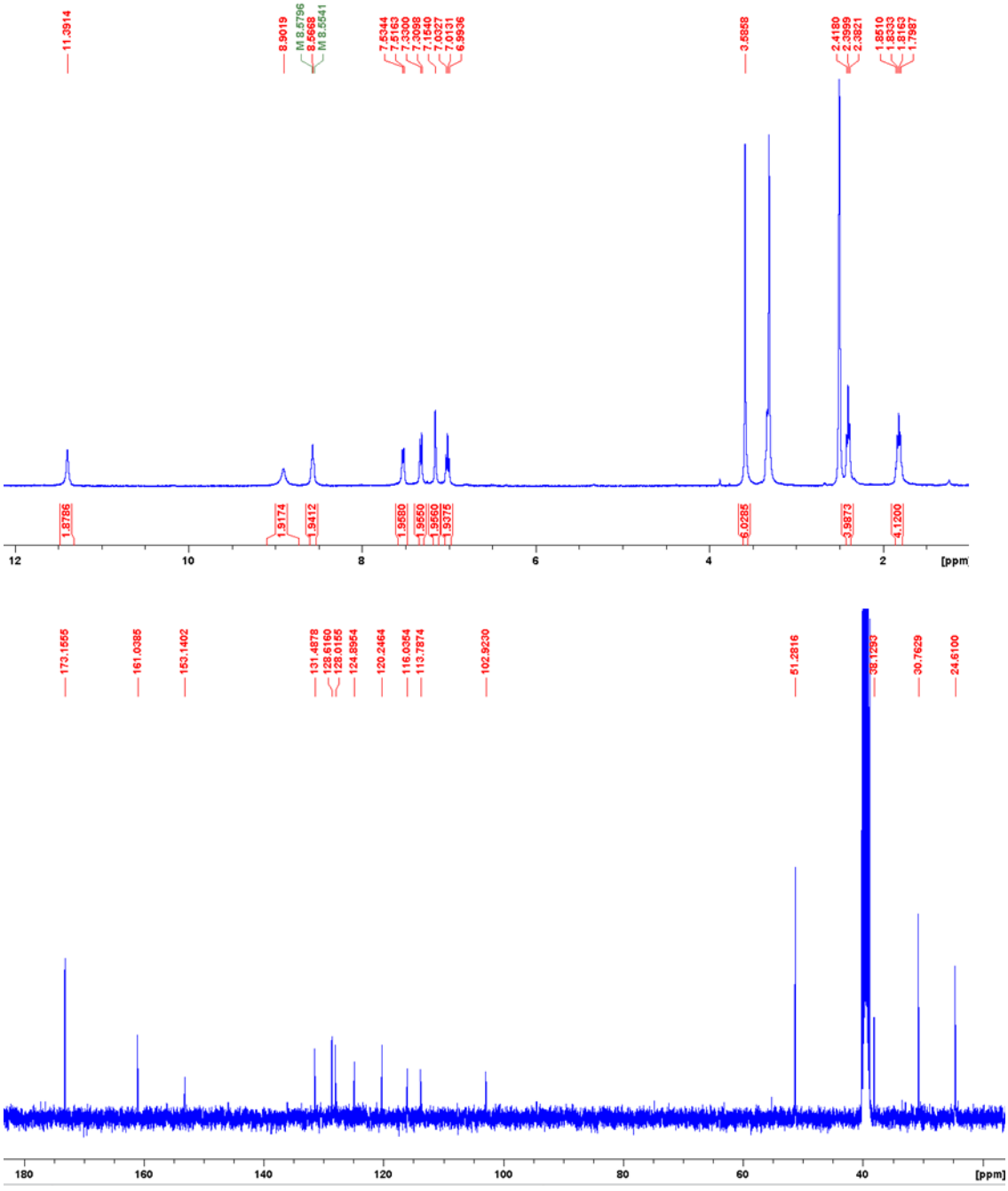

Appendix 4: Top) ^{1}H; Bottom) ^{13}C NMR spectra of compound **3.7** in d_6-DMSO at 298 K.

Compound **3.10**

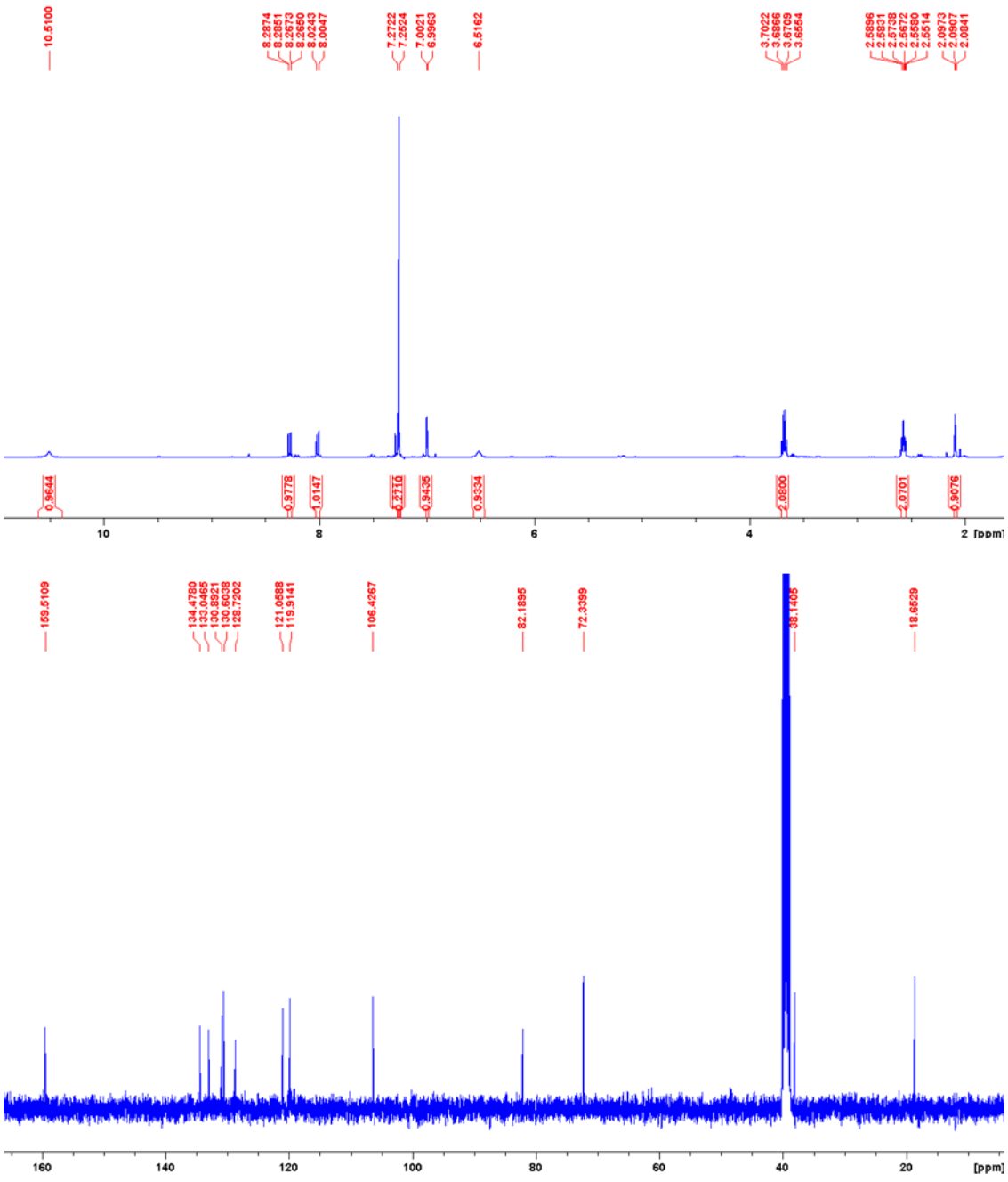

Appendix 5: Top) ^{1}H; Bottom) ^{13}C NMR spectra of compound **3.10** in $CDCl_3$ at 298 K.

Compound **3.11**

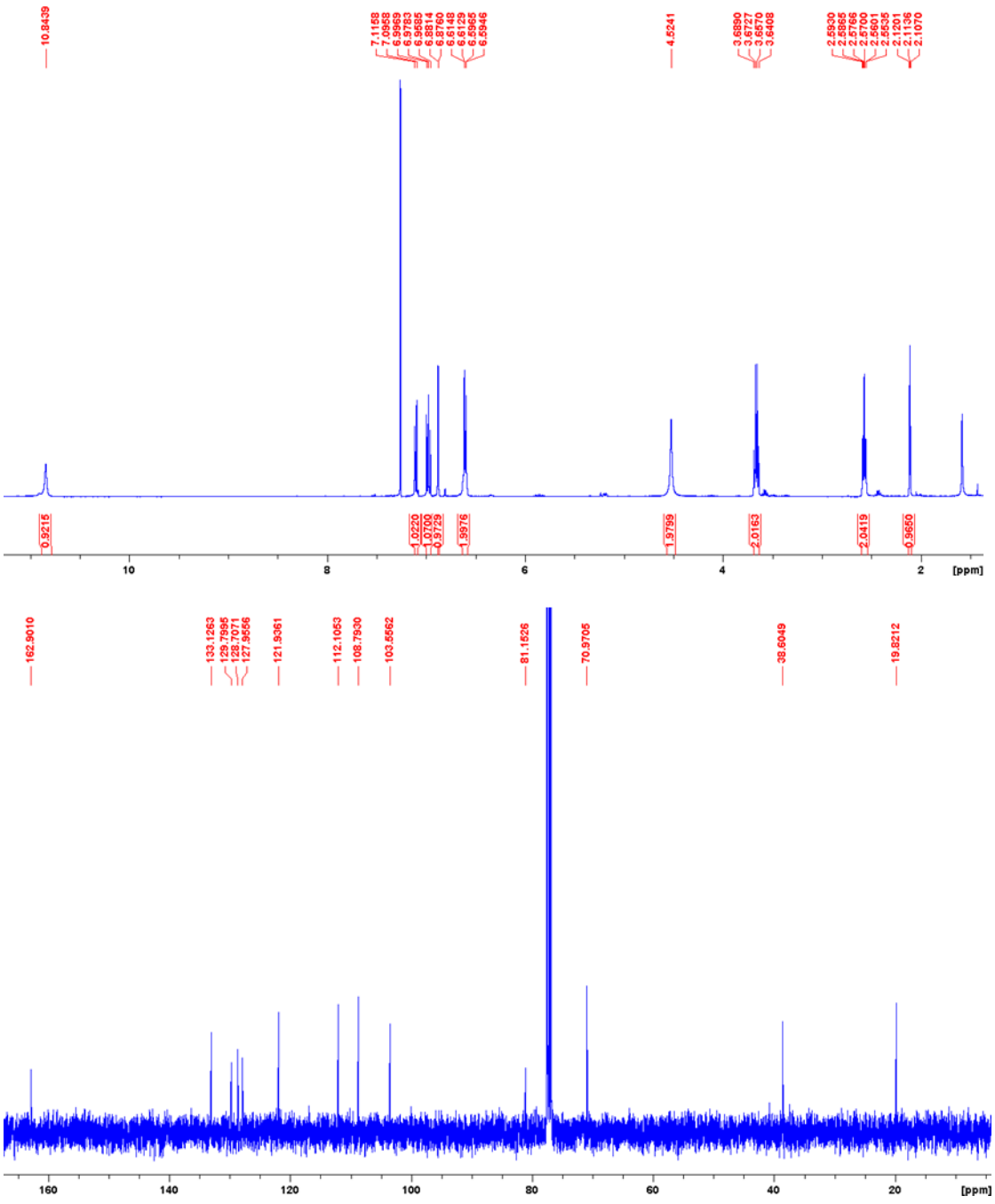

Appendix 6: Top) ^{1}H; Bottom) ^{13}C NMR spectra of compound **3.11** in $CDCl_3$ at 298 K.

Compound **3.12**

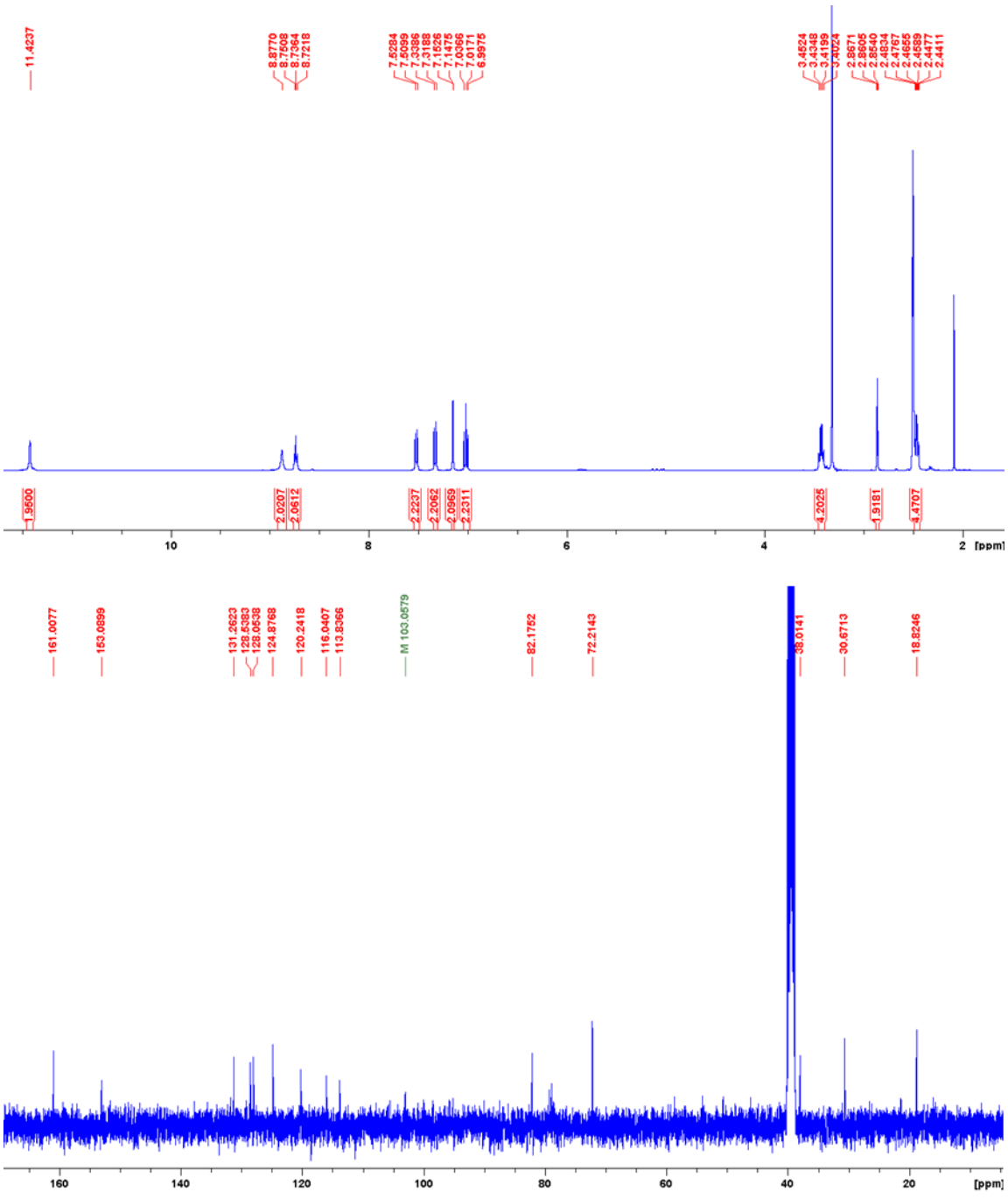

Appendix 7: Top) ^{1}H; Bottom) ^{13}C NMR spectra of compound **3.12** in d_6-DMSO at 298 K.

Compound **4.5**

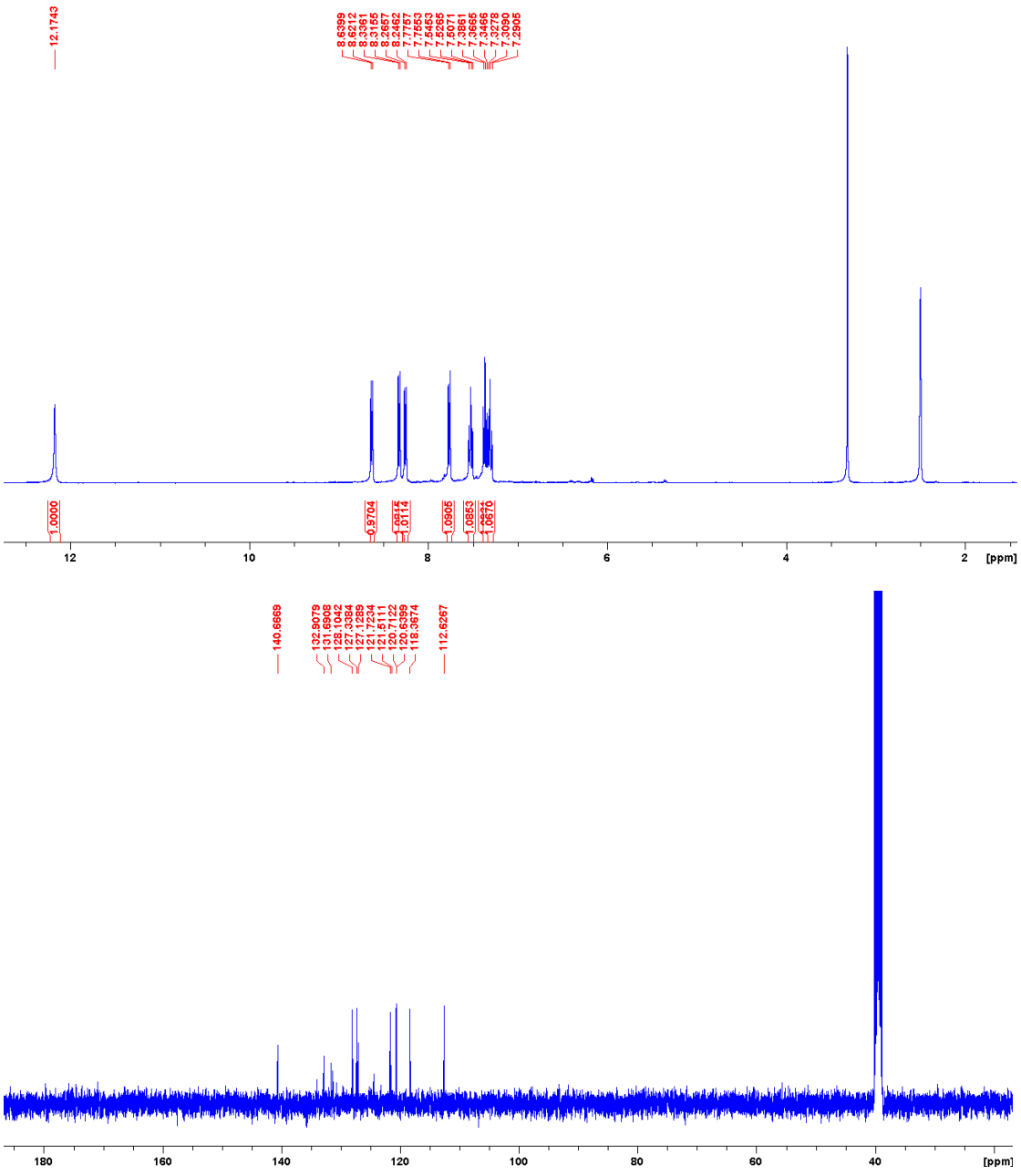

Appendix 8: Top) ^{1}H; Bottom) ^{13}C NMR spectra of compound **4.5** in d_6-DMSO at 298 K.

Compound **4.9**

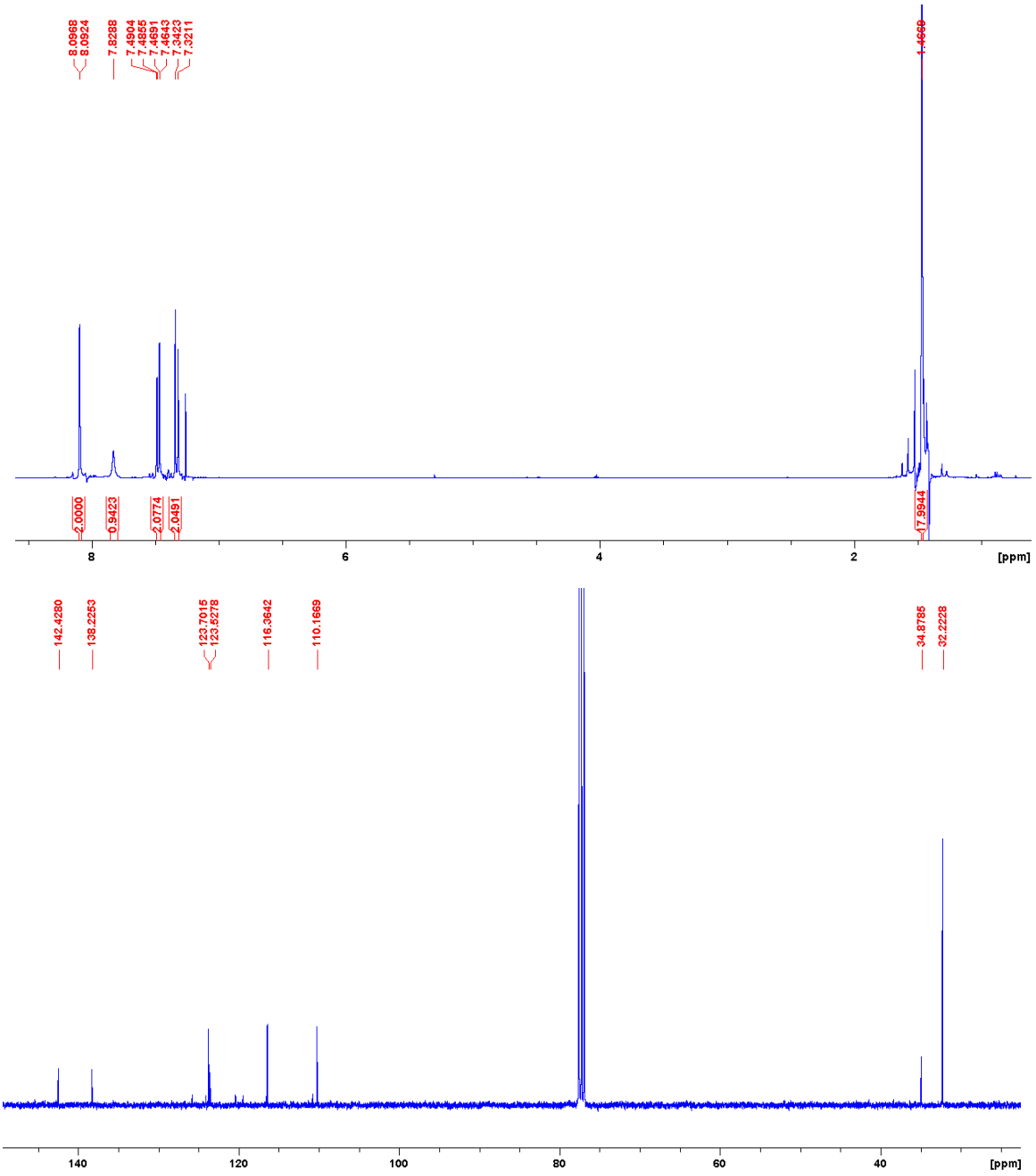

Appendix 9: Top) ^{1}H; Bottom) ^{13}C NMR spectra of compound **4.9** in $CDCl_3$ at 298 K.

Compound **4.10**

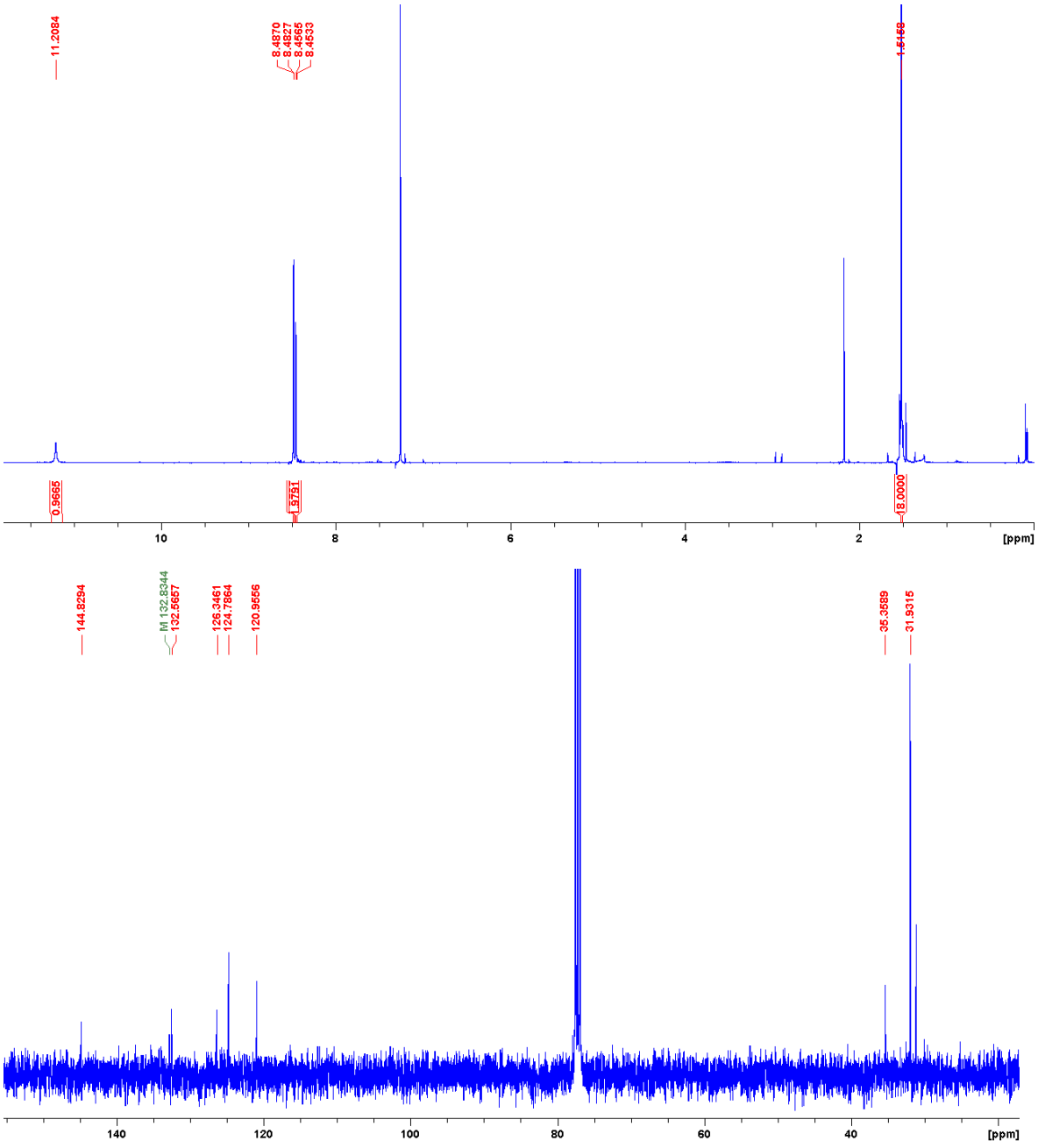

Appendix 10: Top) ^{1}H; Bottom) ^{13}C NMR spectra of compound **4.10** in $CDCl_3$ at 298 K.

Compound **4.11**

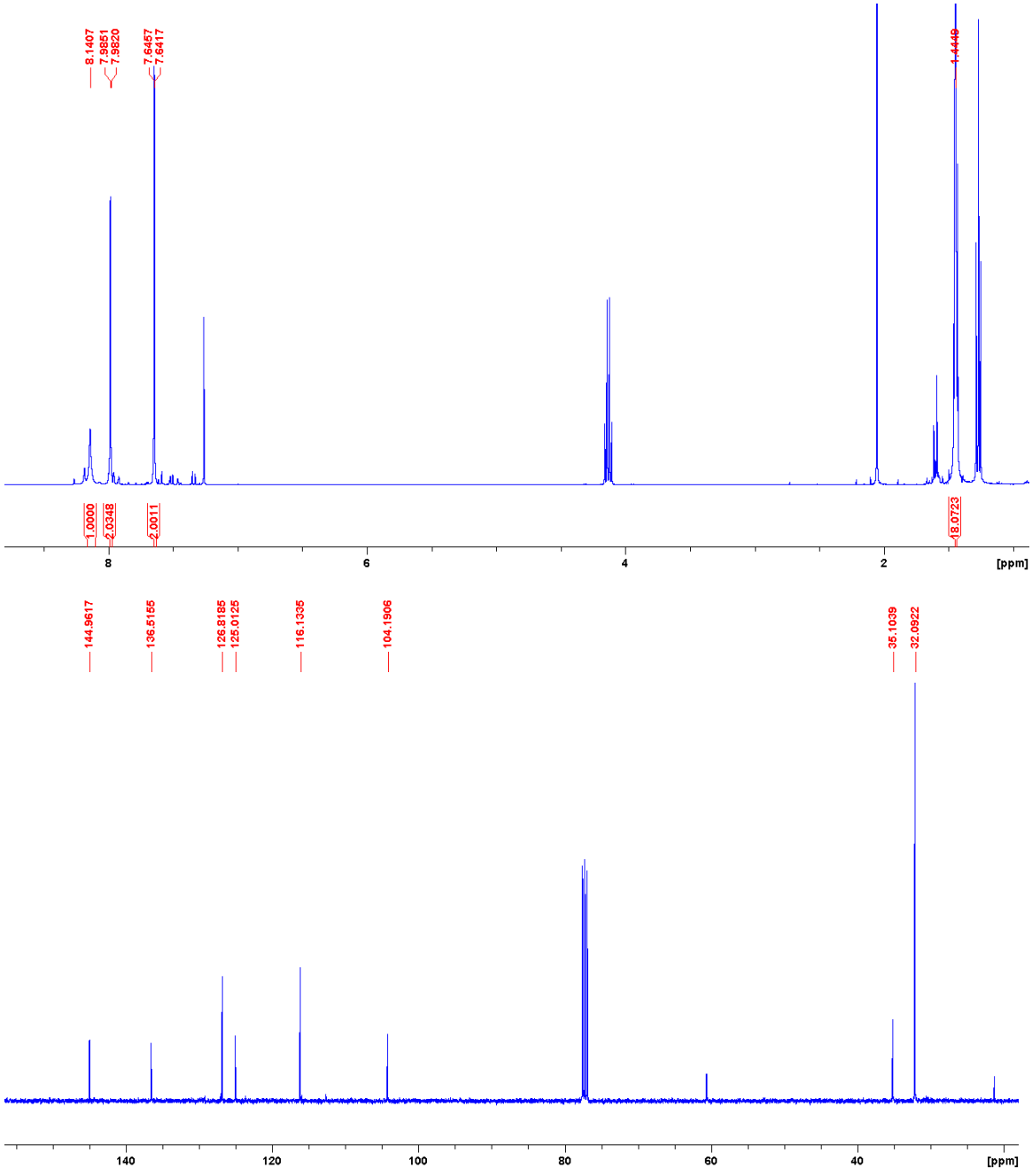

Appendix 11: Top) ^{1}H; Bottom) ^{13}C NMR spectra of compound **4.11** in $CDCl_3$ at 298 K.

Compound **4.12**

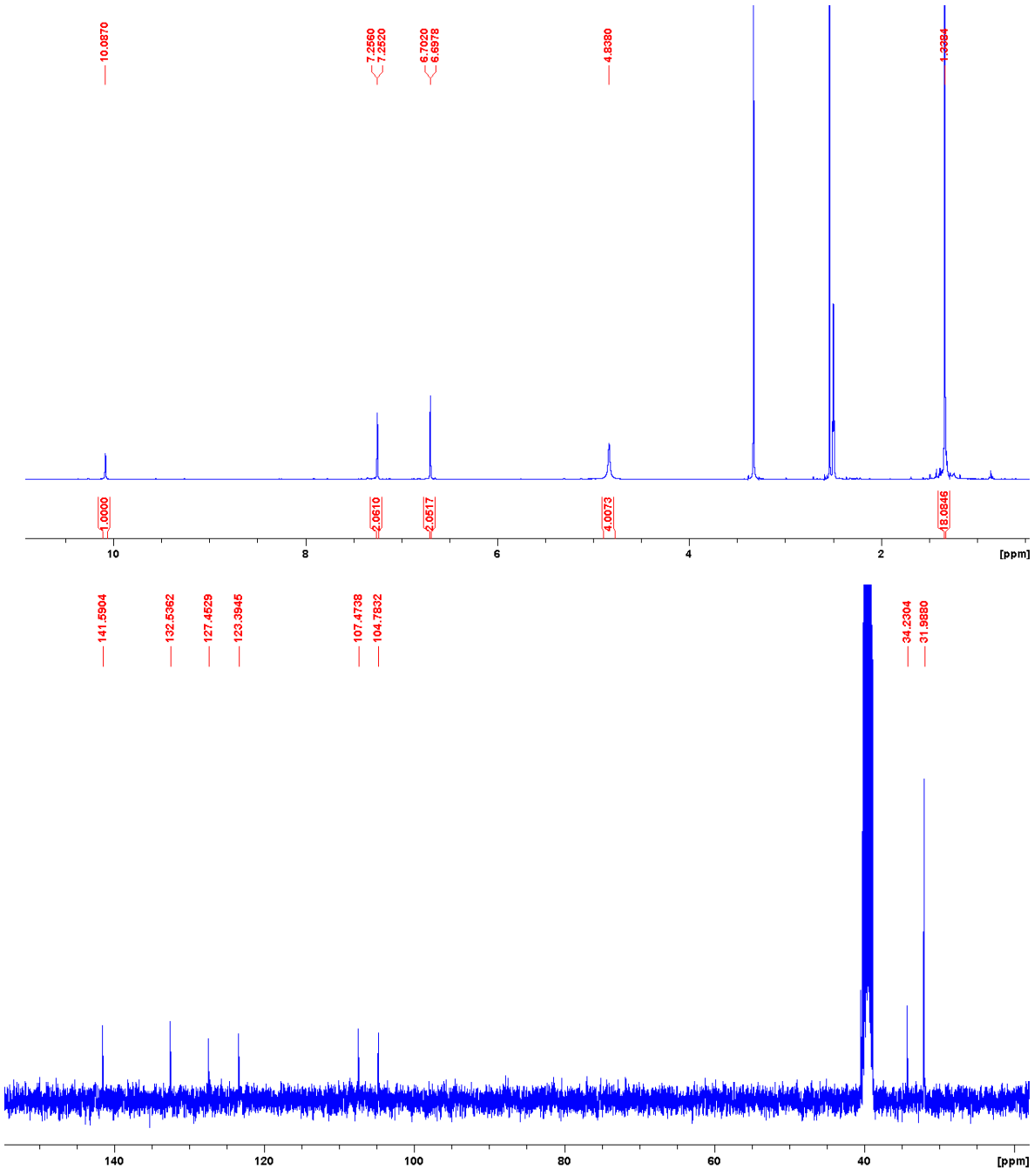

Appendix 12: Top) ^{1}H; Bottom) ^{13}C NMR spectra of compound **4.12** in d_6-DMSO at 298 K.

Compound **4.13**

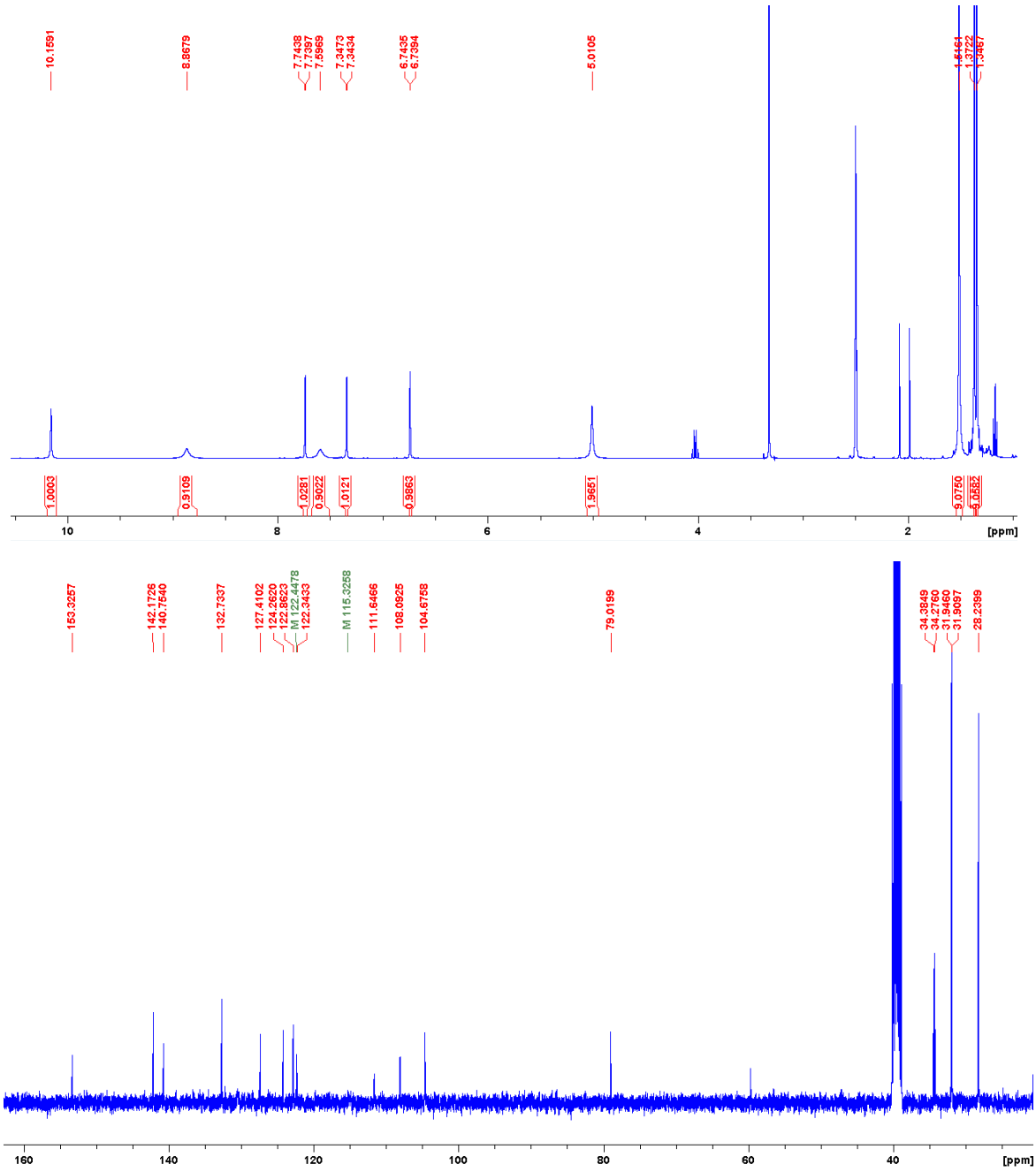

Appendix 13: Top) ^{1}H; Bottom) ^{13}C NMR spectra of compound **4.13** in d_6-DMSO at 298 K.

Compound **4.14**

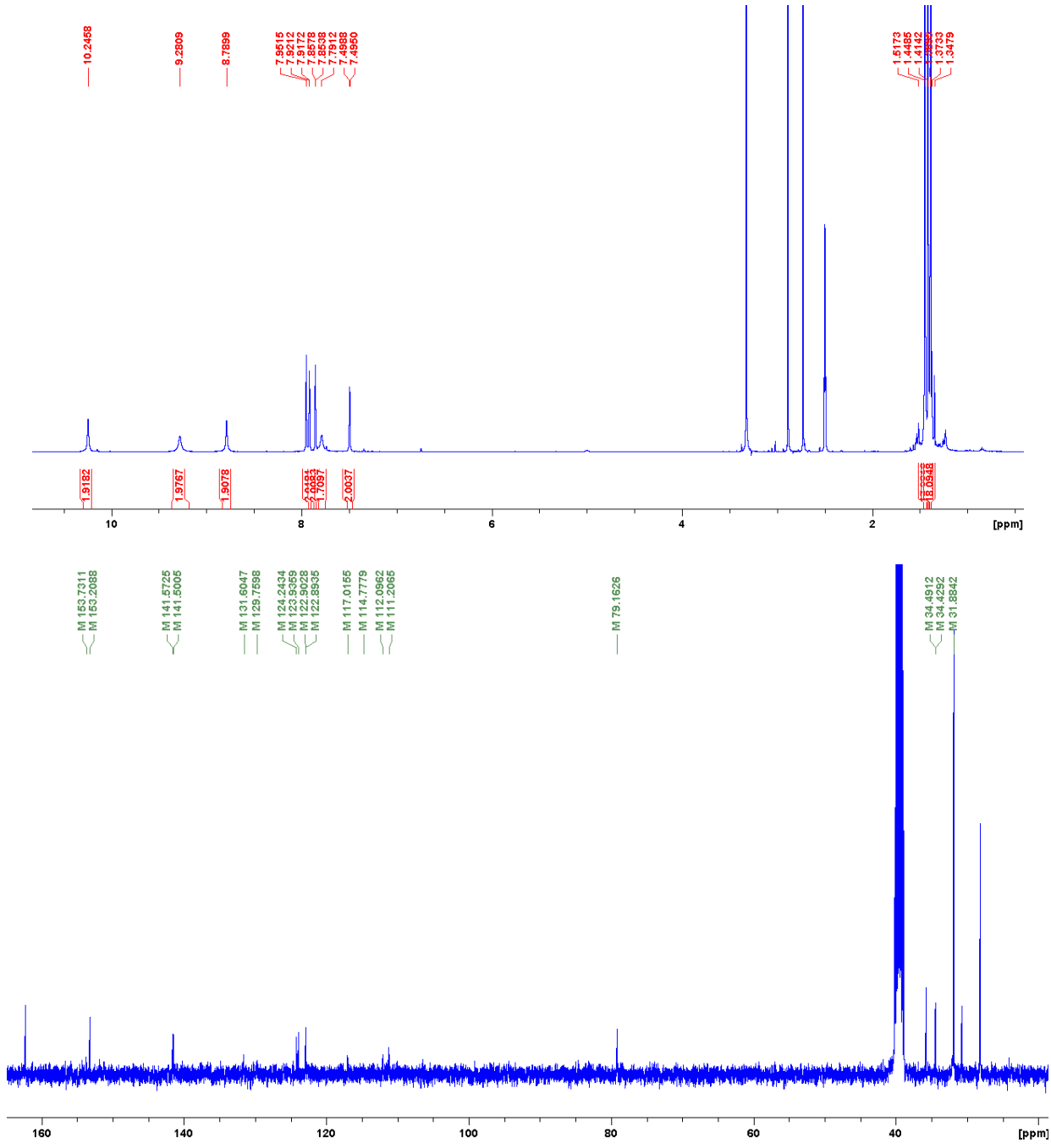

Appendix 14: Top) ^{1}H; Bottom) ^{13}C NMR spectra of compound **4.14** in d_6-DMSO at 298 K.

Compound **4.15**

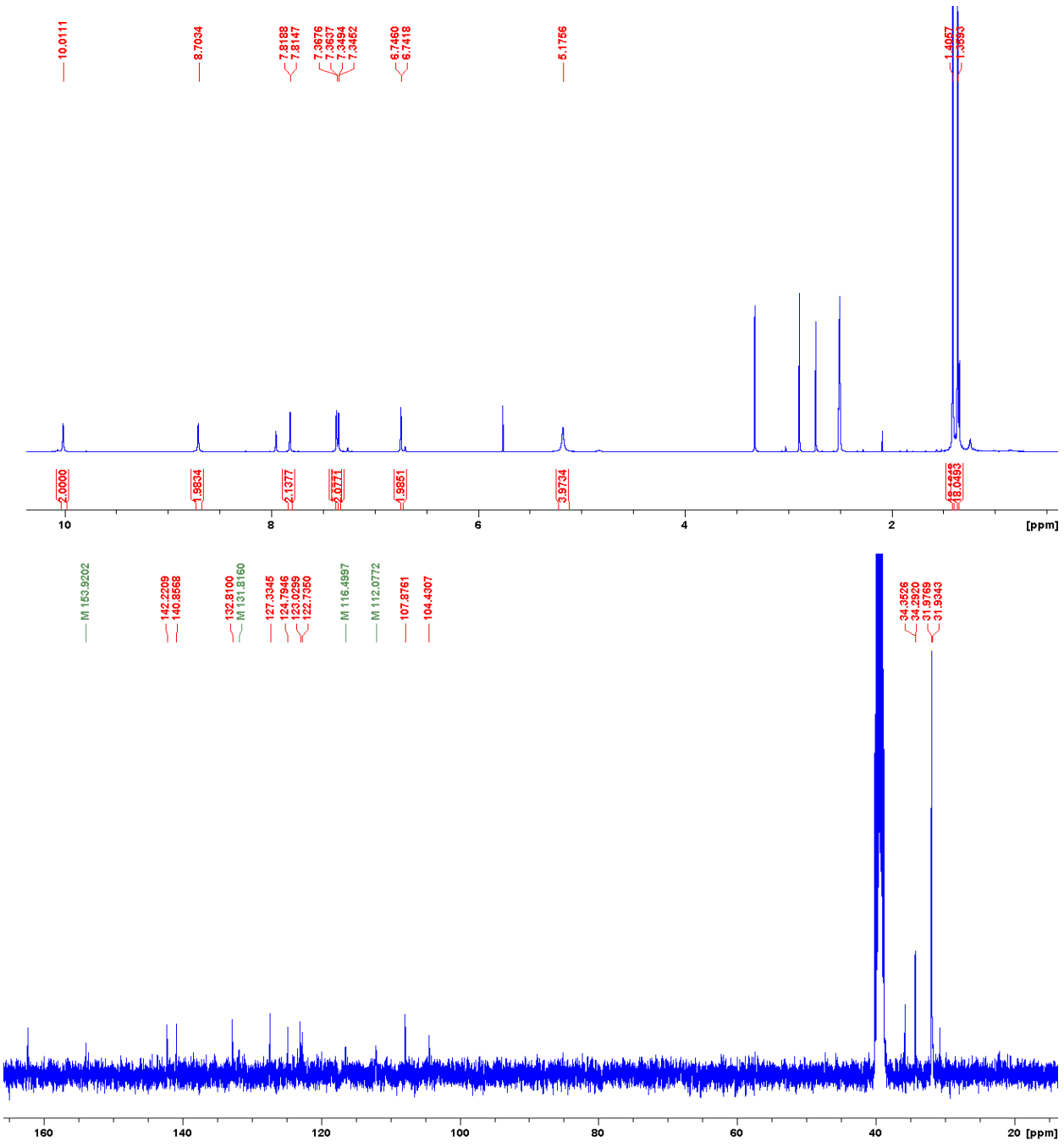

Appendix 15: Top) ^{1}H; Bottom) ^{13}C NMR spectra of compound **4.15** in d_6-DMSO at 298 K.

Compound **5.8**

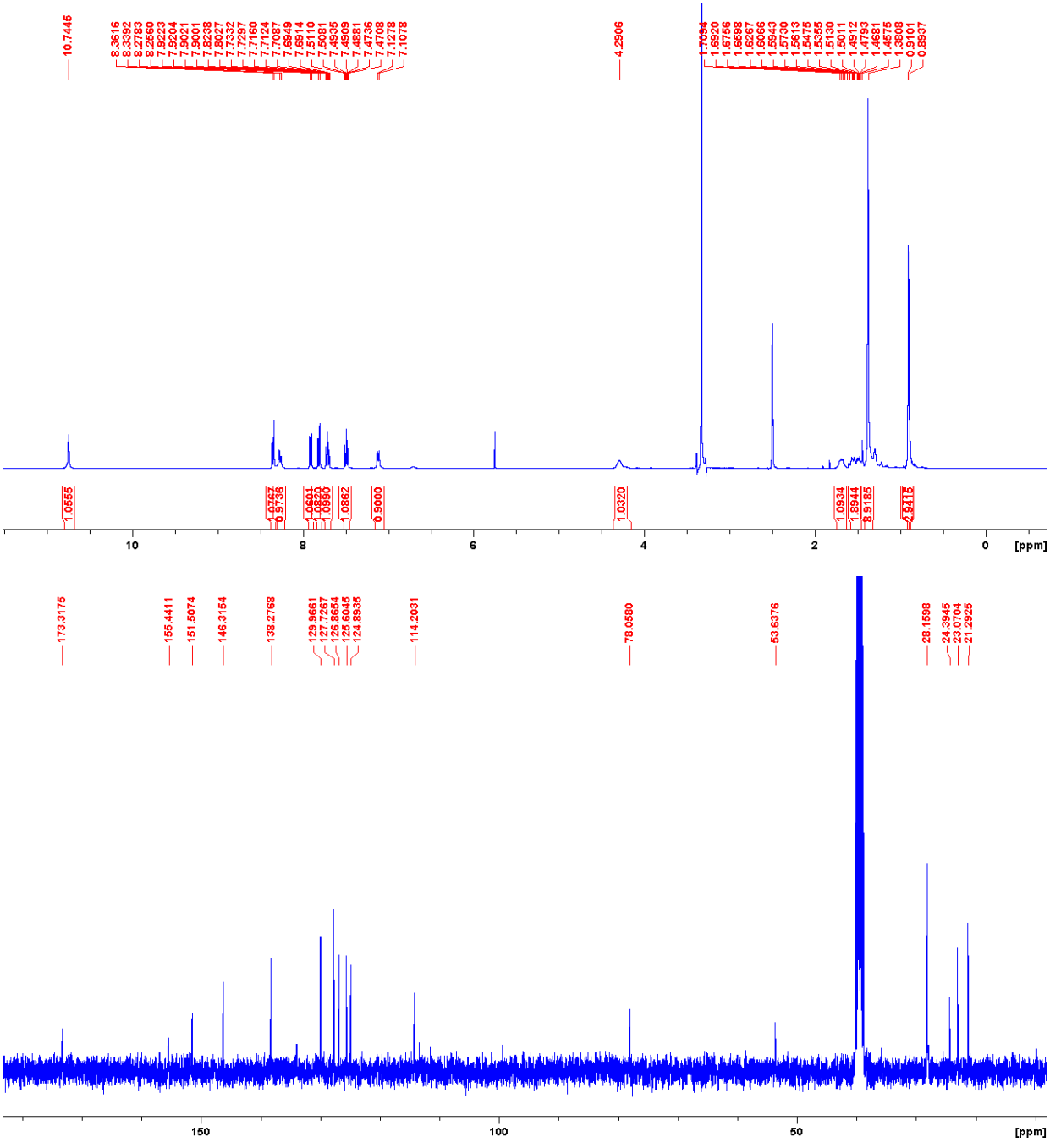

Appendix 16: Top) ^{1}H; Bottom) ^{13}C NMR spectra of compound **5.8** in d_6-DMSO at 298 K.

Compound **5.11**

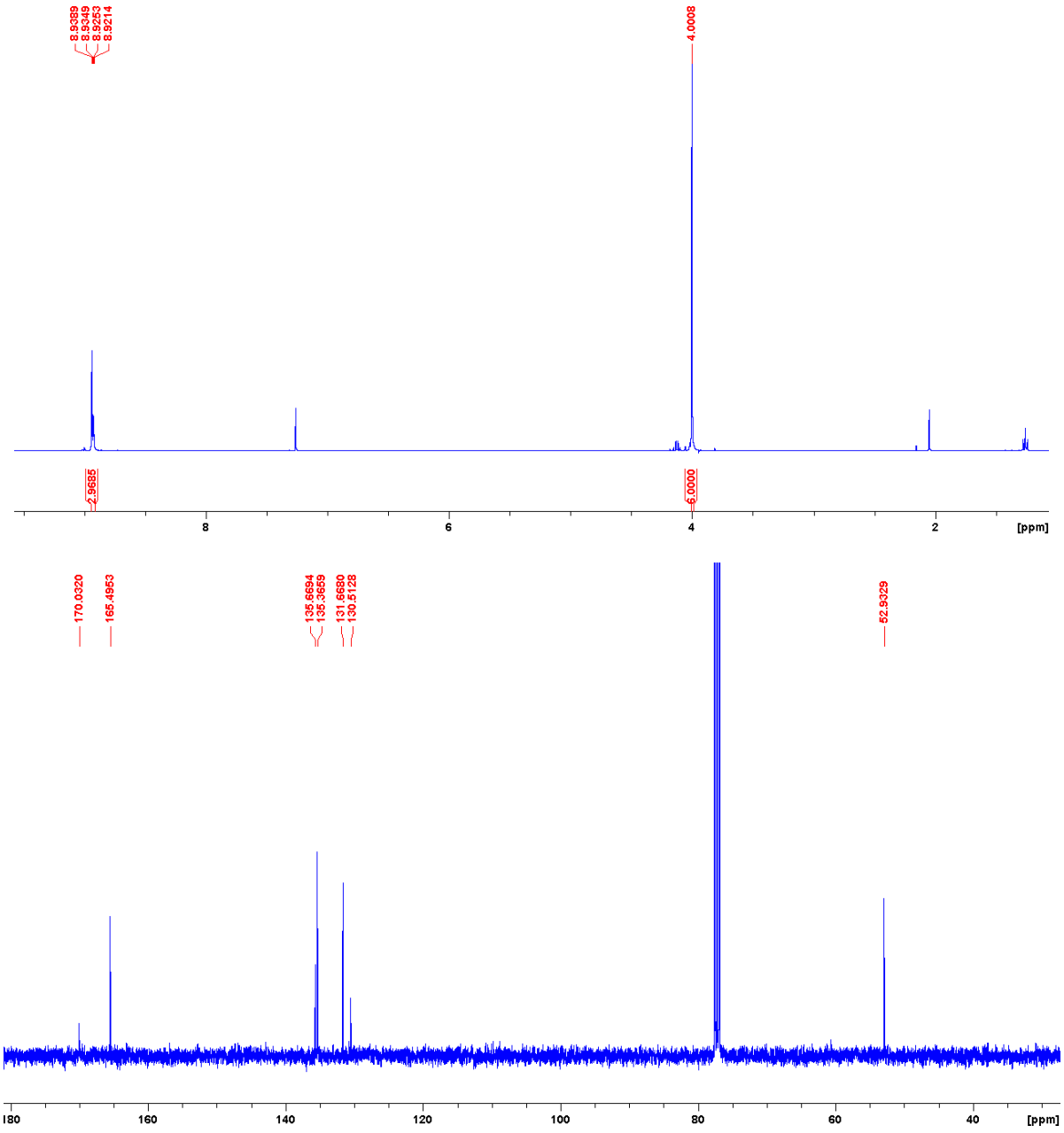

Appendix 17: Top) ^{1}H; Bottom) ^{13}C NMR spectra of compound **5.11** in $CDCl_3$ at 298 K.

Compound **5.12**

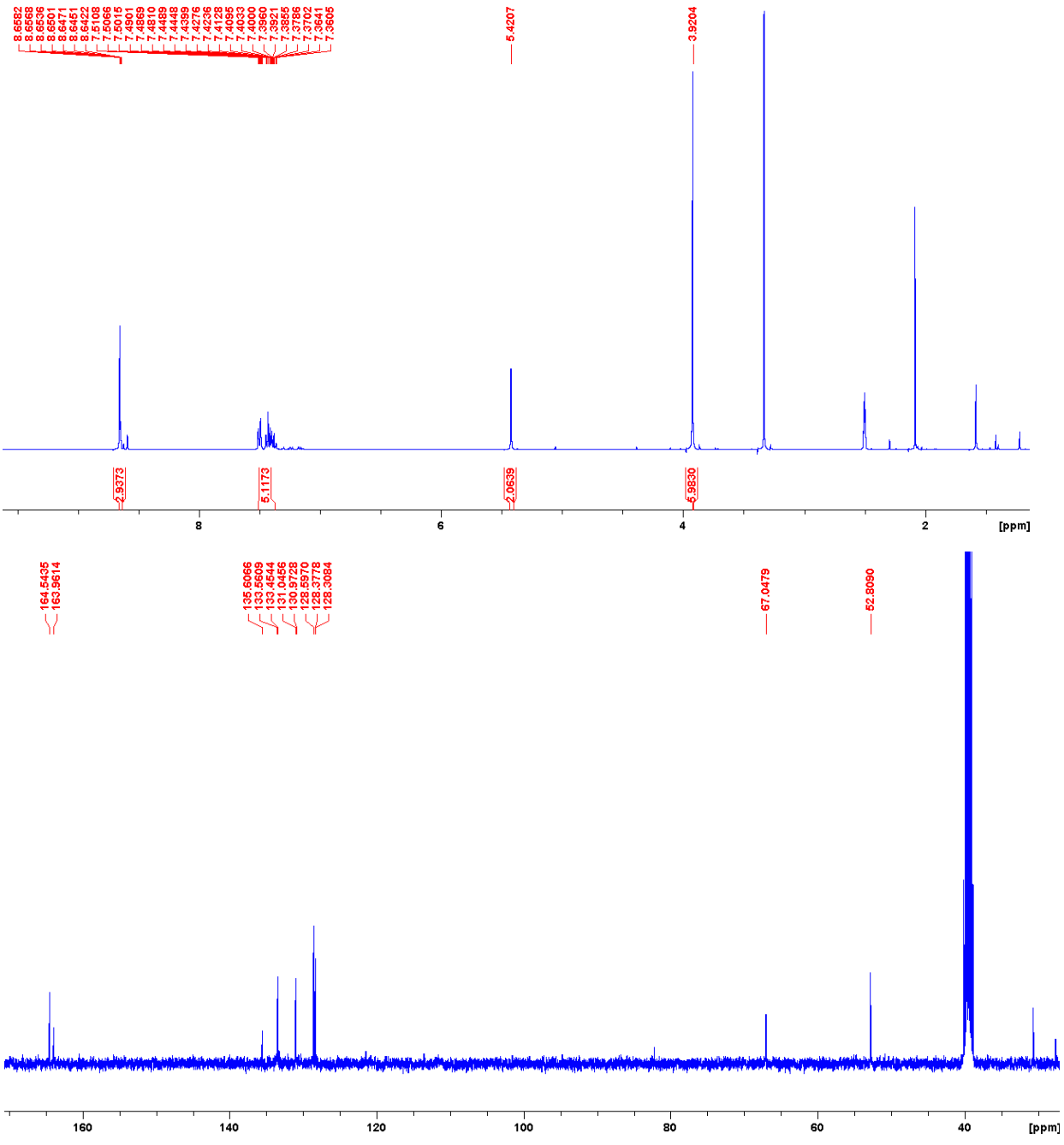

Appendix 18: Top) ^{1}H; Bottom) ^{13}C NMR spectra of compound **5.12** in d_6-DMSO at 298 K.

Compound **5.16**

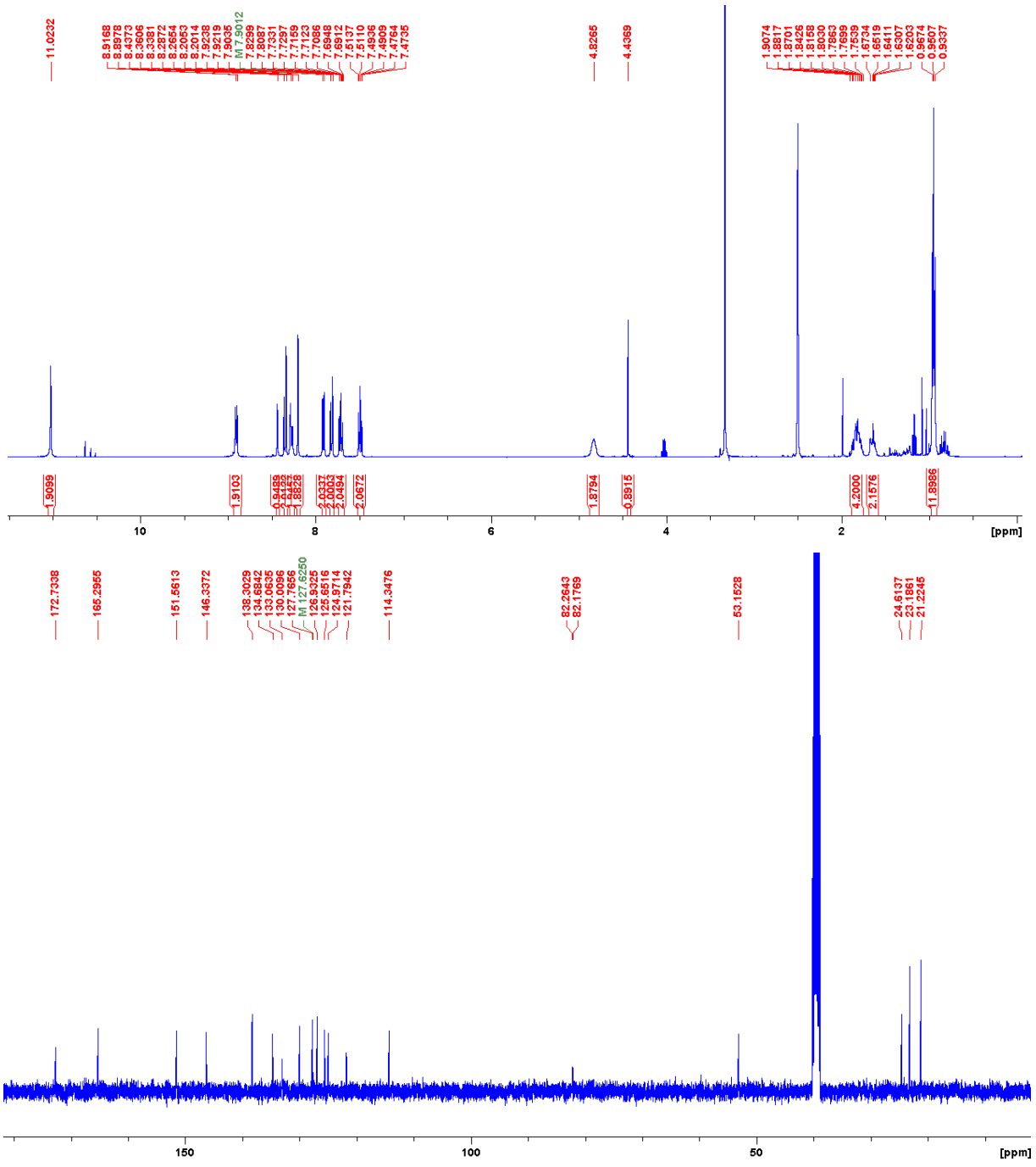

Appendix 19: Top) ^{1}H; Bottom) ^{13}C NMR spectra of compound **5.16** in d_6-DMSO at 298 K

Association Constant Fitting (BindFit)[1,2]

Chapter 3- Compound 3.12

1:1 binding model

http://app.supramolecular.org/bindfit/view/6043dbcf-8647-46e2-9465-ddc805903bcc

2:1 binding model

http://app.supramolecular.org/bindfit/view/541f78b1-4e67-4fba-8949-0eaf321c70e6

1:2 binding model

http://app.supramolecular.org/bindfit/view/949a9556-daff-453c-bc20-f3bda38b9879

Chapter 4- Compound 4.16

http://app.supramolecular.org/bindfit/view/ab721410-d21c-4978-924b-6b79b0cde7d2

Chapter 5- Compound 5.16

http://app.supramolecular.org/bindfit/view/a30832ac-a2ce-4aa0-86aa-c57546f1c740

References

1 D. Brynn Hibbert and P. Thordarson, *Chemical Communications*, 2016, **52**, 12792–12805.

2 http://supramolecular.org